

Dynamical evolution of small bodies in the Solar System

by

Seth A. Jacobson

B.S., Cornell University, 2008

M.S., University of Colorado, 2010

A thesis submitted to the

Faculty of the Graduate School of the

University of Colorado in partial fulfillment

of the requirements for the degree of

Doctor of Philosophy

Department of Astrophysical and Planetary Sciences

2012

This thesis entitled:
Dynamical evolution of small bodies in the Solar System
written by Seth A. Jacobson
has been approved for the Department of Astrophysical and Planetary Sciences

Daniel Scheeres

Glen Stewart

J. Michael Shull

Date _____

The final copy of this thesis has been examined by the signatories, and we find that both the content and the form meet acceptable presentation standards of scholarly work in the above mentioned discipline.

Jacobson, Seth A. (Ph.D., Astrophysical and Planetary Sciences)

Dynamical evolution of small bodies in the Solar System

Thesis directed by Prof. Daniel Scheeres

This thesis explores the dynamical evolution of small bodies in the Solar System. It focuses on the asteroid population but parts of the theory can be applied to other systems such as comets or Kuiper Belt objects. Small is a relative term that refers to bodies whose dynamics can be significantly perturbed by non-gravitational forces and tidal torques on timescales less than their lifetimes (for instance the collisional timescale in the Main Belt asteroid population or the sun impact timescale for the near-Earth asteroid population). Non-gravitational torques such as the YORP effect can result in the active endogenous evolution of asteroid systems; something that was not considered more than twenty years ago.

This thesis is divided into three independent studies. The first explores the dynamics of a binary systems immediately after formation from rotational fission. The rotational fission hypothesis states that a rotationally torqued asteroid will fission when the centrifugal accelerations across the body exceed gravitational attraction. Asteroids must have very little or no tensile strength for this to occur, and are often referred to as “rubble piles.” A more complete description of the hypothesis and the ensuing dynamics is provided there. From that study a framework of asteroid evolution is assembled. It is determined that mass ratio is the most important factor for determining the outcome of a rotational fission event. Each observed binary morphology is tied to this evolutionary schema and the relevant timescales are assessed.

In the second study, the role of non-gravitational and tidal torques in binary asteroid systems is explored. Understanding the competition between tides and the YORP effect provides insight into the relative abundances of the different binary morphologies and the effect of planetary flybys. The interplay between tides and the BYORP effect creates dramatic evolutionary pathways that lead to interesting end states including stranded widely separated asynchronous binaries or tightly

bound synchronous binaries, which occupy a revealing equilibrium. The first results of observations are reported that confirm the theoretically predicted equilibrium.

In the final study, the binary asteroid evolutionary model is embedded in a model of the entire Main Belt asteroid population. The asteroid population evolution model includes the effects of collisions as well as the YORP-induced rotational fission. The model output is favorably compared to a number of observables. This allows inferences to be made regarding the free parameters of the model including the most likely typical binary lifetimes.

These studies can be combined to create an overall picture of asteroid evolution. From only the power of sunlight, an asteroid can transform into a myriad number of different states according to a few fundamental forces.

Dedication

I dedicate this thesis to my family: Bob, Renee, Alec, Tess and Elli.

Acknowledgements

For the construction of this thesis and my graduate career in general, I would like to acknowledge a number of people. Foremost, I acknowledge the incredible guidance provided by my advisor Daniel J. Scheeres. I found both challenge and inspiration inside his laboratory, the Celestial and Spaceflight Mechanics Lab, and amongst his other students including Jay McMahon, Masatoshi Hirabayashi, Paul Sanchez, Christine Hartzell, Marcus Holtzinger, Zubin Olikara, Yu Takahashi, Dylan Boone, and Kohei Fujimoto.

Within the Astrophysical and Planetary Sciences Department, I have found many individuals that have provided positive role models, good advice, and friendship: John Bally, John Stocke, Jeremy Darling, Robbie Citron, Julia Kamenetzky, Susanna Kohler, Erik Larson, Adam Ginsburg, Tyler Mitchell, Tim Ellsworth-Bowers, and Jessica Lovering. I would like to specially acknowledge the members of my thesis committee: Phil Armitage, Larry Esposito, Glen Stewart, Mike Shull, Seth Hornstein.

I must also acknowledge the assistance of a number of individuals outside of the university including Petr Pravec, Petr Scheirich, Francesco Marzari, and Alessandro Rossi. Special acknowledgements to the observatory staffs of Apache Point Observatory and Kitt Peak National Observatory especially Russet McMillan and Dianne Harmer.

Lastly, I must acknowledge the role of my family and friends in keeping me motivated and sane especially Caroline Sczcepanski, Drew Eisenberg, Robbie Citron and Erik Larson.

Contents

Chapter

1	Study of Post-rotational Fission Dynamics	1
1.1	Introduction	1
1.1.1	Observed NEA Classes	1
1.1.2	Motivation	5
1.2	Methods	6
1.2.1	Initial Conditions	6
1.2.2	Rotational Fission Model	7
1.2.3	Dynamical Model	8
1.3	Results	10
1.3.1	Chaotic Binary	10
1.3.2	Two Regimes	12
1.3.3	High Mass Ratio Regime	15
1.3.4	Low Mass Ratio Regime	18
1.3.5	Secondary Spin Fission	22
1.3.6	Chaotic Ternaries	25
1.3.7	Stable Binaries	30
1.3.8	Asteroid Pairs	38
1.4	Discussion	38
1.5	Conclusion	40

1.6	Derivation of the Two-Body Equations of Motion	41
1.7	Derivation of the Three-Body Equations of Motion	45
1.8	Derivation of the Tidal Theory	49
1.9	Secondary Fission Condition	50
1.10	Impact Mass Redistribution	51
1.11	Modeling Tidal Timescales	52
1.12	Limit on the Mass Ratio of Next Secondary Fission	52
2	Study of the Role of Non-gravitational and Tidal Torques on Binary Asteroid Systems	54
2.1	Introduction	54
2.2	Asynchronous Binary Evolution	60
2.2.1	The YORP effect and mutual body tides	61
2.2.2	The tidal YORP coefficient	63
2.2.3	Application to systems with unknown status	72
2.3	Synchronous Asteroid Evolution	73
2.3.1	Tidal Evolution	74
2.3.2	BYORP Evolution	76
2.3.3	Joint Evolution	77
2.4	Joint Expansive Evolution	78
2.4.1	Expansive De-synchronization Hypothesis	79
2.4.2	Adiabatic Invariance	81
2.4.3	Derivation of the Adiabatic Invariance	81
2.4.4	Onset of Circulation	86
2.4.5	Libration Energy	86
2.4.6	Derivation of the libration tides	86
2.4.7	Energy Dissipation in a number of systems	90
2.4.8	Libration growth due to BYORP effect	90

2.4.9	Comparison to Observation	91
2.5	Joint Opposing Evolution	92
2.5.1	Implications for the Synchronous Binary Asteroid Population:	94
2.5.2	Proposed Equilibrium Hypothesis	97
2.5.3	Test of the Hypothesis	98
2.5.4	Observation Design and Methods	99
2.5.5	First Results	102
3	Study of the Effects of Rotational Fission on the Main Belt Asteroid Population	105
3.1	Introduction	105
3.2	Single Asteroid Evolution	108
3.2.1	YORP Evolution	109
3.2.2	Collisional Evolution	110
3.2.3	Spin Limits	112
3.2.4	Outcomes of Rotational Fission	115
3.2.5	Mass Ratio Fraction	118
3.3	Binary Asteroid Evolution	120
3.3.1	“Instantaneous” Binary Evolution	122
3.3.2	“Long-term” Binary Evolution	124
3.3.3	Binaries and Collisions	140
3.3.4	Contact Binaries	140
3.3.5	Asteroid Pair Observability	141
3.4	Results of the asteroid population evolution model	141
3.4.1	Steady-State Binary Fraction	142
3.4.2	Steady-State Mass Ratio Fraction	145
3.4.3	Contact Binary Fraction	150
3.4.4	Best Fit Parameters	150

3.5 Discussion 154

Bibliography **155**

Appendix

Chapter 1

Study of Post-rotational Fission Dynamics

1.1 Introduction

The Near-Earth asteroid (NEA) population has a relatively large amount of data compared to other small body populations, including detailed information on asteroid figures and binary structure, often made possible through the combination of lightcurve and radar techniques. Observers have discovered a wide and complex set of asteroid systems that before this study have not been tied together into a coherent theory. The emergence of radiative forces as a major evolutionary mechanism for small bodies, in particular for NEA systems due to their small size and proximity to the Sun, makes the development of such a theory possible.

A simple model of NEA evolution constructed from the Yarkovsky-O’Keefe-Radzievskii-Paddack (YORP) and binary YORP (BYORP) effects, “rubble pile” asteroid geophysics, and gravitational interactions can incorporate all of the diverse observed asteroid classes as shown in Figure 1.1: synchronous binaries, doubly synchronous binaries, contact binaries, asteroid pairs, re-shaped asteroids, and stable ternaries.

1.1.1 Observed NEA Classes

Binary asteroid systems comprise a significant fraction ($15\pm 4\%$) of the NEA population (Margot et al., 2002; Pravec et al., 2006) and include all compositional classes and size scales (Pravec and Harris, 2007). Most of these systems are synchronous binaries—the orbital and secondary spin periods are equal, but the primary has a faster spin rate. Observed synchronous systems have mass

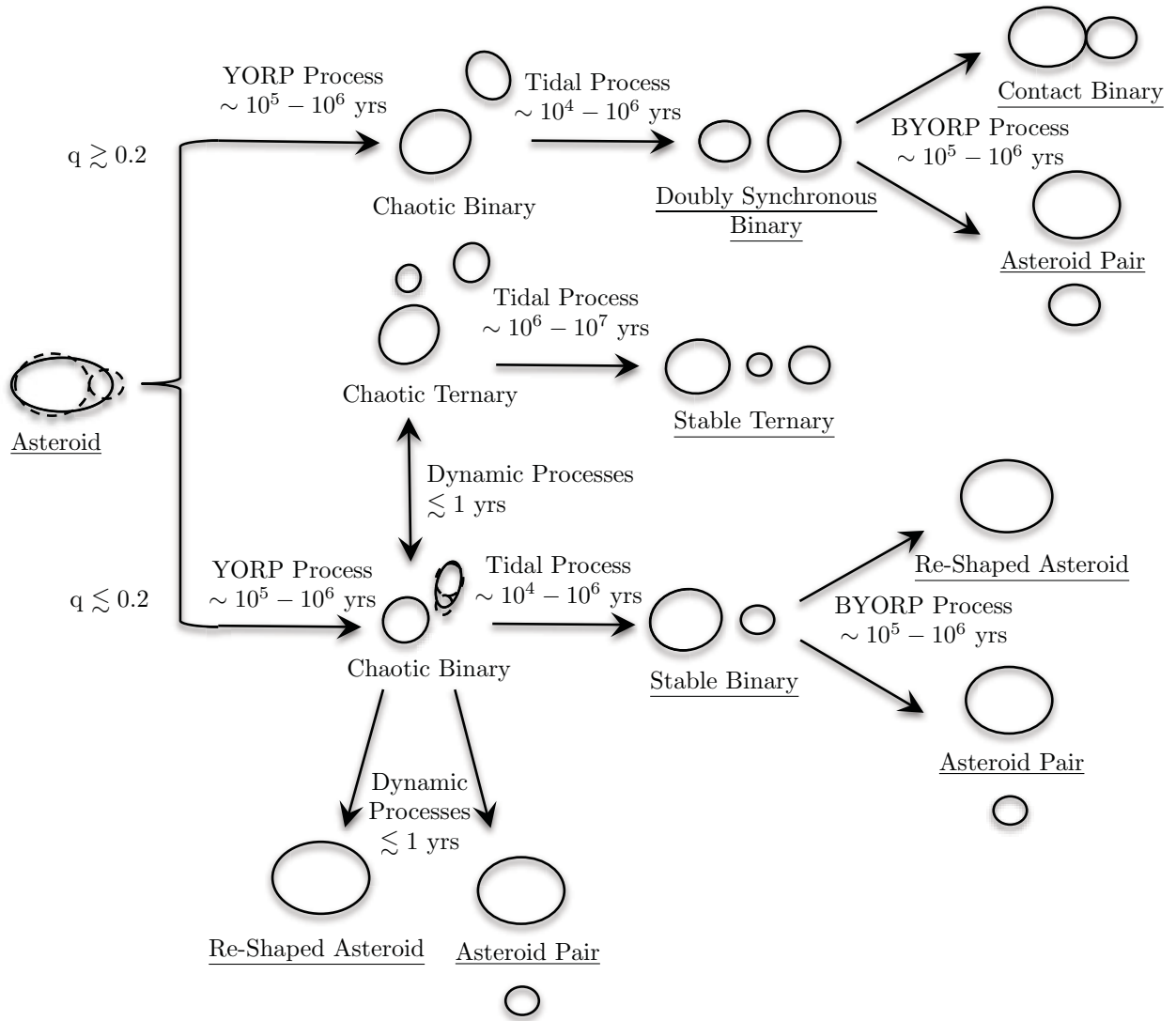


Figure 1.1: Evolutionary tracks for an NEA. q is the rotational fission component mass ratio. Arrows indicate the direction of evolution along with the process propelling the evolution and a typical timescale. Simple schematics show evolutionary states, an underline indicates an observed asteroid class. Stable ternaries are rare, and so their continued evolution is not described here, although it should be noted that ternaries may be formed via multiple primary fission events. It is important to note that the eventual outcomes are single asteroids (re-shaped asteroids, contact binaries, each member of asteroid pairs), so this evolutionary process represents a binary cycle.

ratios $\lesssim 0.2$, a system semi-major axis of 1.5 to 3 primary diameters, and a possibly elongated secondary and a nearly spherical primary with a distinctive shape characterized by an equatorial bulge (Pravec et al., 2006; Pravec and Harris, 2007). The system has a positive free energy, but the tidally locked secondary inhibits disruption. Migration to the inner solar system from the main

Morphology	Observed Examples	Description
Doubly Synchronous Binaries	Frostia, Hermes, and Gavrilin (Behrend et al., 2006; Margot, 2003; Higgins et al., 2008)	All spin rotation periods are equivalent to the orbital revolution period. Mass ratios > 0.2 .
Contact Binaries	Castalia, Bacchus, and 2005 CR ₃₇ (Hudson and Ostro, 1994; Benner et al., 1999, 2006)	Single asteroids with a bi-modal shape appear as two similar-sized components resting on each other. Component mass ratios > 0.2 .
Synchronous Binaries	1999 KW ₄ , 2000 DP ₁₀₇ , and 2002 CE ₂₆ (Ostro et al., 2006; Margot et al., 2002; Shepard et al., 2006)	Secondary spin rotation period is equivalent to the orbital revolution period. Primary is fast rotating and has a characteristic oblate shape with an equatorial bulge. Mass ratios < 0.2 .
High- e Binaries	2004 DC and 2003 YT ₁ (Taylor et al., 2008; Nolan et al., 2004)	Mutual orbit is eccentric and secondaries may not be synchronous. Otherwise resemble synchronous binaries. Mass ratios < 0.2 .
Ternaries	2001 SN ₂₆₃ and 1994 CC (Nolan et al., 2008; Brozović et al., 2011)	All three members are in the same plane, and the primary resembles the primary of the synchronous binary. Mass ratios < 0.2 .
Re-shaped Asteroids	1999 RQ ₃₆ and 2008 EV ₅ (Nolan et al., 2007; Busch et al., 2010)	Single asteroids that resemble the primary of the synchronous binary.

Table 1.1: Examples of each observed NEA class according to a morphological classification scheme.

belt as binaries, binary creation via collision amongst NEAs, and binary creation via tidal disruption from close planetary flybys are not efficient enough mechanisms to create this population nor match the observed synchronous binary properties (Margot et al., 2002; Walsh and Richardson, 2008). Several theories attempt to explain this binary population by a YORP-induced rotational fission process, but do not capture all properties of synchronous binaries and do not predict the other NEA systems that are seen (Scheeres, 2007a, 2009a; Walsh et al., 2008).

The Walsh et al. (2008) theory requires rotational fission induced “landslides” that re-shape the primary, then enter into orbit. Secondaries are built from collections of “landslide” material

in orbit after many “landslide” events, and consequently YORP cycles—the length of the process to rotationally accelerate an asteroid to spin fission from its current state under the YORP effect. However, we will show that material entering orbit via rotational fission will almost always escape on timescales much shorter than a YORP cycle. Furthermore, Holsapple (2010) using continuum approximations of granular theory finds that mass loss would not occur at the equator of small, critically spinning asteroids, but that their shapes would deform, elongating the body until interior failure. These deformations in the shape of the body allow YORP to continue to increase the angular momentum without significant changes to the spin rate, even slightly decreasing the spin rate in some cases. Scheeres (2007a) reports a similar analytic finding that when cohesive theory is considered, failure will most likely occur along interior planes. The analytic theory in Scheeres (2009b) describes the first stage of the model proposed herein, where a chaotic binary system is immediately formed from the rotational fissioning of a “rubble pile.” A rotational fission model related to the one proposed in this work has been implicated in the formation of asteroid pairs (Pravec et al., 2010)—two asteroids with heliocentric orbits that in the recent past ($\lesssim 10^6$ yrs) intersect deep within the other’s Hill radius and with small relative speeds (Vokrouhlický and Nesvorný, 2008). Asteroid pairs are observed in the Main Asteroid Belt with similar sizes to NEAs, but they have not been observed in the NEA population. The theory outlined in this paper predicts them; asteroid pairs are difficult to detect in the NEA population because their orbits are rapidly perturbed and smaller initial asteroids fission into even smaller secondaries for the same mass ratios as the Main Belt asteroid population.

Other observed distinct dynamical and morphological classes include doubly synchronous binaries, high- e binaries, ternaries, contact binaries, and re-shaped asteroids. We describe each in turn. Doubly synchronous binaries: all spin rotation periods are equivalent to the orbital revolution period. They also have high mass ratios $\gtrsim 0.2$ and a system semi-major axis of 2 to 8 primary diameters (Pravec and Harris, 2007). These systems are difficult to detect because of an observational bias in light curve data; doubly synchronous systems and elongated single objects appear similarly. Contact binaries: bimodally-shaped asteroids observed as two similar-sized components resting on

each other, which implies a formation mechanism that brings the two components together very gently. Contact binaries comprise a significant fraction ($> 9\%$) of the NEA population (Benner et al., 2006). High- e binaries: low mass ratio binary systems distinct from the synchronous binaries, because they are asynchronous and have high eccentricities (Taylor et al., 2008). Ternary systems: large primary orbited by two smaller satellites. The primaries are spinning faster than the orbital rates and the mass ratio is low (< 0.1) (Brozović et al., 2011). Re-shaped asteroids: single bodies similar to the primaries of the synchronous binary class—an oblate shaped figure with an equatorial bulge. For reference, examples of each NEA class are given in Table 1.1.

1.1.2 Motivation

A collisionally evolved asteroid can be modeled as a “rubble pile”—a collection of gravitationally bound boulders with a distribution of size scales and very little tensile strength between them (Michel et al., 2001; Richardson et al., 2005; Tanga et al., 2009). “Rubble pile” morphology has been closely examined by the Hayabusa mission to Itokawa, as shown in Figure 1.2, which has no obvious impact craters and appears as collection of shattered fragments of different size scales (Fujiwara et al., 2006). Mass and volume measurements from the NEAR Shoemaker flyby of Mathilde (Yeomans et al., 1997) and radar observations of 1999 KW₄ (Ostro et al., 2006) determine mean densities that are lower than their constitutive elements, which is evidence of voids and cracks in the structures of these bodies. Asteroids with diameters larger than ~ 200 m rarely spin with periods less than ~ 2.2 hours, which corresponds with the critical disruption spin rate of self-gravitating, “rubble pile” bodies (Pravec and Harris, 2007). Both theoretical modeling and direct observation indicate that asteroids within a size range of ~ 100 m to ~ 10 km have “rubble pile” geophysics.

The details of the rotational fission process determine the initial conditions for the binary system. The torque from the YORP effect will increase the centrifugal accelerations acting on each “rubble pile” component. There is a specific spin rate at which each component of the body will go into orbit about the rest determined by the largest separation distance of the mass centers of the

fissioned component and the remainder of body (Scheeres, 2009a). The smaller component is now the secondary, and the remainder is the primary, both in orbit about each other. The motivation for this study was to determine what happens dynamically after a rotational fission event.

This paper will utilize some important concepts throughout that will be briefly introduced here and further defined later. The mass ratio is defined as the secondary mass divided by the primary mass. The primary of a binary system is always larger than the secondary, so the mass ratio is a number between 0 and 1. Secondary fission is rotational fission of the secondary induced via spin-orbit coupling and occurring during the chaotic binary stage of low mass ratio evolution creating chaotic ternaries. Ternary systems have three members. The components in decreasing mass are labeled primary, secondary, and tertiary, however the two smaller members are referred collectively as secondaries. Secondaries may escape the system if the system has a positive free energy. The free energy of an asteroid system is the sum of the kinetic and mutual potential energies of the system (both rotational and translational) neglecting the self-potentials of each body.

1.2 Methods

1.2.1 Initial Conditions

As the rotation rate of an asteroid increases due to the YORP effect, the asteroid will go through a series of reconfiguration events. These events may range from small-scale “rock flows” to significant restructuring of the principal coherent components. A “rubble pile” will have a specific set of local minimum energy configurations that the coherent components will settle into (Scheeres, 2009b). As the spin rate of the asteroid increases due to the YORP effect, the system will act to arrange itself into the global minimum energy configuration. The largest distance between two mass centers, which encompass all of the mass, determines how the system will fission, since systems in this minimum energy equilibrium will undergo rotational fission at lower spin rates than any other configuration (Scheeres, 2009b). The model assumes that the system is in this minimum energy configuration and the two components can be represented by tri-axial ellipsoids resting so that

contact is along the largest axis of each body.

If a system cannot rearrange itself to this configuration and so is not in the relative equilibrium, it will still rotationally fission but at a higher spin rate. The system will then undergo the same dynamics demonstrated below but start with a higher energy increasing the probabilities of disrupting the system and a re-impact event between the two components. An impact event will dissipate energy but conserve angular momentum, so there is no stable single-body configuration for the system, and thus material must immediately lift off the primary and return to orbit (Scheeres, 2009a). The specific details of the impact and ejecta will determine whether the system evolves as a high or low mass ratio system. For the sake of simplicity, the model will assume the minimum energy configuration with the knowledge that the results have a systematic uncertainty due to this initial condition.

1.2.2 Rotational Fission Model

The dynamical simulation begins with a tri-axial asteroid made of two components inspired by objects such as Toutatis or Itokawa. We model “rubble pile” asteroids as having an inherent component mass ratio dividing all of the “rubble” into hierarchical groups determined by the largest distance between mass centers as shown in the upper left panel of Figure 1.2. The mass ratio between the components and the shape ratio of each component are the three initial free parameters. As the asteroid’s rotational rate increases due to the YORP effect, the long axes of each “rubble pile” component ellipsoid will align for rapid rotation rates. This configuration is the only stable relative equilibrium figure for the body while still resting on each other (Scheeres, 2007a). As the YORP effect continues to torque the body, the two components will enter into orbit about each other.

The YORP effect is responsible for spinning the initial body up to the required rotation rate for fission. This is the only time a non-gravitational process (Yarkovsky, YORP, or BYORP) is required for constructing synchronous binary systems. The components will fission at a specific spin rate of the primary body given the internal component mass distribution (Scheeres, 2009a).

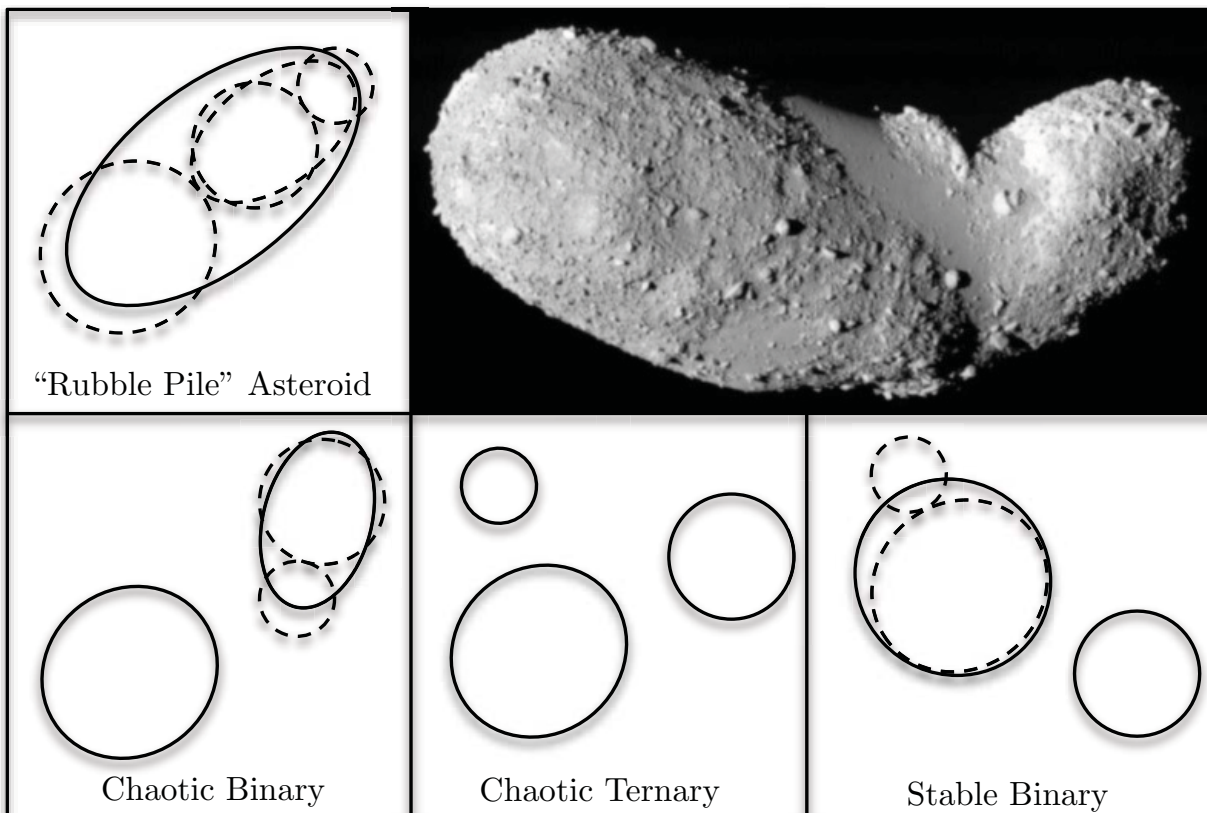


Figure 1.2: The upper right hand corner shows a motivating image of Itokawa taken by the Hayabusa spacecraft (Image courtesy of ISAS/JAXA). The cartoons document the low mass ratio evolutionary model. Solid lines indicate surfaces and dashed lines indicate “rubble-pile” internal substructure. The “rubble pile” asteroid evolves from the upper left to bottom left chaotic binary panel via a YORP-induced rotational fission event. A secondary fission event occurs between the lower left and lower middle panels creating a chaotic ternary system. One of the components impacts the primary as the system evolves from the lower middle to lower right panel forming a less energetic, more stable binary system.

All bodies in these simulations have a density of 2 g/cc and so will fission at rotational periods greater than 2.33 hours dependant only on the mass and shape ratios of the two model components.

1.2.3 Dynamical Model

Post-rotationally fissioned systems were studied by directly integrating the Lagrangian dynamics with an implicit 12th order Runge-Kutta scheme for two bodies (two tri-axial ellipsoids) or three bodies (one tri-axial ellipsoid and two spheres) as described in 1.6 and 1.7, respectively.

Non-spherical gravitational potentials ensure that the model will capture the important effect of spin-orbit coupling. The model incorporates secondary fission (selecting secondary component mass ratios from a flat distribution between 0.01 to 0.99) and impacts (inelastic collisions with total angular momentum and mass conserved) as described in 1.9 and 1.10, respectively. The dynamics also include the torques from mutual body tides, which dissipate energy. The rate of energy dissipation is dependent on the difference between the spin rate of the body and the orbital rate and inversely dependent on the distance between the bodies to the sixth power (Murray and Dermott, 2000). The specifics of the tidal theory is given in 1.8. The effect of solar gravitational perturbations for an orbit about the Sun at 1 AU is also included on the system. In each integrator, total system energy is conserved to greater than 1 part in 10^8 when energy changing effects such as mutual body tides and solar gravitational perturbations are neglected, and angular momentum is conserved to greater than 1 part in 10^8 when angular momentum changing effects such as solar gravitational perturbations are neglected.

Non-gravitational forces (YORP and BYORP effects) were not included in the post-rotational fission dynamical model since the gravitational timescales are much shorter than the radiative timescales. The model assumes planar motion with the intention of implementing 3-D motion and associated non-principal axis rotation in the future, with the expectation that it will increase energy dissipation, lengthen the timescale for ejection of the secondary, and thus increase the binary formation efficiency; more detailed modeling of impact and fission processes may change the efficiencies associated with the evolutionary sequence but should not change the possible outcomes. The dynamics will scale to any realistic size scale for NEAs, although the effects of cohesive attraction are not modeled and may be important on the smallest size scales $\lesssim 100$ m (Scheeres et al., 2010) and the timescale for YORP effect induced rotational fission is too long for the largest size scales $\gtrsim 10$ km.

1.3 Results

1.3.1 Chaotic Binary

The dynamics demonstrated immediately after the initial rotational fission are chaotic. The coupling of the spin and orbit states from the tri-axial gravitational potential is responsible for significant variations of behavior in the system. This coupling can transfer large amounts of energy and angular momentum across the system leading to rapid changes in the spin rates and orbital revolution rates. These changes can repeatedly switch the tidal bulge on each member from leading to lagging and vice versa. Immediate tidal energy dissipation via mutual body tides helps prevent re-impact.

Studying two cases in detail helps illustrate this chaotic evolution. These systems approximate the well-known systems: (66391) 1999 KW₄, an asynchronous binary, and 25143 Itokawa, a contact binary. Ostro et al. (2006) reports the size of the primary of 1999 KW₄ as close to a tri-axial ellipsoid with semi-axes $708.5 \times 680.5 \times 591.5$ m, and the secondary as a tri-axial ellipsoid with semi-axes $297.5 \times 225 \times 171.5$ m. Assuming constant density, the mass ratio of the binary system is close to 0.04. Demura et al. (2006) reports that size of the “body” (primary) of Itokawa approximates a tri-axial ellipsoid with semi-axes $245 \times 130 \times 130$ m, and the “head” (secondary) as a tri-axial ellipsoid with semi-axes $115 \times 90 \times 90$ m. Assuming constant density, the mass ratio of these components is close to 0.3.

For these simulations the bodies are placed into their relative equilibrium state, which is the only stable configuration of the bodies when the rotation rate of the system is just below rotational fission of the two components (Scheeres, 2009b). In this configuration, the primary and secondary are in contact and aligned along their longest axes. The dynamical simulation begins when the rotation rate of the pre-fissioned body reaches the critical disruption spin limit for the two, internal components. The dynamics modeled include spin-orbit coupling and mutual body tides as described in Section 1.2.3, but do not include solar gravitational perturbations, so angular momentum is conserved.

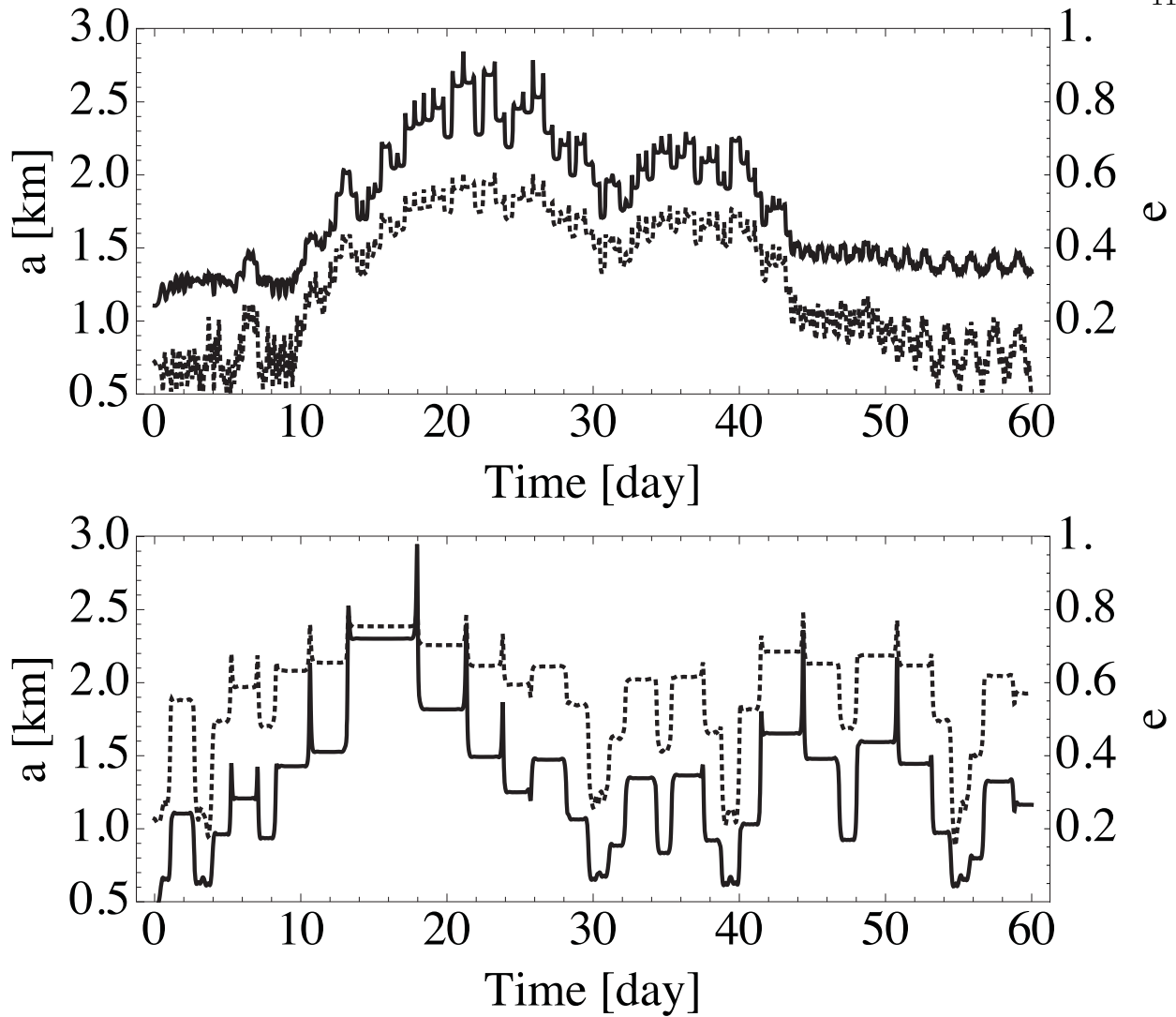


Figure 1.3: The semi-major axis a (solid line and left-hand, vertical axis) and the eccentricity e (dotted line and right-hand, vertical axis) are shown as a function of time for both a 1999 KW₄-like system (top plot) and an Itokawa-like system (bottom plot).

Exploring the evolution of the semi-major axis a and eccentricity e for 1999 KW₄ and Itokawa over the first 60 days after rotational fission in Figure 1.3, the nature of the chaotic evolution is evident. Variations in the semi-major axis track transfers of angular momentum from the orbital state to the spin state and back. The spin of each body is coupled to the orbital motion through the non-Keplerian gravitational potential, and these transfers of angular momentum are apparent in the changing rotational periods of the primary and secondary of each system as shown in Figure 1.4.

The spin rates of both bodies change dramatically, however as the mass ratio decreases the changes in the spin rate of the secondary become more dramatic. The secondary of 1999 KW₄ has intervals of almost no rotation, but also intervals when its rotation rate exceeds and resides near the critical disruption limit for a sphere. The critical disruption limit for a sphere is defined as the rotation rate necessary to lift a massless test particle off the surface, if the secondary had a “rubble pile” internal structure, then it would disrupt at a slower rotation rate. Rotational fission of the secondary due to torques from spin-orbit coupling is called secondary fission and occurs in many simulated systems. This process is discussed further later. If the secondary of 1999 KW₄ is not allowed to fission and the system continues to dynamically evolve, then the system will disrupt after ~ 1600 days. The Itokawa system will never disrupt since the system has a negative free energy and so is always bound.

This chaotic evolution causes the rate of tidal energy dissipation to change radically between intervals of strong and weak or even non-existent tidal dissipation, which depends on the separation distance to the sixth power and the relative spin rates of the bodies to the orbital rate. While the motions of an individual system are chaotic, the systems as a whole do appear to have a general set of dynamics and show trends with mass ratio. The secondary vacillates between libration and circulation more often than the primary which usually displays just circulation. The system evolves rapidly into an eccentric mutual orbit with a quickly changing longitude of pericenter. Secondaries of lower mass ratio systems exhibit stronger instances of these behaviors. This is expected because the lower the mass ratio, the greater the initial spin rate for rotational fission in the parent body. Lower mass ratio systems will thus have more energy to transfer into their orbits after fission.

1.3.2 Two Regimes

The initial spin rate for rotational fission in the parent body quickly divides the dynamics into two regimes: negative and positive free energy. The initial rotation rate necessary to fission the components depends on the mass ratio between the two components (Scheeres, 2009b). For two spherical components the division between the two regimes occurs at a mass ratio of ≈ 0.2 . High

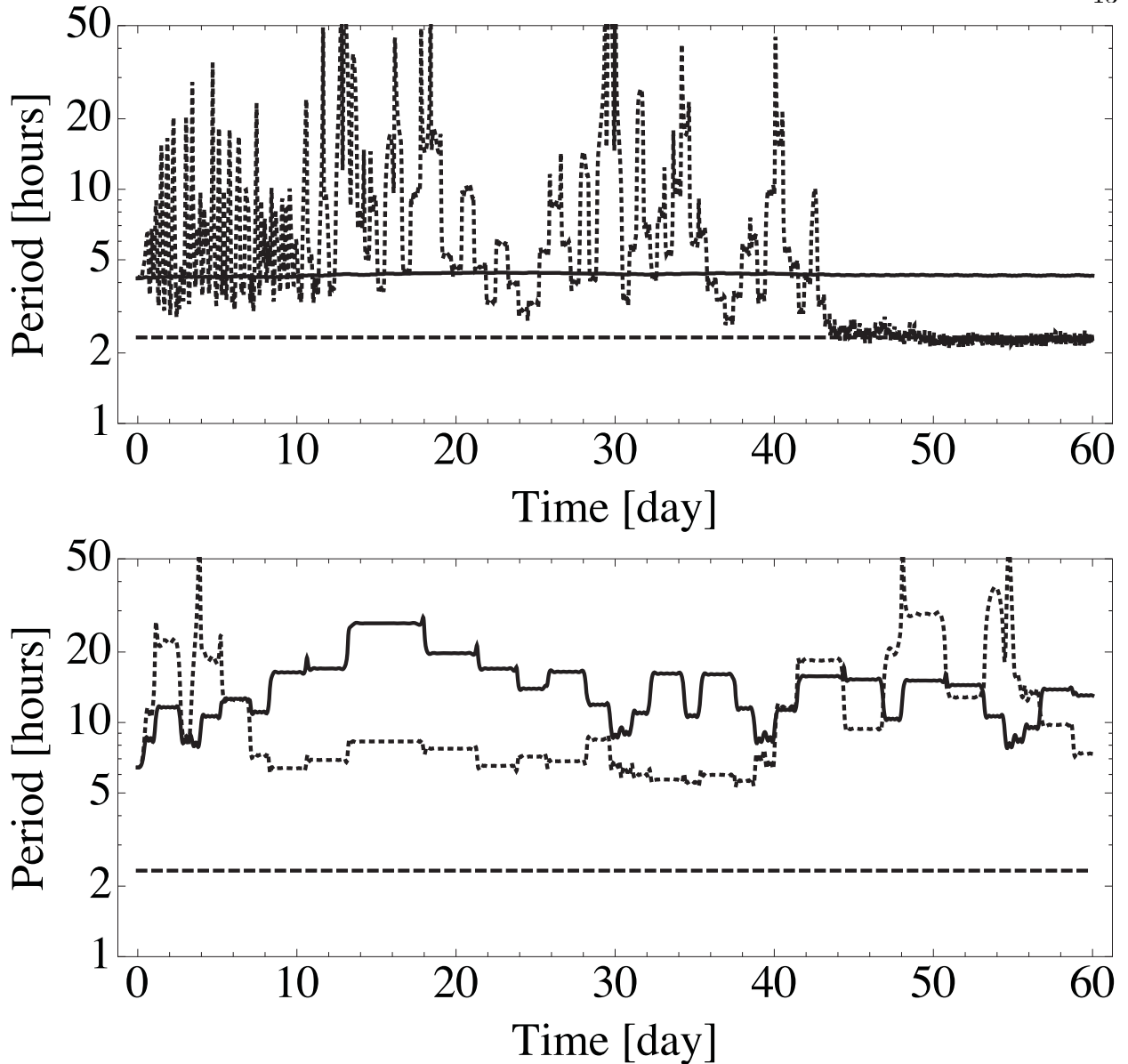


Figure 1.4: The rotational periods of the primary (solid line) and the secondary (dotted line) are shown as a function of time for both a 1999 KW₄-like system (top plot) and an Itokawa-like system (bottom plot). The dashed line is the period (~ 2.33 hours) for the surface disruption of a sphere of density 2 g/cc.

mass ratio systems (mass ratio > 0.2) have a negative free energy and are bound for all time under internal gravitational perturbations. Low mass ratio systems (mass ratio < 0.2) have a positive free energy and may escape if the excess energy is not dissipated. For tri-axial ellipsoids the regime boundary does not have a specific value since there is a dependence on the shape of each body,

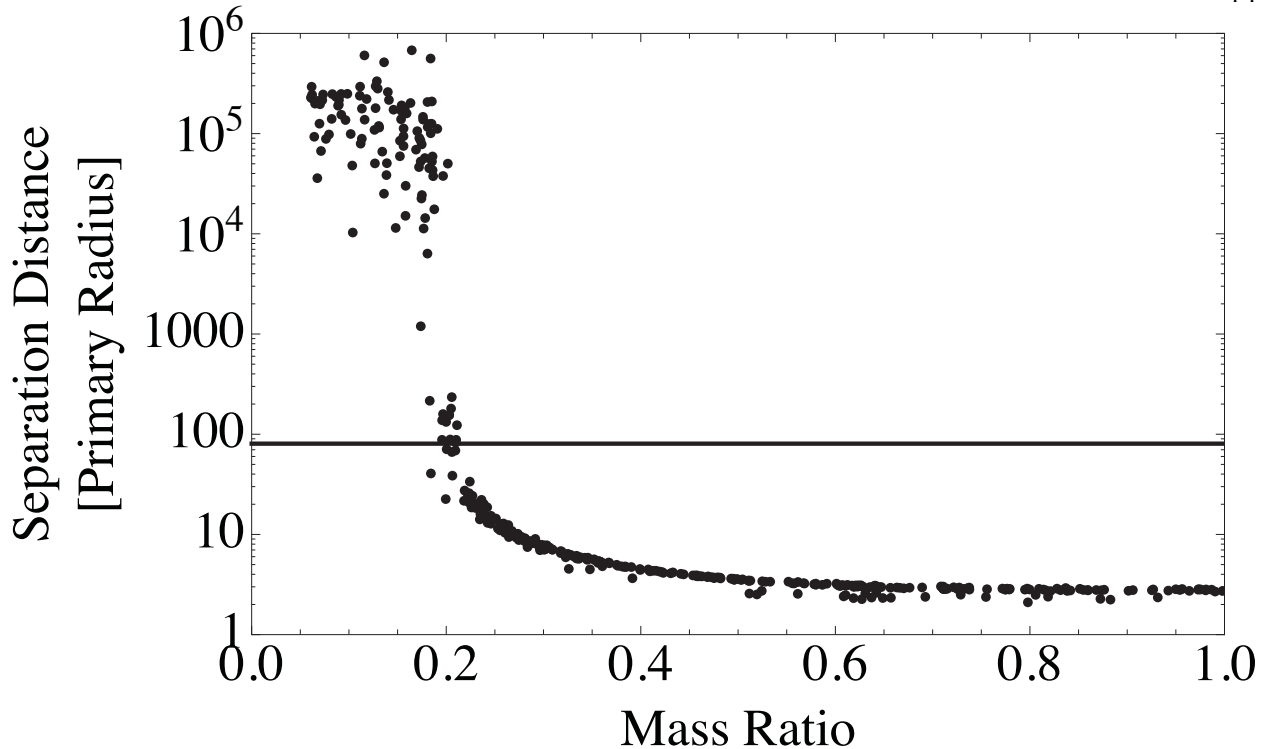


Figure 1.5: The average separation distance between the binary members measured in primary radii after 100 years of evolution as a function of mass ratio for 150 systems. This simulation does not allow secondary fission or include solar gravity perturbations just evolves the system according to the interactions of two aspherical bodies. The dark line indicates the Hill radius (80.5 primary radii) of these systems at 1 AU, crossing this radius is equivalent to escape for the needs of this work.

however the results indicate that the regime boundary is real and can be approximated by a mass ratio of 0.2. Increasing the shape ratio (elongating the objects) decreases the mass ratio of a zero free energy system, but not by much (Scheeres, 2009b).

Figure 1.5 shows the time averaged separation distances of 150 systems with mass ratios from 0.05 to 0.99 after 100 years. The Hill radius (80.5 primary radii at 1 AU) determines boundedness for these systems. The regime change between bound (high mass ratio) and unbound (low mass ratio) is dramatic and has consequences for the subsequent evolutionary path of the systems. Pravec et al. (2010) has directly observed this mass ratio spin limit in the asteroid pairs population, which is discussed further in Section 1.3.8.

Both high and low mass ratio regimes have chaotic early dynamics. These dynamics increase

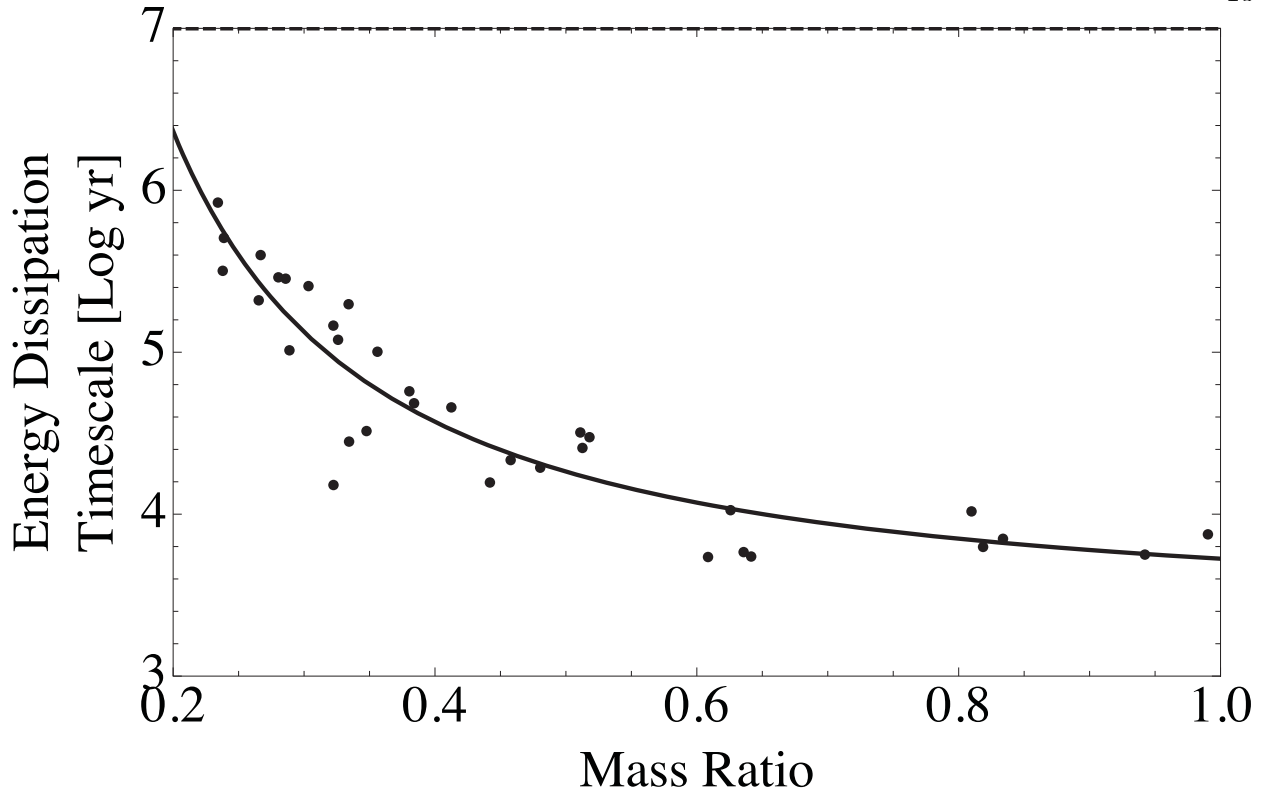


Figure 1.6: The timescale for the tidal evolution to the doubly synchronous state as a function of mass ratio. The nominal ejection timescale from the NEA population is 10^7 years. The black data points are the results of numerical modeling and the black curve is a power law fit to those points.

the eccentricity and thus the energy dissipation from mutual body tides. High mass ratio systems will evolve to an orbital equilibrium state, but low mass ratio systems will disrupt before tidal dissipation can reduce the free energy to a negative value unless they undergo secondary fission. The outcomes of these processes on each of the regimes are detailed below.

1.3.3 High Mass Ratio Regime

High mass ratio systems are defined as those systems that have negative free energy and do not experience secondary fission. The upper branch of Figure 1.1 shows the evolutionary path of high mass ratio systems. The dynamics of these systems are chaotic, but since the bodies are more equal in size, the exchanges of angular momentum and energy through spin-orbit coupling are less severe. This inhibits secondary fission and reduces the eccentricities these systems experience as

they evolve. The tidal energy dissipation rate is inversely related to the separation distance to the sixth power, and so higher mass ratio systems experience faster rates of tidal energy dissipation, since the average separation distance decreases with higher mass ratios, as shown in Figure 1.5.

Tidal dissipation damps systems in the high mass ratio regime so that both the primary and secondary of such systems are trapped in libration states. The libration angle is eventually damped to zero, first in the secondary then the primary, and the bodies become doubly synchronous. Since high mass ratio systems have similarly sized components, the tidal timescale is similar for each member and systems evolve into doubly synchronous binaries. Tidal timescales are a direct function of mass ratio with equal mass members taking $\sim 5 \times 10^3$ years, 0.6 mass ratio systems taking $\sim 10^4$ years, and 0.2 mass ratio systems taking $\sim 2 \times 10^6$ years to reach the doubly synchronous state (see 1.11 for a description of the assumptions behind these timescales). Figure 1.6 shows these timescales as a function of mass ratio, along with a fitted power law showing a clear trend as a function of the system's mass ratio. Both members are tidally locked in the doubly synchronous state, and these asteroids are observed as the Hermes-class.

This numerical tidal dissipation timescale for high mass ratio systems can be compared to the tidal timescales derived analytically by Goldreich and Sari (2009). The corresponding analytic tidal dissipation timescales for equal mass members is $\sim 3 \times 10^4$ years, for 0.6 mass ratio systems is $\sim 4 \times 10^4$ years, and for 0.2 mass ratio systems is $\sim 4 \times 10^6$ years to reach the doubly synchronous state. The analytic theory is within an order of magnitude of the numerical results but consistently overestimates the time necessary to de-spin these systems especially at higher mass ratios. Fundamentally, the analytic theory assumes a quasi-steady state evolution, but this is not how these systems initially evolve. All of these systems engage in a period of chaotic evolution that can increase the spin rates of the bodies relative to the orbit, and since the tidal energy dissipation rate is linearly related to the difference between the spin rate of the body and orbital rate, the energy dissipation is faster than that predicted by the analytic theory.

Once in the doubly synchronous state, the system will contract or expand due to the BYORP effect creating contact binaries or asteroid pairs (Ćuk, 2007; McMahon and Scheeres, 2010b). The

BYORP effect is the summation of radiative effects on synchronous secondaries. It can shrink or expand the semi-major axis. If the semi-major axis expands, the asteroid system will eventually disrupt when the separation distance equals the Hill radius. If the semi-major axis shrinks, the two components will at first remain in the doubly synchronous state since this is also the stable relative equilibrium state until the separation distance reaches a lower limit and the relative equilibrium state becomes unstable (Scheeres, 2009b). Simulations show the impacts occur very soon (< 100 days) after reaching the stability limit, and the perpendicular and tangential impact velocities for 1 km bodies are < 50 mm/s, modest enough to be capable of creating contact binaries. These impact velocities are gentle enough that they would not disrupt the figure of the bodies creating the contact binaries. Thus, high mass ratio evolution is responsible for creating doubly synchronous binaries, which can evolve into contact binaries or asteroid pairs.

The end products of this sequence are single “rubble pile” asteroids, so this is a lifecycle. We propose a possible contact binary loop that high mass ratio systems could get stuck in, whereby the components of a contact binary repeatedly fission and re-impact. Each component maintains its relative orientation to the other, so that the YORP effect, BYORP effect, and mutual body tides all act similarly each time the system goes through the cycle. The estimated timescales of the tidal process and the BYORP process are roughly an order of magnitude shorter than the estimated timescale of the YORP process (Rossi et al., 2009; McMahon and Scheeres, 2010a). This would explain why contact binaries are so prevalent compared to doubly synchronous systems. Contact binaries appear to be 9% of the NEA population, and very roughly this theory would predict that the doubly synchronous population would be ~ 5 times smaller due to timescales. Also, this theory would predict that the ratio of timescales would reflect the ratio of contact binaries to doubly synchronous systems with a caveat regarding asteroid pair production from doubly synchronous systems.

1.3.4 Low Mass Ratio Regime

Low mass ratio systems have positive free energy or undergo secondary fission. These systems typically have mass ratios < 0.2 . Coupling between the spin and orbit states drives a large spin increase in the secondary and an increase in the eccentricity of the system. These systems chaotically explore their phase space until an escape trajectory is discovered or secondary spin fission occurs, which will be further defined in Section 1.3.5.

If low mass ratio systems are evolved after a rotational fission event and they are not allowed to secondary spin fission, then almost all systems will disrupt. 450 low mass ratio systems were simulated starting from rotational fission and evolved considering tri-axial gravitational potentials, mutual body tides, and solar gravitational perturbations starting from the relative resting equilibrium as described in Section 1.2. The systems were evolved until they disrupted, which is when the separation distance equals the Hill radius. The Hill radius is taken to be 80.5 primary radii, which is correct for a system is in a circular heliocentric orbit at 1 AU, but mutual orbits that grow to this separation distance typically reach much larger separation distances if the system is allowed to continue to evolve.

The time to system disruption is shown in Figure 1.7, firstly as a function of mass ratio and secondly as a function of primary shape ratio, defined as the shortest semi-axis divided by the longest semi-axis of the primary in the plane of motion. Similarly, a secondary shape ratio can be defined. The initial component mass ratios, which determined the binary mass ratios, were chosen from a flat distribution ranging from 0.001 to 0.2. Although secondary fission was not allowed to occur in these simulations, each binary was still defined using the hierarchical “rubble pile” internal structure as shown in Figure 1.2. Therefore, the internal component mass ratio of each binary component is chosen from a flat distribution between 0.001 and $q/(1 - q)$, where q is the mass ratio of the previous fission, this requirement is derived in 1.12. The internal component mass ratio also determines the shape ratio of the component, since each component is dynamically modeled as a tri-axial ellipsoid with the same moments of inertia as the hierarchical “rubble pile”

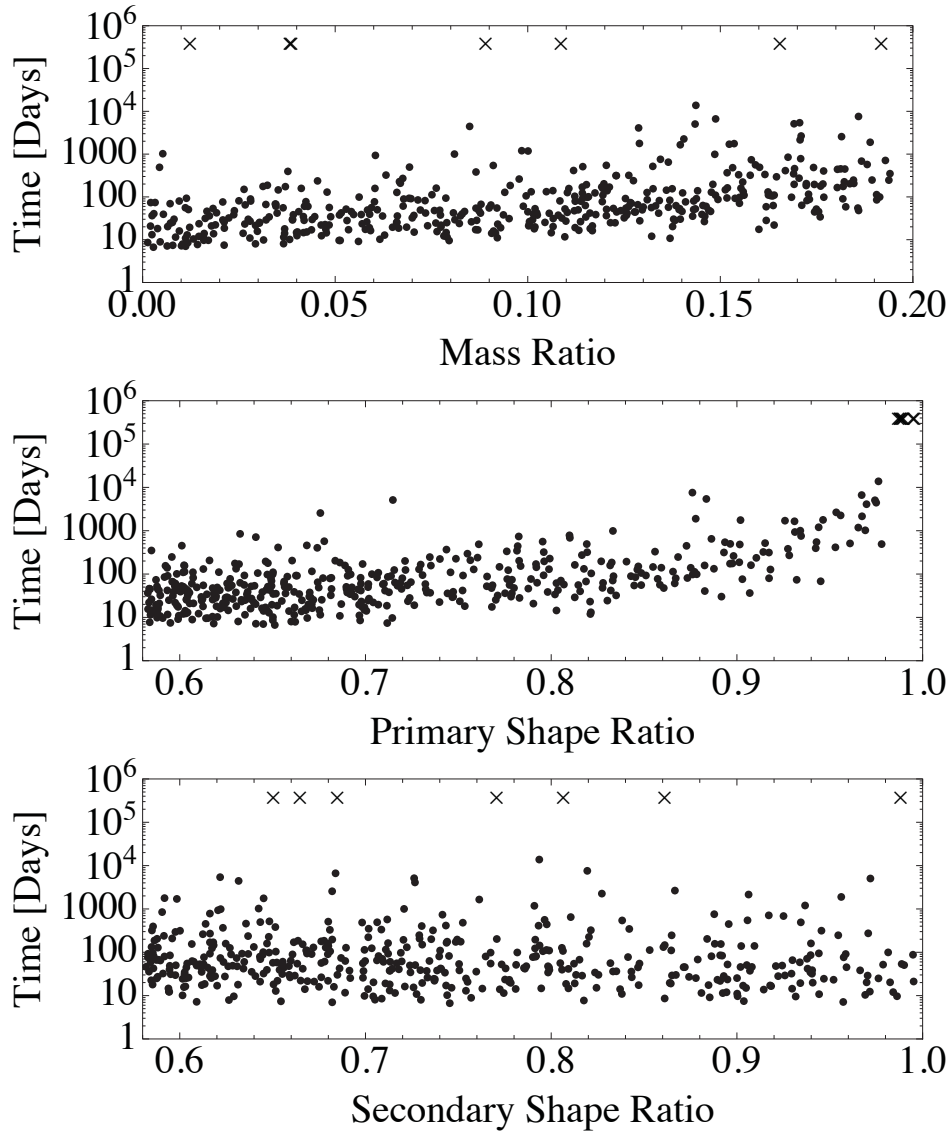


Figure 1.7: Each point shows the time after initial rotational fission for the simulated system to disrupt and each cross indicates a system that survived 1,000 years without disrupting. These simulations include tri-axial gravitational potentials, mutual body tides and solar gravitational perturbations. In order from top to bottom, the time to system disruption is shown as a function of system mass ratio, primary shape ratio, and secondary shape ratio.

internal structure model. Thus the primary shape ratios are distributed between 0.581 and 0.997.

$2 \pm 1\%$ ¹ of systems integrated, 7 out of 450, do not disrupt after 1000 years of integration.

¹ All uncertainties from the model given as $\# \pm \#$ describe the most likely actual proportion and an estimate of the sampling error given as a 90% confidence interval. These likelihoods and confidence intervals are calculated using the Wilson Score Confidence Interval, which best approximates a binomial distribution especially at extreme probabilities—small number of successes compared to number of trials (Agresti and Coull, 1998).

The simulation was ended after 1000 years, because the timescale of the BYORP effect becomes comparable and this effect was not included in the simulation. The 7 binary systems that did not disrupt evolved very differently than the other 443 systems; the secondary rotation and orbital periods remained very close to one another, slowly growing as mutual body tides dissipated energy. The primary rotation period is slightly smaller than the other periods as the system evolves.

These binaries evolved differently than the other systems because their primaries were significantly more spherical as shown in Figure 1.7. All surviving binaries had primary shape ratios greater than 0.98 and all disrupted systems have primary shape ratios below 0.98. The mass ratios and secondary shape ratios do not effect the outcome of the evolution of the system. When 50 more systems were evolved with primary shape ratios restricted to lie between 0.9 and 1 and the mass and secondary shape ratios varied over the same range as before, these conclusions are modified slightly. The boundary between disruption and stability is not as sharp, one system with a primary shape ratio below 0.98 does not disrupt (it had a primary shape ratio of 0.978), and two systems with primary shape ratios greater than 0.98 do disrupt (they had primary shape ratios of 0.981). No observed binaries have primaries with primary shape ratios of 0.98 or greater. The largest known primary shape ratio is 0.96 (Pravec and Harris, 2007), as shown with other observed binaries in Figure 1.13. Therefore, the 2% likelihood of creating a stable binary that evolves along the unstable relative equilibrium is strongly dependent on the assumption of a flat distribution in primary shape ratio, and potentially no primaries after a rotational fission event may ever be that close to spherical.

These systems are evolving outward along a relative equilibria as theoretically shown in Scheeres (2007a), where the case of a small ellipsoid rotationally fissioning from a large sphere is explored. In Scheeres (2009b), it was shown that this relative equilibrium would always been unstable for two ellipsoids, however if the primary shape ratio is nearly one, then the growth of this instability may be slow compared to the tidal dissipation. In this case, the system may evolve outward along the relative equilibrium without chaotically fully exploring its phase space, instead it may only exchange limited angular momentum and energy between the orbit and rotation

states causing libration and circulation in the primary, libration with very rare circulation in the secondary, and small changes in eccentricity and semi-major axis. As the system evolves, tidal energy dissipation will slowly grow the pericenter, and since the higher order gravitational potential terms have a $1/r^3$ functional dependence, the effects of the small non-sphericity of the primary will diminish even more. The secondary rarely circulates and is often librating with a very small angle, so the BYORP effect would significantly effect the evolution of the system in potentially only a few thousand years (Ćuk, 2007; McMahon and Scheeres, 2010a). The properties of these binaries that survive without disruption are shown in Figure 1.13 and more discussion of their continued evolution is further discussed in Section 1.3.7.

For those systems that do disrupt, the median time to disruption for all systems is 32_{18}^{72} days². An exponential decay can be fit to the data $N(> t) = 443e^{-t/\tau}$, where t is the time after rotational fission, $N(> t)$ is the number of asteroid systems remaining after time t , and $\tau = 92.0 \pm 1.8$ days is the exponential decay timescale. The adjusted R^2 value of the fit is 0.996. The half-life to disruption for low mass ratio systems is then $\tau_{1/2} = 63.8 \pm 1.2$ days.

As shown in Figure 1.7 and also shown in a simple binning of the data as done in Table 1.2, there is a trend in the disruption time with the mass ratio. The lower the mass ratio the shorter the median time to disruption. This is a direct result of the added energy necessary to initially fission lower mass ratio systems. Higher mass ratio systems experience lower average eccentricity, explore their orbital phase space more slowly, and thus can find disruption orbits on much longer timescales. A stronger trend than the dependence on mass ratio is the dependance on primary shape ratio. The lower the primary shape ratio the shorter the median time to disruption, despite the energy necessary for rotationally fissioning a system decreasing with a smaller primary shape ratio Scheeres (2007a). This relatively small effect is strongly counteracted by the increase in the size of the second order terms in the gravitational potential, which increase the coupling of the spin and orbit states. The spin-orbit coupling through these non-spherical gravitational terms is how

² All statistics reported from the model are given as $\#_{\#}^{\#}$ and describe quantile statistics that enclose 50% of the data, since the underlying distribution is unknown. In the normal script is the median value, and then in the subscript is the 25th percentile and in the superscript is the 75th percentile.

energy is transferred into the orbit from the rotation states eventually disrupting the system. A useful analogy is the time it takes Theseus to escape the Cretan Labyrinth; the number of exits from the maze and the speed at which Theseus explores different passages increases with the decreasing mass ratio and decreasing primary shape ratio of the chaotic asteroid binary. These trends are nonlinear and appear logarithmic. The disruption time appears to approach a constant value as the mass ratio and primary shape ratio approach zero. There appears to be no or a very weak trend in the disruption time with secondary shape ratio.

The disruption timescales for rotationally fissioned systems are very short compared to the YORP timescales for fissioning the primary again before the system disrupts. This is true even for systems with primaries that are more rotationally symmetric than any of the observed primaries of binary asteroid systems. Stabilization of the secondary via collision with more material fissioned from the primary would require extremely (and unobserved) large YORP accelerations and hence very short YORP timescales. Something else must happen to the system before disruption, in order to form synchronous binaries. We hypothesize from our numerical modeling that this process is spin fission of the secondary.

1.3.5 Secondary Spin Fission

Rotational fission rests on the premise that asteroids are “rubble piles,” and so this naturally leads to the assumption that the primary and secondary members of the chaotic binary formed from rotational fission are also “rubble piles.” During the evolution of the two-body system, spin-orbit coupling can increase the spin rate of the secondary such that it undergoes rotational fission of its “rubble pile” structure. Both asteroids undergo surface fission at similar rotation rates, however because of the large mass difference between the bodies they disrupt at very different rotational kinetic energies. It takes much less energy transferred via spin-orbit coupling to the secondary to fission that body.

The most conservative scenario for secondary spin fission is surface fission—the condition for a massless test particle resting on the surface of the secondary to become unbound. A real massive

component would become unbound at some lesser condition as described in 1.9. The full two-body integrator checked the surfaces of each asteroid as it evolved for this condition at every time step, and then implements Brent’s method (a bracketed root finding method) to determine the time and state of the system when the condition is first satisfied.

During the evolution of the 443 low mass ratio systems simulated above, 178 undergo surface fission of the secondary before orbital disruption. That is $40 \pm 4\%$ of the modeled systems (uncertainties attained using the Wilson Score Confidence Interval). Secondary surface fission is a conservative limit that corresponds to the spin rate necessary to place a massless test particle on the surface of the original body into orbit. If these secondaries have “rubble pile” geophysics then they would secondary fission at lower spin rates Scheeres (2007a). This hypothesis is pursued later in the numerical simulations discussed in Section 1.3.6.

In Figure 1.8, those systems are shown as crosses at the time of secondary fission, while those that did not secondary fission are shown as dots at the time of disruption. For those systems that underwent secondary fission, the median time to surface fission was 51_{27}^{128} hours. Those systems that take the longest to disrupt are also the most likely to go through secondary fission. Spin-orbit coupling transfers free energy throughout the system temporarily storing it in different reservoirs such as the spin states of the bodies at different times. If too much energy is stored in certain kinetic energy reservoirs, the system can be irreversibly changed. These two reservoirs are: the spin energy of the secondary and the relative translational energy of the bodies. If too much energy is stored in the translational energy the system will disrupt, and if too much energy is stored in the spin of the secondary than the secondary will fission. Fission of the primary is theoretically possible, however it was never observed in the numerical experiments. While the rotation rate needed to surface fission the primary is the same as the secondary—the surface fission rate only depends on density (Scheeres, 2007a), the rotational kinetic energy necessary to achieve that rotation rate is much higher, and a transfer of this much energy into the rotation state of the primary does not occur.

Figure 1.8 also shows how the likelihood of secondary fission depends on the three parameters

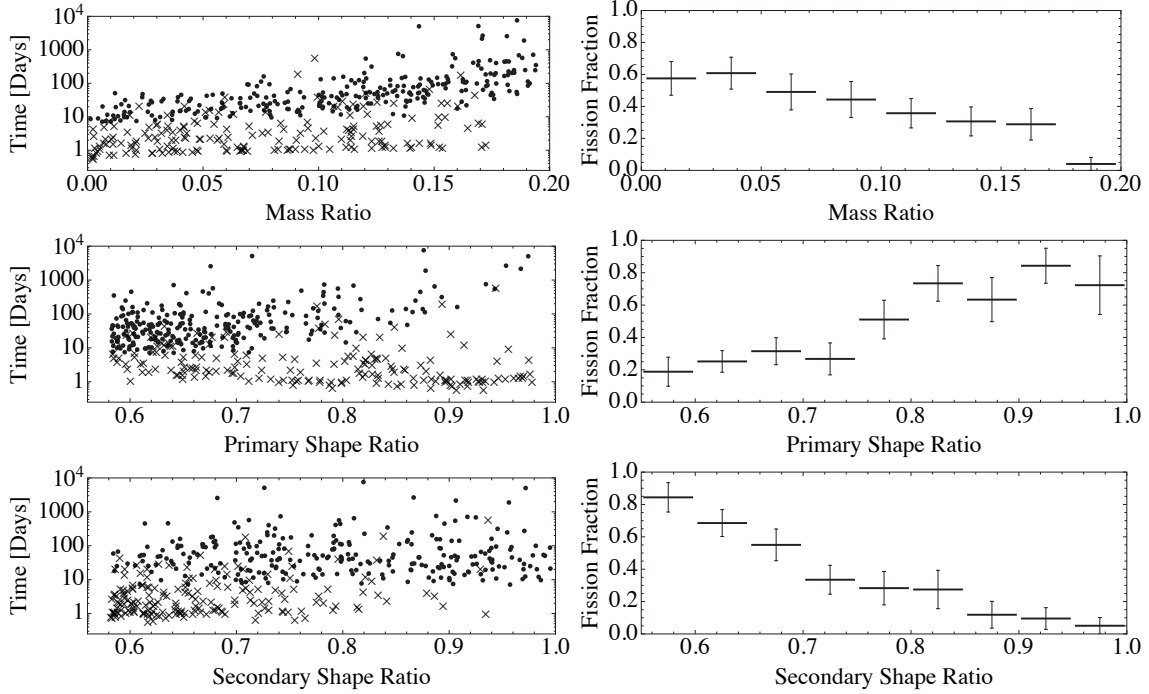


Figure 1.8: These are the same systems as in Figure 1.7 that disrupted, however now those systems that underwent secondary, surface fission are distinguished. In the left hand plots, those system that go through surface fission before disruption are shown as crosses at the time of secondary fission, while those that did not secondary fission are shown as dots at the time of disruption. The right hand plots show the fraction of systems in each bin of width 0.025 for mass ratios and 0.05 for shape ratios that underwent secondary, surface fission. The fraction and errors were calculated using the Wilson Score Confidence Interval. From top to bottom, The time to fission or disruption and the fission fraction are shown as functions of mass ratio, primary shape ratio and secondary shape ratio.

in the simulation. The fraction and errors shown in the plots on the right hand side of Figure 1.8 are given for bins of width 0.025 for mass ratio and 0.05 for each of the shape ratios and were calculated using the Wilson Score Confidence Interval. The fission fraction decreases with increasing mass ratio, which follows naturally from the decreasing amount of energy necessary to initially rotationally fission the original body. If there is less energy to transfer via spin-orbit coupling through the binary system, then there will be less energy to momentarily store in the rotation reservoir of the secondary. The fission fraction decreases with larger secondary shape ratio. The smaller second order gravitational potential terms of the secondary lower the coupling of the spin state to the orbit state decreasing the ability of energy to be transferred into the rotation rate of the

secondary. The fission fraction decreases with smaller primary shape ratio for a very related reason. The increased spin-orbit coupling of the primary to the orbit increases the energy transferred into the orbit and increases the semi-major axis so that the secondary is prevented from being rotationally accelerated.

1.3.6 Chaotic Ternaries

Secondary spin fission drastically alters the evolution of the system. After secondary fission, the asteroid system is now a chaotic ternary. These systems could stabilize via tidal dissipation into the observed ternary asteroid systems, but more likely one of the secondaries will either exit the system: further stabilizing the orbit of the secondary through removal of energy and angular momentum, or impact the primary: increasing its spin rate and potentially creating an equatorial bulge. This process provides a route to the creation of synchronous binaries.

Secondary fission often occurs when the orbit of the secondary is at pericenter and the location of the fission is on the interior (primary facing) side of the secondary. The fissioned material will be at apoapse of a new orbit with periapse close to or inside the primary and so this material will quickly impact the primary. These impacts have speeds < 1 m/s, and so will not disrupt the primary, but may re-organize it's shape. This mechanism may be responsible for forming the observed equatorial bulges seen in the near-Earth asteroid population, specifically primaries of synchronous binaries and fast-spinning, single asteroids. Impacts are modeled to conserve angular momentum and mass, and the collision is treated as inelastic as described in 1.10.

The remainder of the secondary still in orbit is now at periapse of a new larger orbit that is more stable. The secondary fission may repeat many times during the evolution of a system. The model also incorporates tidal effects including solar gravitational perturbations and mutual body tides, which work over time to circularize and synchronize the secondary to create the observed synchronous binaries. The gravitational effects of the Sun on the mutual orbit provide important stability to the system during the transition period between chaotic evolution and quasi-steady state evolution dominated by mutual tidal dissipation.

This process was modeled using the full two-body integrator, as above and initial rotational fission component mass ratios were drawn from a flat distribution between 0.01 and 0.2 to capture the complete low mass ratio regime. After the initial rotational fission the secondary is treated as “rubble pile” itself with initial component mass ratios chosen from a flat distribution between 0.01 and 0.99^3 . The asteroid is treated as a hierarchical structure as depicted in Figure 1.2, only the next. Until the secondary fission condition is met, each component of the binary is treated as a coherent dynamical body. Once the secondary fission condition is met, then the system becomes a chaotic ternary. After one of the chaotic ternary members is ejected from the system or impacts another member, then the smaller of the two remaining members is once again treated as a “rubble pile” with a component mass ratio chosen from a flat distribution with an appropriate upper limit and subject to the secondary fission condition.

The exact condition for secondary fission is described for the case of a primary tri-axial ellipsoid and a secondary composed of two spheres in 1.9. The motion of the chaotic ternary, which is made of one tri-axial ellipsoid and two spheres is determined by the three-body integrator described in 1.7. This integrator includes the effect of solar gravitational perturbations for a circular orbit about the Sun at 1 AU and mutual body tides between the primary and each of the satellites. The three-body system is highly chaotic and rapidly explores its phase space. There are four possible outcomes to this state: stable ternary system, collision between the spherical bodies, impact of one spherical member onto the tri-axial primary, and escape of one of the spherical bodies.

526 systems were evolved for 1000 years unless the system disrupts or the components impact each other. The model defines stable ternary systems as those that last until the end of the simulation, 1000 years ($\sim 10^4$ disruption timescales). Since two of the three members are perfect spheres not all of the dynamics are captured by the three-body integrator and these systems are stable in only a limited sense. The three remaining paths are diagrammed in Figure 1.10. The first path is ejection of one of the satellites. This results in a binary system with a spherical secondary,

³ A flat distribution across all possible values is the simplest assumption. In Section 1.3.5, we chose the more conservative assumption that results in higher secondary fission ratios given by 1.12.

but to capture the spin-orbit coupling the secondary is then given some small prolate-ness and a new internal “rubble pile” structure (shape and mass ratios are randomly drawn from the same initial, flat distributions). The dynamics are then returned to the two-body integrator and the system continues to be evolved. The second path from a chaotic ternary to a chaotic binary is impact of one component of the secondary onto the primary. These impacts occurs at low speeds < 1 m/s. When this occurs the mass and angular momentum are conserved and the collision is treated as inelastic as described in 1.10. The third path is impact of the two satellites with each other and these impacts are treated in the same way. From simulation, the impact velocities of both of these impacts suggest that single re-shaped asteroids are a more likely outcome rather than fragmentation. These velocities are described later in this work.

After a binary system has gone through secondary fission, it will have lost energy which raises the semi-major axis and thereby increasing the periapsis distance. The higher-order gravitational effects responsible for spin-orbit coupling are strongest at periapse, and so these systems will not be as affected by spin-orbit coupling. However, the system will often still be eccentric and solar gravitational perturbations are important for stabilizing and destabilizing these systems. Solar tides will change the energy and angular momentum of the system and when they stabilize the orbit they do so by expanding the pericenter and lowering the apocenter, which keeps the system from impact and disruption.

After 1000 years of evolution, $8 \pm 2\%$ of low mass ratio systems are stable binaries, $67 \pm 3\%$ of simulated systems disrupt and become asteroid pairs, and $25 \pm 3\%$ of the simulations end with the secondary impacting the primary at modest speeds creating re-shaped asteroids. While ternaries exist in some simulations for a number of years, none of the systems remain as stable ternaries; this sets an upper limit on the likelihood of stable ternary formation at $0.3 \pm 0.3\%$ for our simplified model. These intervals capture the statistical or random errors but do not include systematic effects from broad assumptions such as the internal components size distribution (we assumed a flat distribution). Other systematics such as the assumption of planarity and a full body model for the three body system will be developed in the future. There is also another route to stable

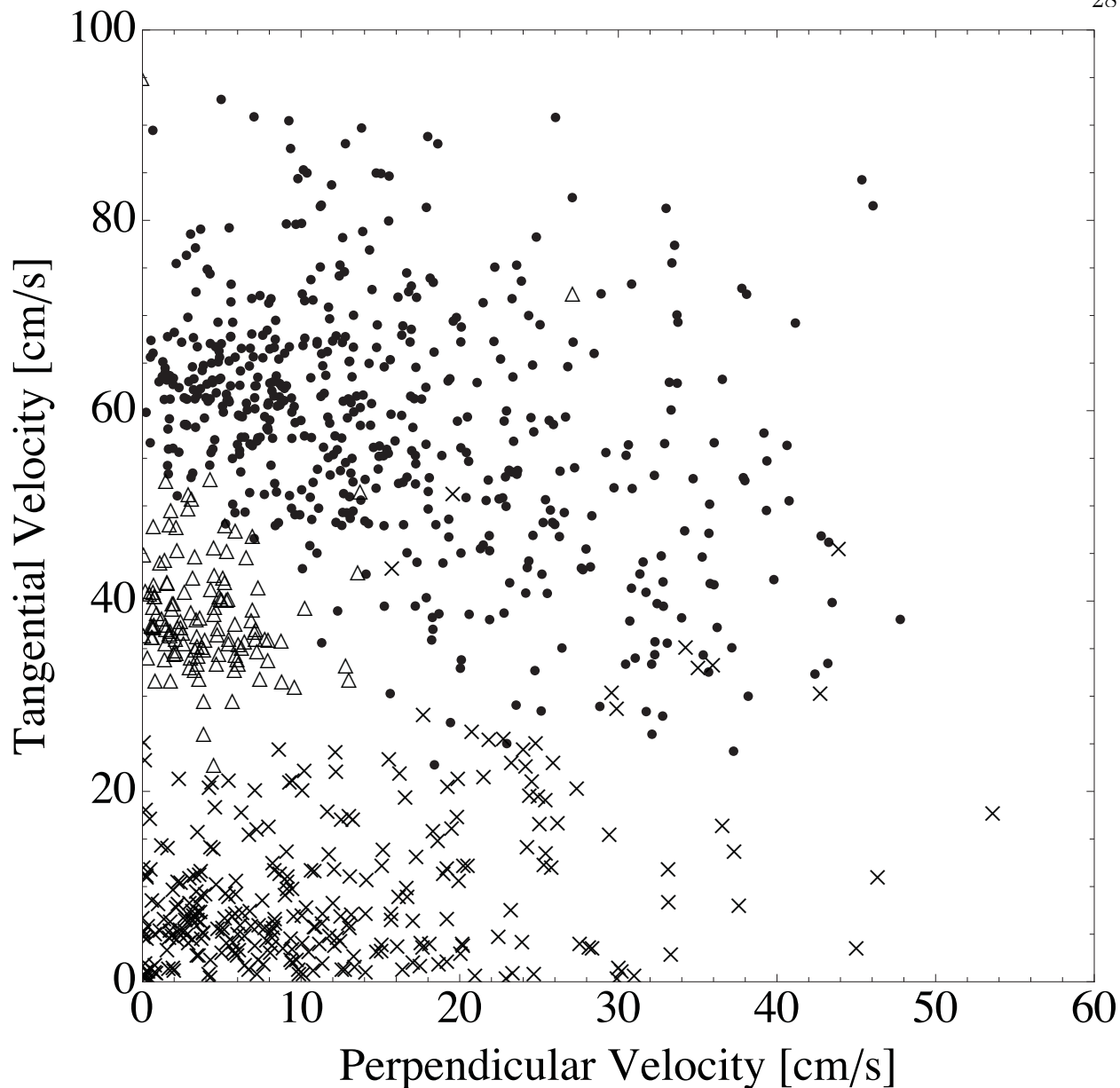


Figure 1.9: The perpendicular and tangential velocities in cm/s for every occurrence of all the three types of impacts occurring in the simulation: The dots represent primary impacts—the collisions that occur between the primary and one of the secondaries of a ternary system, the crosses represent secondary impacts—the collisions that occur between secondary and tertiary members of ternary systems, the triangles represent binary impacts—the collisions that occur between secondary and primary members of binary systems.

ternaries, where the primary of a stable binary goes through YORP-induced fission and the system may evolve such that this new ternary system does not disrupt. These systems were not modeled

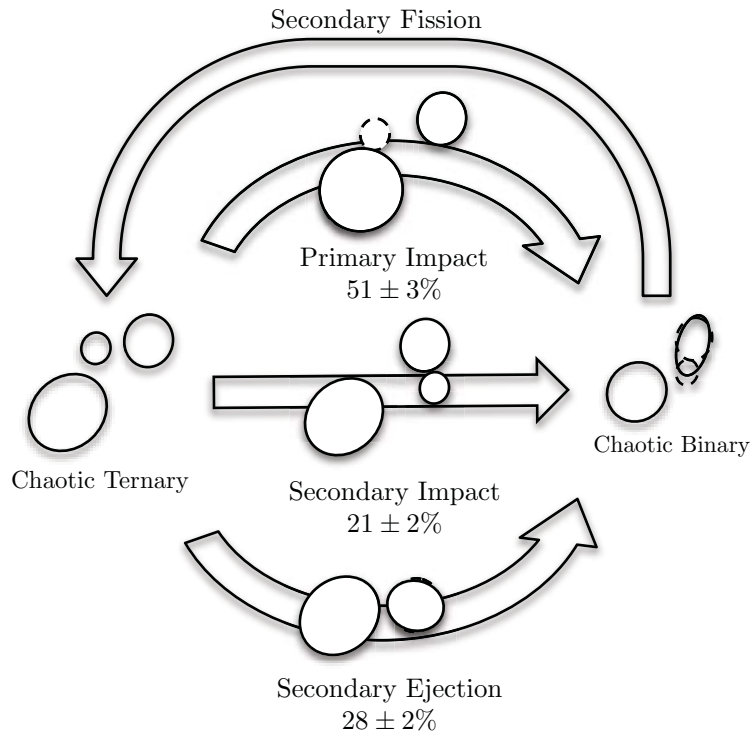


Figure 1.10: Chaotic ternary to binary loop via secondary fission and three ternary processes. Each process has a schematic as well as the percent likelihood a system will follow that path. All of these processes are dynamic and occur on timescales much shorter than a year.

here.

Secondary fission is a dominant process— $64 \pm 3\%$ of low mass ratio systems go through it at least once. Secondary fission creates a chaotic ternary that evolves back into a binary via one of the three routes. One of the secondaries impacts the primary $51 \pm 3\%$ of the time. Otherwise, one of the secondaries is ejected from the system $28 \pm 2\%$ of the time, or the secondaries collide in orbit about the primary $21 \pm 2\%$ of the time. All of these chaotic ternary processes dissipate energy and produce more stable binaries.

Collisions between the secondaries of a ternary system occur in $17 \pm 3\%$ of low mass ratio systems at least once. Impacts also occur on $83 \pm 3\%$ of low mass ratio primaries via either a ternary component impact after a secondary fission or collision with the secondary in a binary. Each of the three collision processes has a unique velocity structure shown in the top plot of Figure 1.11. The median velocity, as well as first and third quartiles are listed in Table 1.3 for all three processes.

Each type of impact has a unique tangential velocity, but similar perpendicular velocities.

The bottom two plots of Figure 1.11 compare the impact velocities that occur in the model to catastrophic disruption limits derived elsewhere. The triangles and dots are piled up in both plots. The middle plot shows the total velocity of the impactor relative to the target and compares this value to the catastrophic disruption velocity of Stewart and Leinhardt (2009). The upper line is the critical velocity for projectiles much smaller than the target, which corresponds with impacts onto the primary of either the binary (triangle) and ternary (dot) systems. The lower line is the critical velocity for nearly equal size projectile and target. The collisions between secondaries of ternary systems do not fall entirely into either domain; they have mass ratios between 0.01 and 0.99. From this analysis a minority of collisions may undergo catastrophic disruption, however analysis of the specific energy of these collisions leads to the opposite conclusion. The bottom plot of Figure 1.11 shows the specific energy of each impact and compares this to the catastrophic disruption limits derived by others. The two curved and dotted lines indicate models that include both internal strength and self-gravity, the two dashed lines only include self-gravity, and the dot-dashed line represent the self-potential energy of the target for reference. With the exception of a single impact, these collisions do not catastrophically disrupt the target body, but will rearrange material on the surface. For impacts on the primary, material will preferentially impact the equator and we hypothesize that it creates the commonly observed equatorial bulge and should fill in gravitational potential lows circularizing the body and further stabilizing the dynamics.

1.3.7 Stable Binaries

There are 41 systems out of 526 forming stable binaries at the end of the post-rotational fission dynamical simulation. They have a median mass ratio of $0.003_{0.001}^{0.008}$ and a median semi-major axis of $3.3_{2.6}^{6.0}$ primary radii. The distribution of semi-major axes is shown in the top panel of Figure 1.13. There is an excess of large semi-major axes compared to the observed systems, however the BYORP effect has not been taken into account, and it will move the semi-major axis of nominally half of these systems inward. The output binary systems also have eccentricities with

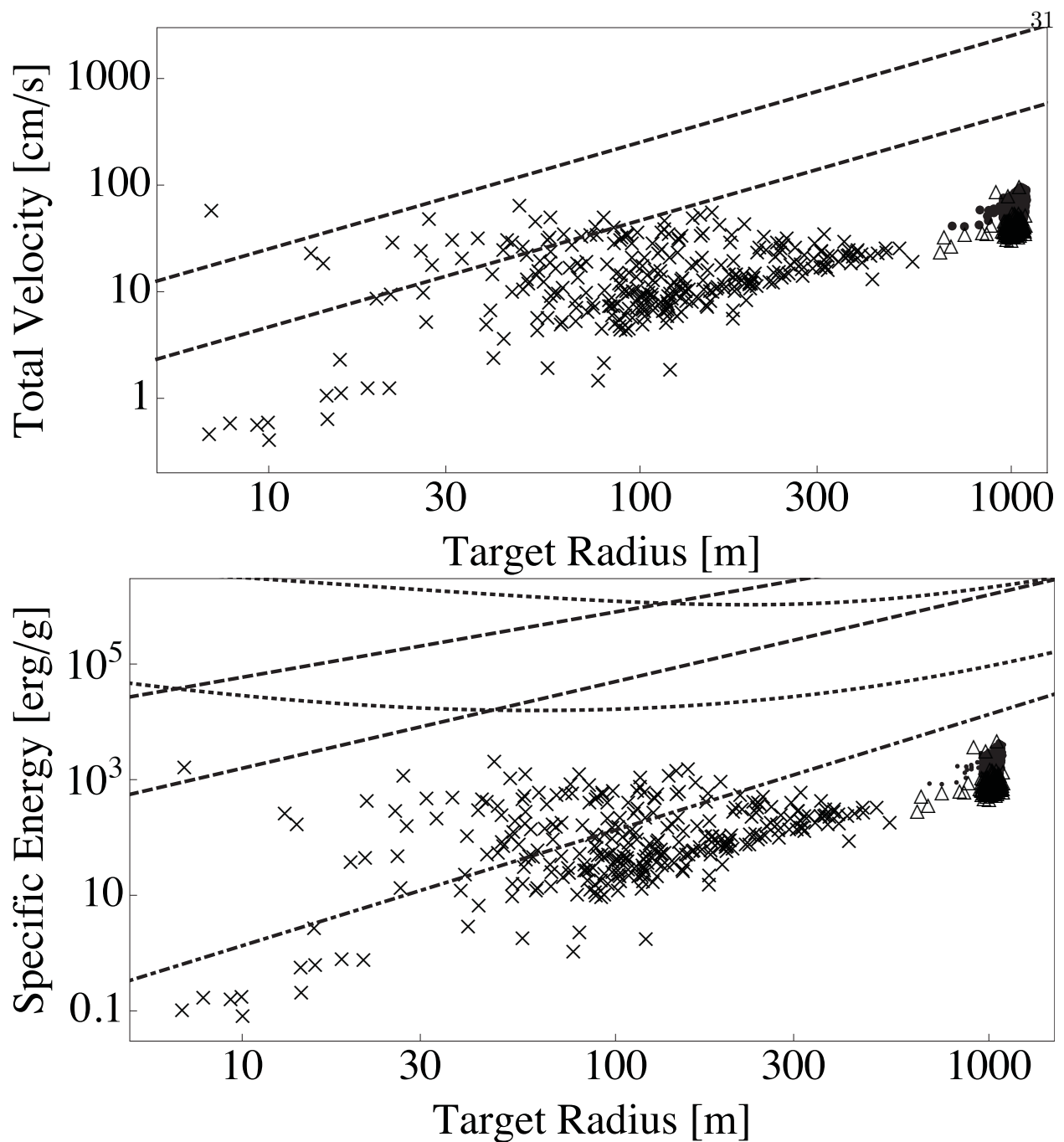


Figure 1.11: The type of each impact is represented by the same symbols as in Figure 1.9. The top plot shows the total velocity in cm/s of each impact comparing them to the critical disruption velocities for rubble piles shown as the dashed line (Stewart and Leinhardt, 2009). The bottom plot shows the specific energy in erg/g for each impact comparing them to derived catastrophic disruption thresholds: the dotted lines represent models that include material strength and self-gravity: the top line is Benz and Asphaug (1999) and the bottom is Durda et al. (1998), the dashed lines represent models that only include self-gravity: the top line is Love and Ahrens (1996) and the bottom is Davis et al. (1995), and the dot-dashed line is the self-potential energy of the target.

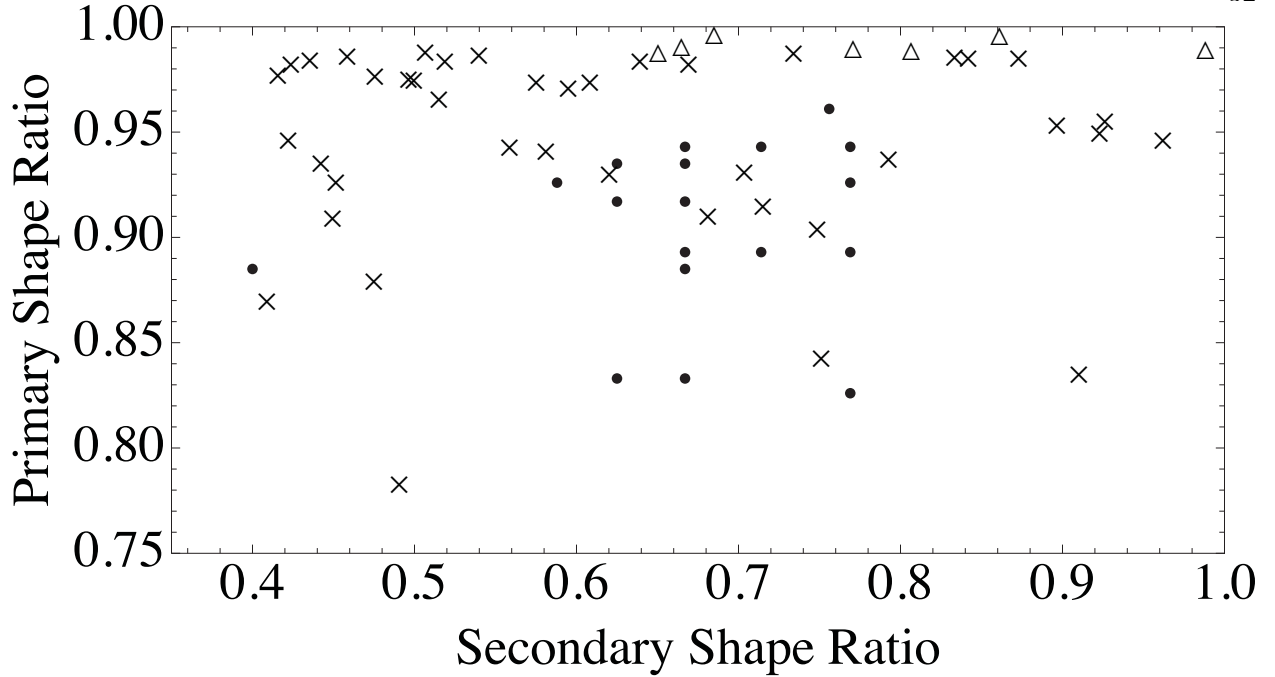


Figure 1.12: This shows the primary and secondary shape ratios of the stable binaries. The symbols are the same as in Figure 1.13.

a median of $0.32_{0.15}^{0.45}$ that will also be tidally damped over time.

The median primary rotation period is $3.9_{3.5}^{4.6}$ hours and are shown in the middle plot of Figure 1.13. Compared to the observed systems, the modeled primaries are spinning slowly, however the YORP effect will continue to spin up the primary and while this effect operates on a timescale longer than the simulation, the YORP timescale is short compared to the lifetime of the asteroid system.

The secondaries have fast spin periods, spun up via spin-orbit coupling; the median secondary spin period is $2.8_{2.1}^{3.7}$ hours. The distribution is shown in the lowest panel of Figure 1.13. $29 \pm 5\%$ of secondaries are retrograde after the chaotic phase. The critical disruption limit only includes mass ratios > 0.01 , which corresponds to secondaries $\gtrsim 100$ m in radius, which are either coherent bodies with internal strength or “rubble piles” bound by cohesive forces. The stable binaries output by the simulation spin too fast compared to the observed synchronous binaries, however tidal dissipation will synchronize these systems.

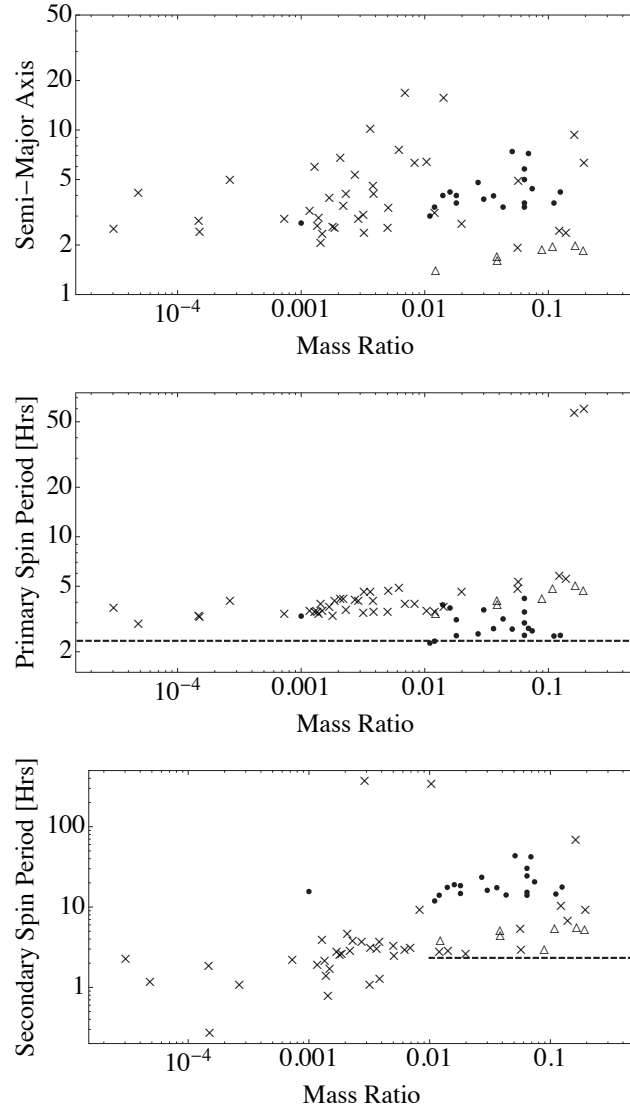


Figure 1.13: From top to bottom, the distribution of semi-major axes, primary rotation periods and secondary rotation periods are shown as a function of mass ratio. The triangles represent the 7 binary systems out of 450 that did not disrupt in the simulation that did not allow secondary fission. The crosses indicate the 41 stable binaries out of 526 that were outputs of the simulation that did allow secondary fission to occur. The dots indicate observed systems (Pravec and Harris, 2007). The dashed line in the bottom two plots is the critical spin disruption limit (2.33 hour period) for a body with a density of 2 g/cc, however it only includes bodies $\gtrsim 100$ m in radius (i.e. secondaries with a mass ratio less than 0.001 for a 1 km primary). Bodies smaller than 200 m in diameter may have internal strength or cohesive binding and so will require greater spin rates to disrupt.

The timescale for a low mass ratio secondary of a binary asteroid system to evolve to the synchronous state, τ_{tidal} , is estimated by dividing the spin rate, ω , by the magnitude of the tidal

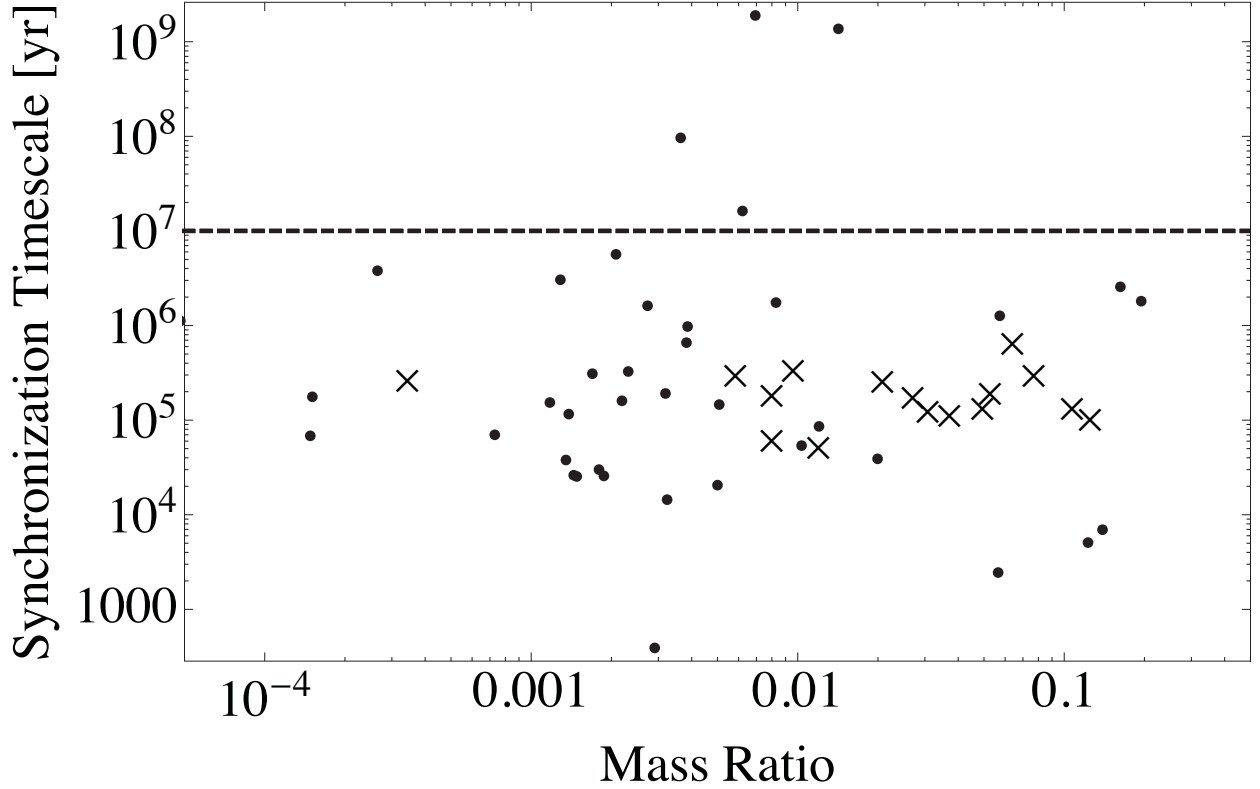


Figure 1.14: The timescale for synchronization due to mutual body tides as a function of mass ratio are shown as dots for each modeled system. The dotted line indicates the nominal lifetime for an NEA asteroid system. The crosses are the analytical de-spinning timescales for known asteroid systems (Goldreich and Sari, 2009).

acceleration of the secondary, $|\dot{\omega}_{\text{tidal}}|$.

$$\tau_{\text{tidal}} = \frac{\omega}{|\dot{\omega}_{\text{tidal}}|} = \frac{Q}{5k} \left(\frac{\omega}{G\pi\rho} \right) a^6 \quad (1.1)$$

where $k = 10^{-5}$ is the tidal Love number, $Q = 100$ is the quality factor, G is the gravitational constant, $\rho = 2 \text{ g cm}^{-3}$ is the asteroid average density, a is the binary system semi-major axis in units of primary radii (Goldreich, 1963; Goldreich and Peale, 1966). Assuming rubble pile geophysics, eccentricity will damp for all mass ratios (Goldreich and Sari, 2009). The secondaries, due to their much smaller dimensions and slower relative spin rate, tidally damp before the primary and create synchronous binaries (Goldreich and Sari, 2009). Assuming a primary radius of 1

km, the median estimate of the tidal spin-down timescale for the created synchronous binaries is $1.6 \times 10^5 \frac{1.7 \times 10^6}{3.0 \times 10^4}$ years, as shown in Figure 1.14. The analytic theory of Goldreich and Sari (2009) predicts a median timescale for the observed synchronous asteroid population within an order of magnitude of the simulated systems, $1.7 \times 10^5 \frac{2.6 \times 10^5}{1.1 \times 10^5}$ years, but a very different dispersion. This dispersion is the result of a few simulated systems having very large and very small secondary spin periods. Those systems with very small secondary spin periods may not synchronize within their lifetime in the NEA population and may be observed as asynchronous, high- e binaries, however these systems seem to only exist for very low mass ratio.

The YORP effect will also evolve the spin state of the primary and secondary, however the YORP effect will be stronger on the smaller secondary and potentially match the timescale for tidal synchronization. The evolution of the secondary may follow three paths depending on the relative directions and strengths of the YORP effect and tides. Firstly, tides and YORP act in the same direction lowering the timescale to synchronization. Once the system is synchronized, the YORP effect will not be able to remove it from that state, because the YORP torques will be much less than the gravity gradient at the separation distances of the observed and simulated systems. The YORP effect may provide a small source of angular momentum through the secondary to the system creating a small leading offset in the orientation of the secondary and very slowly evolving the orbit. The other two ways in which the secondary may evolve occur when the YORP effect and tides. If tides dominate in strength, then the system will synchronize and the YORP effect will act as a small sink of angular momentum causing the system separation to shrink and a small trailing offset in the orientation of the secondary. If the YORP effect dominates, then synchronization may never occur and the BYORP effect will never evolve the system. Tides will continue to expand the system, but the YORP effect will keep the secondaries rapidly rotating. This last path may be responsible for the as asynchronous, high- e binary systems as well, but without the mass ratio dependence apparent in the previously mentioned source of high- e binaries.

The chaotic evolution of low mass ratio systems including the effects of secondary fission and the ensuing consequences of impacts and escapes drastically changes the initial spin rate of the

secondary for the classical tidal theory, which assumes that the secondary starts at the spin fission limit. Chaotic evolution of the secondary appears as a random walk in spin rate. If the secondary walks to higher spin rates it will eventually spin fission, and the random walk will be reset for each of the secondaries. If it walks to slower spin rates, then when the system evolves into classical tidal evolution, the system will de-spin on a shorter timescale. This would be true of all stable binaries output by the dynamical model, however some systems form stable binaries with large semi-major axes. Classical tidal dissipation is inversely related to the separation distance to the sixth power, and so these systems may only be a factor of a few larger in semi-major axis, but that translates into a difference of over two orders of magnitude in tidal dissipation rates. Those systems that take longer than or similarly to the lifetime of an NEA system ($\sim 10^7$ years) to synchronize do not become synchronous binaries, instead they become the rarer high- e binaries.

Once a system is synchronized, the BYORP effect can contract or expand their orbit. Synchronous binaries disrupt once the orbit has expanded to the Hill radius creating asteroid pairs. The BYORP effect can also contract the orbit to the stability limit leading to the secondary impacting the primary, re-shaping the body due to the primary's rapid rotation rate and creating re-shaped asteroids (McMahon and Scheeres, 2010a). Thus, low mass ratio evolution after rotational fission is responsible for creating synchronous binaries, high- e binaries, asteroid pairs, re-shaped primaries, and potentially ternaries.

Mass Ratio Bins	0 - 0.05	0.05 - 0.1	0.1 - 0.15	0.15 - 0.2
Time [Days]	26_{14}^{56}	39_{20}^{82}	59_{37}^{133}	197_{98}^{448}
Primary Shape Ratio Bins	0.6 - 0.7	0.7 - 0.8	0.8 - 0.9	0.9 - 1.0
Time [Days]	35_{18}^{65}	63_{36}^{144}	104_{56}^{197}	532_{270}^{1758}
Secondary Shape Ratio Bins	0.6 - 0.7	0.7 - 0.8	0.8 - 0.9	0.9 - 1.0
Time [Days]	59_{28}^{132}	54_{24}^{163}	45_{23}^{127}	39_{19}^{91}

Table 1.2: The median disruption time (in days) for four bins of width 0.05 in mass ratio and 0.1 in shape ratio are tabulated. In the subscript is the 25th percentile and in the superscript is the 75th percentile of the data from each bin.

Impact Type	Perpendicular Velocity [cm/s]	Tangential Velocity [cm/s]
Primary Impact	13_7^{22}	59_{51}^{66}
Secondary Impact	9_4^{18}	7_4^{13}
Binary Impact	3_2^6	37_{35}^{41}

Table 1.3: For each type of impact, the median impact velocities as well as the first and third quartiles are tabulated for the perpendicular and tangential directions relative to the center of mass of the impacting bodies in cm/s. Collisions between the primary and one of the secondaries of a ternary are shown in the first row, collisions between the secondaries of a ternary are shown in the second row, and collisions between the primary and secondary of a binary are shown in the third row.

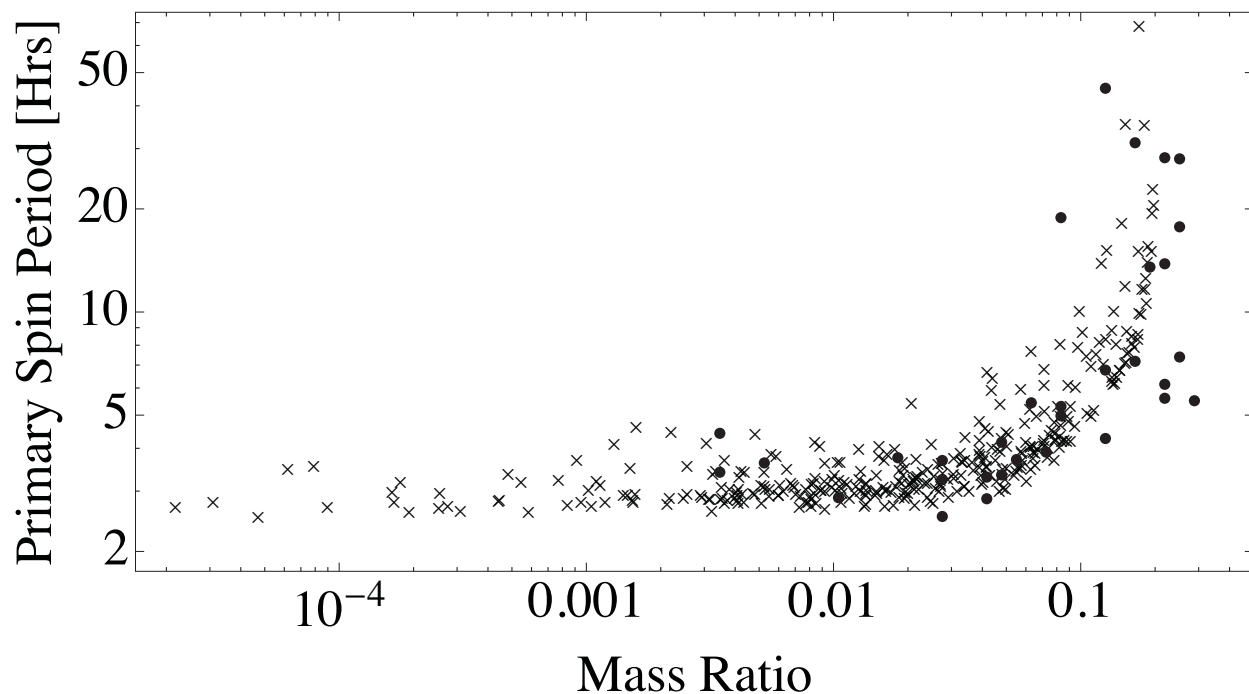


Figure 1.15: The primary spin period of asteroid pairs as a function of mass ratio. The dots are the output from the simulation and the crosses are observed asteroid pairs (Pravec et al., 2010).

1.3.8 Asteroid Pairs

YORP induced fission is a significant source of asteroid pairs (Pravec et al., 2010). Simulated disrupted systems also escape with low escape velocities similar to those modeled for asteroid pairs. The primary spin periods of observed asteroid pairs have a very characteristic dependence on mass ratio. This dependence is captured naturally by the rotational fission process as shown in Figure 1.15—the dots are the primaries of simulated disrupted systems and the crosses are observed asteroids.

1.4 Discussion

This is not the first rotational fission model for asteroid binary systems (Pravec and Harris, 2007; Scheeres, 2007a; Walsh et al., 2008; Holsapple, 2010), but this rotational fission model explains all observed NEA systems and constructs the entire life history of NEA systems into one coherent

theory. This theory agrees with previous authors that the progenitors of the NEA population are disrupted critically spinning asteroids, and that the YORP effect forces asteroids through an effective random walk up to that disruption limit, or away towards the slow rotator population, although eventually slow rotators may be spun back up in the other direction or tumbling might prevent this.

Unlike previously presented rotational fission theories for binary asteroids, this work modeled the evolution of disrupted systems over long timescales and concluded that these systems always disrupt. In order to prevent disruption, these systems need to transfer energy out of the orbit of the system into the spin energy of the bodies, either to stay or be dissipated. In the Walsh et al. (2008) model the energy is dissipated via accretion of more material onto the secondary. This material is from subsequent rotational fission of the primary after the initial rotational fission. However, we discover that rotational fissioned systems disrupt on timescales longer ($\sim 10^2$ to 10^3 orbits) than the Walsh et al. (2008) model allows the system to evolve (~ 5 orbits) before implementing an impulsive YORP torque on the primary, but on timescales much shorter than the equivalent natural YORP torque would take to develop ($\gtrsim 10^6$ orbits, estimated from the YORP timescale).

The dynamical model is scale independent and so predicts that binary formation occurs at the same rate across the entire size distribution of NEAs, but other non-incorporated effects begin to play an important role. Bodies < 100 m in radius may be dominated by cohesive forces so the “rubble pile” approximation no longer applies (Scheeres et al., 2010). This would reproduce the observed disappearance of the spin barrier at small size scales (Pravec and Harris, 2007). The YORP effect depends on the radius of the body to the second power, so at large sizes (> 10 km) the timescale of the YORP effect approaches the NEA lifetime. These effects create a range of sizes for which we expect binary asteroids to be formed from rotational fission in: 0.1 to 10 km. This agrees well with the sizes of the observed binary NEA population—between 0.3 and 3 km Pravec and Harris (2007), although the upper limit may also be set by small number statistics rather than the YORP timescale.

This formation mechanism predicts asteroid pairs amongst the NEA population. These will

be harder to detect than their counterparts amongst the small Main Belt asteroid population, since the orbit scattering time is much shorter due to interactions with the inner planets, and since the progenitors are typically smaller, the secondary member of each pair will have a small absolute size (< 100 m), which makes orbit determination difficult. In the small Main Belt asteroid pair population, this theory agrees with the already accepted idea that each pair is formed in a rotational fission event Pravec et al. (2010).

Shortcomings of the above model fall into two camps: unknown parameters and computational shortcuts. Geophysical parameters including the tidal Love number and the tidal quality number have significant uncertainties. In the model above, we were forced to assume a flat initial mass ratio, essentially the internal component mass distribution, since the actual distribution is unknown. Computationally, we took a number of shortcuts to reduce complexity and computational time including very simple impact physics, first-order tidal models, and second-order gravity. These assumptions probably had only a small impact on the efficiencies in the code. The largest computational time saver was the assumption of a planar system—an assumption supported by the high angular momentum content of rotationally fissioned asteroids, but this assumption removes an energy dissipation mechanism. When these systems fission, the components will most likely not be rotating about their principal axes. Thus, each component may damp energy through internal torques induced from non-principal axis rotation. This model has the ability to be improved with more observations and more complete physics, however we feel that none will change the overall conclusions regarding the evolutionary tracks, but they will have an impact on the efficiencies of the different pathways.

1.5 Conclusion

The evolution of NEA systems is driven by four important processes: initial rotational fission, secondary fission, impacts, and solar gravitational perturbations. The lower the mass ratio, the faster the spin rate required for initial rotational fission, and thus the more energy in the eventual binary system. The free energy transitions from positive to negative at a mass ratio of 0.2 for the

spherical end state, this divides the evolution of rotationally fissioned systems into two paths as shown in Figure 1.1. Secondary fission can occur before low mass ratio systems are ejected. Enough energy is transferred to the secondary via spin-orbit coupling so that it undergoes rotational fission and creates a chaotic ternary as shown in Figure 1.2. Secondary fission grows increasingly likely as mass ratio decreases, since the initial energy in the system increases and rotational energy transferred to the secondary is more effective on a less massive secondary. Chaotic ternaries are formed from secondary fission and evolve quickly back into a chaotic binary state, however impacts dissipate energy and produce more stable binaries. Escape of ternary members can also stabilize the system. Solar gravitational perturbations are important in changing the eccentricity and are responsible for both stabilizing and destabilizing binary systems. NEAs are actively evolving systems driven by these four processes and the observed asteroid classes are stages in this evolution.

Radiative processes dominate the evolution of the NEA population from the Yarkovsky effect which drives small Main Belt asteroids into resonances with Jupiter pushing them into the NEA population, to the YORP effect which dominates their spin evolution and forces them to disrupt forming asteroid systems, to the BYORP effect which drives these systems back together or apart. The lives of NEAs are exciting—each asteroid may go through many iterations of the cycle shown in Figure 1.1 taking different paths each time.

1.6 Derivation of the Two-Body Equations of Motion

The equations of motion of the two-body system will be derived from the Euler-Lagrange equations of motion modified to account for mutual body tides and then placed in the rotating coordinate frame of a body encircling the Sun at 1 AU to account for solar tides (using the Hill approximation).

The two-body integrator models the system as two tri-axial ellipsoids, E_1 and E_2 , expanded to 2nd order in their moments of inertia. A relative coordinate system with four degrees of freedom is defined: r is the separation distance between the centers of mass of the two bodies, θ tracks the rotation of the line connecting the centers of mass relative to an inertial frame, and ϕ_n tracks the

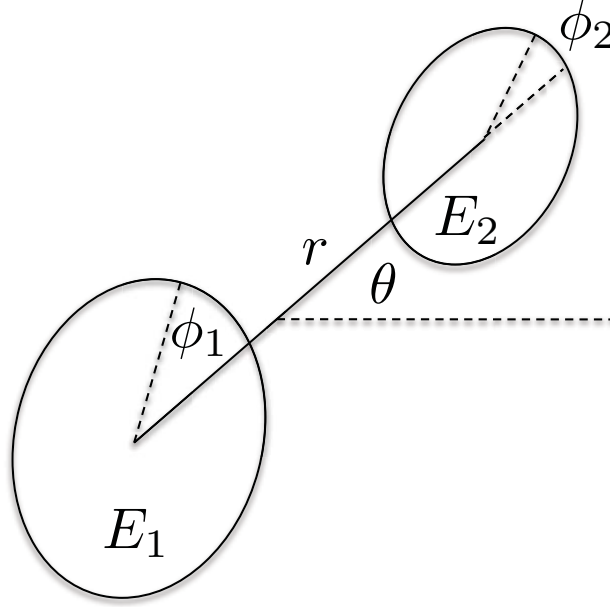


Figure 1.16: Two-body Coordinate System

rotation of the body n with respect to the line connecting the centers of mass. Figure 1.16 shows a schematic of the two-body coordinate system. In order to track the rotation of a body in an inertial frame, ψ_n , the two coordinates would need to be added $\psi_n = \theta + \phi_n$.

The density of each body is $\rho = 2 \text{ g/cc}$ —a typical density for small bodies in the solar system. Each tri-axial ellipsoid is a prolate body with axes $\alpha_n > \beta_n = \gamma_n$, where γ_n is oriented along the rotation axis. All rotation axes are aligned, thus all motion is constrained to a plane.

The kinetic energy of the system T has four independent degrees of freedom when written in the relative coordinate system:

$$T = \frac{1}{2}m \left(\dot{r}^2 + r^2\dot{\theta}^2 \right) + \frac{1}{2} \sum_{n=1}^2 I_{n_z} \left(\dot{\phi}_n + \dot{\theta} \right)^2 \quad (1.2)$$

where m is the reduced mass of the system and I_{n_i} is the moment of inertia of body n along axis i .

The potential energy V used is a 2nd order expansion in the moments of inertia corresponding to tri-axial ellipsoids, and has three independent degrees of freedom when written in the relative coordinate system:

$$V = -\frac{GM_1M_2}{r} \left\{ 1 + \frac{1}{2r^2} \left[\bar{I}_1 + \bar{I}_2 - \frac{3}{2} (\bar{I}_{1x} + \bar{I}_{1y} + \bar{I}_{2x} + \bar{I}_{2y} - \cos(2\phi_1)(\bar{I}_{1y} - \bar{I}_{1x}) - \cos(2\phi_2)(\bar{I}_{2y} - \bar{I}_{2x})) \right] \right\} \quad (1.3)$$

where M_n is the mass of body n , \bar{I}_n is the sum of the reduced (mass normalized) inertial moments of body n , and \bar{I}_{ni} is the reduced (mass normalized) moment of inertia of body n along axis i .

The modified Euler-Lagrange equations of motion for this system:

$$\frac{d}{dt} \left(\frac{\partial L}{\partial \dot{q}} \right) = \frac{\partial L}{\partial q} - \Gamma_q \quad (1.4)$$

where the tidal torque term Γ_q appears only in the relative spin coordinate equations as Γ_{ϕ_1} or Γ_{ϕ_2} , and is zero for all others, $\Gamma_r = \Gamma_\theta = 0$. This tidal torque is responsible for dissipating energy in the form of heat. The exact form of the tidal torque is discussed in 1.8.

The Euler-Lagrange equation of motion for the separation distance r is solved straightforwardly for \ddot{r} :

$$\ddot{r} = r\dot{\theta}^2 - \frac{V_r}{m} \quad (1.5)$$

where V_r is the partial derivative of the potential energy with respect to the separation distance r :

$$V_r = \frac{GM_1M_2}{r^2} \left(1 + \frac{3}{2r^2} \left(\bar{I}_1 + \bar{I}_2 - \frac{3}{2} (\bar{I}_{1x} + \bar{I}_{1y} + \bar{I}_{2x} + \bar{I}_{2y} - \cos(2\phi_1)(\bar{I}_{1y} - \bar{I}_{1x}) - \cos(2\phi_2)(\bar{I}_{2y} - \bar{I}_{2x})) \right) \right) \quad (1.6)$$

Since the Lagrangian does not depend directly on θ , the right-hand side of the orbital Euler-Lagrange equation of motion is zero and so it becomes a statement of the conservation of angular momentum:

$$\frac{d}{dt} \left(I_{1z}\dot{\phi}_1 + I_{2z}\dot{\phi}_2 + I_z\dot{\theta} \right) = 0 \quad (1.7)$$

where $I_z = I_{1z} + I_{2z} + mr^2$ and is an abbreviation for the system or polar moment of inertia.

The modified Euler-Lagrange equations of motion for the relative spin coordinates ϕ_n for each body n :

$$I_{n_z} \ddot{\phi}_n + I_{n_z} \ddot{\theta} = -V_{\phi_n} - \Gamma_n \quad (1.8)$$

where V_{ϕ_n} is the partial derivative of the potential energy with respect to the relative spin coordinate ϕ_n :

$$V_{\phi_n} = \frac{3}{2} \left(\frac{GM_1 M_2}{r^3} \right) (\bar{I}_{n_y} - \bar{I}_{n_x}) \sin(2\phi_n) \quad (1.9)$$

The modified Euler-Lagrange equations of motion for the angular coordinates can be arranged in a matrix representation:

$$\begin{pmatrix} I_{1z} & 0 & I_{1z} \\ 0 & I_{2z} & I_{2z} \\ I_{1z} & I_{2z} & I_z \end{pmatrix} \begin{pmatrix} \ddot{\phi}_1 \\ \ddot{\phi}_2 \\ \ddot{\theta} \end{pmatrix} = \begin{pmatrix} -\Gamma_1 - V_{\phi_1} \\ -\Gamma_2 - V_{\phi_2} \\ -2mr\dot{r}\dot{\theta} \end{pmatrix} \quad (1.10)$$

Solving all three angular equations of motion simultaneously gives the equations of motion for the individual angular coordinates:

$$\ddot{\theta} = -\frac{2\dot{r}\dot{\theta}}{r} + \frac{\Gamma_1 + \Gamma_2 + V_{\phi_1} + V_{\phi_2}}{mr^2} \quad (1.11)$$

$$\ddot{\phi}_1 = \frac{2\dot{r}\dot{\theta}}{r} - \frac{\Gamma_1 + \Gamma_2 + V_{\phi_1} + V_{\phi_2}}{mr^2} - \frac{\Gamma_1 + V_{\phi_1}}{I_{1z}} \quad (1.12)$$

$$\ddot{\phi}_2 = \frac{2\dot{r}\dot{\theta}}{r} - \frac{\Gamma_1 + \Gamma_2 + V_{\phi_1} + V_{\phi_2}}{mr^2} - \frac{\Gamma_2 + V_{\phi_2}}{I_{2z}} \quad (1.13)$$

These relative equations of motion are in the orbiting reference frame of the asteroid system. This system can be transformed to the inertial frame of the Sun via Hill's approximation; planar motion has already been assumed, but we also now assume a circular heliocentric orbit:

$$\ddot{r}_s = \ddot{r} + 3n^2 r \cos \theta + 2nr\dot{\theta} \quad (1.14)$$

$$\ddot{\theta}_s = \ddot{\theta} - 2n\dot{r} \quad (1.15)$$

where n is the mean motion of the asteroid system about the Sun. Thus, the equations of motion for the two-body integrator are:

$$\ddot{r}_s = r\dot{\theta}^2 - \frac{V_r}{m} + 2nr\dot{\theta} + 3n^2r \cos \theta \quad (1.16)$$

$$\ddot{\theta}_s = -\frac{2\dot{r}\dot{\theta}}{r} + \frac{\Gamma_1 + \Gamma_2 + V_{\phi_1} + V_{\phi_2}}{mr^2} - 2n\dot{r} \quad (1.17)$$

$$\ddot{\phi}_1 = \frac{2\dot{r}\dot{\theta}}{r} - \frac{\Gamma_1 + \Gamma_2 + V_{\phi_1} + V_{\phi_2}}{mr^2} - \frac{\Gamma_1 + V_{\phi_1}}{I_{1z}} \quad (1.18)$$

$$\ddot{\phi}_2 = \frac{2\dot{r}\dot{\theta}}{r} - \frac{\Gamma_1 + \Gamma_2 + V_{\phi_1} + V_{\phi_2}}{mr^2} - \frac{\Gamma_2 + V_{\phi_2}}{I_{2z}} \quad (1.19)$$

1.7 Derivation of the Three-Body Equations of Motion

The equations of motion of the three-body system will be derived from the Euler-Lagrange equations of motion modified to account for mutual body tides and then placed in the rotating coordinate frame of a body encircling the Sun at 1 AU to account for solar tides (Hill approximation). The mutual body tide between the two smallest members is neglected.

The three body integrator models the system as one tri-axial ellipsoid, E_1 , and two spheres, S_2 and S_3 . The system is described in an inertial cartesian coordinate system with nine coordinates. Each body n has three coordinates: x_n and y_n track the body's center of mass and ψ_n tracks the rotation angle. Figure 1.17 shows a schematic of the three-body coordinate system.

The rotation ψ_m , orbital angle θ_{1m} and relative spin angles ϕ_{1m} of the sphere m are shown schematically in Figure 1.18 and are related:

$$\phi_{1m} = \theta_{1m} - \psi_1 = \arctan\left(\frac{y_m - y_1}{x_m - x_1}\right) - \psi_1 \quad (1.20)$$

The density of each body is $\rho = 2$ g/cc—a typical density for small bodies in the solar system. The tri-axial ellipsoid is a prolate body with axes $\alpha_1 > \beta_1 = \gamma_1$, where γ_1 is oriented along the

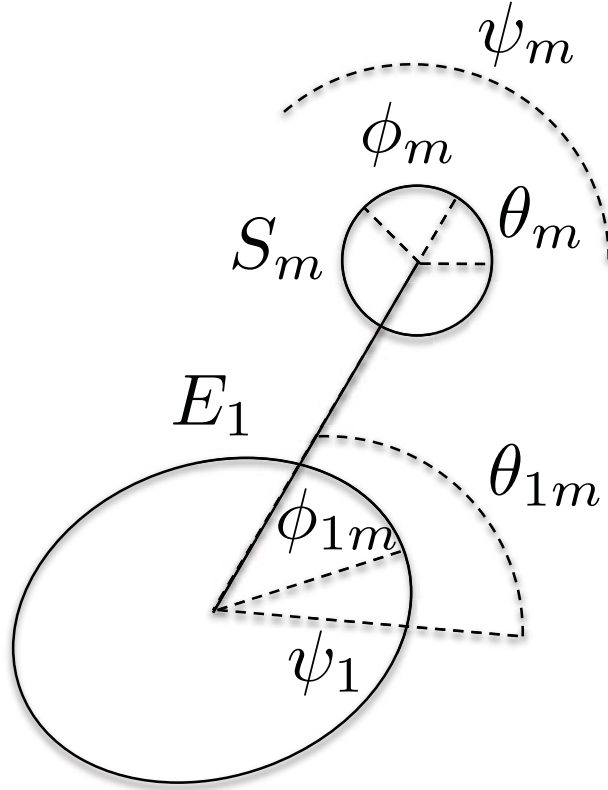


Figure 1.17: Three-body Coordinate System

rotation axis. The spheres are defined by a radius R_m . All rotation axes are aligned, thus all motion is constrained to a plane.

The kinetic energy of the system T has nine independent degrees of freedom when written in the cartesian/angular coordinate system:

$$T = \frac{1}{2} \sum_{n=1}^3 M_n \left(\dot{x}_n^2 + \dot{y}_n^2 + \bar{I}_n \dot{\psi}_n^2 \right) \quad (1.21)$$

where \bar{I}_n is the sum of the reduced (mass normalized) inertial moments of body n .

The potential energy V used for the primary is a 2nd order expansion in the moments of inertia corresponding to a tri-axial ellipsoid, and each of the secondaries is a Keplerian potential corresponding to a sphere. The potential energy has 7 independent degrees of freedom when written in the cartesian/angular coordinate system:

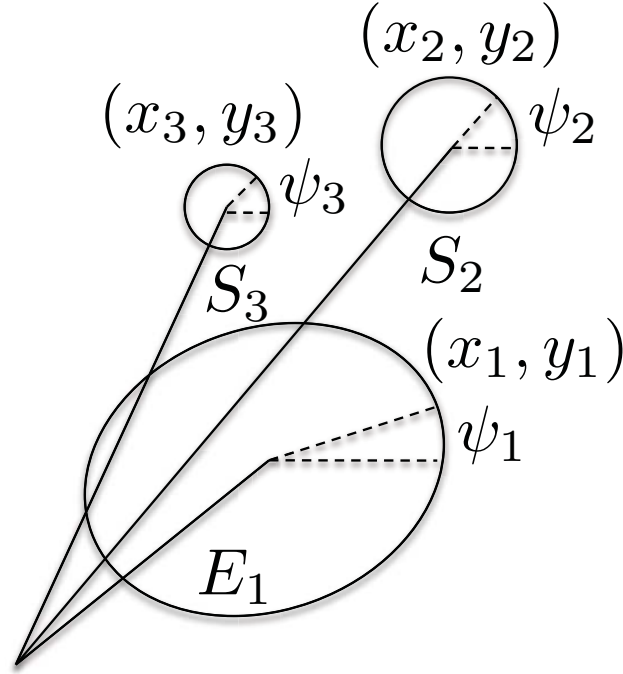


Figure 1.18: Three-body Angular Coordinate System

$$\begin{aligned}
 V = & -\frac{GM_2M_3}{r_{23}} \\
 & -\frac{GM_1M_2}{r_{12}} \left\{ 1 + \frac{1}{2r_{12}^2} \left[\bar{I}_1 - \frac{3}{2} (\bar{I}_{1x} + \bar{I}_{1y} - \cos(2\phi_{12}) (\bar{I}_{1y} - \bar{I}_{1x})) \right] \right\} \\
 & -\frac{GM_1M_3}{r_{13}} \left\{ 1 + \frac{1}{2r_{13}^2} \left[\bar{I}_1 - \frac{3}{2} (\bar{I}_{1x} + \bar{I}_{1y} - \cos(2\phi_{13}) (\bar{I}_{1y} - \bar{I}_{1x})) \right] \right\} \quad (1.22)
 \end{aligned}$$

where \bar{I}_{n_i} is the reduced (mass normalized) moment of inertia of body n along axis i and r_{nm} is:

$$r_{nm} = \sqrt{(x_n - x_m)^2 + (y_n - y_m)^2} \quad (1.23)$$

The Euler-Lagrange equations of motion for the cartesian coordinates are simply solved for \ddot{x} and \ddot{y} :

$$\ddot{x}_n = \frac{1}{M_n} \frac{\partial V}{\partial x_n} \quad \ddot{y}_n = \frac{1}{M_n} \frac{\partial V}{\partial y_n} \quad (1.24)$$

The modified Euler-Lagrange equation of motion for the angular coordinate of the primary can be solved for the $\ddot{\psi}_1$:

$$\ddot{\psi}_1 = \frac{1}{I_1} \left(\frac{dV}{d\psi_1} - \Gamma_{21} - \Gamma_{31} \right) \quad (1.25)$$

There are two tidal torques, Γ_{m1} , from each spherical body m onto the primary. These tidal torques are responsible for dissipating energy in the form of heat. The tidal torque depends linearly on the relative spin angle rate, $\dot{\phi}_{1m}$, and inversely on the distance between the bodies, r_{1m} to the fifth power. The exact form of the tidal torque is discussed in Section 1.8.

The modified Euler-Lagrange equations of motion for the angular coordinates of the spheres are solved:

$$\ddot{\psi}_m = \frac{1}{I_m} \Gamma_{1m} \quad (1.26)$$

where there is only one tidal torque, Γ_{1m} , acting on each spherical body from the primary. The tidal torque between the spherical bodies is neglected. These tidal torques are responsible for dissipating energy in the form of heat. The tidal torque depends linearly on the relative spin angle rate, $\dot{\phi}_m$, and inversely on the distance between the bodies, r_{1m} to the fifth power. The exact form of the tidal torque is discussed in Section 1.8.

These relative equations of motion are in the orbiting reference frame of the asteroid system. This system can be transformed to the inertial frame of the Sun via Hill's approximation; planar motion has already been assumed, but we also now assume a circular heliocentric orbit:

$$\ddot{x}_{ns} = \ddot{x}_n + 2n\dot{y}_n + 3n^2\dot{x}_n \quad (1.27)$$

$$\ddot{y}_{ns} = \ddot{y}_n - 2n\dot{x}_n \quad (1.28)$$

$$\ddot{\psi}_{ns} = \ddot{\psi}_n \quad (1.29)$$

where n is the mean motion of the asteroid system about the Sun. Thus, the equations of motion for the two-body integrator are:

$$\ddot{x}_{ns} = \frac{1}{M_n} \frac{\partial V}{\partial x_n} + 2n\dot{y}_n + 3n^2\dot{x}_n \quad (1.30)$$

$$\ddot{y}_{ns} = \frac{1}{M_n} \frac{\partial V}{\partial y_n} - 2n\dot{x}_n \quad (1.31)$$

$$\ddot{\psi}_{1s} = \frac{1}{I_1} \left(\frac{dV}{d\psi_1} - \Gamma_{21} - \Gamma_{31} \right) \quad (1.32)$$

$$\ddot{\psi}_{ms} = \frac{1}{I_m} \Gamma_{1m} \quad (1.33)$$

1.8 Derivation of the Tidal Theory

The model applies the classical tidal torque presented in Murray and Dermott (2000) for a spherical (point source) satellite j acting on a spherical body i :

$$\Gamma_i = \text{sign}(\dot{\phi}_i) \frac{3}{2} k \left(\frac{3}{4\pi\rho_i} \right)^2 \frac{GM_i^2 M_j^2}{r_{ij}^6 R_i} \sin(2\epsilon_i) \quad (1.34)$$

where k is the tidal Love number and ϵ is the tidal lag angle. R_i is the radius of body i if it were a sphere of equal mass. The tidal bulge is independent of the shape of the body. The sign of $\dot{\phi}_i$ determines whether the tidal bulge is leading or trailing the tide-raising satellite, which determines the direction of angular momentum transfer between the orbit and the spin state. The tidal lag angle can be related to the specific tidal dissipation function Q , which describes how effective the body is at tidally dissipating energy:

$$Q = \frac{1}{\tan 2\epsilon} \approx \frac{1}{2\epsilon} \quad (1.35)$$

However this classical torque presents a problem when $\dot{\phi}_i$ changes through zero, which occurs for many of these systems due to the chaotic nature of their evolution and the large spin-orbit coupling. When $\dot{\phi}_i$ crosses zero, Γ_i changes sign instantaneously. This is unphysical since the bulge is a real phenomenon and would have some finite crossing time. Instantaneous switching is a difficulty for numerical integration as well. We introduce a modified torque that will linearize Γ_i when $\dot{\phi}_i \approx 0$.

$$\Gamma_i = \begin{cases} \Gamma_i & |\dot{\phi}_i| > \delta_i \\ \Gamma_i \frac{\dot{\phi}_i}{\delta_i} & |\dot{\phi}_i| \leq \delta_i \end{cases} \quad (1.36)$$

where δ_i is some small characteristic angular spin rate for body i . We can derive an appropriate small characteristic angular spin rate from the torque equation $\ddot{\phi}_i = \Gamma_i/I_{i_z}$:

$$\delta_i = \Delta \dot{\phi}_i = \frac{\Gamma_i}{I_{i_z}} \Delta t \quad (1.37)$$

where Δt is some characteristic time, which can be derived from the crossing time of a pressure (seismic) wave:

$$\Delta t = \frac{\Delta l}{\Delta v} \quad (1.38)$$

where $\Delta l = 2R_i$ is the characteristic length scale of the body, and Δv is the pressure (seismic) wave velocity c_i . The pressure wave velocity can be found from the central pressure P_i :

$$c_i = \sqrt{\frac{P_i}{\rho_i}} = \sqrt{\frac{2\pi G \rho_i}{3}} R_i \quad (1.39)$$

The small characteristic angular spin rate δ_i is now determined:

$$\delta_i = \frac{\Gamma_i}{I_{i_z}} \frac{2R_i}{c_i} = \frac{\Gamma_i}{I_{i_z}} \sqrt{\frac{6}{\pi G \rho_i}} \quad (1.40)$$

This gives the modified tidal torque:

$$\Gamma_i = \begin{cases} \text{sign}(\dot{\phi}_i) \frac{3}{2} k \left(\frac{3}{4\pi\rho_i} \right)^2 \frac{GM_i^2 M_j^2}{r_{ij}^6 R_i} \sin(2\epsilon_i) & |\dot{\phi}_i| > \delta_i \\ \sqrt{\frac{\pi G \rho_i}{6}} I_{i_z} \dot{\phi}_i & |\dot{\phi}_i| \leq \delta_i \end{cases} \quad (1.41)$$

1.9 Secondary Fission Condition

The coordinate system is given in Figure 1.19, and the condition for secondary fission is:

$$\ddot{\vec{r}}_{2B}^R \cdot \hat{r}_{2B} > 0 \quad (1.42)$$

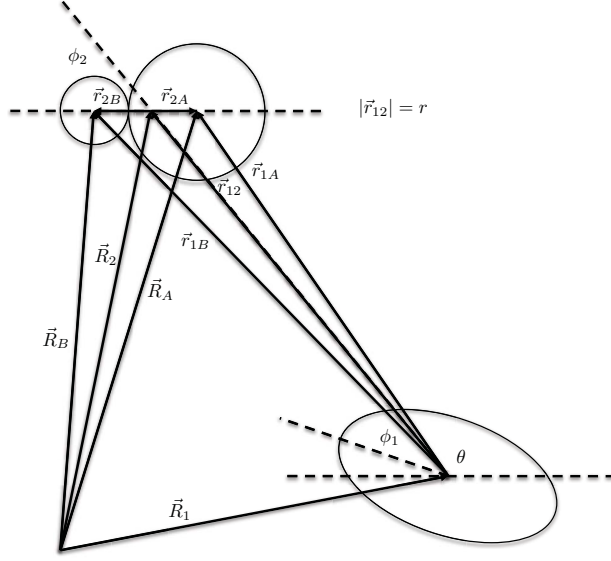


Figure 1.19: New Relative Coordinate System

$$\begin{aligned}
 \ddot{\vec{r}}_{2B}^R \cdot \hat{r}_{2B} = & -\frac{GM_A}{|\vec{r}_{AB}|^2} + |\vec{r}_{2B}||\Omega_2|^2 - \left(1 + \frac{M_B}{M_A}\right)^{-1} \frac{GM_1}{|\vec{r}_{1B}|^2} \left[1 + \frac{3}{2|\vec{r}_{1B}|^2} \times \right. \\
 & \left. \left(\bar{I}_1 - \frac{3}{2}(\bar{I}_{1x} + \bar{I}_{1y} + (\bar{I}_{1x} - \bar{I}_{1y}) \cos 2\psi_{1B})\right)\right] (\hat{r}_{1B} \cdot \hat{r}_{2B}) - \frac{GM_1}{|\vec{r}_{1A}|^2} \times \\
 & \left[1 + \frac{3}{2|\vec{r}_{1A}|^2} \left(\bar{I}_1 - \frac{3}{2}(\bar{I}_{1x} + \bar{I}_{1y} + (\bar{I}_{1x} - \bar{I}_{1y}) \cos 2\psi_{1A})\right)\right] (\hat{r}_{1A} \cdot \hat{r}_{2B})
 \end{aligned} \tag{1.43}$$

1.10 Impact Mass Redistribution

When the spherical secondary re-impacts the tri-axial primary, the mass of the secondary is placed onto the primary so as to bring the surface closer to a geopotential along the equator (oblate spheroid). The smaller β axis is increased by a height:

$$h = \frac{R_s^3}{\alpha\beta} \tag{1.44}$$

where R_s is the radius of the secondary and α and β are the original tri-axial axes.

1.11 Modeling Tidal Timescales

High mass ratio systems (mass ratio > 0.2) were evolved from YORP induced rotational fission according to the two-body integrator described exactly as above with the exception of solar gravitational perturbations which were neglected for this case. According to theory developed in Scheeres (2009b), if the secondary does not undergo secondary fission and without the influence of external events, then these systems will evolve from their initial orbital state immediately after rotational fission to the doubly synchronous (relative equilibrium) state with the same angular momentum. Mutual tidal dissipation naturally weakens and eventually turns off as the system approaches and reaches the doubly synchronous state.

The doubly synchronous state has lower energy than the initial state, and this energy is dissipated via mutual body tides. After evolving each system for 10^4 years, some of the systems had reached the doubly synchronous state, and the time that the energy dissipation rate went effectively to zero was recorded as the time the system became a doubly synchronous system. Many systems had not reached the doubly synchronous state within 10^4 years, due to limited computation resources the timescale for transformation to the doubly synchronous state was determined by extrapolation. The energy dissipation as a function of time for each system could be fit with a power law (with greater than 99% confidence in the fit) and that power law was then extrapolated to zero when the system would be in the doubly synchronous state and there would be no more mutual tidal energy dissipation.

1.12 Limit on the Mass Ratio of Next Secondary Fission

Let there be a body made of two components M_1 and M_2 . The first component is made up of two components M_{11} and M_{12} , so that $M_{11} + M_{12} = M_1$. Without loss of generality assume that:

$$M_{12} > M_{11} \tag{1.45}$$

In order that the M_2 component fission first the following condition must be met:

$$M_2 > M_{12} > M_{11} \quad (1.46)$$

Divide by M_1 to put in terms of mass ratio.

$$\frac{M_2}{M_1} = q_2 > \frac{M_{12}}{M_1} \quad (1.47)$$

$$\frac{1}{q_2} < \frac{M_{11}}{M_{12}} + 1 = \frac{1}{q_{12}} + 1 \quad (1.48)$$

$$q_{12} < \frac{q_2}{1 - q_2} \quad (1.49)$$

This condition is not a strong condition since it doesn't require the mass ratio of a future rotational fission event to decrease after an initial rotational fission event.

Chapter 2

Study of the Role of Non-gravitational and Tidal Torques on Binary Asteroid Systems

2.1 Introduction

The previous study determined the post-rotational fission dynamics of binary asteroid systems, and showed how these dynamics may lead to the formation of all classes of observed near-Earth asteroid (NEA) binaries. In this study, we focus on the non-gravitational and tidal torques that evolve these systems when they occupy specific evolutionary states. We will consider asynchronous binary evolution and then synchronous evolution, which is broken into two parts: joint expansive evolution and joint opposing evolution. The joint opposing evolution leads to a newly discovered tidal-BYORP equilibrium and my participation in an observing campaign to confirm that the synchronous binary population occupies this equilibrium. That campaign, my contributions and its first results are discussed at the end of the study.

The secular evolution of binary systems is determined by three important torques: mutual body tides, the YORP effect, and the binary YORP effect. Mutual body tides in the context of binary asteroids have been considered in the past by Margot et al. (2002) and Taylor and Margot (2011), but the NEA population is constantly evolving due to the incredible influence of electromagnetic radiation and the importance of those torques has not been fully appreciated. The YORP effect, torque from the incident solar irradiation and thermal radiation of an asymmetric body, can rotationally accelerate individual asteroids until centrifugal accelerations match gravitational accelerations, releasing part of the body into orbit and creating a binary asteroid system

(i.e. rotational fission). The YORP effect can also delay tidal synchronization and accelerated newly de-synchronized binary members. The BYORP effect can contract and expand binary systems creating non-binary asteroid classes such as contact binaries and asteroid pairs. Lastly it's important to realize that for the near-Earth asteroid population planetary flybys have a strong, stochastic influence on binary systems. Figure 2.1 shows the evolutionary pathways from rotational fission to each of the observed binary classes indicated by an underline and is an update from the flowchart shown in the previous study to better specify long-term evolutionary states and the role of planetary flybys.

A remark on the assumptions going forward. For the rest of this thesis, we will assume that these binaries formed via rotational fission and so share a common parent body (Margot et al., 2002; Scheeres, 2007a; Walsh et al., 2008; Pravec et al., 2010; Jacobson and Scheeres, 2011a). Each component of the binary will share the same intensive properties such as density ρ , tidal dissipation number Q , rigidity μ , and yield strain ϵ_Y . Extensive properties such as radius R , mass ratio q , and tidal Love number k depend on the absolute sizes of the binary members. Having made this assumption, it is important to realize that there are measurements that are consistent with differences in quantities such as density between the primary and secondary of a binary system Ostro et al. (2006), but these differences are only of order tens of percent and often do not exceed the uncertainties. The added clarity from these assumptions to the analytical treatment is valuable and is likely not to effect the results of any particular calculation by a substantial amount.

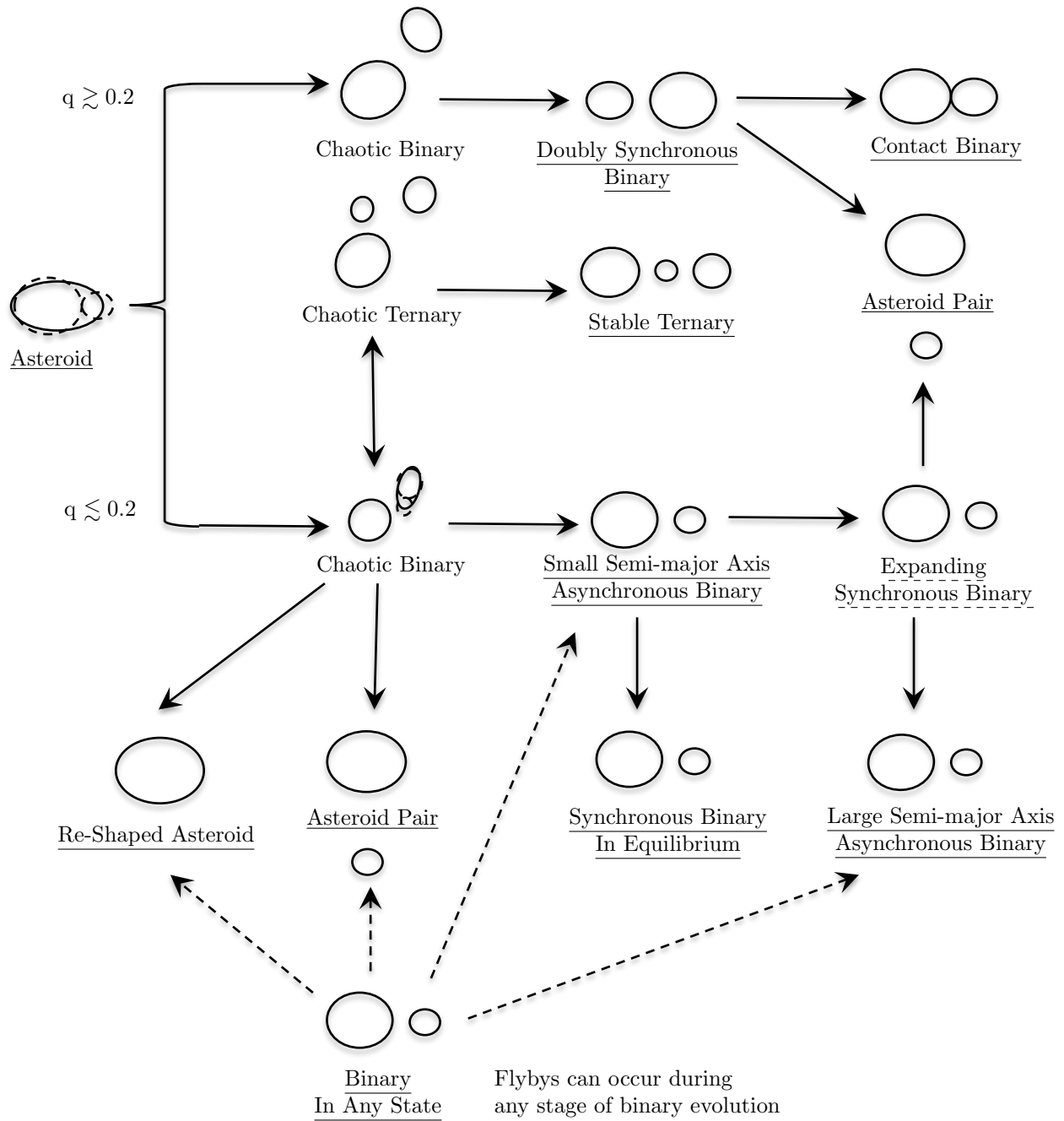


Figure 2.1: This evolutionary flowchart includes both the role of flybys, the tidal-BYORP equilibrium, and the large asynchronous binaries.

Asteroid System	a_{\odot} [au]	e_{\odot}	q	R_p [km]	a [R_p]	a [km]	P_p [P_d]	P_p [h]	P_s [P_d]	P_s [h]	P_o [P_d]	P_o [h]	ρ [g/cc]
Doubly synchronous binary asteroids													
(69230) Hermes	1.66	0.62	0.729	0.3	4.0	1.2	6.0	13.9	6.0	13.9	6.0	13.9	2.0
(809) Lundia	2.28	0.19	0.705	3.4	4.4	15.2	6.6	15.4	6.6	15.4	6.6	15.4	2.0
(1089) Tama	2.21	0.13	0.729	4.7	4.6	21.6	7.0	16.4	7.0	16.4	7.0	16.4	2.0
(2478) Tokai	2.22	0.07	0.636	3.5	6.0	21.0	11.1	25.9	11.1	25.9	11.1	25.9	2.0
(1313) Berna	2.66	0.21	0.913	5.0	6.2	31.0	10.9	25.5	10.9	25.5	10.9	25.5	2.0
(1139) Atami	1.95	0.26	0.512	2.5	6.2	15.5	11.8	27.4	11.8	27.4	11.8	27.4	2.0
(4492) Debussy	2.77	0.18	0.804	5.5	6.4	35.2	11.4	26.6	11.4	26.6	11.4	26.6	2.0
(854) Frostia	2.37	0.17	0.941	4.5	8.2	36.9	16.2	37.7	16.2	37.7	16.2	37.7	2.0
(7369) Gavrilin	2.37	0.32	0.343	2.4	8.8	20.7	21.0	49.1	21.0	49.1	21.0	49.1	2.0
(4951) Iwamoto	2.26	0.17	0.681	2.0	16.8	33.6	50.5	118.0	50.5	118.0	50.5	118.0	2.0

Synchronous binary asteroids

(276049) 2002 CE ₂₆	2.23	0.56	0.001	1.7	2.7	4.7	0.9	3.3	4.2	15.6	4.2	15.6	0.8
(65803) Didymos	1.64	0.38	0.011	0.4	3.0	1.1	1.0	2.3	5.1	11.9	5.1	11.9	2.0
(137170) 1999 HF ₁	0.82	0.46	0.012	1.8	3.4	6.0	1.0	2.3	6.0	14.0	6.0	14.0	2.0
(76818) 2000 RG ₇₉	1.93	0.10	0.043	1.4	3.4	4.8	1.4	3.2	6.1	14.1	6.1	14.1	2.0
(31345) 1998 PG	2.02	0.39	0.064	0.4	3.4	1.5	1.1	2.5	6.0	14.0	6.0	14.0	2.0

Asteroid System	a_{\odot} [au]	e_{\odot}	q	R_p [km]	a [R_p]	a [km]	P_p [P_d]	P_p [h]	P_s [P_d]	P_s [h]	P_o [P_d]	P_o [h]	ρ [g/cc]
2005 NB ₇	2.04	0.52	0.064	0.2	3.6	0.9	1.5	3.5	6.5	15.3	6.5	15.3	2.0
(66063) 1998 RO ₁	0.99	0.72	0.111	0.4	3.6	1.4	1.1	2.5	6.2	14.5	6.2	14.5	2.0
(17260) 2000 JQ ₅₈	2.20	0.18	0.018	1.6	3.6	5.8	1.3	3.1	6.3	14.7	6.3	14.8	2.0
(175706) 1996 FG ₃	1.05	0.35	0.030	0.8	3.8	2.8	1.5	3.6	6.9	16.1	6.9	16.1	2.0
(66391) 1999 KW ₄	0.64	0.69	0.036	0.6	4.0	2.6	1.2	2.8	7.5	17.4	7.5	17.4	2.0
(3309) Brorfelde	1.82	0.05	0.018	2.4	4.0	9.4	1.1	2.5	7.9	18.4	7.9	18.5	2.0
(1338) Duponta	2.26	0.11	0.014	3.7	4.0	14.8	1.7	3.9	7.5	17.6	7.5	17.6	2.0
(85938) 1999 DJ ₄	1.85	0.48	0.125	0.2	4.2	0.7	1.1	2.5	7.6	17.7	7.6	17.7	2.0
(2044) Wirt	2.38	0.34	0.016	2.8	4.2	11.8	1.6	3.7	8.1	19.0	8.1	19.0	2.0
(7088) Ishtar	1.98	0.39	0.074	0.6	4.4	2.6	1.1	2.7	8.8	20.6	8.8	20.6	2.0
(2131) Mayall	1.89	0.11	0.027	3.7	4.8	17.8	1.1	2.6	10.1	23.5	10.1	23.5	2.0
(5477) Holmes	1.92	0.08	0.059	1.4	5.0	7.2	1.3	3.0	10.5	24.4	10.5	24.4	2.0
(9069) Hovland	1.91	0.12	0.064	1.5	5.8	8.7	1.8	4.2	13.0	30.3	13.0	30.3	2.0
(185851) 2000 DP ₁₀₇	1.37	0.38	0.069	0.4	7.2	2.9	1.2	2.8	18.1	42.2	18.0	42.1	2.0
(6084) Bascom	2.31	0.24	0.051	2.9	7.4	21.5	1.2	2.7	18.6	43.5	18.6	43.5	2.0

Short semi-major axis asynchronous binary asteroids

(5381) Sekhmet	0.95	0.30	0.027	0.5	3.1	1.5	1.1	2.7	4.1	10.0	5.1	12.5	1.8
----------------	------	------	-------	-----	-----	-----	-----	-----	-----	------	-----	------	-----

Continued on next page
58

Asteroid System	a_{\odot} [au]	e_{\odot}	q	R_p [km]	a [R_p]	a [km]	P_p [P_d]	P_p [h]	P_s [P_d]	P_s [h]	P_o [P_d]	P_o [h]	ρ [g/cc]
(162000) 1990 OS	1.68	0.46	0.003	0.1	4.4	0.7	1.1	2.5	3.4	8.0	9.0	21.0	2.0
2004 DC	1.63	0.40	0.008	0.1	4.6	0.7	0.9	2.0	2.8	6.5	9.9	23.0	2.0
(35107) 1991 VH	1.14	0.14	0.055	0.6	6.0	3.6	1.1	2.6	5.5	12.8	14.0	32.7	2.0
(16635) 1993 QO	2.30	0.29	0.043	1.9	6.0	11.4	0.9	2.2	3.3	7.6	13.8	32.2	2.0
(164121) 2003 YT ₁	1.11	0.29	0.006	0.5	6.4	3.2	1.0	2.3	2.6	6.0	15.7	36.7	2.0
(2577) Litva	1.90	0.14	0.039	2.0	6.4	12.8	1.2	2.8	2.4	5.7	15.4	35.9	2.0

Large semi-major axis asynchronous binary asteroids

(1717) Arlon	2.20	0.13	0.216	4.5	15.0	67.5	2.2	5.1	7.8	18.2	50.1	117.0	2.0
1998 ST ₂₇	0.82	0.53	0.003	0.4	16.5	6.6	1.3	3.1	2.6	6.0	72.0	168.0	2.0
(32039) 2000 JO ₂₃	2.22	0.28	0.275	0.9	32.0	28.8	1.4	3.3	4.8	11.1	154.0	360.0	2.0
(1509) Esclangona	1.87	0.03	0.036	3.9	54.0	211.0	1.4	3.3	2.8	6.6	374.0	874.0	2.0

Table 2.1: Small binary asteroid systems with well-defined parameters.

This study makes strong use of the July 1, 2011 binary parameter release from <http://www.asu.cas.cz/asteroid/binastd.htm>, which is compiled by methods described in Pravec et al. (2006) and Pravec and Harris (2007) and maintained by Petr Pravec and collaborators. It contains entries for many asteroid binary systems, however we make special use of the systems shown in Table 2.1. They are divided into the four categories established in this thesis: tight asynchronous binaries, wide asynchronous binaries, singly synchronous binaries and doubly synchronous systems. These morphologies are determined by the spin rates of the secondary and primary relative to the orbit rate, as well as the separation distance for the case of asynchronous systems.

In Table 2.1, the first two columns are the heliocentric semi-major axis a_{\odot} and eccentricity e_{\odot} , which are important for the radiative torques. The mass ratio q is in column three. The primary radius R_p is in column four. For many calculations, we use a spherical approximation for both bodies and the secondary radius $R_s = q^{1/3}R_p$. Then the mutual semi-major axis a is given in both primary R_p and kilometers. The next three sets of columns contain the primary period P_p , the secondary period P_s , and the orbital period P_o in two different units P_d , which is the period disruption limit $P_d = 2\pi/\omega_d = \sqrt{3\pi/\rho G}$, and hours. If a period is near P_d then it is spinning near its rotational fission limit.

2.2 Asynchronous Binary Evolution

As shown in the previous study, the outcome of rotational fission does not always lead to binary formation. When it does, the binary orbits are often eccentric and the spin states are not synchronous with orbit. For all of these systems mutual body tides play a stabilizing role. These tides damp eccentricity and act to synchronize each member of the system. The rotational acceleration due to the YORP effect is always occurring though (except for the special case when the YORP coefficient is precisely zero). The YORP effect acts on each member and while it does not directly influence the mutual orbit evolution, it can both assist or resist the synchronization of each member, independently. There is a competition between tides and the YORP effect as to whether a binary member synchronizes or not.

2.2.1 The YORP effect and mutual body tides

The YORP effect is the cumulative torque due to incoming solar irradiation and outgoing thermal emission and its effect on the rotational dynamics of the body (Rubincam, 2000). The YORP effect secularly evolves the spin rate and the obliquity, but the obliquity change is slow compared to the rotational acceleration of the body. The YORP coefficient Y depends strongly on the shape of the body, but does not depend on its size (extent or mass). Scheeres (2007b) showed that YORP coefficients are on order 2.5×10^{-2} when calculated solely from the shape of the body and this was found to be in general agreement with spin model comparisons with observed asteroid population (Rossi et al., 2009). Golubov and Krugly (2012) has shown that there may be another component of the YORP torque due to thermal radiation from heat that has been conducted across the surface of the body. Interestingly, this new YORP torque is preferentially prograde, whereas the original YORP torque is not biased in either direction. So far, the theory for this torque is in its infancy but it is clear that regolith properties, asteroid size, and spin rate will play an important role. For now, Golubov and Krugly (2012) showed that the torque may be of the same order of magnitude as the more theoretically developed Rubincam (2000) YORP torque (Scheeres, 2007b; Nesvorný and Vokrouhlický, 2008).

The orbit and rotation averaged YORP rotational acceleration $\dot{\omega}_Y$ to first order in e for the primary and secondary, respectively, is:

$$\dot{\omega}_{Y,p} = \frac{Y_p H_\odot}{2\pi\rho R_p^2} \quad \dot{\omega}_{Y,s} = \frac{Y_s H_\odot}{2\pi\rho R_p^2 q^{2/3}} \quad (2.1)$$

where $H_\odot = (2/3)F_\odot/(a_\odot^2\sqrt{1-e_\odot^2})$ and F_\odot is the solar radiation constant ($F_\odot \sim 10^{14}$ kg km s⁻²) (Scheeres, 2007b). These YORP acceleration equations do not include the Golubov and Krugly (2012) YORP torque and so for rapid (few hour period) and small (0.1 to 1 km) asteroids, there may be a significant additional acceleration. In the following analysis, we incorporate this torque by designating a large region of uncertainty (factor of ten) to the YORP coefficient.

Since the YORP torque depends on the surface area of the binary components, the YORP acceleration of the primary is a factor of $q^{2/3}$ smaller if both members have similar YORP coefficients.

The YORP coefficient is independent of size and only dependent on shape.

Relative motion between components in a binary system leads to tidal dissipation of energy and the transfer of angular momentum between spin and orbit states. Assuming spherical, homogeneous bodies with identical compositions and a mutual orbit with low eccentricity, an asteroid's first order geophysics can be characterized by two parameters: the tidal Love number and the tidal dissipation number. The tidal Love number k is the ratio of the additional gravitational potential produced by the redistribution of mass relative to the deforming potential, and theoretically is thought to depend on the size and internal properties of the body. The tidal dissipation number Q describes how effective the body is at tidally dissipating energy. It is a quality factor defined as: $Q = 2\pi E_0 / \oint \frac{dE}{dt} dt$, where E_0 is the maximum energy stored in the tidal distortion during a cycle and $\oint \frac{dE}{dt} dt$ is the energy dissipated over one cycle.

For systems with $\omega > n$, the rotational acceleration $\dot{\omega}_T$ is to first order in e for both the primary and the secondary, respectively:

$$\dot{\omega}_{T,p} = -\frac{15k_p\omega_d^2q^2}{4Qa^6} \quad \dot{\omega}_{T,s} = -\frac{15k_s\omega_d^2}{4Qa^6} \quad (2.2)$$

where $\omega_d = (4\pi G\rho/3)^{1/2}$ is the surface disruption spin limit for a sphere, G is the gravitational constant, and a is the semi-major axis measured in primary radii R_p (Murray and Dermott, 2000). If $\omega < n$ the sign is opposite, and when $\omega = n$ there is no longer any tidal damping to first order in e . This process is often referred to as tidal locking of the satellite and will occur unless the YORP acceleration of the secondary is greater than the tidal rotational damping.

The tidal rotational acceleration of the primary is a factor of q^2 smaller than the secondary, if they have the same tidal Love numbers. The tidal-BYORP equilibrium theory presented later in this study suggests that the tidal Love number $k \propto R^{-1}$. In this case the factor is $q^{7/3}$. This strong dependence on mass ratio is why systems with high mass ratios can synchronize on similar timescales while low mass ratio systems cannot. It is important to note that this factor of $q^{7/3}$ is different than the $q^{2/3}$ for YORP rotational acceleration. For instance, if the secondary of a system has nearly equal YORP and tidal torques, the primary will be dominated by the YORP torque.

2.2.2 The tidal YORP coefficient

It is useful to quantify the tidal acceleration in terms of a tidal YORP coefficient Y_t . This coefficient can be calculated from the current binary parameters of a systems and estimates of the tidal parameters and then compared to the range of possible YORP coefficients. The tidal YORP coefficient for the primary and secondary, respectively, is:

$$Y_{t,p} = \frac{15\pi k_p \omega_d^2 \rho R_p^2 q^2}{2QH_\odot a^6} \quad Y_{t,s} = \frac{15\pi k_p \omega_d^2 \rho R_p^2 q^{2/3}}{2QH_\odot a^6} \quad (2.3)$$

The tidal YORP coefficient of the primary is a factor of $q^{5/3}$ smaller than the tidal YORP coefficient for the secondary using the tidal-BYORP equilibrium theory for the tidal Love number.

If the YORP coefficient of a body is less than the tidal YORP coefficient, then that body will synchronize. If the YORP coefficient is greater than the body will rotational accelerate away from synchronization towards rotational fission. Using the tidal-BYORP equilibrium theory and assuming a typical BYORP coefficient of 10^{-2} , which is consistent with the estimate from 1999 KW₄ (McMahon and Scheeres, 2010a) and the results in the third study of this thesis, an estimate for the tidal parameters can be made. Since the tidal Love number and the tidal quality number are degenerate in this problem, we devise that their ratio is:

$$\frac{k}{Q} = 4 \times 10^{-6} \left(\frac{1 \text{ km}}{R} \right) \quad (2.4)$$

where R is the radius of the body.

Using this tidal theory and the known binary parameters shown in Table 2.1, the tidal YORP coefficients for each primary and secondary can be calculated. The big caveat is that the current semi-major axis is not necessarily the only semi-major axis, the system has occupied. Particularly if the system is currently synchronous, then the gravity gradient due to a permanent bulge or non-spherical figure would prevent the YORP torque from de-synchronizing the system at a new semi-major axis. Therefore, systems that have undergone significant semi-major axis evolution due to the BYORP effect which requires synchronization may now have evolved to a semi-major axis where the tidal YORP coefficient is very small.

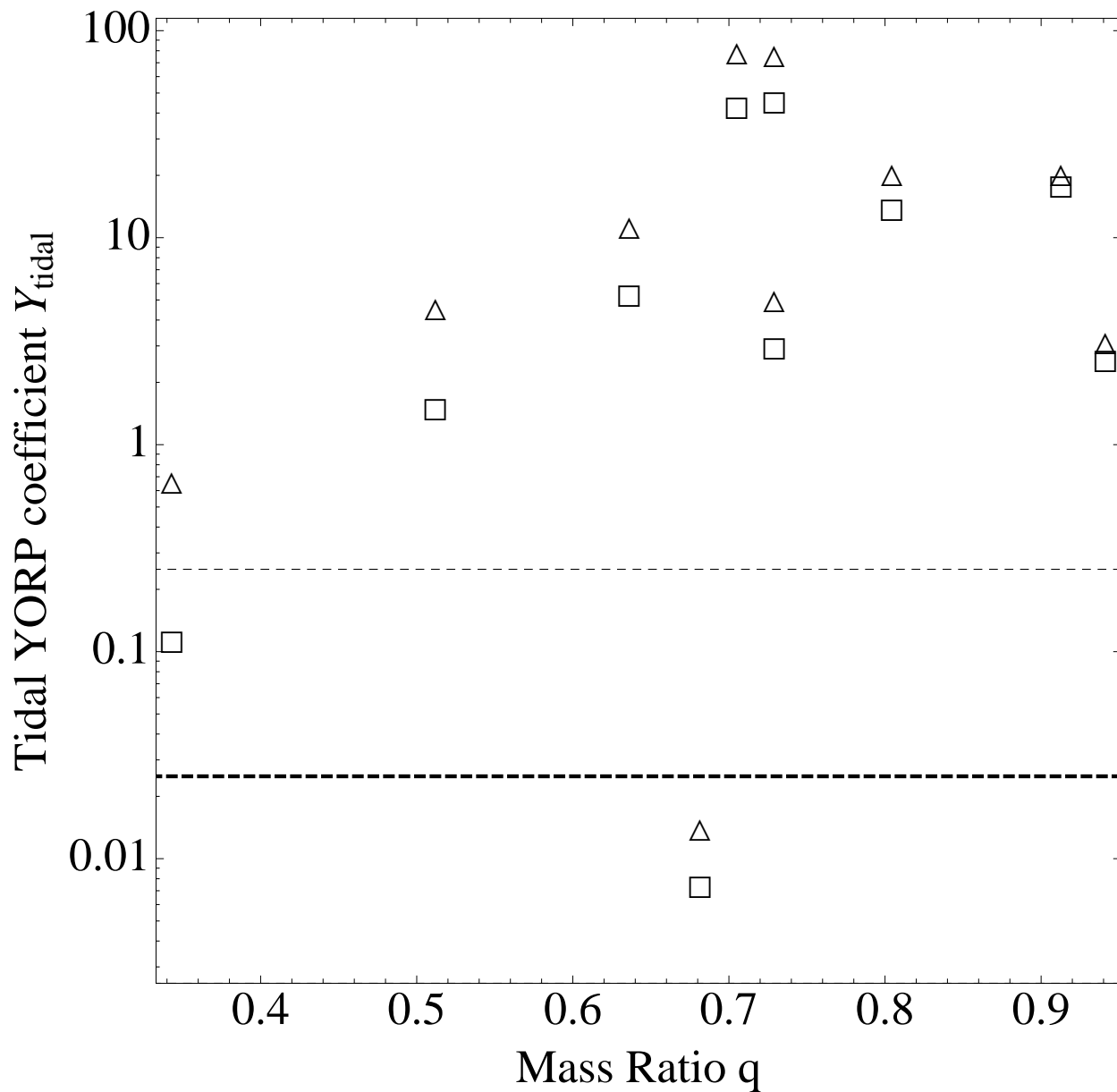


Figure 2.2: The tidal YORP coefficients for each of the 10 doubly synchronous binary systems as a function of mass ratio (to spread them out and make them identifiable). The primaries are marked with squares and the secondaries are marked with triangles. Dashed lines at 0.25, 0.025 and 0.0025 demarcate, a plausible range for the YORP coefficient.

The doubly synchronous population is a good example of a population that we theoretically predict to have undergone significant BYORP evolution. Even so, 8 of 10 systems (809 Lundia, 854 Frostia, 1089 Tama, 1139 Atami, 1313 Berna, 2478 Tokai, 4492 Debussy and 69230 Hermes) have tidal YORP coefficients for both binary members that are significantly larger than any plausible YORP coefficients. These are shown in Figure 2.2. Both members of these systems should be tidally dominated and they are. The remaining two systems may represent special cases. The secondary of 7369 Gavrilin has a significantly large tidal YORP coefficient but the primary has a large but not necessarily implausible coefficient. It could be that the primary of Gavrilin has a low YORP coefficient or a YORP coefficient in the direction of synchronization. 4951 Iwamoto is a more peculiar case, both members have low tidal YORP coefficients and this would suggest that the YORP effect should dominate and the bodies not be synchronous unless the YORP torque is in the direction of synchronization. It is also possible that the BYORP effect is expanding the mutual orbit of Iwamoto and Gavrilin, and this expansion has weakened tides relative to the YORP effect, which is independent of the mutual orbit. The YORP effect is not strong enough to overcome the gradient until the system has expanded to much larger semi-major axes often larger than the Hill radius. This is shown at the very end of this study.

The singly synchronous binary population is proposed to be in a tidal-BYORP equilibrium, which keeps these systems at similar semi-major axes as when the systems stabilized after rotational fission, which is shown in the previous study in this thesis. As shown in Figure 2.3, Every synchronous binary system (1338 Duponta, 2044 Wirt, 2131 Mayall, 3309 Brorfelde, 5477 Holmes, 6084 Bascom, 9069 Hovland, 17260 (2000 JQ₅₈), 65803 Didymos, 137170 (1999 HF₁), 175706 (1996 FG₃), 276049 (2002 CE₂₆), 2005 NB₇, 31345 (1998 PG), 66063 1998 RO₁, 66391 (1999 KW₄), 7088 Ishtar, 76818 (2000 RG₇₉, and 85938 (1999 DJ₄)) except 185851 (2000 DP₁₀₇) has a secondary with a very high tidal YORP coefficient and a secondary with a tidal YORP coefficient comparable to the plausible ranges of the YORP coefficient or lower, which is consistent with synchronization of the secondary and YORP acceleration of the primary or very slow rotational acceleration of the primary. All of these primaries are rapidly rotating and many are observed to be prograde, which

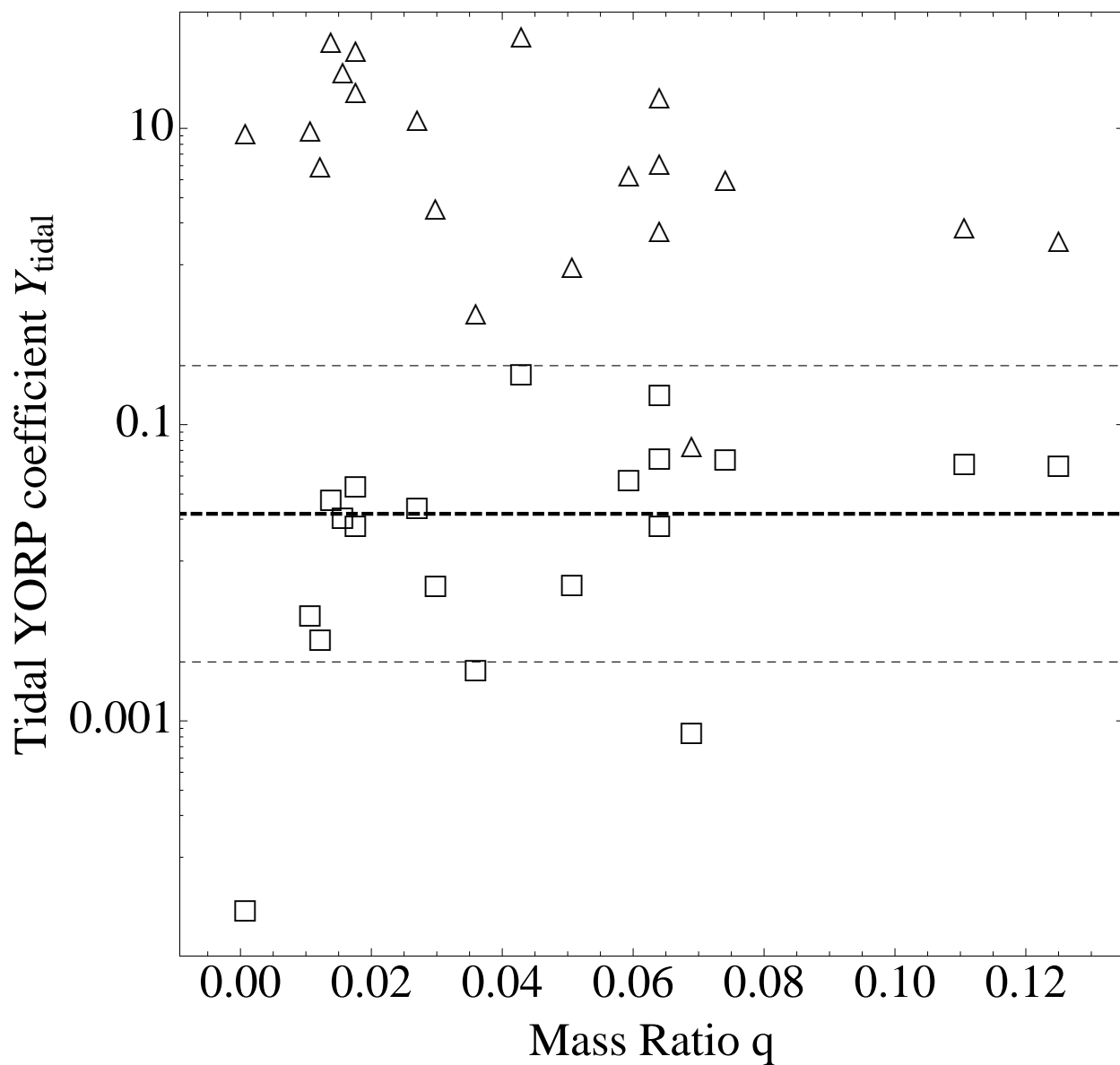


Figure 2.3: The tidal YORP coefficients for each of the 20 singly synchronous binary systems as a function of mass ratio (to spread them out and make them identifiable). The primaries are marked with squares and the secondaries are marked with triangles. Dashed lines at 0.25, 0.025 and 0.0025 demarcate, a plausible range for the YORP coefficient.

may be a result of the Golubov and Krugly (2012) YORP torque. The one exception, 185851, is notable because it also is an outlier when discussing the tidal-BYORP equilibrium below. It's large semi-major axis is out-of-character for a singly synchronous binary system in the equilibrium, however it may be not in the equilibrium and expanding due to the BYORP effect on the synchronous secondary. If this is so, it is a good candidate for the direct detection of the BYORP effect since the other singly synchronous systems are likely in the equilibrium.

In the next section of this thesis, it is proposed that wide asynchronous binary population has undergone synchronization and BYORP evolution but also de-synchronization at a larger semi-major axis due to an adiabatic invariance. At their current semi-major axes all (1509 Esclangona, 32039 (2000 JO₂₃, and 1998 ST₂₇) but 1717 Arlon have significantly small tidal YORP coefficients and Arlon has a small tidal YORP coefficient. This is shown in Figure 2.4. Since typical YORP coefficients exceed these values, the spin states of the primary and secondary of these systems are controlled by the YORP effect. The rapid rotation of the primary may be controlled by the Golubov and Krugly (2012) YORP torque similar to the singly synchronous binary population, and the secondary having just de-synchronized due the adiabatic invariance is now rotationally accelerating due to the YORP effect.

The tidal YORP coefficients for each primary of the tight asynchronous binary population is significantly small compared to the plausible range of YORP coefficients. However, the tight asynchronous binary population may be divided into two categories according to the tidal YORP coefficients of the secondaries as shown in Figure 2.5. The first population consists of four members (35107 (1991 VH₁), 162000 (1990 OS), 164121 (2003 YT₁), and 2004 DC) and share the property of having secondary tidal YORP coefficients within or near the plausible range of YORP coefficients. After formation the secondaries of these systems are locked in close race between tides and the YORP effect. Eventually the YORP effect may drive the secondary to rotational fission creating a chaotic triple system that may stabilize or de-stabilize into something else. If tides are slightly stronger the system will eventually drive the system to synchronization but may do so on a timescale much longer than a typical tidal timescale.

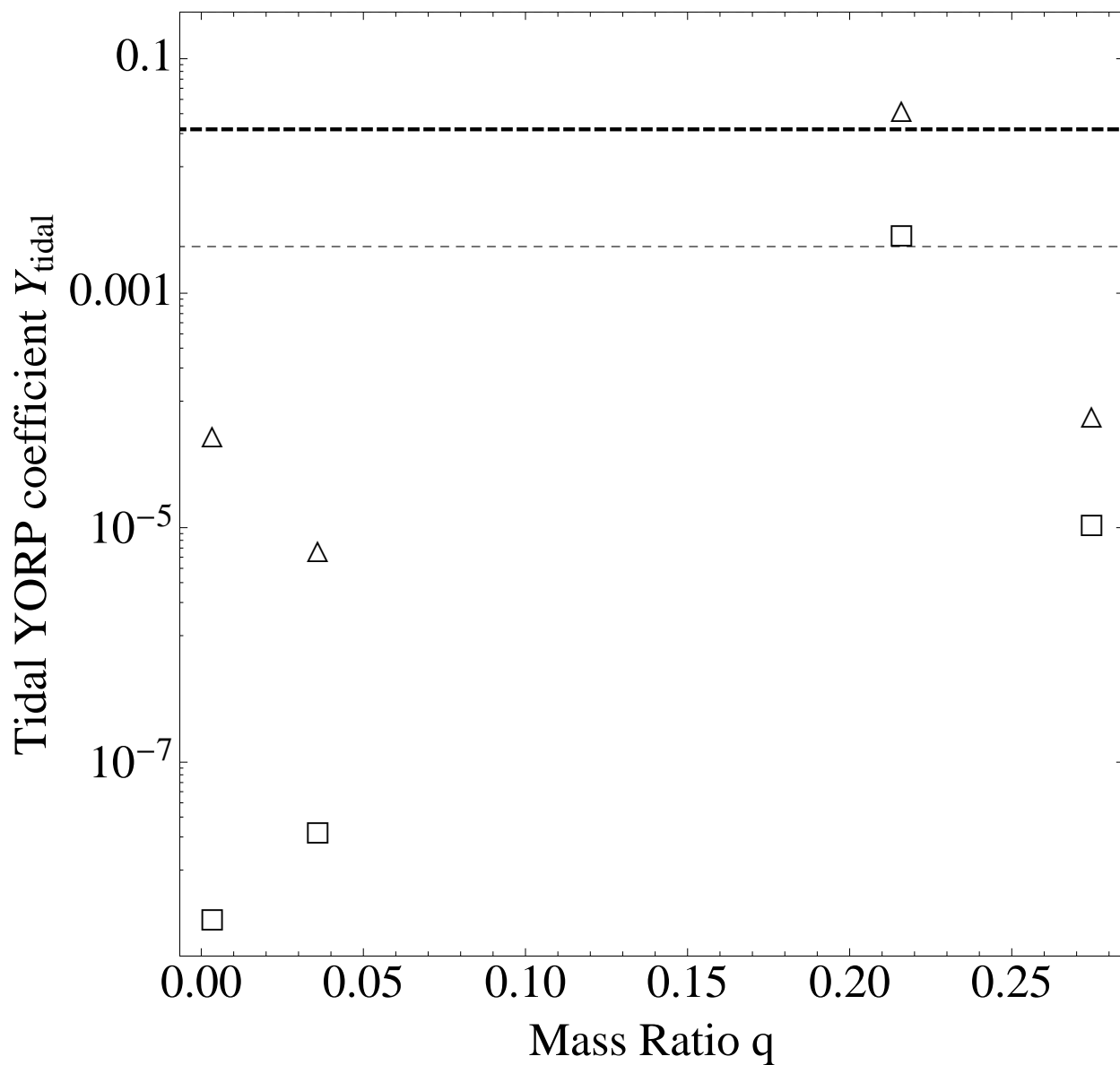


Figure 2.4: The tidal YORP coefficients for each of the 4 wide asynchronous binary systems as a function of mass ratio (to spread them out and make them identifiable). The primaries are marked with squares and the secondaries are marked with triangles. Dashed lines at 0.25, 0.025 and 0.0025 demarcate, a plausible range for the YORP coefficient.

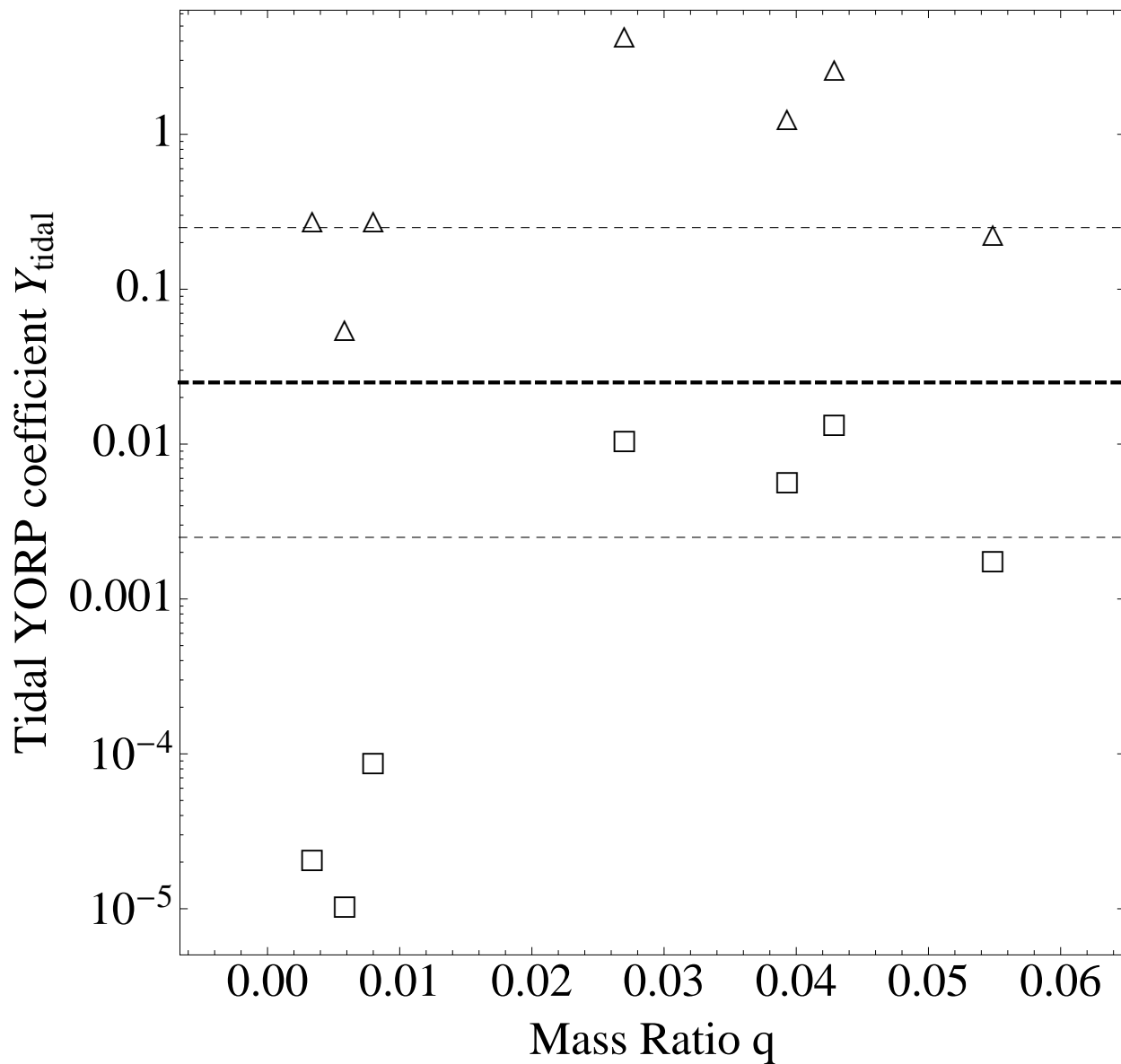


Figure 2.5: The tidal YORP coefficients for each of the 7 tight asynchronous binary systems as a function of mass ratio (to spread them out and make them identifiable). The primaries are marked with squares and the secondaries are marked with triangles. Dashed lines at 0.25, 0.025 and 0.0025 demarcate, a plausible range for the YORP coefficient.

An example using the parameters for 1991 VH₁ is shown in Figure 2.6. The strength of the YORP coefficient is changed to demonstrate different behaviors including assistance and resistance to tidal synchronization. If a secondary of a newly created binary system has a YORP torque that is aligned with the tidal torque then the system will synchronize faster, whereas if the YORP torque is anti-aligned with the tidal torque then two scenarios can occur. If the YORP coefficient is smaller than the tidal YORP coefficient, then the system will still synchronize but it will take longer. If the YORP coefficient is larger than the tidal YORP coefficient, then the system will not synchronize and may eventually rotationally fission. The first category of tight asynchronous binaries may represent systems where the YORP torque and the tidal torque are anti-aligned but nearly of the same magnitude creating long-lasting asynchronous binary systems.

The second category of wide asynchronous binary systems includes 5381 Sekhmet, 16635 (1993 QO) and 2577 Litva. These systems are also shown in Figure 2.5, but they have secondary tidal YORP coefficients significantly larger than the range of plausible YORP coefficients. This is consistent with these systems being relatively young or having experienced a planetary flyby in the recent past. A note, 5381 Sekhmet may already be synchronous, the radar observation that measured the spin rate of the secondary is consistent with synchronous given the uncertainties (Howell, personal communication). 2577 Litva is in the Main Belt asteroid population and so is only consistent with recent binary formation from rotational fission.

Fang and Margot (2012) found that planetary flybys that pass within 10 planetary radii typically grow the mutual orbit and de-synchronize the secondary. They also found that for many near-Earth asteroid binary systems this occurs on a timescale of ~ 1 Myrs. Since synchronization timescales are $\sim 100kyrs$, then for every 10 near-Earth asteroid binaries, 1 system recovering from a planetary flyby induced synchronization is expected. This is consistent with the two large tidal YORP coefficient systems that are tight asynchronous binaries from a population of 18 near-Earth asteroid binary systems.

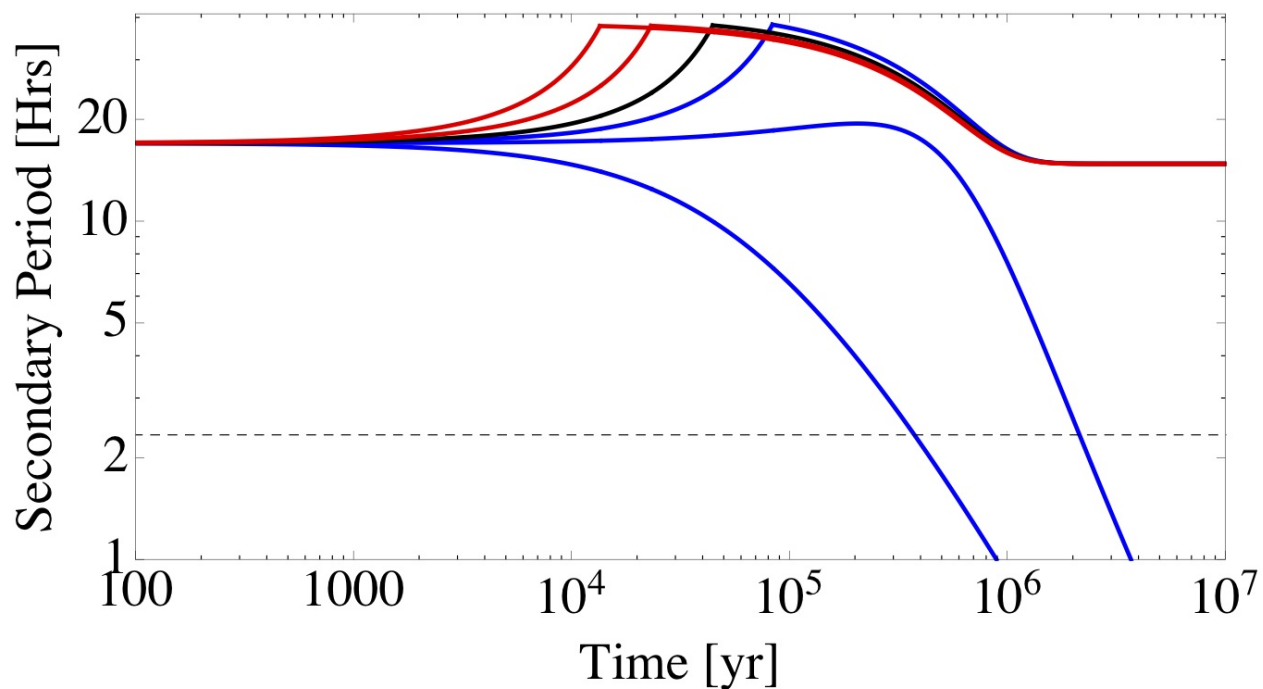


Figure 2.6: The spin period evolution of a 1991 VH₁-like system given different YORP coefficients. The red lines indicate negative YORP coefficients that assist the tidal torques towards synchronizing the system, the black line is no YORP torque, and the blue lines are positive YORP torques resisting tidal synchronization. The cusp occurs at synchronization, because the BYORP effect is contractive for this system and drives it towards a tidal-BYORP equilibrium. The time along the x-axis is logarithmic.

2.2.3 Application to systems with unknown status

Out of 41 known binary systems, comparing the strengths of the tidal and YORP torques correctly predicts 92% of them. Since this technique appears so powerful, we can use it to make predictions for systems who have yet to be classified according to rotation state morphology because of a lack of knowledge about the secondary rotation period but who have been observed well enough to determine their tidal YORP coefficients Y_{tidal} , which are plotted in Figure 2.7.

Using the rules as above for the stronger condition for each morphology, we can predict that (617) Patroclus and (6708) Bobbievaile are most likely doubly synchronous, that (121) Hermione, (1453) Fennia, (15268) Wendelinefroger, (1830) Pogson, 2005 AB, 2006 GY2, (2006) Polonskaya, 2007 DT103, (2121) Sevastopol, (22) Kalliope, (2577) Litva, (26471) 2000 AS152, (2754) Efimov, (34706) 2001 OP83, (3673) Levy, (3749) Balam, (3782) Celle, (3868) Mendoza, (4607) Seilandfarm, (4786) Tatianina, (5407) 1992 AX, (6244) Okamoto, (7225) Huntress, (8116) Jeanperrin, (87) Sylvia, (88710) 2001 SL9, (9260) Edwardolson, (9617) Grahamchapman, and (99913) 1997 CZ5 are most likely synchronous, and (17246) 2000 GL74, (22899) 1999 TO14, (379) Huenna, and (4674) Pauling are most likely asynchronous. When we use the weaker condition as given above for each morphology, systems may fall into two or even three possible categories. (10208) 1997 QN1, (107) Camilla, (130) Elektra, (162000) 1990 OS, (164121) 2003 YT1, 1994 AW1, (283) Emma, (3073) Kursk, (32008) 2000 HM53, (3671) Dionysus, (45) Eugenia and (762) Pulcova may be either synchronous or asynchronous and (11264) Claudiomaccone, (3703) Volkonskaya, (4029) Bridges, (5481) Kiuchi, (5899) Jedicke, (5905) Johnson, (6265) 1985 TW3 and (8373) Stephengould may be doubly synchronous or synchronous. Only 2000 UG11 defies prediction with both members having tidal YORP coefficients that fall within the plausible range. These predictions may be useful in planning future observation campaigns and when considering evolutionary paths.

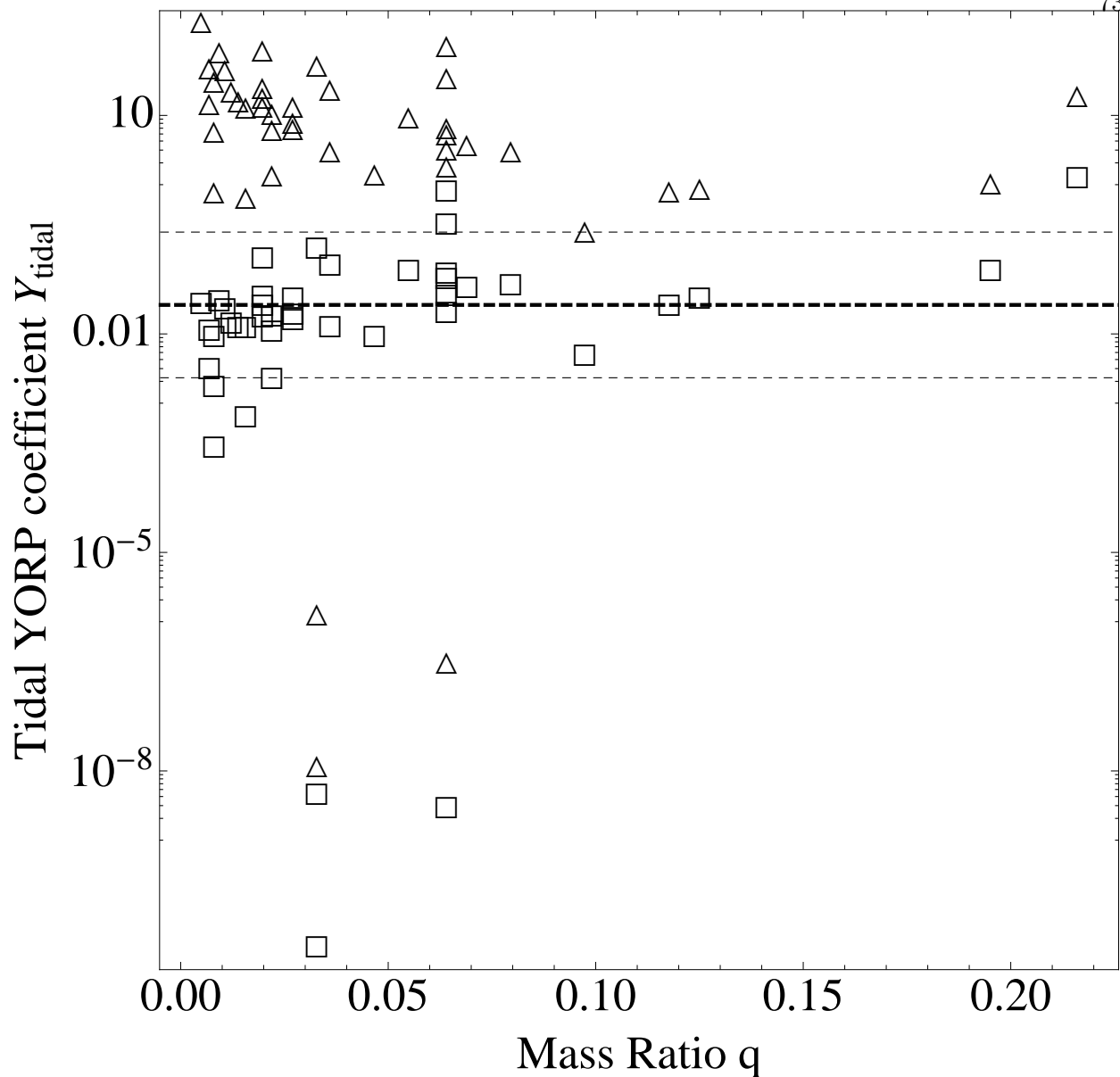


Figure 2.7: The tidal YORP coefficients for each of the 43 unknown asynchronous binary systems as a function of mass ratio (to spread them out and make them identifiable). The primaries are marked with squares and the secondaries are marked with triangles. Dashed lines at 0.25, 0.025 and 0.0025 demarcate, a plausible range for the YORP coefficient.

2.3 Synchronous Asteroid Evolution

As has been mentioned in the previous study of this thesis, the members of high mass ratio systems synchronize on similar timescales due to their similar sizes. These systems then evolve

according to the BYORP effect. Since the BYORP effect acts independently on both members, the torques can add to drive the system apart to the Hill radius and become an asteroid pair or together to become a contact binary. If the two BYORP torques are anti-aligned, then the system may persist as it moves slowly towards one of those end states. High mass ratio systems are not numerous in the near-Earth asteroid population and their evolution appears to be simplified because either tides are operating or the BYORP effect is operating, but not both at once.

Low mass ratio systems are more numerous and only the secondary is likely to synchronize, which is likely to happen first according to the tidal theory (Goldreich and Sari, 2009) and the theory developed in the preceding section. After the secondary has been tidally locked, the system will evolve due to both tides and the BYORP effect, which is not active when the secondary is asynchronous. In the next few sections, both tidal evolution, BYORP evolution and their joint evolution are discussed in the context of singly synchronous binary systems. Joint evolution is dictated by the alignment or anti-alignment of the two torques. Each of these situations is described in detail: Joint expansive evolution and joint opposing evolution. Joint expansive evolution leads to more asteroid pairs but perhaps also the wide asynchronous binary population. Joint opposing evolution leads to the tidal-BYORP equilibrium and the most numerous singly synchronous binary population.

2.3.1 Tidal Evolution

Tidal evolution continues after synchronization of the secondary. The strongest tides are those raised by the secondary onto the primary, but there also tides associated with an eccentric orbit that are raised on both bodies as well as tides from the primary onto the secondary libration state. These last tides on the free libration state of the secondary do not secularly evolve the orbit because the tidal bulge switches directions on the body. As tides dissipate energy from the rotation state of the primary, the semi-major axis and the eccentricity of the mutual orbit change over time. Only after the rotation period of the primary is synchronous with the mutual orbital period (doubly synchronous) and the orbit is circularized as well will binary systems not experience any

tidal evolution.

When the system is singly synchronous, tides raised on the primary by the secondary cause the semi-major axis to expand. From the first order theory, the semi-major axis time rate of change due to tides is:

$$\dot{a}_T = 3 \frac{k_p}{Q} \left(\frac{\omega_d}{a^{11/2}} \right) q \sqrt{1+q} \quad (2.5)$$

where a is the semi-major axis measured in primary radii R_p , k_p is the tidal Love number of the primary, $\omega_d = (4\pi G\rho/3)^{1/2}$ is the surface disruption spin limit for a sphere, and G is the gravitational constant (Murray and Dermott, 2000). Due to the fast rotation of the primary compared to the mean motion, tidal evolution always expands the semi-major axis of the binary system.

Tides raised on the primary by the secondary cause the eccentricity to grow, while tides raised on the secondary by the primary cause eccentricity to damp. From the first order theory, the tidal eccentricity time rate of change due to tides is:

$$\dot{e}_T = \frac{57k_p q^{1/3} - 84k_s}{8Q} \left(\frac{\omega_d e}{a^{13/2}} \right) q^{2/3} \sqrt{1+q} \quad (2.6)$$

where e is the eccentricity and k_s is the tidal Love number of the secondary (Murray and Dermott, 2000). Tidal evolution can cause excitation or damping of the eccentricity depending on the system mass ratio and the tidal Love numbers of each component.

There are two developed theories for the internal structure of asteroids: “monolith” and “rubble pile.” Evidence that asteroids have a “rubble pile” internal structure rather than a “monolithic” interior includes: the Hayabusa mission to Itokawa showing no obvious impact craters and the appearance of a structure made entirely from shattered fragments of different size scales (Fujiwara et al., 2006), numerical modeling of collisions of asteroids (Michel et al., 2001), mass and volume measurements from the NEAR Shoemaker flyby of Mathilde (Yeomans et al., 1997) and radar observations of 1999 KW₄ (Ostro et al., 2006) showing mean densities that are lower than their constitutive elements, the rotational speed limit period (~ 2.2 hours) observed amongst asteroids with diameters larger than ~ 200 m, which corresponds to the critical disruption spin rate

of a self-gravitating, strengthless body (Pravec and Harris, 2007), and that rotational fission of strengthless bodies is responsible for the asteroid pair population (Pravec et al., 2010). All of this evidence suggests that a “rubble pile” internal structure is a more realistic assessment than a “monolith” internal structure, however for completeness we will consider both theories. The two theories become distinct when assessing the functional form of the tidal Love number.

The dimensionless rigidity of the body $\tilde{\mu}$, which can be thought of as the ratio of the fluid strain to the elastic strain, can be used to define the tidal Love number: $k = 1.5/(1 + \tilde{\mu}) \approx 1.5/\tilde{\mu}$, this approximation is true when the fluid strain dominates the elastic strain (Goldreich and Sari, 2009). According to the canonical “monolith” theory the dimensionless rigidity has the form $\tilde{\mu} = 19\mu/(2\omega_d^2\rho R^2)$, where μ is the rigidity of the body. To first order, the tidal Love number for a “monolith” depends on the size of the body as $k_M \propto R^2$.

Goldreich and Sari (2009) developed an alternative “rubble pile” tidal Love number theory by studying how introducing voids increases the stress across contact areas. The dimensionless rigidity of a “rubble pile” is smaller than that of a “monolith” of the same size. Using conceptual and dimensional arguments, Goldreich and Sari (2009) determine that the “rubble pile” dimensionless rigidity should scale as $\tilde{\mu}_R \gtrsim (\tilde{\mu}/\epsilon_Y)^{1/2}$ where ϵ_Y is the yield strain. To first order, the tidal Love number for a “rubble pile” depends on the size of the body as $k_R \propto R$. The observational results which will be discussed at the end of this chapter suggest that the “rubble pile” tidal Love number law is $k_R \propto 1/R$. All of these theories will be explored in later sections.

2.3.2 BYORP Evolution

The BYORP effect is the summation of radiative effects on a synchronous secondary (Ćuk and Burns, 2005). McMahon and Scheeres (2010b) using averaging theory showed that this effect secularly evolves both the semi-major axis and the eccentricity, because radiative forces acting on asymmetries in the shape of the secondary create torques on the mutual orbit that persist after averaging over the mutual orbit, the heliocentric orbit, and the precession of the node. To first order, the evolution of the semi-major axis and the eccentricity only depends upon a single

constant term B that represents the averaged acceleration in the direction parallel to the motion of the secondary (McMahon and Scheeres, 2010a). The BYORP coefficient B depends only on the shape of the secondary, and can be thought of as a ratio relating the asymmetric area, on which the average force of the BYORP effect acts, to the total area. A symmetric body—a sphere or an ellipsoid—has a value: $B = 0$. The BYORP coefficient has a maximum magnitude: $B = 2$ in either direction, but commonly has a small value: $B \sim 10^{-3}$. The BYORP effect can either expand or shrink the semi-major axis, with the sign of the eccentricity evolution always opposite that of the semi-major axis evolution. From the first order theory, the evolution of the semi-major axis and eccentricity is:

$$\dot{a}_B = \pm \frac{3H_\odot B}{2\pi} \left(\frac{a^{3/2}}{\omega_d \rho R_p^2} \right) \frac{\sqrt{1+q}}{q^{1/3}} \quad (2.7)$$

$$\dot{e}_B = \mp \frac{3H_\odot B}{8\pi} \left(\frac{a^{1/2} e}{\omega_d \rho R_p^2} \right) \frac{\sqrt{1+q}}{q^{1/3}} \quad (2.8)$$

where $H_\odot = (2/3)F_\odot/(a_\odot^2 \sqrt{1-e_\odot^2})$, F_\odot is the solar radiation constant, and a_\odot and e_\odot are the heliocentric semi-major axis and eccentricity (McMahon and Scheeres, 2010a).

2.3.3 Joint Evolution

Synchronous binary asteroids will evolve under the influence of both tides and BYORP. There are two scenarios: joint expansive evolution and joint opposing evolution depending on the direction of the BYORP torque, which nominally has an equal chance of pointing in either direction. Both tides and the BYORP effect can change the energy of the system over time, and the BYORP effect can also change the system angular momentum. It is convenient to define a parameter A , which compares the strengths of these two effects on the semi-major axis of the system, and E which does the same for the eccentricity:

$$A = \frac{|\dot{a}_T|}{|\dot{a}_B|} = \frac{2\pi\omega_d^2 \rho k_p R_p^2 q^{4/3}}{BH_\odot Q a^7} \quad (2.9)$$

$$E = \frac{|\dot{e}_T|}{|\dot{e}_B|} = \frac{|19 - 28K|}{2} A \quad (2.10)$$

where $K = k_s/(k_p q^{1/3})$ is an important tidal Love number relation. For the “monolith” model $k \propto R^2$, so $K = q^{1/3}$, for the Goldreich and Sari (2009) “rubble pile” model $k \propto R$, so $K = 1$, and for the observation tidal-BYORP equilibrium theory $k \propto R^{1-}$ and so $K = q^{-2/3}$. If $A < 1$ then the BYORP effect dominates semi-major axis evolution, $A > 1$ then tides dominate the semi-major axis evolution, and if $A = 1$ then the two are balanced and the system semi-major axis will not evolve via either effect. Which effect dominates eccentricity is shown similarly by E .

2.4 Joint Expansive Evolution

During joint expansive evolution, both effects are growing the semi-major axis. Tides are removing energy by spinning down the primary and transferring angular momentum from the primary spin to the orbit, while the BYORP effect is directly adding both energy and angular momentum to the orbit. The eccentricity of the mutual orbit can be excited or damped depending on the system mass ratio and the tidal Love numbers of the components. The condition for stability or damping in eccentricity is:

$$\frac{19 - 28K}{2} A \leq 1 \quad (2.11)$$

For “monoliths,” $K = q^{1/3}$ and so low mass ratio systems can have growing eccentricity, if $q < (19/28)^3$ and $A > 2/(19 - 28q^{1/3})$. For “rubble pile” systems, $K = 1$ or $K = q^{-2/3}$ and thus the condition is always satisfied, and so the eccentricity of binary asteroids with “rubble pile” internal structures will always damp.

“Rubble pile” asteroids expand due to both tides and the BYORP effect and without some intervening process would do so until the system Hill radius and disrupt. However, there are a number of wide asynchronous binary systems whose origins are a mystery. In the following sections, we propose that these systems are expanding systems that were de-synchronized due to an adiabatic invariance. If the synchronous secondary were to de-synchronize, then the BYORP effect would turn off. Once tides have been significantly weakened and the BYORP effect disengaged, the mutual orbit would become stranded at a large semi-major axis. Furthermore, when the secondary

overcomes the gravity gradient and breaks synchronicity, the YORP effect can begin to change the spin rate of the secondary.

2.4.1 Expansive De-synchronization Hypothesis

The observation that most small near-Earth and Main Belt asteroid binary systems have a rapidly rotating primary is one of the key pieces of evidence that led astronomers to more closely investigate rotational fission as possibly the dominant binary formation mechanism (Margot et al., 2002). Walsh et al. (2008) and Jacobson and Scheeres (2011a) showed that the creation of stable binaries is possible via YORP-induced rotational fission. These newly created binaries are asynchronous with generally members and always the primary rotating rapidly compared to the mutual orbit rate, and these systems were tight with small semi-major axes ($a < 8 R_p$). Goldreich and Sari (2009) showed that synchronization of the secondary is the fastest tidal process and for given estimates of the relevant tidal parameters is quick compared to the dynamical or collisional lifetime of kilometer and sub-kilometer binary systems. Singly synchronous binary systems are the most prevalent small ($R_p < 10$ km), binary asteroid systems (Pravec et al., 2006). But as discussed earlier, not all binary systems fit this pattern. Some are doubly synchronous, both spin periods are equal to the orbit period, due to similar tidal synchronization timescales because of similarities in mass (Jacobson and Scheeres, 2011a). Others are asynchronous, neither spin period is equal to the orbit period. Tight asynchronous binary systems, those which have semi-major axes similar to synchronous binary systems $a < 8 R_p$, are consistent with either new formation from rotational fission or a recent strong planetary perturbations (Jacobson and Scheeres, 2011a; Fang and Margot, 2012).

There also exists a population of wide asynchronous binary systems: 1717 Arlon, 1509 Esclangona, 32039 (2000 JO₂₃) and 1998 ST₂₇. Their properties are listed at the beginning of this study. Each has a rapidly rotating primary consistent with formation from rotational fission but a large semi-major axis. In the cases of 32039 (2000 JO₂₃) or 1509 Esclangona, their semi-major axes greatly exceed those created from models of rotational fission events (Jacobson and Scheeres,

2011a). The spin-orbit coupling responsible for the location of the stable semi-major axis conserves angular momentum resulting in a relationship between the semi-major axis and eccentricity. Systems scattered to semi-major axes of 32 or 54 R_p primary radii would likely have eccentricities very nearly 1, and so would be quickly lost to either collision between the members or system disruption.

Radar observations of 1998 ST₂₇ report a significant eccentricity of at least 0.3 (Benner et al., 2003). The $a-e$ relationship for stable binaries formed from rotational fission shown in Jacobson and Scheeres (2011a) predicts an eccentricity around 0.8 for a separation distance of 16.5 R_p indicating either tidal damping or possibly a different excitation process. Planetary perturbations may be very important for 1998 ST₂₇, which crosses the orbits of Venus, Earth and Mars. However, the three other systems are not planet crossers. The other three objects do not have well constrained mutual orbit eccentricities. The distinctive feature of the four systems specified is a mutual semi-major axis $a > 10 R_p$ primary radii, but they otherwise share characteristics with the rest of the small, low mass ratio of a rapidly rotating primary indicative of formation via rotational fission likely induced by the YORP effect.

In the case of joint expansion, both the BYORP torque and the tidal torque are acting to grow the mutual orbit:

$$\dot{a} = \frac{3k_p\omega_d q\sqrt{1+q}}{Qa^{11/2}} + \frac{3H_\odot B a^{3/2}\sqrt{1+q}}{2\pi\omega_d\rho R_p^2 q^{1/3}} \quad (2.12)$$

where the first term is due to tidal evolution and the second term is due to BYORP evolution (Goldreich and Sari, 2009; McMahon and Scheeres, 2010b). However it can be seen from above that while these torques may be of equal order at a few primary radii, they will be substantially different as the system expands. If the ratio of the BYORP torque to tidal torque is 1 at some semi-major axis and then the system doubles in semi-major axis that ratio becomes ~ 181 . For this reason, we will consider only the BYORP torque in the following analytical treatment. The final results were tested with and without the tidal torque and were unchanged.

As stated above, the synchronicity of the secondary in an expanding mutual orbit may be broken by an adiabatic invariant relationship between the semi-major axis (or mean motion) and the

maximum libration angle of the secondary. In the next section, the adiabatic invariant relationship is derived using a simple model and discussed. Then, since librations of the secondary are subject to tides, a tidal model is developed based on Wisdom (2004) and comparisons are made regarding the libration energy excitation due to orbit expansion and dissipation due to tides. Finally, the results of the theory are applied to the four known wide asynchronous binaries and discussed.

2.4.2 Adiabatic Invariance

We want to study the dynamics of synchronous binary asteroid systems as they expand due to the BYORP effect and tides. Both of these non-conservative effects damp the eccentricity of the mutual orbit and the expansion is very slow compared to the orbital period (i.e. largest mutual orbit period at Hill radius ~ 1 year \ll fastest BYORP predicted expansion timescale ~ 10000 years) (McMahon and Scheeres, 2010b). Tides damp the inclination of the system and the spin and orbit poles of observed synchronous systems are observed to be aligned (Pravec et al., 2012). The primaries of observed synchronous systems are rotating much faster than the orbital period and are observed to be nearly oblate and so well-approximated by spherical potentials as the mutual separation increases (Pravec and Harris, 2007).

2.4.3 Derivation of the Adiabatic Invariance

We will use a simple model of a sphere and a triaxial ellipsoid in a mutual planar orbit (i.e. all spin and orbit poles are aligned). The triaxial ellipsoid is spinning in its relaxed state about the direction of the shortest body semi-axis \hat{z}_s , where \hat{x}_s is the longest body semi-axis direction and \hat{y}_s is the intermediate axis direction. Thus, the secondary moments of inertia are related $I_{sz} = CI_s \geq I_{sy} = BI_s \geq I_{sx} = AI_s$ where $I_s = M_s R_s^2$. The mass ratio is the secondary mass divided by the primary mass $q = M_s/M_p$.

The coordinate tracking the instantaneous separation distance between the centers of mass of the two bodies is r , where r and \dot{r} are measured in primary radii R_p and primary radii per unit time, respectively. The instantaneous rotation of the line between the two mass centers relative to

inertial space is θ and the spin angle of the n th body relative to the line connecting the centers is ϕ_n . Since the potential of the sphere is independent of its orientation, the relative spin angle of the primary sphere ϕ_p does not need to be tracked.

Given these conditions, the system free kinetic and potential energies can be determined from similar equations in Scheeres (2009b):

$$T = \frac{I_s}{2q^{2/3}(1+q)} \times \left[\dot{r}^2 + r^2\dot{\theta}^2 + Cq^{2/3}(1+q) \left(\dot{\theta} + \dot{\phi}_s \right)^2 \right] \quad (2.13)$$

$$V = -\frac{I_s\omega_d^2}{4q^{2/3}r^3} \times \left[4r^2 - q^{2/3}(A+B-2C+3(B-A)\cos 2\phi_s) \right] \quad (2.14)$$

where $\omega_d = \sqrt{4\pi\rho G/3}$ is the surface disruption spin limit for a sphere of density ρ and G is the gravitational constant. The Lagrangian of the system is $L = T - V$, and the three generalized coordinates of the system are the separation distance $q_r = r$, instantaneous rotation of the line connecting the mass centers $q_\theta = \theta$, and the relative spin angle of the secondary to the line connecting the mass centers $q_{\phi_s} = \phi_s$. The related generalized momenta and generalized velocities for each coordinate are determined using the Lagrangian:

$$p_r = \frac{I_s\dot{r}}{q^{2/3}(1+q)} \quad (2.15)$$

$$p_\theta = \frac{I_s r^2 \dot{\theta}}{q^{2/3}(1+q)} + CI_s \left(\dot{\theta} + \dot{\phi}_s \right) \quad (2.16)$$

$$p_{\phi_s} = CI_s \left(\dot{\theta} + \dot{\phi}_s \right) \quad (2.17)$$

From these generalized momenta and the Lagrangian, the Hamiltonian can be determined:

$$H = \frac{p_{\phi_s}^2}{2CI_s} + \frac{q^{2/3}(1+q)}{2I_s} \left[p_r^2 + \frac{(p_\theta - p_{\phi_s})^2}{q_r^2} \right] + V \quad (2.18)$$

The instantaneous equations of motion for the system can be determined from this Hamiltonian, but we can reduce the number of canonical pairs by introducing an integral of motion. From the equations above, it is clear that the coordinate θ is ignorable: $\partial L/\partial\theta = 0$. This is conservation of

angular momentum.

$$K = \frac{\partial L}{\partial \dot{\theta}} = \frac{I_s r^2 \dot{\theta}}{q^{2/3} (1+q)} + C I_s (\dot{\phi}_s + \dot{\theta}) = p_\theta \quad (2.19)$$

The generalized momentum for the relative spin angle of the secondary p_{ϕ_s} can then be expressed solely in terms of its coordinate. The relationship above changes to:

$$p_{\phi_s} = \frac{r^2 C I_s}{r^2 + C q^{2/3} (1+q)} \dot{\phi}_s \quad (2.20)$$

Considering the system that we wish to study, we can make the following approximation. The changes in the instantaneous separation distance δr are very small compared to the instantaneous separation distance $\delta r \ll r$. This means that $\dot{r} \approx 0$. This assumption implies that the orbit is circular so $r \approx a$, where a is the semi-major axis measured in primary radii. The semi-major axis will change over time, but as stated above that change is very slow. In the Hamiltonian system, the generalized momenta $p_r = 0$ and $q_r = a$. Furthermore, the instantaneous rotation of the line between the two mass centers relative to inertial space is the mean motion $\dot{\theta} = n$ when $\delta r \ll r$. This approximation means that Kepler's third law is valid and $a^3 n^2 = \omega_d^2 (1+q)$.

We can now re-express the Hamiltonian introducing a collection of constant terms:

$$H = H_0 + H_1 p_{\phi_s}^2 - H_2 \cos 2q_{\phi_s} \quad (2.21)$$

where

$$H_0 = \frac{I_s \omega_d^2}{a} \left(\frac{A + B - 2C}{4a^2} - \frac{1}{q^{2/3}} \right) - \frac{K^2 q^{2/3} (1+q)}{2I_s (a^2 + C q^{2/3} (1+q))} \quad (2.22)$$

$$H_1 = \frac{a^2 + C q^{2/3} (1+q)}{2C I_s a^2} \quad (2.23)$$

$$H_2 = \frac{3I_s \omega_d^2}{4a^3} (B - A) \quad (2.24)$$

The Hamiltonian equations of motion are:

$$\dot{p}_{\phi_s} = -2H_2 \sin 2q_{\phi_s} \quad (2.25)$$

$$\dot{q}_{\phi_s} = 2H_1 p_{\phi_s} \quad (2.26)$$

For maximum libration angles Φ_s where $\sin 2\Phi_s \approx 2\Phi_s$, the natural libration frequency ω_l is:

$$\begin{aligned}\omega_l &= \sqrt{8H_1H_2} \\ &= n\sqrt{\frac{3S}{1+q}} \left(1 + Ca^{-2}q^{2/3}(1+q)\right)^{1/2}\end{aligned}\quad (2.27)$$

where S is a shape parameter of the secondary determined by the principal moments of inertia $S = (B - A)/C$.

We can identify some features of this system. First, there is a separatrix that divides the motion of the secondary between libration and circulation. The separatrix goes through the equilibrium point at $\phi_s = \pi/2$ and $\dot{\phi}_s = 0$, which corresponds to $q_{\phi_s} = \pi/2$ and $p_{\phi_s} = 0$. The Hamiltonian for the separatrix H_s is:

$$H_s = H_0 + H_2 \quad (2.28)$$

If $H < H_s$ the secondary is librating, if $H > H_s$ circulating, and if $H = H_s$ on the separatrix.

Second, the Hamiltonian can be expressed in terms of the libration angle amplitude of the secondary Φ_s as it librates about $\phi_s = 0$. When the secondary is at the maximum libration angle, the relative spin velocity is $\dot{\phi}_s = 0$ so that the conjugate momentum is $p_{\phi_s} = 0$. Therefore, the Hamiltonian can also be expressed as:

$$H = H_0 - H_2 \cos 2\Phi_s \quad (2.29)$$

Using the equations above, the conjugate momentum of the relative spin angle of the secondary can be re-expressed in terms of the Hamiltonian constant terms, the relative spin angle, and the maximum libration angle:

$$p_{\phi_s} = \sqrt{\frac{H_2}{H_1}} \sqrt{\cos 2\phi_s - \cos 2\Phi_s} \quad (2.30)$$

The action of the system is the integrated phase space for a full cycle of the coordinate: $J_{\phi_s} = \oint p_{\phi_s} dq_{\phi_s}$. The action is an adiabatic invariant, since we are considering very slow orbit expansion due to the BYORP effect relative to both the libration and orbital periods.

$$J_{\phi_s} = 2\sqrt{\frac{2H_2}{H_1}} \sin \Phi_s \int_{-\Phi_s}^{\Phi_s} \sqrt{1 - \frac{\sin^2 \phi_s}{\sin^2 \Phi_s}} d\phi_s \quad (2.31)$$

This can be integrated directly but the result is an incomplete elliptical integral of the second kind. An analytic solution can be found if we substitute the variables: $\sin^2 \chi = \sin^2 \phi_s / \sin^2 \Phi_s$. Then the action is transformed to:

$$J_{\phi_s} = 4\sqrt{\frac{2H_2}{H_1}} \int_0^{\pi/2} \frac{\sin^2 \Phi_s \cos^2 \chi}{\sqrt{1 - \sin^2 \Phi \sin^2 \chi}} d\chi \quad (2.32)$$

The generalized solution $G(k)$ to this integral can be expressed in terms of complete elliptic functions of the first $K(k)$ and second $E(k)$ kind:

$$\begin{aligned} G(k^2) &= \int_0^{\pi/2} \frac{k^2 \cos^2 x}{\sqrt{1 - k^2 \sin^2 x}} dx \\ &= E(k^2) - (1 - k^2) K(k^2) \end{aligned} \quad (2.33)$$

The function $G(\sin^2 \Phi_s)$ can be well by cutting off the expansion of the elliptic function definitions at low order:

$$G(\sin^2 \Phi_s) \approx \frac{\pi}{4} \left(\sin^2 \Phi_s + \frac{\sin^4 \Phi_s}{8} + \frac{3 \sin^6 \Phi_s}{64} \right) \quad (2.34)$$

The adiabatic invariance can be expressed exactly as:

$$J_{\phi_s} = \sqrt{\frac{3S}{1 + Ca^{-2}q^{2/3}(1+q)}} \left(\frac{4CI_s\omega_d}{a^{3/2}} \right) G(\sin^2 \Phi_s) \quad (2.35)$$

This relationship can be used to study the system at two different times (indicated by subscripts):

$$\sqrt{\frac{a_1(a_1^2 + Cq^{2/3}(1+q))}{a_2(a_2^2 + Cq^{2/3}(1+q))}} = \frac{G(\sin^2 \Phi_1)}{G(\sin^2 \Phi_2)} \quad (2.36)$$

These are all low mass ratio systems and while secondaries may be possibly elongated, the second term in both the numerator and the denominator is likely much less than 1. If that term is neglected and we keep only the first order term of the function $G(\sin^2 \Phi_s) \approx (\pi/4) \sin^2 \Phi_s$, then the relationship can be re-expressed as:

$$\frac{a_1^{3/2}}{a_2^{3/2}} = \frac{n_2}{n_1} = \frac{\sin^2 \Phi_1}{\sin^2 \Phi_2} \quad (2.37)$$

Using Kepler's Third Law to convert to mean motion. As the system expands the maximum libration angle increases as well. While the small angle approximation is valid, as the semi-major axis doubles the libration angle amplitude increases by a factor of $2^{3/4} \approx 1.7$.

2.4.4 Onset of Circulation

These relationships between the maximum angle of libration and the mean motion determine when the system may cross the separatrix and the secondary will begin to circulate. This occurs when the maximum angle of libration is $\pi/2$. We set this to occur at time 2. The simpler relationship can be re-arranged to solve for the semi-major axis a_{onset} at which onset of circulation occurs given an initial semi-major axis a_1 and maximum libration angle Φ_1 :

$$a_{\text{onset}} = a_1 \sin^{-4/3} \Phi_1 \quad (2.38)$$

The exact relationship can be expressed analytically but is long and won't be repeated here.

2.4.5 Libration Energy

What are reasonable values for the initial semi-major axis and maximum libration angle? The semi-major axis of the system at synchronization seems a natural choice but the maximum libration angle immediately after synchronization is $\pi/2$. It is only after continued tidal dissipation of the libration of the secondary that the maximum libration angle damps to zero. Tides on the free libration due not secularly evolve the orbit because the tidal bulge oscillates from leading to trailing and so the angular momentum transfer to the orbit averages to zero.

In the next section we determine the energy dissipation rate of the libration state due to tides from the primary. From the previous section we can then determine the rate of change of the maximum libration angle as a function of the adiabatic invariance and the tidal energy dissipation. We can use that information and the characteristics of the known wide asynchronous systems to test this hypothesis.

2.4.6 Derivation of the libration tides

We are searching for the energy dissipated within the rotation state of binary asteroid member in a mutual orbit. To simplify this problem, we will de-couple the system and, for the determination

of the tidal energy dissipation only, treat each body as a sphere.¹ This derivation follows those given in Wisdom (2004, 2008). We repeat material to inform the reader. Both Wisdom papers treat various forced librations and obliquity, we derive the tides for a free libration in a circular orbit below. Deriving these tides for an eccentric orbit requires more than one set of tidal responses due to the multiple forcing frequencies (libration frequency, mean motion, and their harmonics) and is left for future work (MacDonald, 1964).

The energy dissipated within the interior of a homogenous (constant density) body moving through the gravity field of a point mass is the work done on each individual element within the body. The work can be expressed as the dot product of the tidal force on that element of the body \vec{F}_T with the displacement of the element $\delta\vec{x}$ or the instantaneous velocity \vec{v} of the element over an instant of time δt .

$$\delta W_T = \vec{F}_T \cdot \delta\vec{x} = \vec{F}_T \cdot \vec{v} \delta t \quad (2.39)$$

which can be arranged to express a rate of work done on each element.

The tidal force F_T is a negative gradient of the perturbing potential energy V_T , which is the perturbing tidal potential U_T multiplied by the mass of the element $dm = \rho dV$. The expression for the rate of work on each element can be integrated of all volume elements of the body to determine the total rate of change in energy.

$$\dot{E}_T = \iiint_{\text{Body}} \dot{W}_T dV = -\rho \iiint_{\text{Body}} \vec{v} \cdot \nabla U_T dV \quad (2.40)$$

Assuming that the body is incompressible $\nabla \cdot \vec{v} = 0$, then the product rule allows a simple substitution:

$$\nabla (U_T \vec{v}) = \vec{v} \cdot \nabla U_T + U_T \nabla \cdot \vec{v} = \vec{v} \cdot \nabla U_T \quad (2.41)$$

Furthermore, Gauss's theorem can be used to express this volume integral as a surface integral:

$$\dot{E} = -\rho \iiint_{\text{Body}} \nabla (U_T \vec{v}) dV = -\rho \iint_{\text{Body}} U_T \vec{v} \cdot \vec{n} dS \quad (2.42)$$

¹ Arbitrary shapes could be treated for either the potential of the tide raising body if it is expanded in spherical harmonics or the surface of the secondary if it is expanded in surface spherical harmonics. This may be future work.

where dS is the area of the particular surface element and \vec{n} is the normal to that surface.

Love (1948) determined that the radial displacement height Δr of a surface element is related to the delayed tidal potential U'_T because the dissipative response lags the forcing, the acceleration of gravity at the surface g and the displaced Love number $h = 5/3k$, which is the potential Love number:

$$\Delta r = -\frac{hU'_T}{g} \quad (2.43)$$

The rate of change of this displacement is conveniently $\vec{v} \cdot \vec{n}$. The energy dissipation can now be expressed directly as the response of the surface of the body to the tidal potential and its time derivative:

$$\dot{E} = \frac{\rho h}{g} \iint_{\text{Body}} U_T \frac{d}{dt} (U'_T) dS \quad (2.44)$$

The tidal potential U_T is:

$$U_T = -\frac{GM_1 R_2^2}{r^3} P_2(\cos \alpha) \quad (2.45)$$

where M_1 is the mass of the perturbing body, R_2 is the radius of the second perturbed body, r is the distance between the two bodies, P_2 is the second Legendre polynomial, α is the angle at the center of the second perturbed body between the vector from the center of the second body to the first \vec{o} and the vector from the center of the second body and the surface element \vec{s} . The length of each vector is known: $|\vec{o}| = R_2$ and $|\vec{s}| = r$. Using the dot product this angle is easily determined:

$$\vec{o} \cdot \vec{s} = rR_2 \cos \alpha \quad (2.46)$$

The vector from the center of the secondary to the center of the primary \vec{o} in cartesian coordinates is:

$$\vec{o} = (r \cos f, r \sin f, 0) \quad (2.47)$$

with true anomaly f .

The vector from the center of the secondary to a surface element can be decomposed into the motion of the surface of the body relative to the center of the secondary \mathcal{R} (i.e. some rotation

matrix or matrices) and a vector from the center of the secondary to a surface element described by a planetocentric longitude λ and colatitude θ at some initial time:

$$\vec{s}_0 = (R_2 \sin \theta \cos \lambda, R_2 \sin \theta \sin \lambda, R_2 \cos \theta) \quad (2.48)$$

$$\vec{s} = \mathcal{R} \vec{s}_0 \quad (2.49)$$

From these equations, we can determine the tidal potential U_T .

In order to determine the delayed potential, Wisdom (2004) says, “The delayed potential U'_T is found by replacing nt by $nt + \Delta$ in the expression for U_T .” Accordingly, Wisdom (2004, 2008) utilizes the relation $\sin \Delta = 1/Q$ where Δ is the tidal lag angle and the tidal quality number Q is inversely proportional to the tidal frequency.

Some Further Qualification

In other words, this model assumes that there is a constant tidal lag time rather than a constant tidal lag angle and that lag time is $\delta t = \Delta/\omega \sim 1/Q\omega$ where ω is the tidal forcing frequency. In Wisdom (2004, 2008), the tidal forcing frequency is always n or a rational factor of n (e.g. $1/3$), but this does not necessarily have to be the case.

This theory shares the same difficulty as the Mignard (1979, 1980) model where the tidal bulge could potentially wrap around the body. We can determine a condition for this to occur, and make sure that we are safely outside of those bounds. If we set the maximum tidal bulge angle to $\Delta < \pi/2 \sim 1$ before wrapping occurs, then this constrains the tidal quality number to $Q > 1$, which implies that the system must be underdamped in order for the bulge not to wrap. This also limits the tidal lag time $\delta t < 1/\omega \sim P$ where P is the tidal forcing period. Conceptually, this is essentially a superposition condition. If the tidal forcing is considered impulsively, then the tidal response must significantly relax the system before the next forcing.

Advantageously, this relationship between the tidal forcing and response avoids the awkward tidal switching that occurs with a constant tidal lag angle model. This discontinuity, which occurs when the tidal frequency goes through zero, causes the tidal bulge to jump across the body.

2.4.7 Energy Dissipation in a number of systems

We can consider a number of surface motions that the second body could be making, but for now we will only consider free libration. For a circular orbit, the following are appropriate:

$$r^{-1} = a^{-1} \quad \cos f = \cos nt \quad \sin f = \sin nt \quad (2.50)$$

The body is rotating at the rate of the mean anomaly M but the body is librating with a libration frequency ω and an amplitude f . The surface rotation matrix \mathcal{R} is:

$$\mathcal{R} = \begin{pmatrix} \cos(M + \Phi_s \sin \omega_l t) & -\sin(M + \Phi_s \sin \omega_l t) & 0 \\ \sin(M + \Phi_s \sin \omega_l t) & \cos(M + \Phi_s \sin \omega_l t) & 0 \\ 0 & 0 & 1 \end{pmatrix} \quad (2.51)$$

where ω is the libration frequency as before. The rotation matrix is expanded to first order in the libration angle max amplitude. Then the procedure described above is followed. Very little insight is gained by showing the gory algebra. The energy dissipation rate for a librating secondary is:

$$\dot{E} = -\frac{2\pi\Phi_s^2 k_s \rho \omega_l \omega_d^2 q^{5/3} R_p^5}{Qa^6} \quad (2.52)$$

Using the time derivative of the expression for the Hamiltonian of spin-coupled system, this expression can be re-arranged to determine the time rate of change of the maximum libration angle divided by the maximum libration angle:

$$\frac{\dot{\Phi}_s}{\Phi_s} = -\frac{\pi k_s q^{5/3} R_p^{5/3} \rho \omega_l \omega_d^2}{2H_2 Q a^6} \left(\frac{\Phi_s}{\sin \Phi_s \cos \Phi_s} \right) \quad (2.53)$$

where the term in parentheses can be dropped if we assume the small angle approximation.

2.4.8 Libration growth due to BYORP effect

There is a competition between libration energy loss due to tides on the secondary and libration energy gain due to the orbit expansion through the adiabatic invariance. We can determine the libration growth due to the BYORP effect through the adiabatic invariance by taking the time

derivative of the invariance, which is equal to zero, and solving for the same time rate of change of the maximum libration angle divided by the maximum libration angle:

$$\frac{\dot{\Phi}_s}{\Phi_s} = \frac{Cq^{2/3}(1+q) + 3a^2}{4a(Cq^{2/3}(1+q) + a^2)} \dot{a} \left(\frac{\tan \Phi_s}{\Phi_s} \right) \quad (2.54)$$

where the term in parentheses can be dropped if we assume the small angle approximation. For a simpler analytic treatment, we can also drop the $Cq^{2/3}(1+q)$ terms since they are typically less than 1 and much less than a^2 . Numerically, we can calculate the final answer with them in, but they do not change the results substantially.

The BYORP effect is principally responsible for the change in semi-major axis \dot{a} , the libration angle growth can be re-stated simply:

$$\frac{\dot{\Phi}_s}{\Phi_s} = \frac{9H_\odot B a^{1/2} \sqrt{1+q}}{8\pi\omega_d \rho R_p^2 q^{1/3}} \quad (2.55)$$

2.4.9 Comparison to Observation

Using these equations, the semi-major axis at which damping due to tides on the libration state and excitation due to BYORP is:

$$a^\dagger = \left(\frac{16\pi^2 k_s q^2 R_p^7 \rho^2 \omega_d^2}{9QBH_\odot I_s \sqrt{3S(1+q)}} \right)^5 \quad (2.56)$$

This semi-major axis is then transition point from decreasing maximum libration angle to increasing as the secondary expands. For our four wide asynchronous binary systems, these semi-major axes are $26 R_p$ for (1509) Esclangona, $25 R_p$ for (1717) Arlon, $20 R_p$ for (32039) 2000 JO₂₃ and $12 R_p$ for 1998 ST₂₇. These calculations used the known parameters for these systems and the tidal and BYORP values determined by the following sections of this thesis. What's notable about these semi-major axes is that they are not very large or very small, but just about right. Given the large uncertainty in the tidal and BYORP parameters and the fifth root, that uncertainty translates into less than an order of magnitude possible adjustments. It's also notable that the separation distance for Arlon is exterior to its current orbit. It is not clear that the tidal dissipation due to libration would be the same as due to rotation, if less than a^\dagger it could move inside the current orbit of Arlon.

We imagine a scenario where the secondary is synchronized at a^\dagger . The librations start at $\pi/2$ but begin to damp. As they damp, the mutual orbit expands due to the BYORP effect. When the system reaches this transition semi-major axis a^\dagger , the maximum libration angle transitions from shrinking to growing. If the current semi-major axis of the binary system is the semi-major axis at which the onset of circulation occurred then we can determine the necessary maximum libration angle at a^\dagger :

$$\Phi^\dagger = \arcsin\left(\frac{a^\dagger}{a_{onset}}\right)^{3/4} \quad (2.57)$$

For the three wide asynchronous binaries with interior a^\dagger 's, the initial maximum libration angles are 35° for (1509) Esclangona, 44° for (32039) 2000 JO₂₃ and 51° for 1998 ST₂₇. These seem like large libration angles, but these systems may expand to a^\dagger very quickly due to the BYORP effect without having their libration angles damped to below these levels. Since the synchronization semi-major axis is unknown, it is difficult to determine how likely this scenario is.

It's also worth mentioning that the outer satellites of the triple systems 1994 CC and 2001 SN₂₆₃ are also asynchronous. The expansion of the outer member may have allowed primary to undergo a second round of rotational fission creating the triple system that is observed.

Although this process may be more likely than creation from initial conditions, the rarity of this class of binary asteroid speaks to the strength of the BYORP effect and the difficulty of this process. Most expanding synchronous binary asteroid systems likely do make it all the way to the Hill radius and become asteroid pairs. The systems that tighten rather than widen are discussed next.

2.5 Joint Opposing Evolution

Returning to the general case of joint evolution after synchronization, we now study the case where tides are acting to grow the semi-major axis, but the BYORP effect is acting to shrink it. Thus the system evolves towards an equilibrium point, where these two effects balance. An

equilibrium exists for the evolution of the semi-major axis at

$$a^* = \left(\frac{2\pi k_p \omega_d^2 \rho R_p^2 q^{4/3}}{BH_\odot Q} \right)^{1/7} \quad (2.58)$$

This is a stable equilibrium, and regardless of the initial semi-major axis, the system will evolve to this equilibrium point. Tides are still transferring angular momentum to the orbit and removing energy from the system, but now the BYORP effect is removing angular momentum and energy from the system. Interior to the equilibrium semi-major axis, tides dominate and the orbit grows due to the increase of angular momentum to the orbit. Exterior to the equilibrium, the BYORP effect controls the evolution and the orbit shrinks due to the decrease of orbital angular momentum. At the equilibrium the amount of angular momentum removed from the orbit equals the amount tidally transferred into the orbit from the primary, de-spinning it. The torque on the primary is equal in strength to the BYORP torque Γ_B and so the rate of the de-spinning of the primary is:

$$\dot{\omega}_p = -\frac{\Gamma_B}{I_p} = -\frac{15BH_\odot a_p}{8\pi R_p^2 \rho} \quad (2.59)$$

The eccentricity of the mutual orbit can be excited or damped depending on the system mass ratio and the tidal Love numbers of the components. The condition for stable evolution without growth in eccentricity is:

$$\frac{19 - 28K}{2} A \leq -1 \quad (2.60)$$

For “monolith” asteroids, $K = q^{1/3}$ and so it is possible for any mass ratio system to be unstable in eccentricity if $A < 2/(28q^{1/3} - 19)$ and in fact, any system with a mass ratio $q < (19/28)^3 \approx 0.31$ will be unstable regardless of A . At the equilibrium, $A = 1$ and so binaries with “monolith” internal structures will grow in eccentricity if the system mass ratio $q < 27/64 \approx 0.42$. This would exclude the observed synchronous binaries from existing in this equilibrium condition, since they all have mass ratios $q < 0.2$ as shown in Table 2.2. Therefore these systems might enter equilibrium but could not remain there for a long period of time since their eccentricities would continue to grow.

For binary asteroids with “rubble pile” internal structures, $K = 1$ or $K = q^{-2/3}$ depending on the theory, the stability condition is always satisfied, and thus the eccentricity will always be

damped. Thus the observed synchronous binary population can exist in the equilibrium without growth in eccentricity.

2.5.1 Implications for the Synchronous Binary Asteroid Population:

If the observed synchronous population is assumed to be in this joint opposing evolutionary equilibrium state, then $A = 1$ and Eqn. 2.9 is solved for the three unknown quantities (B , Q , and k_p):

$$\frac{BQ}{k_p} = \frac{2\pi\omega_d^2\rho R_p^2 q^{4/3}}{H_\odot a^7} \quad (2.61)$$

Table 2.2 lists and Fig. 2.8 plots BQ/k_p for each of the known synchronous binary systems using observational data (Pravec et al., 2006; Pravec and Harris, 2007). The tidal dissipation number Q is an intensive property that we expect to be similar for all of these bodies, and for small bodies has been estimated to be $Q = 10^2$ (Goldreich and Sari, 2009). The scatter and size dependence in Fig. 2.8 should be from B and k_p , respectively. The BYORP coefficient B does not depend on size; B does depend on the shape of the secondary. Asteroid shapes can vary greatly introducing scatter in the BYORP coefficient. McMahon and Scheeres (2010a) estimate $|B| = 10^{-2}$ from the shape model of the secondary of 1999 KW₄, which does not appear symmetric, and this is consistent with the model developed in the third study in this thesis. The BYORP coefficient may vary over a few orders of magnitude, especially towards smaller values corresponding to secondaries that are more symmetric. The tidal Love number may have a dependance on size, and Goldreich and Sari (2009) predict that the tidal Love number $k_p = 10^{-5}R_p$ for a “rubble pile” internal structure.

In the top plot of Fig. 2.8, the solid line plots a simple theoretical model of BQ/k_p using the estimates of each value from above, so that $BQ/k_p = 10^4 R_p^{-1}$. Fitting the proportionality constant of the Goldreich and Sari (2009) tidal Love number model does not significantly change the results. Dashed lines indicate scatter from the BYORP coefficient (one order of magnitude larger and two orders of magnitude smaller). This model works acceptably well for systems with primary radii $R_p = 2$ km but predicts values too large for systems with much smaller primaries. Deviations away from the model appear to be correlated with primary size, and so this may indicate that the tidal

Asteroid System	a_{\odot} (AU)	e_{\odot}	ρ (g/cc)	q	R_p (km)	a (R_p)	BQ/k_p
(1338) Duponta	2.264	0.113	$2.0_{0.7}^{1.0}$	$0.014_{0.010}^{0.031}$	$3.70_{0.51}^{0.59}$	$4.00_{0.52}^{0.60}$	33287_{29924}^{296172}
(2044) Wirt	2.382	0.341	$2.0_{0.7}^{1.0}$	$0.016_{0.011}^{0.035}$	$3.50_{0.81}^{1.05}$	$4.20_{0.55}^{0.63}$	26098_{23478}^{233865}
(2131) Mayall	1.887	0.111	$2.0_{0.7}^{1.0}$	$0.027_{0.019}^{0.065}$	$3.70_{0.27}^{0.30}$	$4.80_{0.63}^{0.72}$	15759_{14175}^{141055}
(3309) Brorfelde	1.818	0.053	$2.0_{0.7}^{1.0}$	$0.018_{0.012}^{0.039}$	$2.50_{0.58}^{0.75}$	$4.00_{0.52}^{0.60}$	13564_{12201}^{121476}
(5477) 1989 UH2	1.917	0.076	$2.0_{0.7}^{1.0}$	$0.064_{0.045}^{0.147}$	$1.50_{0.24}^{0.28}$	$5.00_{0.65}^{0.75}$	6369_{5729}^{56949}
(6084) Bascom	2.313	0.236	$2.0_{0.7}^{1.0}$	$0.051_{0.035}^{0.110}$	$2.90_{0.52}^{0.64}$	$7.40_{0.97}^{1.11}$	1590_{1429}^{14111}
(7088) Ishtar	1.981	0.390	$2.0_{0.7}^{1.0}$	$0.074_{0.051}^{0.159}$	$0.60_{0.14}^{0.18}$	$4.40_{0.57}^{0.66}$	2989_{2688}^{26623}
(9069) Hovland	1.913	0.118	$2.0_{0.7}^{1.0}$	$0.064_{0.047}^{0.176}$	$1.50_{0.35}^{0.45}$	$5.80_{0.76}^{0.87}$	2235_{2017}^{20728}
(17260) 2000 JQ58	2.204	0.183	$2.0_{0.7}^{1.0}$	$0.018_{0.012}^{0.041}$	$1.60_{0.26}^{0.30}$	$3.60_{0.47}^{0.54}$	16807_{15121}^{150731}
(31345) 1998 PG	2.016	0.391	$2.0_{0.7}^{1.0}$	$0.064_{0.047}^{0.176}$	$0.45_{0.10}^{0.14}$	$3.40_{0.44}^{0.51}$	8703_{7856}^{80712}
(65803) Didymos	1.644	0.384	$2.0_{0.7}^{1.0}$	$0.011_{0.007}^{0.024}$	$0.38_{0.04}^{0.05}$	$3.00_{0.39}^{0.45}$	886_{797}^{7886}
(66063) 1998 RO1	0.991	0.720	$2.0_{0.7}^{1.0}$	$0.111_{0.076}^{0.242}$	$0.40_{0.06}^{0.08}$	$3.60_{0.47}^{0.54}$	1740_{1564}^{15444}
(66391) 1999 KW4	0.642	0.688	$2.0_{0.2}^{0.2}$	$0.036_{0.025}^{0.077}$	$0.64_{0.02}^{0.02}$	$3.98_{0.12}^{0.12}$	217_{193}^{1709}
(76818) 2000 RG79	1.930	0.096	$2.0_{0.7}^{1.0}$	$0.043_{0.029}^{0.093}$	$1.40_{0.17}^{0.20}$	$3.40_{0.44}^{0.51}$	48949_{43976}^{432852}
(85938) 1999 DJ4	1.852	0.483	$2.0_{0.7}^{1.0}$	$0.125_{0.090}^{0.325}$	$0.18_{0.04}^{0.05}$	$4.20_{0.55}^{0.63}$	588_{530}^{5390}
(137170) 1999 HF1	0.819	0.463	$2.0_{0.7}^{1.0}$	$0.012_{0.009}^{0.029}$	$1.75_{0.58}^{0.88}$	$3.40_{0.44}^{0.51}$	2287_{2062}^{20955}
(175706) 1996 FG3	1.054	0.350	$2.0_{0.7}^{1.0}$	$0.030_{0.020}^{0.065}$	$0.75_{0.14}^{0.17}$	$3.80_{0.50}^{0.57}$	1114_{1001}^{9907}
(185851) 2000 DP107	1.366	0.377	$2.0_{0.7}^{1.0}$	$0.069_{0.047}^{0.148}$	$0.40_{0.07}^{0.08}$	$7.20_{0.94}^{1.08}$	18_{17}^{163}
2002 CE26	2.234	0.559	$0.8_{0.2}^{0.3}$	$0.001_{0.001}^{0.002}$	$1.72_{0.18}^{0.20}$	$2.72_{0.31}^{0.35}$	277_{250}^{2582}
2005 NB7	2.044	0.518	$2.0_{0.7}^{1.0}$	$0.064_{0.051}^{0.262}$	$0.25_{0.04}^{0.05}$	$3.60_{0.47}^{0.54}$	1721_{1567}^{17579}

Table 2.2: Properties and calculated BQ/k_p of synchronous binary asteroid systems. Data with 1-sigma uncertainties taken from the July 1, 2011 binary asteroid parameter release from <http://www.asu.cas.cz/~asteroid/binastdata.htm> as compiled by methods and assumptions described in Pravec et al. (2006) and Pravec and Harris (2007).

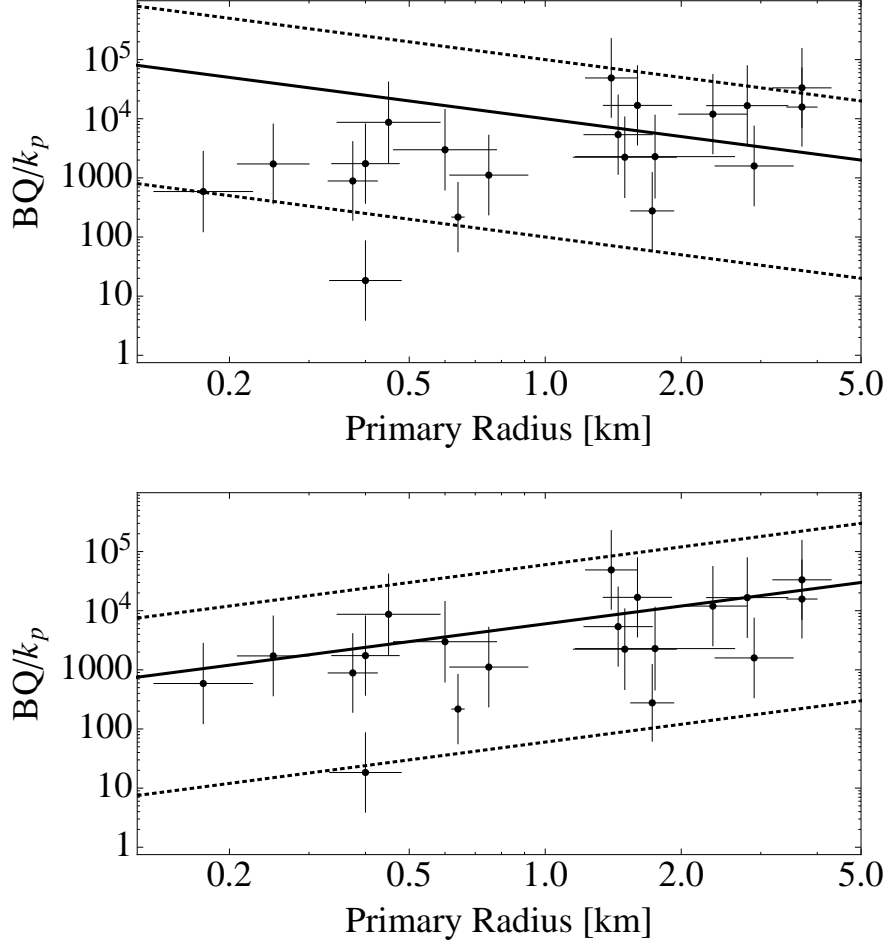


Figure 2.8: BQ/k_p were calculated directly from observed quantities according to equation 2.61 for each known synchronous binary, and plotted as a function of primary radius R_p along with 1-sigma uncertainties (for clarity, the same data are shown in both plots). This data is also listed in Table 1. The solid line in the top plot shows the tidal Love number model from Goldreich and Sari (2009) for asteroids with “rubble pile” internal structures: $k_p = 10^{-5}R_p$. The bottom plot is a fitted model to the data: $k_p = 4 \times 10^{-4}R_p^{-1}$. For both models, the tidal dissipation number $Q = 10^2$ and the BYORP coefficient $B = 10^{-2}$ is assumed. The dashed lines indicate the range of predicted scatter in the model due to the BYORP coefficient (possibly 10 times stronger or 100 times weaker).

Love number has the wrong primary radius dependence.

If a power law is fit to the logarithmic data, then the best fit is $BQ/k_p = 2500R_p$ (shown as the solid line in the bottom plot of Fig. 2.8). Using the same models for B and Q as above, then the tidal Love number dependence is $k_p = 4 \times 10^{-4}R_p^{-1}$. Systems with this tidal Love number

dependence are stable in eccentricity at the long-term equilibrium in semi-major axis. Deviations from this model do not appear to have a dependence on primary radius, and furthermore the scatter follows our expectations for scatter due to the BYORP coefficient, namely that the largest deviations are about two orders below, while most systems fall within an order below and above.

2.5.2 Proposed Equilibrium Hypothesis

Both Čuk (2007) and McMahon and Scheeres (2010a) determined that if the BYORP effect dominates the evolution, then synchronous binaries can disrupt in much less than a million years, this required the hypothesis of frequent binary creation to maintain the observed population. If binaries are trapped in a long-term stable equilibrium, then binary creation could be infrequent. This conclusion is corroborated by evidence that the binary formation process from rotational fission is inefficient, requiring many rotational fission events per asteroid (taking many YORP timescales), in order to create a stable binary system that does not immediately disrupt (Jacobson and Scheeres, 2011a). The observed synchronous binary population may be residing in this equilibrium.

Small, singly synchronous binary asteroids may be residing in a long-term stable equilibrium and they may now provide a method of directly probing an asteroid’s internal structure. They may be inhabiting a long-term stable equilibrium created by the opposing torques from mutual body tides and the binary YORP (BYORP) effect. From the tidal theory, this equilibrium would allow direct study of an asteroid’s geophysics for the first time. To inhabit the equilibria, asteroids cannot have a “monolith” internal structure but must have “rubble pile” interior. The tidal Love number is expected to vary with size, however the data suggest $k \propto R^{-1}$, which is different than the $k_R \propto R$ predicted by the Goldreich and Sari (2009) “rubble pile” theory. This may highlight the difficulty of using a modified continuum theory to model “rubble piles.” This suggests that the tidal Love number theory is incomplete, and future work should examine this closely. In the future, if B is determined through secondary shape modeling for each system, the geophysical parameters k/Q could be assessed directly.

2.5.3 Test of the Hypothesis

Directly measuring the change in mean motion or the period using lightcurves would take more than a century. Instead, the mutual orbit plane of each of these systems crosses the Earth's orbit plane about the Sun. During these epochs it is possible to observe mutual events—either occultations (one member between the observer and the other member) or eclipses (an observable shadow cast on one member by the other). From these mutual events, the relative orientation of the system (i.e. mean anomaly) can be determined accurately (typically to within 3 degrees).

For Keplerian motion, the mean anomaly M grows linearly with time: $M = n(t - t_0)$ where n is the mean motion, t is the time, and t_0 is some reference time. The time derivative of the mean anomaly is $\dot{M} = \dot{n}(t - t_0) + n$ and this can be integrated to show that $M = n(t - t_0) + \frac{1}{2}\dot{n}(t - t_0)^2$ for a system with changing mean motion. Therefore, as the mutual orbit contracts or expands, the mean anomaly will change quadratically in time and the rate of change is related to the orbit expansion or contraction. For convenience define $\Delta M_d = \frac{1}{2}\dot{n}$.

In order to test the hypothesis that these binary systems occupy an orbital equilibrium, an estimate needed to be made for the possible strengths of BYORP or tidal evolution in the absence of an equilibrium. The tidal parameters are so poorly known that no such estimate could be made. However, McMahon and Scheeres (2010a) made an estimate of the strength of the BYORP effect and Pravec and Scheirich (2010) used that estimate to create similar estimates for a subpopulation of seven candidate systems: 7088 Ishtar $\Delta M_d = -0.24$, 65803 Didymos $\Delta M_d = -2.51$, 66063 (1998 RO₁) $\Delta M_d = -3.14$, 88710 (2001 SL₉) $\Delta M_d = -3.27$, 137170 (1999 HF₁) $\Delta M_d = -0.42$, 175706 (1996 FG₃) $\Delta M_d = -0.89$ and 185851 2000 DP₁₀₇ $\Delta M_d = -0.72$. We participated in this campaign to directly detect the BYORP effect or to measure a non-detection below the predicted level. Petr Pravec is the lead collaborator and he maintains a large database of lightcurve observations including observations that go back many years and even decades for each of these systems.

2.5.4 Observation Design and Methods

Using Petr Pravec’s database of binary asteroid lightcurves, most of the proposed systems only needed a couple more apparitions before the predicted growth in the mean anomaly should be detectable. We proposed to both the Apache Point Observatory 3.5-m and the Kitt Peak National Observatory 2.1-m to make many of these measurements. I was awarded 31.5 nights to observe all seven of these objects. We lost half our time to weather (including an entire 4 night run) and never took any data on Didymos.

We need to observe each candidate through at least one mutual event. The absolute time of mutual events cannot be extrapolated from previous apparitions due to uncertainties in the measured orbital periods. Observation of a single, entire mutual event is only guaranteed when we observe $\geq 60\%$ of the orbital period over consecutive nights. We always try to observe both the primary and secondary eclipses, which is only guaranteed when the entire orbital period has been observed; this is not often possible. We propose within each apparition window to maximize our coverage of the orbital period. At least two nights per target are always required to accurately measure the shorter period lightcurve due to the rotational period of the primary asteroid, so that it can be removed as was done in Figure 2.10. For this experiment, exposures times are a balance between properly sampling the orbit of the satellite and reaching the necessary signal to noise. The uncertainty in the mean anomaly must be $\leq 3^\circ$ if its drift is to be detected in as few as three epochs (Pravec and Scheirich, 2010). The sampling rate is constrained directly by the orbital period of the target binary. We track all imaging at half the target’s rate of motion using non-sidereal tracking. The target and the field stars will then be trailed the same and systematic uncertainties in the photometric reduction process is then reduced. The integration time is designed to be long enough in order to properly measure the mutual events and shape variations of the bodies as they rotate. It has been shown empirically that if the photometric errors ≤ 0.02 mag ($S/N \sim 54$), then the mutual events in the binary model can be fit to the data with the mean error of the mean anomaly $\leq 3^\circ$ (Pravec et al., 2006). We used standard time-series differential aperture photometry

in the R-band for all nights following procedures from Warner (2006) using biases, dome flats, twilight flats and dark sky flats. On photometric nights, we observed Landolt standard stars and transferred our relative magnitudes to an absolute scale. This photometric data forms a lightcurve that we can then analyze according to techniques in Pravec et al. (2006).

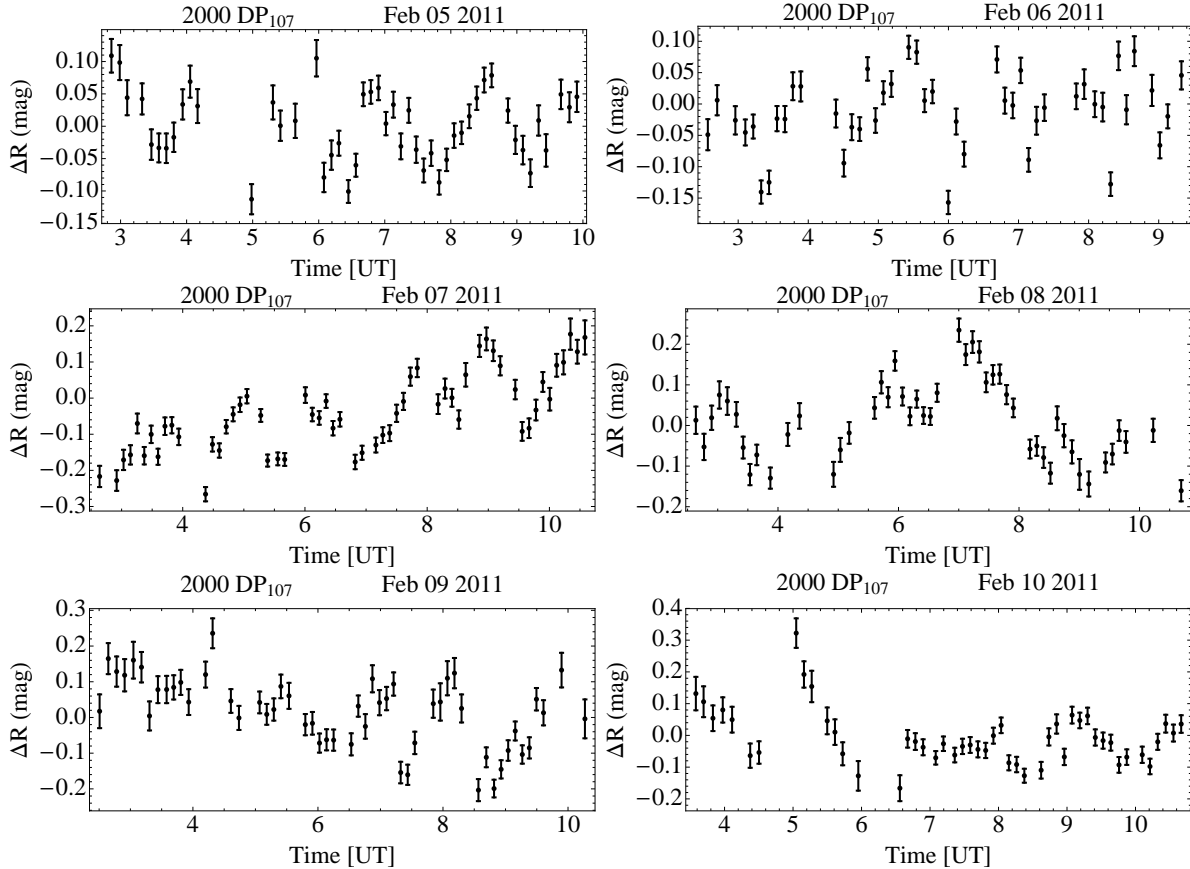


Figure 2.9: Photometric data on a relative magnitude scale for each night taken at the KPNO 2.1-m telescope using the T2KB chip on the CFIM imaging camera. This is the complete lightcurve so there is a 2.8 hour primary rotational period and a 42.2 hour orbital and secondary rotational period mixed with each other. There is also a number of mutual events which are shown in Figure 2.10.

An example of a dataset is shown in Figure 2.9. Petr Scheirich provided a lightcurve analysis tool to deconvolve the primary period, the orbit period and any mutual events. Using this tool on this dataset, we were able to nicely capture the primary period and also capture two occultation mutual events. These are shown in Figure 2.10. This dataset was also used to make predictions for Spitzer observations which are being analyzed by a colleague.

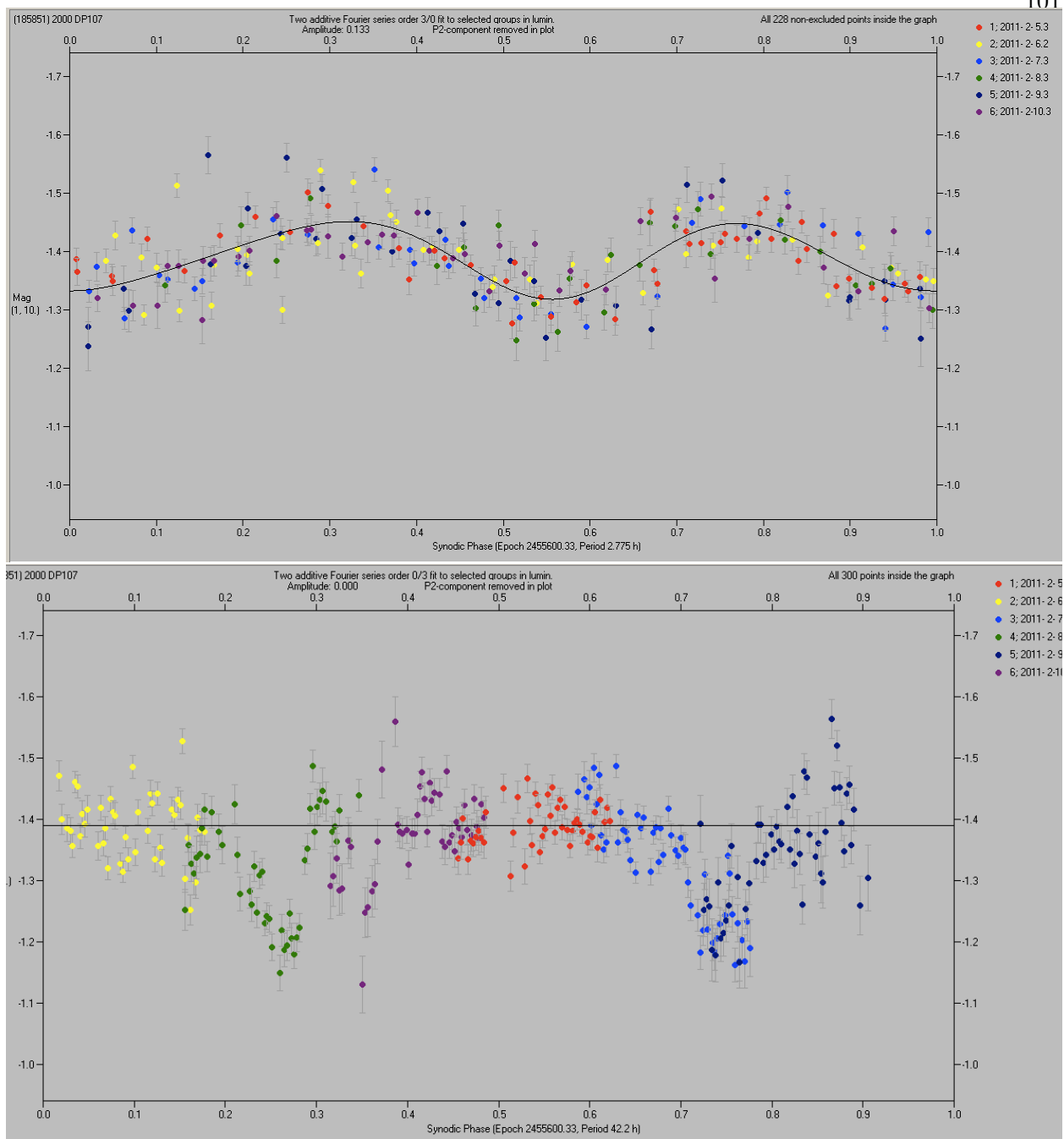


Figure 2.10: From the photometric data in Figure 2.9, the following two lightcurves could be built. The top lightcurve is the primary with a period of 2.775 hours and an amplitude of 0.133 mags. The bottom lightcurve is the remainder. From this remainder lightcurve only it is difficult to see the secondary lightcurve partially because of the noise but also because of the two occultations each of depth 0.2 mags. The colors indicate the date of the observations.

2.5.5 First Results

Six of the seven targets will require at least one more apparition before uncertainty on the growth in the mean anomaly is less than the projected growth due to the BYORP effect. However, for 1996 FG₃, which had the longest baseline of 16 years, we can report no change in the mean anomaly. This is consistent with the tidal-BYORP equilibrium and may be considered a confirmation of the theory.

Photometric data for 1996 FG₃ was taken in 5 apparitions (1996, 1998/1999, 2009, 2010 and 2011) over 16 years. I contributed observations from the APO 3.5-m in 2010 and KPNO 2.1-m in 2011. A selection of the entire dataset is shown in Figure 2.11 with the best fit to the drift in the mean anomaly $\Delta M_d = 0.00$ (-0.1 $+0.18$) with three sigma stated uncertainties. The drift in the mean anomaly was treated as a free parameter to the fit routine similar to the semi-major axis, rotation periods, orbit and spin pole of the primary and the ellipsoidal shapes of the two binary members. The spin pole of the secondary is assumed to be aligned with the orbit pole.

The prediction based on the strength of the BYORP effect alone was $\Delta M_d = -0.89$. To further demonstrate that this signal would have been detected if it existed, Figure 2.12 shows the same data as in Figure 2.11 but the red line indicates the best fit.

Currently this dataset relies on the 1996 observations for much of the reduction in uncertainty due to their long lever arm. Observations to be taken in January 2013 will alleviate this problem. Also radar data from 2011 will be input into the model as well. The combination of these improvements should dramatically reduce the uncertainty. If the result holds with order of magnitude smaller uncertainty and similar results are obtained for the other members of the sample then the tidal-BYORP prediction will be confirmed.

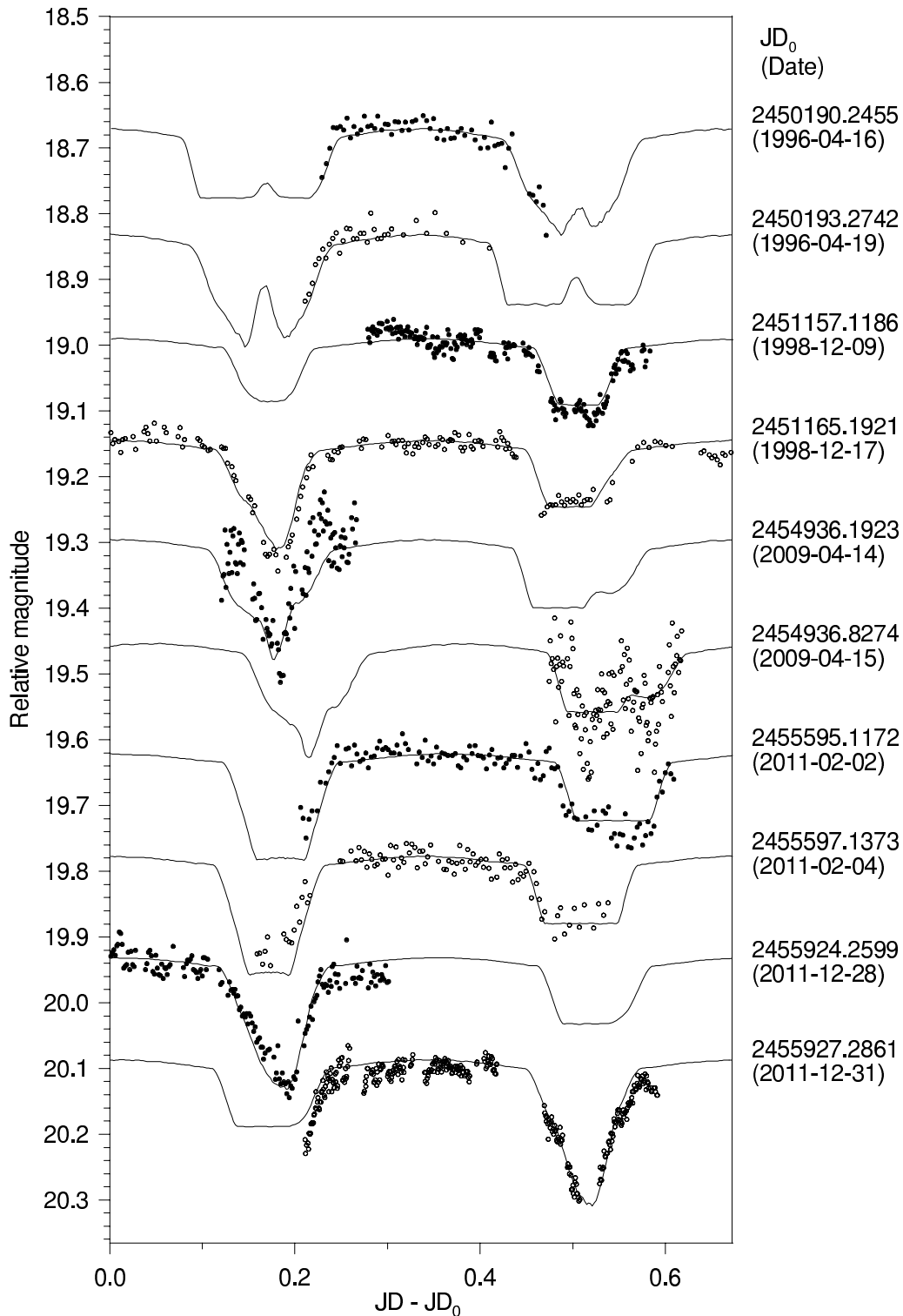


Figure 2.11: Examples of photometric data from each epoch compared to the best fit line.

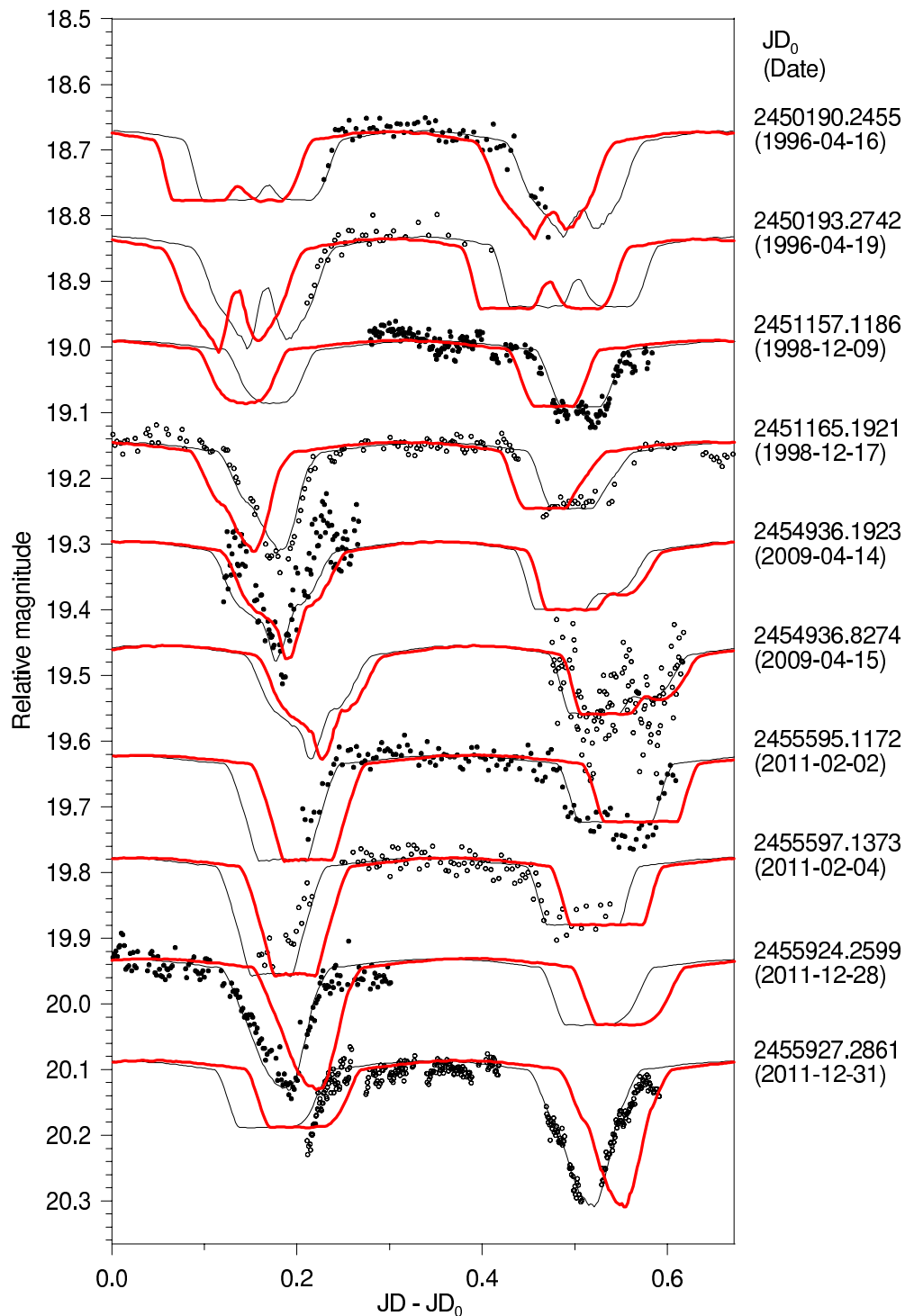


Figure 2.12: Examples of photometric data from each epoch compared to the best fit line in black and a model with a imposed $\Delta M_d = 0.1$ in red (all other model parameters were free).

Chapter 3

Study of the Effects of Rotational Fission on the Main Belt Asteroid Population

3.1 Introduction

The YORP-induced rotational fission hypothesis predicts that the Yarkovsky-O’Keefe-Radzievskii-Paddack (YORP) effect can rotationally accelerate “rubble pile” asteroids until internal stresses within the body due to centrifugal accelerations surpass the gravitational strength holding the “rubble pile” elements in their current configurations. Subsequently these asteroids rotationally fission into mutually orbiting components that can dynamically evolve into the observed binary populations (Rubincam, 2000; Scheeres, 2007a; Walsh et al., 2008; Jacobson and Scheeres, 2011a). Pravec et al. (2010) observationally confirmed that asteroid pairs are the result of YORP-induced rotational fission confirming that rotational fission due to the YORP effect occurs and creates a predicted relationship between the spin states and asteroid pair member sizes (Scheeres, 2007a). Jacobson and Scheeres (2011a,b) numerically modeled the post-rotational fission process determining the outcomes (e.g. asteroid pairs, binaries, triples, etc.) and their likelihoods. After including mutual body tides and the binary YORP (BYORP) effect, Jacobson and Scheeres (2011a,b, 2012) showed how the observed binary systems are natural end-members of these evolutionary processes, however many of these processes occur too quickly (on Solar System timescales) and too infrequently (on human timescales) to be likely observed *in situ*. The observed relative abundances of each end-member, especially binary systems, reflects this process though, and a detailed asteroid population evolution model that can reproduce the observed abundances is a strong test of the YORP-induced rotational fission hypothesis.

The asteroid population evolution model presented herein is designed to provide this test. The model will inform whether the proposed evolutionary mechanisms are sufficient to create the observed populations. Successes and deficiencies in the model will lead to insight regarding the proposed theory, either confirmation or necessitated changes. The asteroid evolution population model is a continuation of Marzari et al. (2011), which studied the spin rate evolution of the Main Belt asteroid (MBA) population including both the YORP effect and collisions and was already an improvement and continuation of earlier studies by Scheeres et al. (2004) and Rossi et al. (2009). Similar to Marzari et al. (2011), we use a Monte Carlo approach to simulate the evolution of 2×10^6 asteroid systems for 4.5×10^9 years. To ease computation, each asteroid system is propagated forward in time individually. The spin state of the asteroid evolves constantly due to the YORP effect and collisions exactly as in Marzari et al. (2011) and summarized in Section 3.2. However, when the rotation rate of an asteroid exceeds a specified spin limit, the asteroid can rotationally fission and form a binary system. These binary systems can persist for short or long intervals of time depending on their initial conditions and characteristics; their survival and lifetimes are determined from a separate set of calculations based on the results of Jacobson and Scheeres (2011a, b). This evolution is described in Section 3.3. Binary asteroid systems may also be destroyed via catastrophic collisions.

Both the single and binary evolution schemes are built from well-developed theory in the literature, and there are very few free parameters within the uncertainties built into the assumptions of the model. For instance, the intrinsic probability of collision for the Main Belt $\langle P_i \rangle$, the fundamental parameter determining the influence of collisions in the model, has been established by the efforts of a series of authors to at least the order of uncertainty inherent in other parts of the asteroid population evolution model (Farinella and Davis, 1992; Bottke Jr et al., 1994; Veder, 1996, 1998). Likewise, the binary evolution model utilizes the the evolutionary flowchart and derived probabilities given in Jacobson and Scheeres (2011a, b).

The binary evolution model does contain two free input parameters that are not well constrained by either observation or current theory. The first is the initial mass ratio fraction F_i ,

which is the ratio of high mass ratio to low mass ratio binary systems created from rotational fission events. This parameter is determined from the interior structure of the rotationally fissioning asteroid and the mechanics of the fission event itself; neither of which are currently known to the significant accuracy needed to generate this number. The second parameter is the mean of the logarithmic normal distribution of BYORP coefficients μ_B . The basic shape and width of the distribution is determined from the equilibrium occupied by the synchronous binary asteroid population. The BYORP coefficient distribution determines the overall binary lifetimes for most systems. As discussed below, there has only been a single estimation of a BYORP coefficient and the shape model used may not have had the necessary accuracy. These parameters are the knobs that will control the output from the asteroid population evolution model.

After evolving the population for the age of the Solar System, we can compare the model population to the observed asteroid population. There are four particular observables that we can compare with our model population: The binary fraction F_B , which is the number of binaries over the total number of asteroid systems, the fast-rotating binary fraction, F_F , which is a more specific comparison of the number of binaries with rapidly rotating primaries to the number of rapidly rotating asteroids, the steady-state mass ratio fraction, which is defined similarly to the initial mass ratio fraction F_i above, and the contact binary fraction F_C , which is the number of contact binaries divided by the entire asteroid population. These comparisons are discussed in Section 3.4, and then a simple log-likelihood model is used to assess which model parameters, F_i and μ_B , are the most likely to match the model population to the observations.

Then in Section 3.5, the asteroid population evolution model, which utilized those most likely model parameters can be used to make predictions regarding the binary and asteroid pair populations. From the success of the binary evolution scheme, we can predict typical binary lifetimes and from assuming a typical asteroid pair observability lifetime, we can predict the fraction of asteroids that we expect to be able to pair in the current Main Belt asteroid population.

3.2 Single Asteroid Evolution

Each asteroid system within the asteroid population evolution model is individually evolved. Similar to Marzari et al. (2011), the asteroid population evolution model utilizes the intrinsic probability for impact $\langle P_i \rangle$ and a projectile size distribution to determine the collision history of each model asteroid. Between collisions, single asteroids undergo YORP evolution potentially rotationally fissioning. The specific conditions for triggering rotational fission and the process itself are discussed in Sections 3.2.3 and 3.2.4. Similarly, binary asteroid systems evolve and age.

Each single asteroid system is characterized by a number of fixed and evolving parameters. The mean radius of the asteroid is drawn from the size distribution given in Bottke Jr et al. (2005b) but limited to be between 50 m and 20 km. From the mean radius and the density $\rho = 2 \text{ g cm}^{-3}$, the mass of the asteroid is determined and each body is assigned a shape from an ellipsoidal semi-axis ratio distribution given by Giblyn et al. (1998). Every asteroid is also assigned a semi-major axis a_{\odot} and eccentricity e_{\odot} from the Main Belt asteroid orbital element distribution. The source of each asteroid is also recorded, whether it was created as an initial asteroid, an outcome of a collision, a member of an asteroid pair (i.e. member of a disrupted binary) or a contact binary (i.e. member of a collapsing high mass ratio binary).

Along with these permanent parameters, the spin rate ω and obliquity ϵ of the asteroid are evolved. The initial spin rate is drawn from a Maxwellian distribution consistent with Fulchignoni et al. (1995) and Donnison and Wiper (1999) and the obliquity is drawn from a flat distribution. The spin rate is evolved according to both the YORP effect and collisions, while the obliquity is only updated due to the impulsive changes in angular momentum delivered by collisions. The spin rate is the important variable for triggering rotational fission, however large changes in the obliquity can change the YORP coefficient significantly, which feedbacks to evolve the spin rate. Cratering (sub-catastrophic) collisions lead to changes in the obliquity and spin rate, which can lead to collision-induced rotational fission and changes to the YORP coefficient due to the new crater (Statler, 2009). Catastrophic collisions lead to destruction of the asteroid.

Asteroid destruction whether through a catastrophic collision, rotational bursting, or destruction of a binary, is a mass transfer from one size asteroid (the progenitor in the case of a binary) into two or more smaller size bodies. Each asteroid in the asteroid population evolution model resides in a logarithmic diameter bin and then the model tracks the mass flow into two or more smaller diameter bins after each destructive event. This mass flow from large asteroids into smaller asteroids is a well-studied phenomena in the context of collisional evolution of an asteroid population (Davis et al., 1979; Bottke Jr et al., 2005a). After a destructive event the asteroid is then replaced with an asteroid from the original diameter bin. This replacement is motivated by the constant flux of material into the original bin from even larger bins, and similar model's have been used in the past (Farinella et al., 1992; Marzari et al., 2011). The asteroid population evolution model does not include a full feedback collisional evolution, but bootstraps itself forward using an already established projectile size distribution and collision frequency as a first estimate from the Sloan Digital Sky Survey (Ivezić et al., 2001). The never before included effects of YORP-induced rotational fission modify the asteroid size distribution (therefore the projectile size distribution) and the collision frequency, but feeding these effects back into the model is a future work. For now, the tracked mass flow from the asteroid population evolution model can be used to determine the first order corrected size distribution due to rotational fission. This method can be viewed as the first step in a long iterative process, but this first iteration already provides valuable insight.

3.2.1 YORP Evolution

In order to calculate the evolution due to the YORP effect, each object is also assigned a non-dimensional YORP coefficient¹ Y from a gaussian distribution with a mean of 0 and a standard deviation of 0.0125 motivated by the measured values of 1862 Apollo (1932 HA) $Y = 0.022$ (Kaasalainen et al., 2007) and 54509 YORP (2005 PH₅) $Y = 0.005$ (Taylor et al., 2007). In Rossi et al. (2009), the results were found to be invariant on the order of the uncertainty of the model to the particular distribution used. The YORP coefficient is re-drawn whenever the obliquity changes

¹ In Rossi et al. (2009); Marzari et al. (2011) the non-dimensional coefficient Y is notated C_Y .

by more than 0.2 rad and evolves according to: $Y' = Y (3 \cos^2 \epsilon - 1) / 2$ for smaller changes in the obliquity due to collisions as in Nesvorný and Vokrouhlický (2008). A similar scheme was utilized in the past (Scheeres, 2007b; Rossi et al., 2009; Marzari et al., 2011).

The YORP effect changes the spin rate $\dot{\omega}$ as:

$$\dot{\omega} = \frac{Y}{2\pi\rho R^2} \left(\frac{F_{\odot}}{a_{\odot}^2 \sqrt{1 - e_{\odot}^2}} \right) \quad (3.1)$$

where $F_{\odot} = 10^{14} \text{ kg km s}^{-2}$ is the solar radiation constant. This is the same as Equation 1 in Marzari et al. (2011) with slightly different notation. If the YORP coefficient $Y > 0$, then the spin rate is accelerating. If uninterrupted by collisions, the spin rate will eventually reach the spin limit, which is described in Section 3.2.3. If the YORP coefficient $Y < 0$, then the spin rate is decelerating and the asteroid may enter a tumbling state. Since this model cannot assess the evolution of this state, an artificial lower spin barrier is enforced. Asteroids have a set maximum spin period limit of 10^5 hours. At this very slow rotation rate the YORP torque switches directions. This is modeled by switching the sign of the YORP coefficient. Collisions often control the spin state of bodies with such low rotation rates since even the smallest projectiles can deliver impulsive torques that are the same order of magnitude as the angular momentum of the target body.

3.2.2 Collisional Evolution

The collisional evolution of each asteroid follows a similar protocol as Marzari et al. (2011). The population of potential impactors is derived from the Sloan Digital Sky Survey size distribution of asteroids (Ivezić et al., 2001) distributed over logarithmic size bins. Using Poisson statistics, the number of collisions and their timing is computed for each asteroid with projectiles from each size bin using the intrinsic probability of collision for the Main Belt $\langle P_i \rangle$ (Farinella and Davis, 1992; Bottke Jr et al., 1994). Each collision is assigned an impact velocity of 5.5 km s^{-1} from Bottke Jr et al. (1994). In order to determine from these parameters the change in spin rate due to each collision, a random geometry is assigned to the collision within the limits of the Main Belt orbital distribution.

Cratering collisions do not appreciably change the mass or size of the target asteroid, but they do change the angular momentum of the asteroid. The angular momentum of the projectile and the target and the geometry of the collision determine the new angular momentum of the cratered asteroid. This new angular momentum vector is used to update both the spin rate and the obliquity. Sub-catastrophic impacts create a random walk in spin rate if there is no significant YORP effect rotational acceleration. After each cratering collision the YORP coefficient Y is newly drawn from the distribution. Statler (2009) showed that newly emplaced craters of a similar scale as the diameter of the asteroid can dramatically change the YORP coefficient. We are only really considering cratering collisions of those scales.

If the collision is too large for a cratering event, then the original asteroid is shattered and a new object is created with the same size but a new initial spin state and YORP coefficient. Shattering collisions are defined as those that deliver specific kinetic energy greater than the critical specific energy of the target, which defined as the energy per unit target mass delivered by the collision required for catastrophic disruption (i.e. such that one-half the mass of the target body escapes).

As mentioned above, the asteroid population evolution model only handles the collision evolution to first order. The intrinsic probability for collision determined by Bottke Jr et al. (1994) is not updated to include the heliocentric dependent changes in the size distribution due to the YORP effect. In order to avoid very large computations, the current model is the first step in a potentially iterative process whereby the collision-only size distribution is used as a good first-hypothesis for generating the collision probabilities. After the new size distribution is established in the asteroid population evolution model, it can be used to generate a new collision probability which can be then inserted back into the asteroid population model, and so on. This iterative process may improve the accuracy of the steady-state size distribution of the asteroid population evolution model, but we leave this to future work with a more sophisticated model. The current first order approximation is consistent with other approximations in the asteroid population evolution model.

3.2.3 Spin Limits

Collisions fracture and catastrophically disrupt asteroids into many coherent elements, which individually retain a “monolithic” internal structure (i.e. lithic material strength properties, meteoritic densities, etc.). Post-impact the relative velocities of these elements do not often exceed the local escape velocity and these elements re-accumulate into new bodies with “rubble pile” internal structures. A “rubble pile” is defined as a collection of gravitationally bound boulders with a distribution of size scales and with very little tensile strength between them (i.e. granular material strength properties, densities below meteoritic due to high porosity, etc.) (Asphaug et al., 2002, for a review). It has been shown numerically that very few collision events are necessary before a “monolithic” progenitor resembles a “rubble pile” (Michel et al., 2001). There is a large body of evidence supporting the determination that small asteroids have “rubble pile” geophysics including measured low bulk densities implying high porosities (Yeomans et al., 1997; Ostro et al., 2006), the resolved surface of Itokawa (Fujiwara et al., 2006), the observed spin limit amongst the asteroid population as shown in Figure 3.1 (Pravec et al., 2007), and evidence that asteroid pairs form from rotational fission events (Pravec et al., 2010).

As an asteroid is rotationally accelerated due to either a continuous YORP torque or sudden collisional torque the centrifugal accelerations increase on each component of the “rubble pile.” These accelerations counter the gravitational accelerations holding each of the components against the others. Scheeres (2009a) showed that for every partitioning of the body in two along “rubble pile” component boundaries, there is a specific rotation rate at which the centrifugal accelerations will exceed the mutual gravity and the two sections will no longer rest against each other but enter into orbit. As the body rotationally accelerates it will reach the slowest of these rotation rates first and it will be along this partitioning that the body rotationally fissions. The smaller of the two sections is now the secondary, and the remainder is the primary, both in orbit about each other. This simple story of rotational fission is complicated by but reaffirmed when the asteroid’s shape is also allowed to evolve (Sánchez and Scheeres, 2012).

Collision-induced rotational fission requires that the combined angular momentum from both precursor bodies and the cratering impact geometry exceeds the critical angular momentum necessary for the body to gravitationally hold itself together against centrifugal accelerations. This is similar to the YORP-induced rotational fission hypothesis described below with three exceptions. Firstly, the collision may significantly change the internal component distribution itself. Secondly, the torque is delivered impulsively. These first two differences are not significant since we are not modeling the internal component distribution nor are we resolving the rotational fission event itself. Thirdly, the new system angular momentum may exceed the critical angular momentum by a measurable amount. Even though an asteroid that undergoes collision-induced rotational fission may be rotationally accelerated past the critical disruption rotation rate, for the purposes of the asteroid population evolution model these events will be treated the same as the YORP-induced rotational fission, which occurs at the critical disruption rotation rate. Consequences of ignoring the excess include overestimating the binary creation rate at the expense of the asteroid pair creation rate.

Since the exact rotational breakup spin rate is a complex function of the internal component distribution, the Monte Carlo asteroid population model utilizes the simple approximation that all “rubble piles” rotationally disrupt at the critical disruption spin limit: $\omega_d = \sqrt{4\pi\rho G/3}$ where ρ is the density and G is the gravitational constant. This approximation requires the system to rotationally accelerate for a longer period of time before undergoing rotational fission. With respect to the YORP timescale for rotational fission, this may accurately reflect delays in rotational fission due to shape evolution.

The theory described in the preceding paragraphs is consistent with the rotational spin limit observed amongst asteroids with diameters larger than 250 m (Pravec et al., 2007). This spin barrier is clearly shown in Figure 3.1, however it is also clear that a fundamental change occurs at an approximate diameter of 250 m. Asteroids with diameters smaller than 250 m cross the barrier and can exceed that spin rate by one or two orders of magnitude. Theoretically, hypotheses for this behavior include given these size scales that cohesive forces can trump the centrifugal forces (Scheeres, 2012; Holsapple, 2007) or that these are the “monolithic” remnants of “rubble

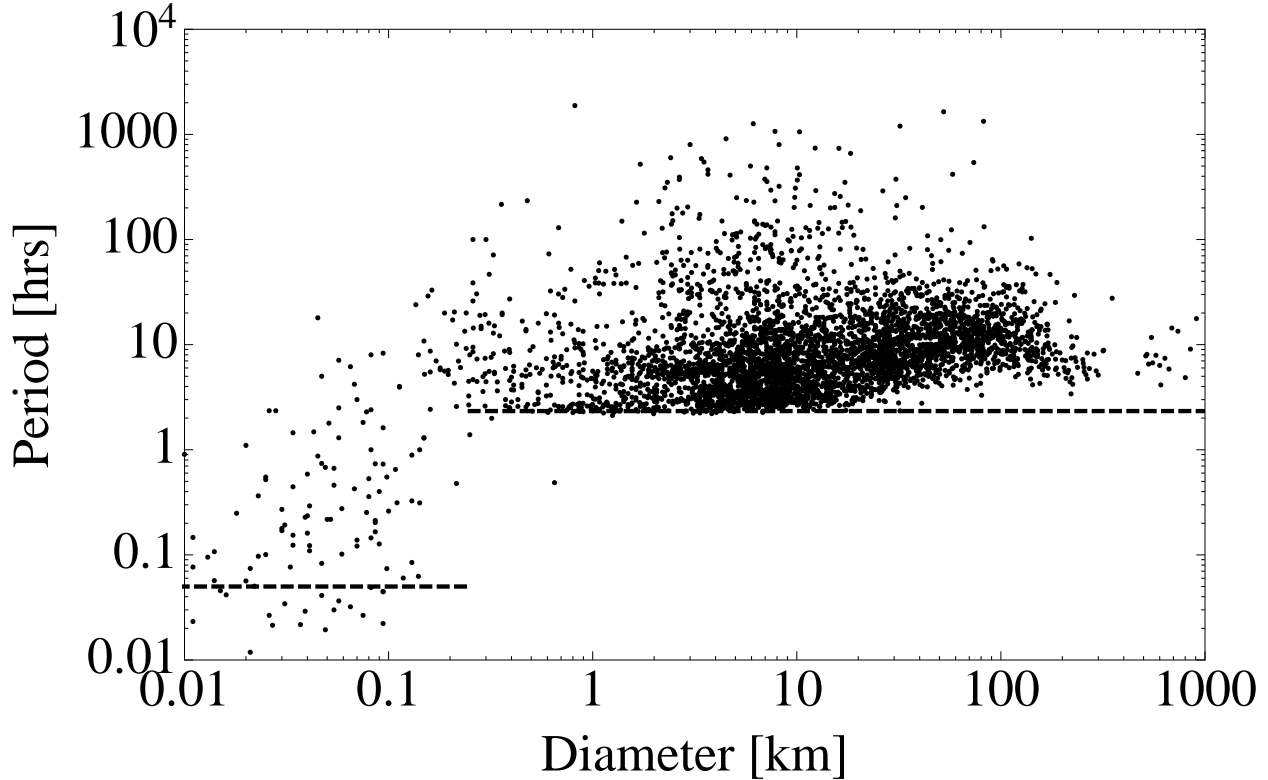


Figure 3.1: Spin period distribution as a function of diameter for near-Earth (NEA), Mars crossing (MCA) and Main Belt (MBA) asteroids as reported in the Asteroid Lightcurve Database (Warner et al., 2009). The dashed lines indicate the critical rotation break-up periods: 2.33 hrs for diameters $D > 250$ m and 0.05 hrs for $D < 250$ m.

pile” progenitors that have undergone multiple YORP induced rotational fissioning (Pravec et al., 2007).

In the asteroid population evolution model, the asteroid population is divided in two diameter bins: $D > 250$ m and $D < 250$ m. Large asteroids ($D > 250$ m) are treated as traditional “rubble piles.” These bodies are given a lower spin period limit that is set by the critical rotational disruption period: $P_d = \sqrt{3\pi/\rho G} \approx 2.33$ hrs where $\rho = 2$ g / cm³ is the density and G is the gravitational constant. Small asteroids ($D < 250$ m) are treated as “monolithic.” Those treated as “monoliths,” whether they are actually monoliths or cohesively bound bodies, only rotationally disrupt at spin periods in excess of 0.05 hours. This period is representative of the maximum

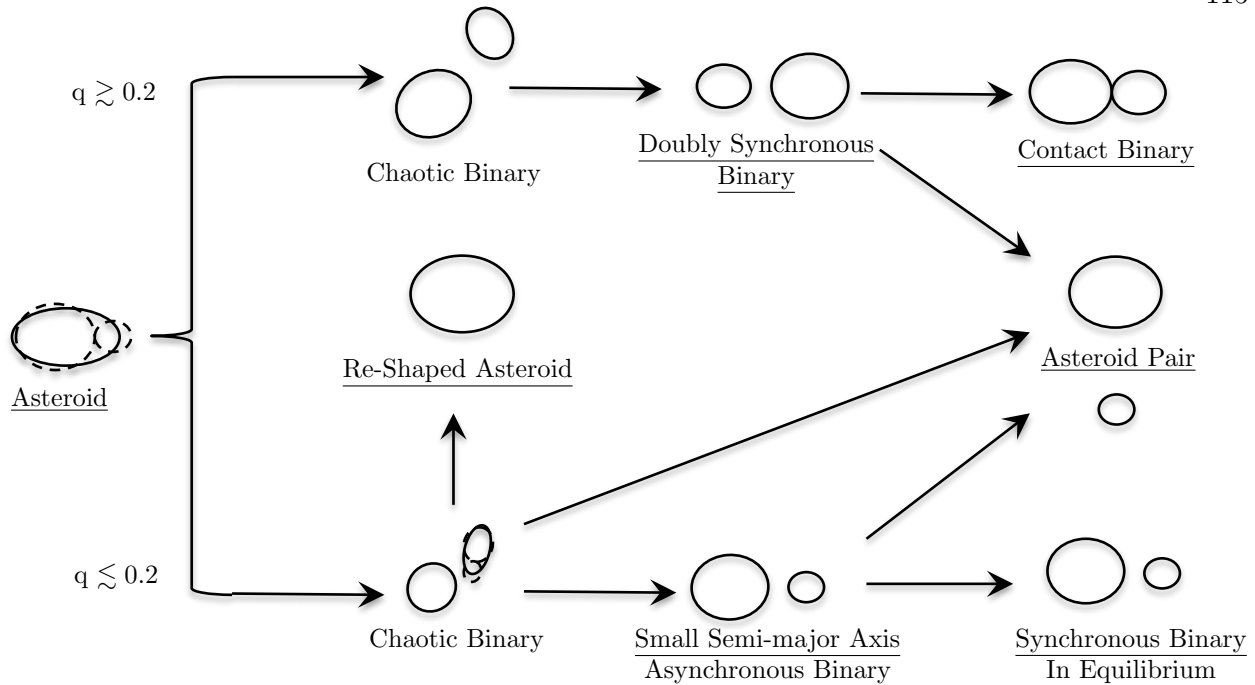


Figure 3.2: Evolutionary tracks for a small asteroid after it has undergone rotational fission according to the theory in Jacobson and Scheeres (2011a) and Jacobson and Scheeres (2011b). Each evolutionary step is indicated by an arrow. Most of this diagram is cycle, since the end states are singles asteroids: re-shaped asteroids, contact binaries or each member of asteroid pairs. Collisions can destroy synchronous binaries in equilibrium. Figure similar to that in Jacobson and Scheeres (2012) but simplified by removing intermediate states and less likely states (e.g. triples).

rotation speeds that small asteroids are observed and was chosen arbitrarily.

3.2.4 Outcomes of Rotational Fission

If the critical spin rate is reached at least once for an asteroid during a timestep, then the asteroid population evolution model simulates a rotational fission event for that asteroid. This can happen when a collision brings the asteroid above the rotational breakup limit or when the rotational breakup period is reached due to YORP acceleration. If the asteroid is in the small diameter regime $D < 250$ m, then the asteroid is rotating super-critically due to internal strength. When this strength fails, the energy released is enough to immediately disrupt the system sending the components on escape trajectories and destroying the asteroid.

If the asteroid is in the large diameter regime $D > 250$ m, then the system rotational fissions

at the critical disruption spin rate. Pravec et al. (2010) observationally showed that these types of events are the progenitors of the observed asteroid pair population. Jacobson and Scheeres (2011a) numerically showed that rotationally fissioned asteroid systems can evolve into a number of different outcomes, as shown in Figure 3.2, but the chaotic nature of the system allows for only a probabilistic determination of the outcome. A binary system formed via rotational fission can temporarily occupy a number of evolutionary morphologies before settling into three enduring states: single, binary and pair. None of these categories are truly permanent since single asteroids can undergo rotational fission forming binaries and pairs, binaries can be disrupted forming pairs or internally collided to make re-shaped asteroids (i.e. singles), and asteroid pairs, which are really sets of single asteroids, can be rotationally fissioned.

Scheeres (2007a) shows that the rotational breakup spin rate is dependent on the mass ratio of the components that will enter into mutual orbit. If a spherical approximation of each component is made, then the rotational breakup spin rate ω_q necessary to fission as a function of mass ratio² q is:

$$\omega_q = \omega_d \sqrt{\frac{1+q}{(1+q^{1/3})^3}} \quad (3.2)$$

where $\omega_d = \sqrt{4\pi\rho G/3}$ is the critical disruption speed, ρ is the density, and G is the gravitational constant. This is the exact solution for two spheres resting on each other with a mass ratio of q rotating about the system maximum moment of inertia. It is important to note, that the asteroid population evolution model utilizes the conservative³, zeroth order approximation that each “rubble pile” asteroid disrupts at the critical disruption speed ω_d . While the mass ratio q does not determine the rotation rate at fission in the asteroid population evolution model, it plays an important role in the determination of the final outcome of rotational fission.

The spherical component model described above demonstrates the important reality that the larger the mass ratio q of the two future binary members the slower the required rotation rate necessary to create the binary system. This slower required rotation rate translates into a small

² Mass of the secondary (smaller) member divided by the mass of the primary (larger) body.

³ It is conservative by requiring longer times to disruption.

initial free energy for the ensuing binary system. The free energy E_f is the energy that is accessible to the different energy reservoirs in the system including the rotation states of each member and the orbit. It does not include the internal binding energy of each object. The free energy is an important quantity because it determines the boundedness of the system. Bound systems have negative free energy, while unbound systems have positive free energy. An unbound binary system implies that the system is capable of disruption but does not imply that the system will disrupt. For the idealized case of two spheres, the free energy can be expressed as:

$$E_f = \frac{2\pi\rho\omega_d^2 R_p^5}{15} \left(\frac{2 - 4q^{\frac{1}{3}} + 6q^{\frac{2}{3}} - 11q + 6q^{\frac{4}{3}} - 4q^{\frac{5}{3}} + 2q^2}{1 + q^{\frac{1}{3}}} \right) \quad (3.3)$$

where R_p is the radius of the primary. For the equation above corresponding to two spheres, the function crosses zero when $q \approx 0.204316$. Similar equations can be written for any two component shapes, but $q \sim 0.2$ remains near the binding energy transition point, and so the model uses this point as a simple approximation. This crossing point divides bound systems with negative energy and mass ratios $q > 0.2$ and unbound systems with positive energy and mass ratios $q < 0.2$. Because of this fundamental difference, high mass ratio $q > 0.2$ and low mass ratio $q < 0.2$ binary systems evolve differently (Scheeres, 2009b; Jacobson and Scheeres, 2011a). Primarily, positive energy low mass ratio systems will chaotically explore orbital phase space until the majority find a disruption trajectory creating an asteroid pair; this evolutionary route is unavailable to high mass ratio systems.

Jacobson and Scheeres (2011a) numerically modeled the evolution of binary asteroids after rotational fission and determined that high and low mass ratio systems evolve along separate tracks that give rise to a different set of outcomes. From these numerical experiments, it was determined that the mass ratio is not necessarily a fixed quantity and may change via a process termed secondary fission. This process is well described in Jacobson and Scheeres (2011a) and has the ability to change the initial mass ratio to a lower value as a binary system evolves. During secondary fission, mass is shed from the secondary either onto the primary or out of the system. This process was only observed numerically to occur with low mass ratio systems. Since it reduces

the mass ratio of low mass ratio systems, no binary systems can evolve across the $q \sim 0.2$ threshold between high and low mass ratio systems. Since these two populations are independent, their long-term evolution will be dealt with separately.

3.2.5 Mass Ratio Fraction

Before describing the possible outcomes and their likelihoods for both high and low mass ratio systems, the relative number of high to low mass ratio systems must be determined. The initial mass ratio of a binary system after rotational fission is determined by the internal component (i.e. “rubble pile” element) distribution of the parent asteroid before rotational fission (Scheeres, 2007a), so it is the distribution of internal structures amongst an ensemble of asteroids that will determine the initial distribution of binary mass ratios. The direct determination of the distribution of mass ratios after rotational fission would perhaps require the gentle and complete disassembly of a number of asteroids into their component pieces understanding their masses, shapes and relative locations, however an approximate understanding of this distribution may soon be available via detailed numerical modeling using discrete element methods (Walsh et al., 2008, 2012; Sánchez and Scheeres, 2011, 2012).

Until then, we can constrain the initial mass ratio fraction F_i that is input in the asteroid population evolution model by comparing the observed steady-state mass ratio fraction to the steady-state fraction output by the model F_q . The steady-state distribution reflects a balance between creation and destruction of binary systems as a function of mass ratio. The mass ratio fraction F is defined as the number of high mass ratio systems divided by the number of low mass ratio systems. The mass ratio fraction is a function of time as high and low mass ratio systems are created and destroyed. The initial mass ratio fraction F_i reflects the distribution of possible internal component distributions of parent asteroids. This initial distribution then evolves into the observed steady-state mass ratio fraction F_q due to the differences between binary creation and destruction timescales in high and low mass ratio systems. The initial mass ratio fraction F_i is an input into the asteroid population evolution model, and the steady-state mass ratio fraction F_q is

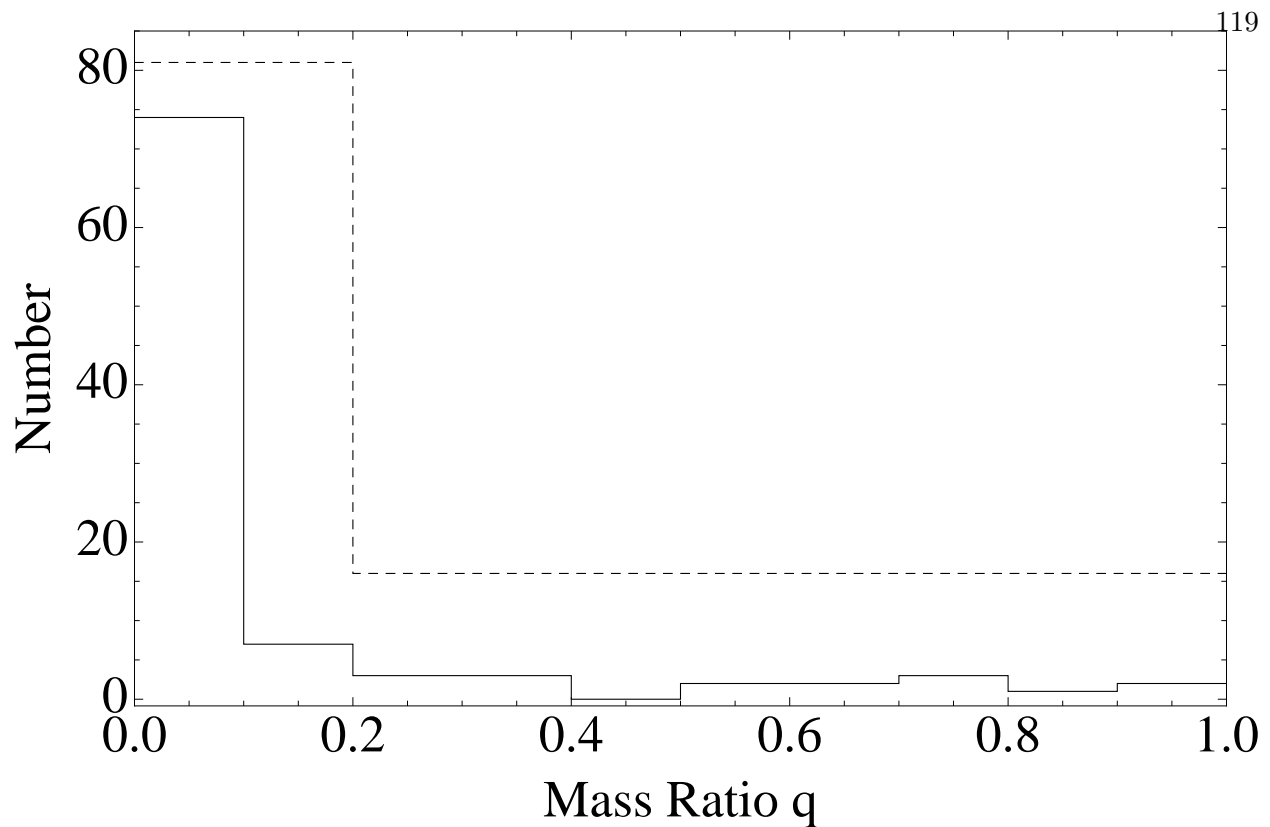


Figure 3.3: Two histograms of the same observed binary distribution as a function of mass ratio. The solid histogram shows the number of binaries in bins of width 0.1 in mass ratio. The dashed histogram simply outlines the number of binaries in the low mass ratio ($0 < q < 0.2$) and the high mass ratio ($0.2 < q < 1$) populations, of which there are 81 and 16 observed binary systems, respectively. The observed binaries are the 97 characterized binaries with small primary diameters $\lesssim 11$ km according to the July 1, 2011 binary asteroid parameter release from <http://www.asu.cas.cz/asteroid/binastdata.htm> as compiled by methods and assumptions described in Pravec et al. (2006) and Pravec et al. (2007).

one of the observable outputs.

This evolution in mass ratio fraction is due only to the creation and destruction of specific binary systems and not due to the possible evolution in mass ratio of those systems, since high mass ratio systems were not observed in numerical models to transform into low mass ratio binaries and vice versa (Jacobson and Scheeres, 2011a). As discussed above, binary systems cannot cross the mass ratio $q \sim 0.2$ boundary between the two regimes via secondary fission. The simplest approximation within each mass ratio regime is to assume that the members are selected from a flat distribution. As is shown in Figure 3.3, this description is imperfect but is an appropriate

assumption, since the asteroid population evolution model is only being used to determine the steady-state mass ratio fraction F_q and not the detailed steady-state mass ratio distribution. In the future, a treatment that includes a more advanced binary evolution model with a more detailed dependence on mass ratio will also need to explore more complex initial mass ratio distributions.

The range of initial mass ratio fractions F_i to be tested in the asteroid population evolution model is motivated by the observed population as shown in Figure 3.3. The observed steady-state mass ratio fraction is $F_q \sim 1/5$, but low mass ratio systems face much steeper odds of surviving as binary systems (8%), as discussed in Section 3.3.1. To examine a broad range of initial conditions and their outcomes: F_i is varied between 32, 16, 8, 4, 2, 1, 1/2, 1/4, 1/8, 1/16, and 1/32. Every time a binary system is created via rotational fission in the asteroid population evolution model, the binary is assigned to either the low or high mass ratio regime, such that $(1 + F_i)^{-1}$ of the time the system is low mass ratio and $1 - (1 + F_i)^{-1}$ of the time it is high mass ratio. This is the first knob in the model; the other knob is the BYORP coefficient distribution.

3.3 Binary Asteroid Evolution

After a rotational fission event, a binary system is formed. Binary systems undergo complex dynamics immediately afterwards (Jacobson and Scheeres, 2011a). If they stabilize, then non-gravitational and tidal torques control the fate of the system. Since this evolution is complex, binary systems are not individually evolved from fission to end state, since this would be computationally expensive. Instead, a lifetime for each system is drawn from a distribution, which has been determined from a separate Monte Carlo model of binary asteroid evolution as described in Section 3.3. Each binary system is placed in a mass ratio bin, low ($q < 0.2$) or high ($q > 0.2$), after formation. These mass ratio bins determine the “instantaneous” survival of the binary system according to Section 3.3.1. If the binary survives, then the binary’s “long-term” evolutionary path is drawn. This is dependent on the assigned mass ratio bin. Each evolutionary path is associated with a binary lifetime distribution, and after a lifetime is drawn from the appropriate distribution, this lifetime is then scaled by the heliocentric orbit of the system and the absolute size of the system

(radius of the primary). The heliocentric semi-major axis and eccentricity remain the same as its rotationally fissioned progenitor. Therefore, each binary system has four permanent parameters: the heliocentric semi-major axis and eccentricity, the mass ratio⁴ and the binary lifetime. The evolved parameter is not the spin rate as in the single asteroid case, but rather the age of the binary. The final outcome of the evolutionary path is also recorded, so that when the binary lifetime is over, the system is replaced with a new asteroid the same size as the progenitor but labeled as either an asteroid pair or a re-shaped asteroid. This evolution may be interrupted by a collision, and this is discussed in Section 3.3.3.

The evolution of a binary asteroid system from rotational fission to a long term stable outcome is deterministic but the evolution is chaotic and only weakly a function of the shape of each body and the mass ratio within each of two distinct dynamical regimes: low and high mass ratio (Jacobson and Scheeres, 2011a). The initial evolution of the spin and orbit states of the system are controlled by dynamical coupling between the spin and orbit by non-Keplerian gravity terms, solar gravitational perturbations, and mutual body tides. This dynamical evolution is quick often finishing in tens of years (Jacobson and Scheeres, 2011a) and much shorter than the 10^6 year timestep in the asteroid population evolution model. Due to the chaotic and swift nature of this evolution it occurs “instantaneously” and probabilistically within the model. After this “instantaneous” evolution, surviving binary systems evolve according to “long-term” binary evolution which is detected by both the BYORP effect and mutual body tides. If the rotational fission event results in the creation of a re-shaped asteroid or an asteroid pair, then these objects are returned to the asteroid population evolution model as single asteroids sharing the same heliocentric orbit properties as their progenitors. If the systems settles into a stable (i.e. long-lasting) binary state, then the binary may exist for many timesteps. According to the theory established in Jacobson and Scheeres (2011b), the longevity of a binary system is determined by mutual body tides, the YORP effect, and the BYORP effect. The BYORP effect is the most important, and can destroy systems in as little as 10^5 years or permanently stabilize them until some exogenic process (e.g.

⁴ The primary radius is determined from the mass ratio and the progenitor radius assuming the same density

planetary flyby) destroys the system (McMahon and Scheeres, 2010a). Upon creation each stable binary is assigned a lifetime that is drawn from a distribution determined by Monte Carlo modeling of binary asteroids. This modeling is explained in Section 3.3.2.2. This allows the preservation of large timesteps within the asteroid population evolution model. At the end of a binary system’s lifetime, the binary disrupts forming a re-shaped asteroid or an asteroid pair similar to the “instantaneous” evolution case. Some binaries do not have endogenic lifetimes, these exist until a collision occurs that is capable of disrupting the mutual orbit or catastrophically destroys one of the binary members. Even binary systems with natural lifetimes can be destroyed via these mechanisms, if they occur. Binary destruction via collision is discussed further in Section 3.3.3.

3.3.1 “Instantaneous” Binary Evolution

After every timestep, each system that rotationally fissioned undergoes binary evolution. Within the Monte Carlo asteroid evolution program, there are two stages for binary evolution: “instantaneous” and “long-term.” This distinction is made between processes that occur immediately after rotational fission and last less than 10^6 years (i.e. the asteroid population evolution model timestep), and those that are gradual or require the completion of some other process such as tidal synchronization of the secondary and take more than 10^6 years. “Instantaneous” evolution is described below and “long-term” evolution in Section 3.3.2. Since the timescales of these processes are often dependent on a large number of parameters, a small minority of systems may violate these assumptions. Where this is possible, it will be noted and discussed. In general, the effect of underestimating the length of “instantaneous” processes results in the reduction of binary lifetimes by only a 10^6 year timestep or two. Since this effects only a small number of systems, the steady-state solution should still predict the relative number of binary systems and the steady-state mass ratio fraction to first order.

If the mass ratio of a system is determined to be high, then that system evolves along the high mass ratio evolutionary track as shown along the top branch of Figure 3.2 reproduced from Jacobson and Scheeres (2011a). Rotationally fissioned binary systems have very compact

mutual orbits. Variations in the orientations and distances between the two members produce changing gravitational fields. Each body is inelastically distorted by the gravitational field of the other. Since these fields are varying time, so are the distortions, which lead to energy dissipation in the form of heat. These mutual body tides lead to circularization of the orbit and synchronization of the spin to the orbit period. Tidal dissipation and subsequent synchronization of each component of a high mass ratio binary occurs at similar rates, since they are of nearly equal size. For “rubble pile” tidal parameters, these systems typically synchronize in much less than 10^6 years (Goldreich and Sari, 2009), and so this process is considered an “instantaneous” process in the asteroid population evolution model. For high mass ratio systems, systems larger than 5 km and with mass ratios $0.2 < q \lesssim 0.3$ may take more than a million years to synchronize. Since high mass ratio systems have negative free energy, none of these systems can disrupt endogenously and all systems emerge as doubly synchronous binaries. Once synchronous, the BYORP effect will expand or contract the mutual orbit. Since this process can last many millions of years, further evolution of high mass ratio binary systems is discussed in Section 3.3.2.

If the mass ratio of a system is determined to be low, then that system evolves along the low mass ratio evolutionary track as shown along the bottom branch of Figure 3.2. In Jacobson and Scheeres (2011a), this track is shown to immediately branch into four possible states, however most chaotic ternary systems formed via secondary fission return to the chaotic binary state via escape of a member or impact between two of the members. None in the original study were found to stabilize for the duration of the simulation although that remains a possibility. This track is not shown in Figure 3.2. Escape from low mass ratio systems is possible because they have positive free energy, and Jacobson and Scheeres (2011a) found numerically that $\sim 67\%$ of low mass ratio binaries do disrupt. Collisions between the two members occur in another $\sim 25\%$ of these systems. Only $\sim 8\%$ of low mass ratio binaries survive for more than 10^3 years. Typically, the secondary of these binaries synchronizes due to mutual body tidal dissipation in less than 10^6 years (Goldreich and Sari, 2009). The primary synchronizes on a timescale proportional to the mass ratio squared q^2 , and so these binaries become singly synchronous systems within the “instantaneous” period

of the asteroid population evolution model. The model stochastically assigns an outcome to each rotationally fissioned low mass ratio system according to the probabilities indicated above creating members of asteroid pairs, re-shaped asteroids, and singly synchronous binary systems. Further evolution of singly synchronous binary systems due to the BYORP effect and tides is discussed in Section 3.3.2 since the relevant timescales typically exceed a million years.

All resultant asteroid systems from both mass ratio regimes are propagated forward using the asteroid population evolution model with all of the asteroids that did not undergo rotational fission. Members of asteroid pairs and re-shaped asteroids are subject to the YORP effect and collisions exactly as single asteroid systems that did not undergo rotational fission. In fact, these systems are now single asteroid systems having complete one rotational fission lifetime cycle. They can eventually rotationally fission again if they are accelerated to the appropriate rotational break-up speed of their size regime.

3.3.2 “Long-term” Binary Evolution

Binary systems that have survived “instantaneous” evolution are treated differently than single systems in the asteroid population evolution model. These systems are still subject to collisions and this is discussed in Section 3.3.3, but they are not subject to the YORP effect in the same way as single asteroids since the internal (i.e. spin and orbit states) evolution of binary systems is complicated by mutual body tides and the BYORP effect. Typically, mutual body tides initially control the internal evolution tidally locking first the secondary and then possibly the primary (Goldreich and Sari, 2009). The BYORP effect then evolves the orbit according to the properties of the synchronous members of the system (Ćuk and Burns, 2005). Jacobson and Scheeres (2011b, 2012) determined that the YORP torque can delay tidal synchronization, but in most cases synchronization will still occur in less than a million years. In rare cases, the YORP torque may be stronger than the tidal torque and evolve the system outside of the proposed evolutionary paths, but it is acceptable to neglect these cases in this model due to the rarity of the required parameters necessary. In most cases, the direction of the BYORP torque has the largest

impact on the lifetime of the system and determines the final end state. At the end of the binary lifetime, the binary system is automatically destroyed and replaced by either a re-shaped asteroid if the mutual orbit contracted until contact or an asteroid pair if the mutual orbit expanded until the Hill radius. Only low mass ratio singly synchronous contracting systems are predicted to not be destroyed by endogenic processes, so in the Main Belt they must be destroyed by collisions, but all binary systems are susceptible to destruction via collision.

The BYORP effect acts as cumulative torque on the orbit of synchronous satellites due to asymmetrical incident solar radiation and emitted thermal radiation (Ćuk and Burns, 2005; Ćuk, 2007; McMahon and Scheeres, 2010a,b). Synchronicity is required in order for the torques from thermal photons to add cumulatively to a non-zero orbital acceleration over all the phases of the mutual orbit, heliocentric orbit, and the precession of the ascending node. The strength of the BYORP effect is strongly dependent on the properties of the mutual orbit as well as the shape and size of the synchronous body. The effect acts independently on each body. If both bodies are synchronous as in doubly synchronous binaries, then there is a BYORP torque on each. For singly synchronous systems, the BYORP effect only acts on the synchronous secondary. Detailed numerical modeling in Jacobson and Scheeres (2011a,b) showed that the direction of the BYORP torques is the fundamental parameter for determining the final evolutionary state of the system. The strength of the BYORP torques determine the timescale of the evolution. The BYORP effect eventually destroys all doubly synchronous and half of all singly synchronous binary systems, shown in Figure 3.2 reproduced from Jacobson and Scheeres (2011a). The exception to BYORP destruction are the singly synchronous systems which occupy an equilibrium between tides and the BYORP effect and are predicted to survive indefinitely unless there is exogenous interference (Jacobson and Scheeres, 2011b).

Evolutionary Track		Likelihood	Binary Lifetime Distributions						σ_τ	
q	Direction	Aligned	Given q	μ_τ	μ_τ	μ_τ	μ_τ	μ_τ	μ_τ	
Low	Out	-	0.5	4.88	5.88	6.88	7.88	8.88	9.88	0.71
Low	In	-	0.5	∞	∞	∞	∞	∞	∞	-
High	Out	No	0.25	4.95	5.95	6.95	7.95	8.95	9.95	0.76
High	Out	Yes	0.25	4.61	5.61	6.61	7.61	8.61	9.61	0.55
High	In	No	0.25	4.42	5.42	6.42	7.42	8.42	9.42	0.75
High	In	Yes	0.25	4.09	5.09	6.09	7.09	8.09	9.09	0.55
BYORP Coefficient Distributions \rightarrow				$\mu_B = -1$	$\mu_B = -2$	$\mu_B = -3$	$\mu_B = -4$	$\mu_B = -5$	$\mu_B = -6$	

Table 3.1: Binary lifetime distributions for each binary evolutionary track and for each BYORP coefficient distribution.

The asteroid population evolution model does not calculate the specific mutual orbit evolution of each binary system due to computational constraints. Instead, each binary is assigned an evolutionary path determined by the system mass ratio and direction of the BYORP torque(s) in the system. There are six distinct evolutionary paths as shown in Table 3.1: low mass ratio stable equilibrium with tides (contractive BYORP), low mass ratio expansive, high mass ratio expansive anti-aligned, high mass ratio expansive aligned, high mass ratio contractive anti-aligned, and high mass ratio contractive aligned. Within each mass ratio regime, there is an equal likelihood to follow a specific track since there is nominally the same chance for a positive as negative BYORP coefficient and the BYORP coefficient of each body is independent of the other (Ćuk and Burns, 2005; McMahon and Scheeres, 2010a). For instance, 25% of high mass ratio systems evolve along the expansive track with aligned BYORP coefficients, since there is a 50% chance that the primary will have a positive BYORP coefficient and a 50% chance that the secondary will also have a positive BYORP coefficient. Once the evolutionary track has been established for a binary system, it continues down that track for the rest of its lifetime.

The lifetime of a binary system is determined principally by the BYORP effect. After synchronization of both members, tides may damp eccentricity from the system but do not strongly evolve the semi-major axis. If only the secondary is synchronized, then tides are still important for contractive systems (i.e. the tidal-BYORP equilibrium) and while tides assist BYORP in expanding systems, tides are a strong function of semi-major axis and soon become much weaker than the BYORP effect. There are also possible interruptions by exogenous processes (e.g. collisions, see Section 3.3.3). The rate of expansion or contraction is determined primarily by the heliocentric orbit, absolute size of the system, and the BYORP coefficient.

The BYORP effect torques synchronous members about the system barycenter expanding or contracting the mutual orbit. The strength of the BYORP torque depends principally on the mutual orbit, the heliocentric orbit, and the size and shape of the synchronous member (McMahon and Scheeres, 2010b). McMahon and Scheeres (2010a) showed that to first order in eccentricity, the

semi-major axis a measured in primary radii R_p evolves as:

$$\dot{a} = \frac{3B_c}{2\pi\omega_d\rho} \left(\frac{a^{3/2}\sqrt{1+q}}{R_p^2q} \right) \left(\frac{(2/3)F_\odot}{a_\odot^2\sqrt{1-e_\odot^2}} \right) \quad (3.4)$$

where $B_c = B_p + B_s q^{2/3}$ is the combined BYORP coefficient. The mass ratio $q^{2/3}$ factor is a direct result of the BYORP effect evolutionary equations (McMahon and Scheeres, 2010a). For doubly synchronous systems, there is a BYORP coefficient for the primary B_p and the secondary B_s , but for singly synchronous systems, there is only a BYORP torque on the secondary so the BYORP coefficient for the primary $B_p = 0$. This evolutionary equation was designed so that the BYORP coefficient is scaleless and depends solely on the shape of the synchronous member. The BYORP coefficients of each synchronous member of the system determine the direction and rate of orbit evolution.

3.3.2.1 BYORP coefficient distributions

Determining the appropriate distribution of plausible BYORP coefficients is very difficult. The effect is similar to the detected Yarkovsky and YORP effects (Chesley et al., 2003; Taylor et al., 2007; Lowry et al., 2007) and so the BYORP effect rests on strong theoretical support despite a lack of direct observation of BYORP-driven evolution. The BYORP effect has never been directly measured, so a BYORP coefficient distribution cannot be derived from direct observation. A detection may be precluded by the BYORP-tidal equilibrium hypothesis and the possibly fast destruction of doubly synchronous binary systems.

BYORP coefficients are determined solely by the shape of the asteroid. Since there are very few well resolved asteroid shapes particularly of binary asteroid members, the distribution of BYORP coefficients is uncertain. The only current BYORP prediction, McMahon and Scheeres (2010a) estimated that $B_s = 2 \times 10^{-2}$ for the secondary of the 66391 (1999 KW₄) system using a vertice-and-facet shape model from Ostro et al. (2006). This shape model is an order 8 spherical harmonic representation with an average 26 m facet edge length (corresponding to 7° angular resolution). Using this BYORP coefficient and the observed parameters of 66391, McMahon and

Scheeres (2010a) determined a Hill radius expansion timescale of $\sim 5.4 \times 10^4$ years. This expansion is very rapid compared to the typical YORP timescales of possible progenitors of $\sim 10^6$ years assuming formation from YORP-induced rotational fission (Rubincam, 2000; Vokrouhlický and Čapek, 2002; Čapek and Vokrouhlický, 2004). Nominally, half of all synchronous binary asteroids are expected to expand due to the BYORP effect and 66391 may be a member of this population but observing this system as a binary rather than an asteroid pair is very unlikely given the difference between those two timescales. This estimated BYORP coefficient also contradicts the BYORP-tidal equilibrium hypothesis in Jacobson and Scheeres (2011b), which states that the observable singly synchronous binary asteroids occupy an equilibrium between a contractive BYORP torque and the expansive mutual body tidal torque. This hypothesis requires a negative BYORP coefficient.

Further study by McMahon and Scheeres (2012, pers. comm.) concluded that the shape of 66391 should be known to a mean facet edge length of 8 m (an angular resolution of 2.2°), using results scaled from an analysis of 25143 Itokawa (1998 SF₃₆), in order to model the BYORP coefficient with sufficient accuracy to prevent significant changes including sign changes. For the related YORP effect, Statler (2009) concluded that spherical harmonic fits of order ≤ 10 produce expected errors of order 100% and for errors under 10%, the harmonic order of the fit must be at least 20. Furthermore, Statler (2009) showed that a crater half the object's radius can produce errors of several tens of percent; the observations of the secondary of 66391 did not uniformly cover the surface, a significant portion of the southern hemisphere is systematically not as accurate as the 7° angular resolution of the rest of the model, and features such as craters may have not been observed (Ostro et al., 2006). Alarming, Rozitis and Green (2012) conclude that the related YORP effect is very sensitive to surface roughness due to thermal-infrared beaming and that accurate YORP (and perhaps BYORP) coefficient estimation from shape models may require 1 cm resolution.

Pravec and Scheirich (2010) determined that the direct detection of the BYORP effect and measurement of the BYORP coefficient would require multi-decade observations of small (semi-major axes of < 10 primary radii and secondary radii < 1 km) binaries. Furthermore, this analysis

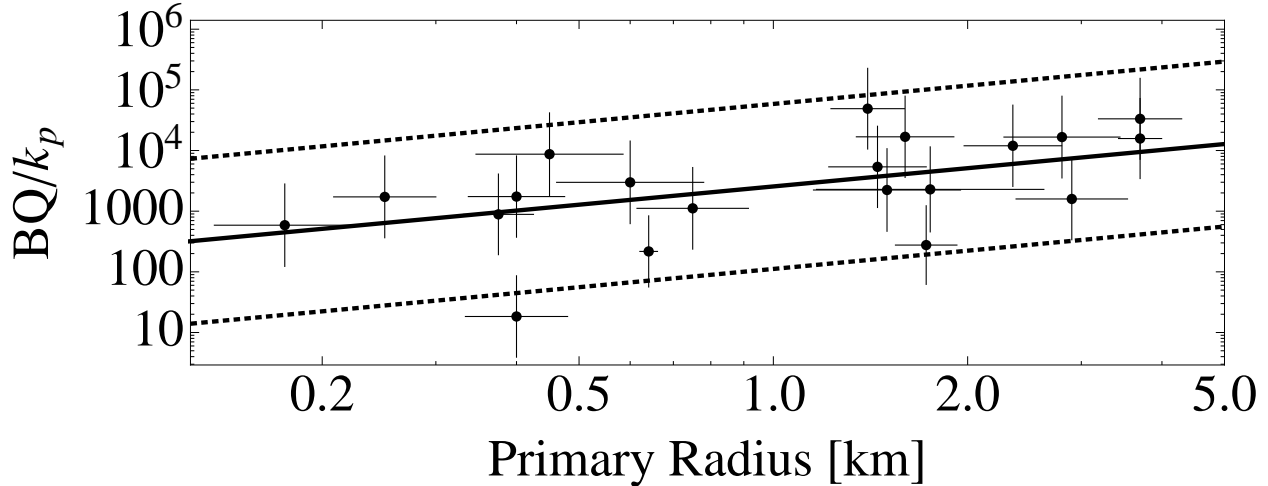


Figure 3.4: The BYORP and tidal coefficients BQ/k_p as determined from the observed singly synchronous population. This plot has been reproduced from Jacobson and Scheeres (2011b) but updated using data from the most recent July 7, 2011 binary asteroid parameter release from <http://www.asu.cas.ca/asteroid/binastdata.htm> as compiled by the methods and assumptions described in Pravec and Harris (2007). Errors are $1\text{-}\sigma$ uncertainties in the observed parameters propagated simply forward. The solid line is the fitted coefficient law $BQ/k_p = 2557R_p \text{ km}^{-1}$, and the dashed lines are the $2\text{-}\sigma$ bounds of the scatter in BQ/k_p as described in the text.

did not include mutual body tides, which Jacobson and Scheeres (2011b) predicted would create a stable equilibrium and halt mutual orbit evolution. Only the less numerous doubly synchronous systems do not have mutual body tides capable of creating the stable equilibrium⁵. The non-existence of a stable equilibrium is the hypothesized reason for the rarity of these systems. Jacobson and Scheeres (2011b) predicts that the mutual orbits of the more numerous singly synchronous systems are not evolving since they occupy the equilibrium. Preliminary results from Scheirich et al. (2012) conclude that for 175706 (1996 FG₃) this is true for at least this system.

While the hypothesized BYORP-tidal equilibrium prevents the direct measurement of the BYORP coefficients of singly synchronous binaries, it may be used to determine the relative distribution of BYORP coefficients. In Jacobson and Scheeres (2011b), it is shown how for each system the balance between the BYORP and tidal torques determines the value of the combination of the BYORP coefficient B and the tidal parameters: tidal quality number divided by the tidal Love

⁵ 69230 Hermes (1937 UB) is the smallest doubly synchronous system in both absolute size and heliocentric orbit, and is therefore the likeliest system for a direct detection of BYORP-driven orbit evolution.

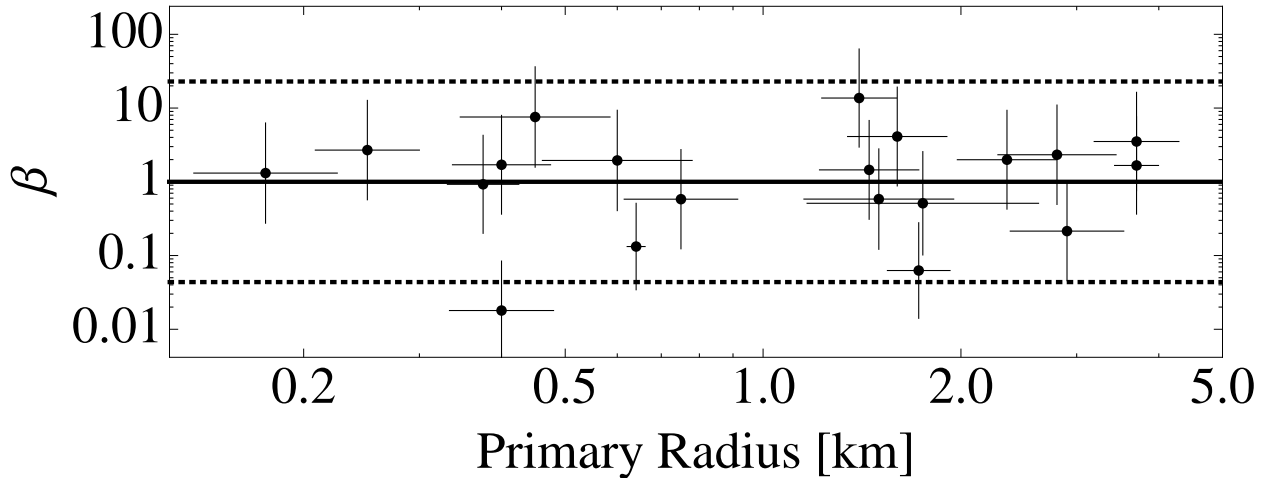


Figure 3.5: The scatter of the BYORP coefficient B due to the variety of secondary shapes. This scatter is determined from the scatter of the calculated BQ/k_p about the fitted coefficient law $BQ/k_p = 2557R_p \text{ km}^{-1}$ as discussed in the text.

number Q/k_p of the primary, degenerately:

$$\frac{BQ}{k_p} = \frac{2\pi\omega_d^2\rho R_p^2 q^{4/3}}{F_\odot a^7} a_\odot^2 \sqrt{1 - e_\odot^2} \quad (3.5)$$

The values of this unitless BQ/k_p coefficient combination for each singly synchronous system is shown in Figure 3.4. This is very similar to Figure 1 in Jacobson and Scheeres (2011b). The solid line is a fit to the logarithm of the data and is $BQ/k_p = 2557R_p \text{ km}^{-1}$. Each asteroid system should follow a similar tidal law and the tidal parameters may have a dependence on absolute size unlike the BYORP coefficient, which is designed to have no dependence on absolute size and only be a function of shape. Jacobson and Scheeres (2011b) argued from this data that $Q/k_p \propto R_p$. Since the BYORP coefficient is not a function of size (R_p), then when the data is divided by a $Q/k_p \propto 2557R_p \text{ km}^{-1}$ model, the resulting scatterplot reflects the distribution of BYORP coefficients B . These normalized BYORP coefficients β are shown in Figure 3.5.

While this trick does not determine the absolute magnitude of the BYORP coefficient, it does provide information about the width of the BYORP coefficient distribution. Figure 3.6 shows the same data as in Figure 3.5 but as a logarithmic histogram. Each system's normalized BYORP coefficient $\beta = 10^v$ are shown in the histogram. The distribution of v is fit with a simple normal

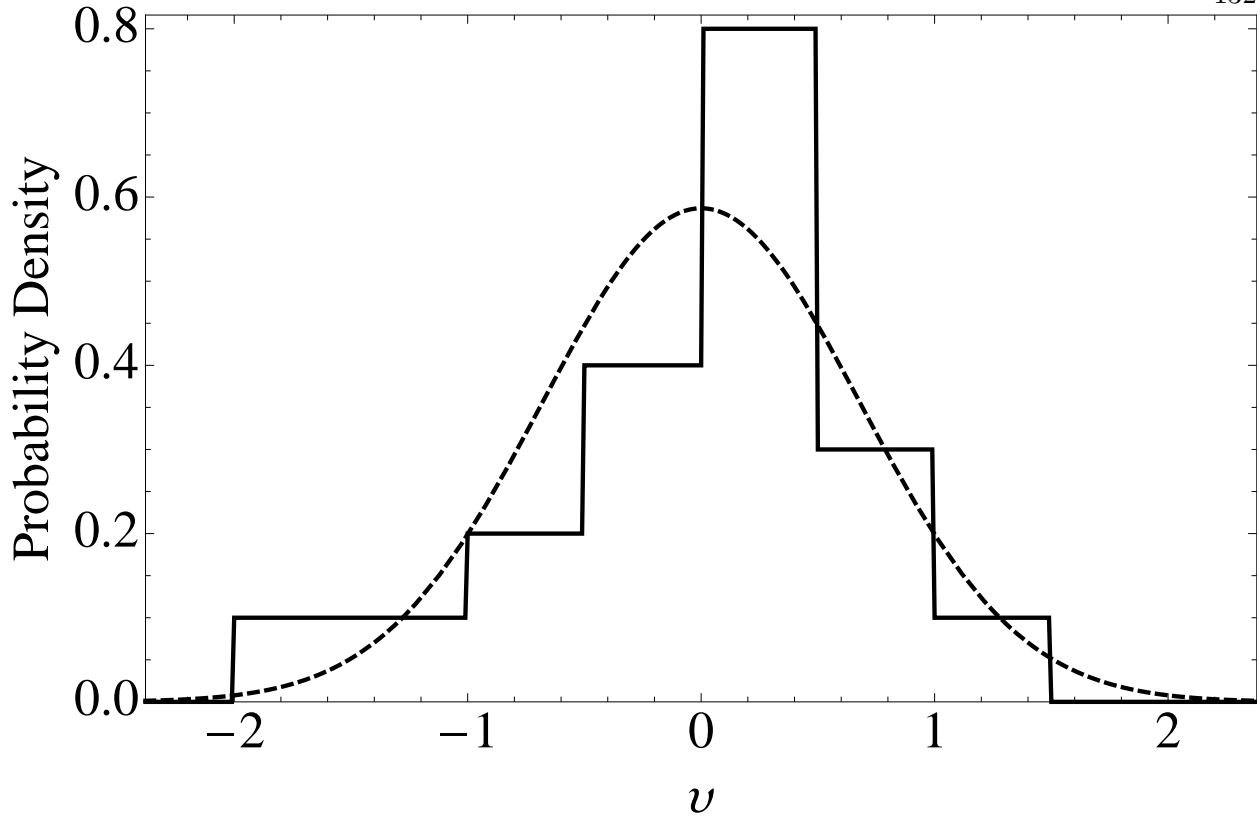


Figure 3.6: A probability density histogram of ν of the observed singly synchronous population (bins are of width 0.5). The dashed line is the probability density function of a central normal distribution fit to the data where $\sigma_\nu = 0.68$. Data is the same as in Figure 3.4.

distribution with mean $\mu_\nu = 0$ and standard deviation $\sigma_\nu = 0.68$. The observed distribution has a slight negative skew and a positive kurtosis compared to the normal distribution. While the normalization of the singly synchronous data removed information about the absolute value of the BYORP coefficients, the standard deviation of those absolute coefficients is the same as the normalized coefficients so $\sigma_B = \sigma_\nu = 0.68$, where σ_B is the standard deviation of y and the absolute BYORP coefficients $B = 10^y$.

The mean μ_B of the distribution of y is difficult to determine. Estimating the absolute magnitude of the BYORP coefficient from McMahon and Scheeres (2010a) suggests a value for the mean of the distribution near $\mu_B = -2$. Even though this value is correct for the radar shape model of the secondary of 66391 rotated 180° about either the radial or body axis orthogonal to

the along track direction, however as discussed above, this estimation may not be accurate due to deficiencies of the shape model.

Another possible estimation scheme for the absolute values of the BYORP coefficient is to determine possible ranges for the tidal parameters and use the equilibrium relationship to determine the likely mean BYORP coefficient. Margot et al. (2002) and Taylor and Margot (2011) show how tidal parameters can be constrained from estimating the age of the binary system. This age constraint is usually an upper limit on tidal parameters since the utilized age is either an estimate of the near-Earth asteroid (NEA) lifetime or the Main Belt asteroid (MBA) collisional timescale. These constraints could be useful in limiting the necessary parameter space in the asteroid population evolution model, however the conducted studies did not consider the role of the YORP or BYORP effect or the similarity between the initial and final semi-major axes of low mass ratio singly synchronous binary systems. The YORP effect can expedite or delay the onset of synchronization. The BYORP effect has the unhelpful characteristic of preventing straightforward tidal evolution of the mutual orbit after synchronization.

After careful consideration of these effects, only the doubly synchronous population can be used to find a useful constraint. The asynchronous binary population must be dismissed since it is not clear if the YORP effect or tides is the dominant evolutionary mechanism. For the singly synchronous population, the combination of the BYORP effect and tides also prevents the useful application of the age constraint on tidal parameters. According to the tidal-BYORP equilibrium, low mass ratio singly synchronous systems are observed at final semi-major axes very similar to the semi-major axes that they settled into after forming via rotational fission Jacobson and Scheeres (2011a), and these systems are stable in this configuration in excess of the near-Earth asteroid lifetime.

The BYORP effect is currently torquing the observed doubly synchronous population, but each member of each binary synchronized on a similar timescale since these are high mass ratio systems (Jacobson and Scheeres, 2011a). Also high mass ratio systems do not undergo secondary fission and so evolve directly from contact to the doubly synchronous relative equilibrium. Since

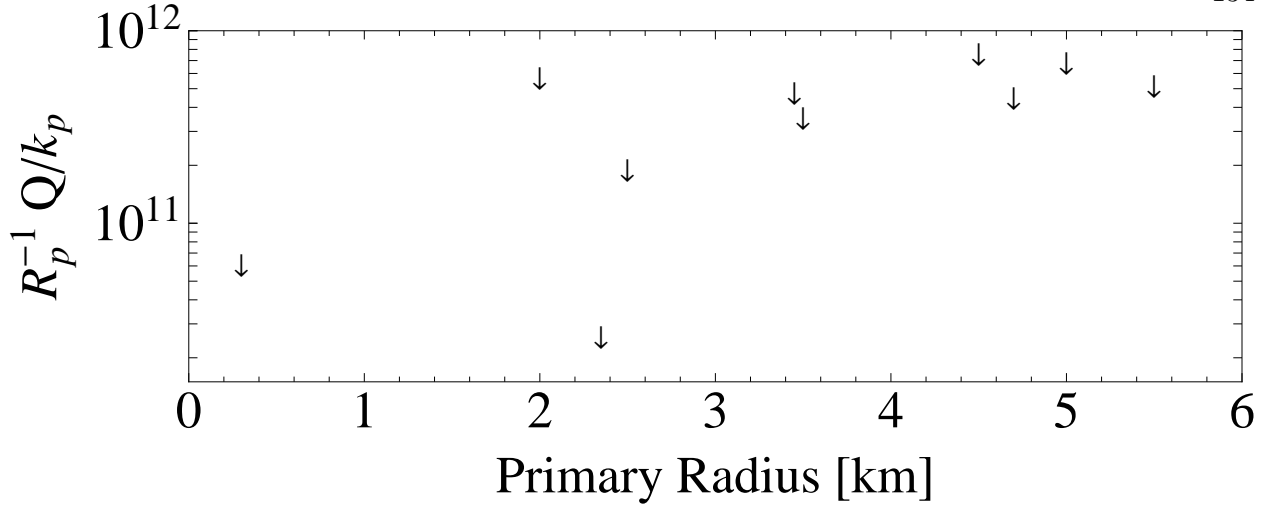


Figure 3.7: The upper limits of $R_p^{-1}Q/k_p$ for each doubly synchronous system from the Ondrejov Binary Parameter Release.

both members are synchronous, the YORP effect must be weaker than the tidal torque on the spin state. The estimated timescale of the system, either the NEA lifetime or the MBA collision timescale τ_l depending on the heliocentric orbit of the system, is equal to the $\tau_t + \tau_b$, where τ_b is the time since synchronization that the system has been evolving due to the BYORP effect. The tidal timescale τ_t is determined from the initial semi-major axis a_c and the final doubly synchronous semi-major axis a_d , as defined in Section 3.3.2.2, as well as the binary system parameters:

$$\tau_t = \frac{2Q}{39k_p\omega_d q\sqrt{1+q}} \left(a_d^{13/2} - a_c^{13/2} \right) \quad (3.6)$$

This is an integration of the standard tidal evolution equations (e.g. as given in Murray and Dermott (2000)). Using the relationship $\tau_t \leq \tau_l$, the tidal parameters can be constrained:

$$\frac{Q}{k_p} \leq \frac{39}{2}\omega_d q\sqrt{1+q} \left(a_d^{13/2} - a_c^{13/2} \right)^{-1} \tau_{NEA} \quad (3.7)$$

The tidal-BYORP equilibrium hypothesis establishes the relationship: $BQ/k_p = 2557R_p$. The BYORP coefficient B is not dependent on the size (R_p) of the body, only the shape. Thus the tidal parameter arrangement $R_p^{-1}Q/k_p$ should be a constant independent of size. Figure 3.7 shows these constraints $R_p^{-1}Q/k_p$ for each doubly synchronous system in the July 1, 2011 binary asteroid parameter release from <http://www.asu.cas.cz/asteroid/binastdata.htm> as compiled by methods

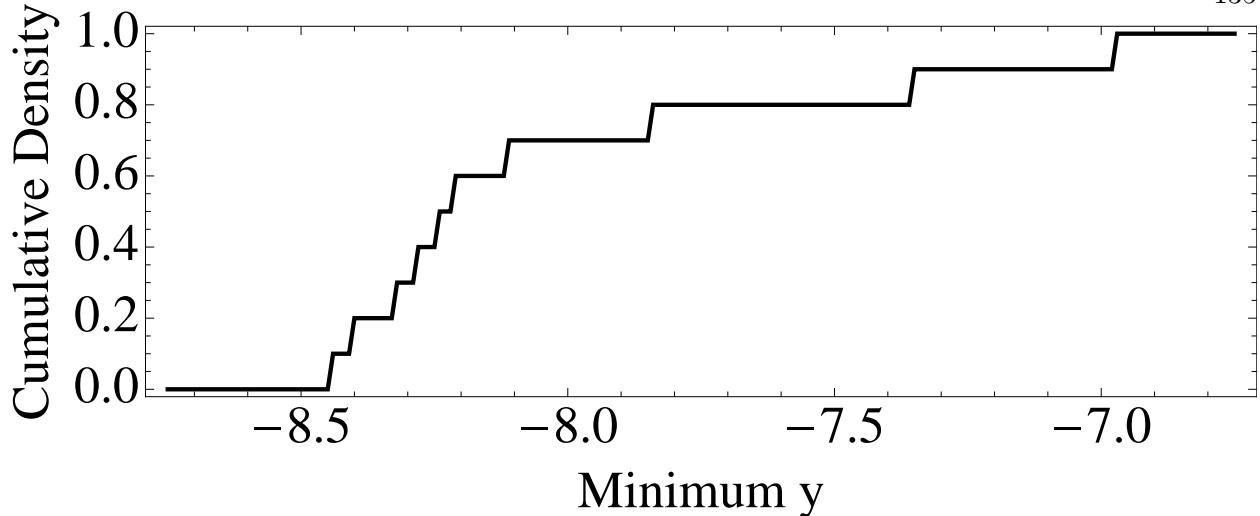


Figure 3.8: The cumulative density distribution for the maximum value of the mean BYORP coefficient given the possible tidal parameter estimations.

and assumptions described in Pravec et al. (2006), Pravec and Harris (2007), and Pravec et al. (2012), for which this constraint on Q/k_p can be determined (i.e. that double synchronicity can be established, and the necessary parameters are known).

If the very plausible assumption is made that the tidal parameters are similar between the doubly and singly synchronous populations, then the equilibrium relationship establishes a constraint on the BYORP coefficients $B = 2557R_p(Q/k_p)^{-1} = 10^y$ for the singly synchronous systems in the equilibrium. In Figure 3.8, the lower limit for the BYORP coefficient is shown as a cumulative density function. The minimum, median, maximum values for y are -7.0 , -8.2 , -8.4 . However, none of these constraints are useful since a value of $y = -6$ produces binary lifetimes longer than the age of the Solar System.

Since we cannot constrain the BYORP coefficient distribution, five different distributions are tested in the asteroid population evolution model: $\mu_B = 0, -1, -2, -3, -4, -5, -6$ and -7 . This is the second knob in the model; the other knob is the initial mass ratio fraction as described in Section 3.2.5. These BYORP coefficient distributions are used to generate the binary lifetime distributions that are then assigned to each binary system in the asteroid population evolution model. Each BYORP distribution is tested independently and the entire asteroid population is then

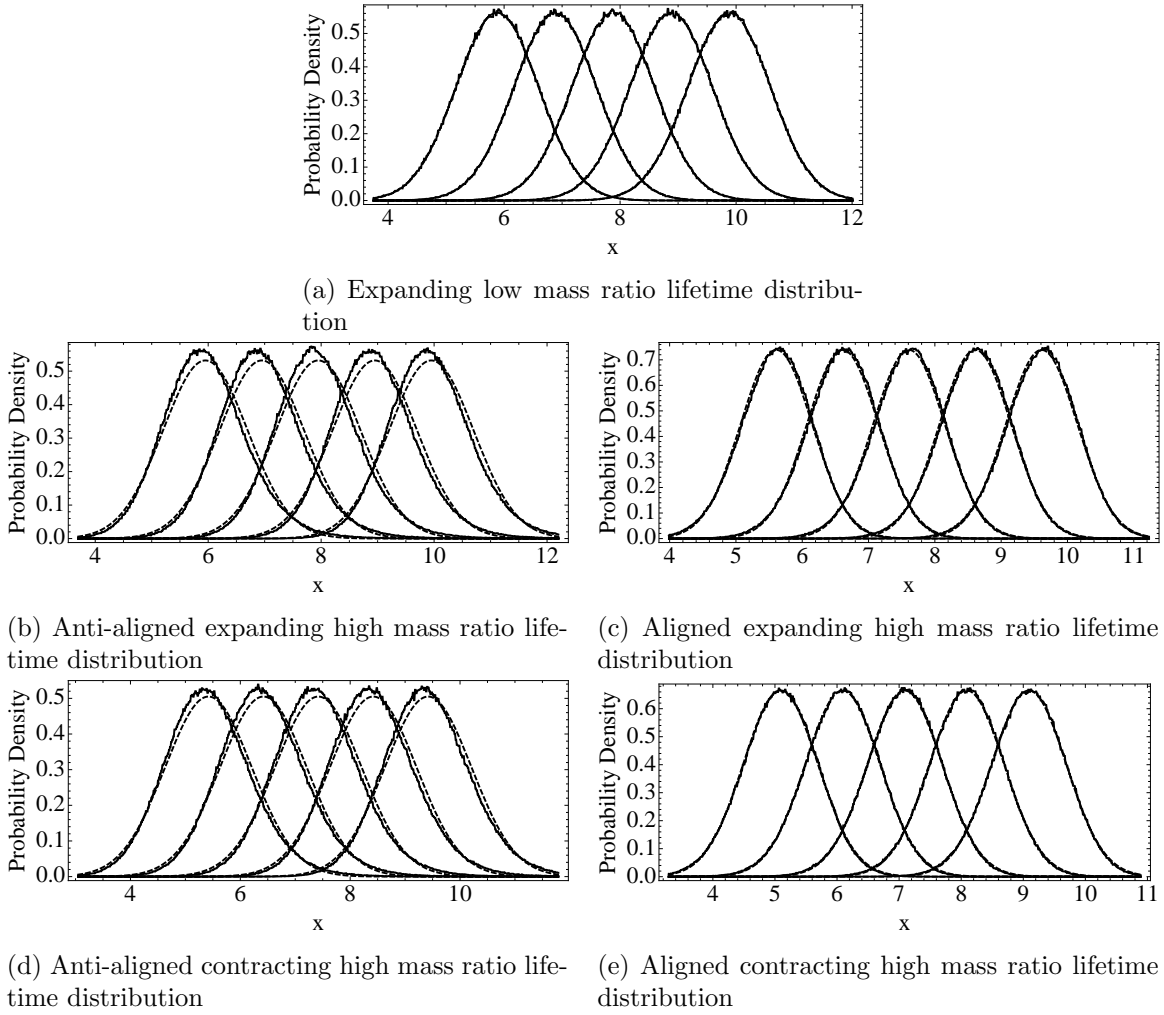


Figure 3.9: Binary lifetime distributions for each evolutionary track are shown as probability density functions (pdfs) of x as defined in the text. Each track (a, b, c, d and e) shows five Monte Carlo generated lifetime distributions and five fitted Normal distributions corresponding to the BYORP coefficient distributions, which from left to right are: $\mu_B = -2, -3, -4, -5,$ and -6 . The solid lines are the result of Monte Carlo generation of a million binary systems for each distribution. The dashed lines are fitted normal distributions to this generated data, and the fit parameters are given in Table 3.1.

evolved from within the chosen distribution for the entirety of the run. Each of these distributions is defined such that $B = 10^y$ and y is drawn from a normal distribution with standard deviation $\sigma_B = 0.68$ and mean μ_B as listed above and in Table 3.1.

3.3.2.2 Binary lifetime distributions

The BYORP lifetime τ is determined by the evolution of the mutual orbit from a tidally synchronized semi-major axis to single member end states either re-shaped asteroids (e.g. contact binaries) or asteroid pairs. This evolution can be described as the evolution from an interior semi-major axis a_{interior} to an exterior semi-major axis a_{exterior} or vice versa:

$$\tau = 10^x R_p^2 a_\odot^2 \sqrt{1 - e_\odot^2} \quad (3.8)$$

$$x = \log_{10} \left[\frac{4\pi\omega_d\rho q}{3F_\odot B_c \sqrt{1+q}} \left(\frac{1}{a_{\text{interior}}^{1/2}} - \frac{1}{a_{\text{exterior}}^{1/2}} \right) \right] \quad (3.9)$$

where $F_\odot = 4.5 \times 10^{-5} \text{ g cm}^{-1} \text{ s}^{-2}$ is the solar constant at a 1 AU circular orbit. The BYORP lifetime τ is determined by the primary radius R_p , the heliocentric semi-major axis a_\odot and eccentricity e_\odot , and x . x is the logarithm of all the other system parameter dependencies. Rather than generating the necessary parameters to determine x for each system, a million systems were generated outside of the asteroid population evolution model for each evolutionary path and the distribution of x was determined. Logarithmic normal distributions were fit to these generated distributions of x with means of μ_τ and standard deviations of σ_τ . Each distribution depends on the BYORP coefficients of the synchronous members, and the particular evolutionary track. For each of the million systems, the BYORP coefficients are drawn from the distribution with the prescribed μ_B for that run. Distributions of x are shown in Figure 7, such that if R_p is in km, a_\odot is in AU, then τ is in years.

Each evolutionary pathway is defined by the sign of the BYORP coefficient for each synchronous member and the mass ratio of the system. As mentioned earlier, the only evolutionary track that does not self-destruct is the BYORP contracting singly synchronous track. These systems may contract or expand to some degree in semi-major axis, but the BYORP-tidal equilibrium hypothesis predicts that these systems reach a stable semi-major axis. This is a fundamental assumption by this model. The interior a_{interior} and exterior a_{exterior} semi-major axes are given below for each of the evolutionary tracks in Table 3.1.

Asteroids undergo rotational fission at some critical disruption rotation rate; this has been

shown with analytic theory, observations of asteroid pairs, and computational numerics (Scheeres, 2007a; Pravec et al., 2010; Sánchez and Scheeres, 2012). This disruption rate and the shape of the asteroid at fission determine the angular momentum of the system during the “instantaneous” binary evolution stage identified in Section 3.3.1. For high mass ratio doubly synchronous systems, the initial semi-major axis is always the tidally synchronized semi-major axis with the equivalent angular momentum as the rotational fissioned system at the time of fission. Tidal dissipation will remove energy from the system, but angular momentum is conserved until the system is synchronized and the BYORP effect evolves the system. This semi-major axis can be either the interior or exterior semi-major axis depending on the sign of the BYORP coefficient. By making some idealizing approximations, the conservation of angular momentum is used to derive a tidal synchronization semi-major axis for the doubly synchronous systems a_d .

The angular momentum of an idealized binary system approximating each body as a constant density sphere is

$$H = I_p\omega_p + I_s\omega_s + ma^2\Omega \quad (3.10)$$

where $I_n = 2M_nR_n^2/5$ are the moments of inertia, R_n are their radii, $M_n = 4\pi\rho R_n^3/3$ are their masses, $m = M_pq/(1+q)$ is the reduced mass, a is the distance between each body’s center of mass, and Ω is the rotation rate about the system barycenter. Additionally, the mass ratio is defined as $q = M_s/M_p = R_s^3/R_p^3$ and the critical disruption rate for a specific mass ratio as $\omega_q = \sqrt{(1+q)/(1+q^{1/3})^3}$.

In the idealized system described above, the initial angular momentum at the moment of rotational fission is a function of the mass ratio, the density and the primary radius. Before entering into orbit, the two idealized components are initially separated only by their radii $a = R_p + R_s = R_p(1+q^{1/3})$. All three rotation rates in the system are equivalent to the critical disruption rate for

a specific mass ratio $\omega_p = \omega_s = \Omega = \omega_q$. Therefore, the initial angular momentum of the system is

$$H_i = \frac{4\pi\rho\omega_d R_p^5}{15} \sqrt{\frac{1+q}{(1+q^{1/3})^3}} \times \left(\frac{2 - 2q^{1/3} + 2q^{2/3} + 5q + 5q^{4/3} + 2q^{5/3} - 2q^2 + 2q^{7/3}}{1 - q^{1/3} + q^{2/3}} \right) \quad (3.11)$$

Doubly synchronous systems dissipate energy until all three rotation rates of the system are equivalent to the keplerian orbit rate $\omega_p = \omega_s = \Omega = \omega_d \sqrt{(1+q)/a_d^3}$ where $a_d = a/R_p$ is the doubly synchronous synchronization semi-major axis normalized by the primary radius. The synchronization angular momentum for a doubly synchronous is:

$$H_d = \frac{4\pi\rho\omega_d R_p^5}{15} \left(\frac{(1+q)(2 + 2(q + q^{5/3} + q^{8/3}) + 5qa_d^2)}{(a_d(1+q^{1/3})(1 - q^{1/3} + q^{2/3}))^{3/2}} \right) \quad (3.12)$$

Since angular momentum is conserved, $H_i = H_d$ and we obtain the synchronization semi-major axis a_d . If we assume $a_d > 0$ and $0 \leq q \leq 1$, then

$$a_d^{-3/2} \left(5qa_d^2 + 2(1 + q + q^{5/3} + q^{8/3}) \right) = \frac{2 - 4q^{1/3} + 6q^{2/3} + q + 2q^{4/3} + 2q^{5/3} + q^2 + 6q^{7/3} - 4q^{8/3} + 2q^3}{(1 - q^{1/3} + q^{2/3}) \sqrt{1 + q^{1/3}}} \quad (3.13)$$

A power series approximation to the solution of this equation

$$a_d = 0.344 + \frac{0.00406}{q^3} + \frac{0.01322}{q^2} + \frac{0.815}{q} + 1.23q \quad (3.14)$$

is the initial tidally doubly synchronous semi-major axis measured in primary radii R_p .

For contracting high mass ratio systems, the interior semi-major axis a_{interior} is contact between the two bodies:

$$a_c = 1 + q \quad (3.15)$$

For both singly and doubly synchronous expanding systems, the exterior semi-major axis a_{exterior} is the Hill radius a_{Hill} . The Hill radius can be approximated in primary radii R_p :

$$a_{\text{Hill}} = q_{\odot} \left(\frac{4\pi\rho}{9M_{\odot}} \right)^{1/3} \quad (3.16)$$

where $\rho = 2 \text{ g cm}^{-3}$ is the density of the primary, $M_{\odot} = 1.99 \times 10^{33} \text{ g}$ is the mass of the Sun, and q_{\odot} is the heliocentric perihelion of the barycenter of the system. Asteroids at the outer edge of the Main Belt in circular orbits $q_{\odot} = 3.28 \text{ AU}$ have the largest Hill radii $a_{\text{Hill}} = 549$ primary radii and those at the inner edge in highly eccentric orbits with periapses just exterior to the Earth $q_{\odot} = 1 \text{ AU}$ have the smallest Hill radii $a_{\text{Hill}} = 168$ primary radii, but these radii are very large compared to the interior semi-major axes a_{interior} . Since the BYORP lifetime is proportional to the difference between the inverse square roots of the interior and exterior semi-major axes, this factor of three difference in exterior semi-major axis translates to an at most 10% difference in BYORP lifetime, if one extreme was chosen relative to the other. To simplify the calculations, we use a single perihelion $q_{\odot} = 2.25 \text{ AU}$, very close to the mean and median of the Main Belt Asteroid distribution. This corresponds to a Hill radius $a_{\text{Hill}} = 377$ primary radii.

3.3.3 Binaries and Collisions

If a binary participates in a catastrophic shattering collision then the binary is always destroyed. This is determined by the same condition as a single asteroid from a comparison of the imparted specific kinetic energy and the critical impact specific energy. Unlike single asteroids, cratering collisions can destroy a binary systems. While these collisions by definition deliver less energy than the critical impact energy, these impacts can deliver enough energy to the system to disrupt the binary. A simple condition for this disruption is a comparison of the delivered change in momentum to the system (ΔV) and the escape velocity from the primary. If the former exceeds the latter, then the system disrupts.

3.3.4 Contact Binaries

Contact binaries are formed from the merging of BYORP contracting high mass ratio binary systems. These systems exist until either they undergo a rotational fission event or are subject to a catastrophic collision. This probably too optimistic a scenario since the binary system crosses a instability before contact (Scheeres, 2009b). This instability causes the two components to begin

to circulate and the orbit to evolve, but from simulations, these systems still collide and do so gently (Jacobson and Scheeres, 2011a). These gentle collisions may be enough to reshape the new combined mass into a non-bifurcated shape that would not be easily identifiable as a contact binary. The subjectivity of the contact binary label adds some uncertainty to the population statistics.

3.3.5 Asteroid Pair Observability

Asteroid pairs are formed from the disruption of asteroid systems either low mass ratio systems during “instantaneous” evolution or high mass ratio systems due to long-term BYORP evolution. Similar to contact binaries, asteroid pair members are tracked until catastrophic collision or rotational fission. Furthermore, due to planetary and asteroidal perturbations this pair information is eventually lost to observers. Most asteroid pairs will lose this information in about 2×10^6 years Pravec and Vokrouhlický (2009). Therefore, the asteroid population evolution model tracks asteroid pairs for only this period of time.

3.4 Results of the asteroid population evolution model

The asteroid population evolution model produces a spin period distribution as a function of diameter similar to the observed population. This is not of great surprise since the spin limit constraints were designed to reproduce the observed population and the model has been used successfully in the past for this purpose (Marzari et al., 2011). The model had two input parameters initial mass ratio fraction F_i and mean of the log-normal distribution of BYORP coefficients μ_B , and these inputs were permuted so that each combination produced a full set of model outputs. We discuss each observable quantity output from the model and how that observable depends on the model free parameters: F_i and μ_B . Combining all of the observables, we assemble a log-likelihood metric that can determine the best fit parameters. Since the computational cost of running the asteroid population evolution model is high and we utilized a population of 2×10^6 asteroids, there is small variance when a particular set of input parameters is run a second time. We use a Monte Carlo method to propagate the observed uncertainties to the comparison tests.

There are two equally good model fits and they are discussed in detail in Section 3.5. Population wide statistics for those models are provided and we discuss in particular the role of YORP-induced rotational fission on the Main Belt asteroid size distribution.

3.4.1 Steady-State Binary Fraction

The asteroid population evolution model traces the evolution of a population with diameters from 50 m to 20 km. However, observations typically do not go to such small sizes. To replicate them, we will only consider asteroids with diameters > 300 m, which corresponds to an absolute magnitude $H \sim 21$ for asteroid albedos. For most observables, changing this diameter does change the results of the model so for each the trend in diameter cut-off is stated.

In Figure 3.10, the steady-state binary fraction is shown as a function of both the initial mass ratio fraction and the log-normal BYORP coefficient distribution mean. Long binary lifetimes (small BYORP coefficients) naturally correspond to a high binary fraction. The relationship with initial mass ratio fraction is more complicated, when binary lifetimes are short then low initial mass ratio fraction cases have higher binary fractions due to the more likely creation of synchronous long-lasting binary systems. Whereas if binary lifetimes are long, then the binary fractions are very similar.

Radar and photometric lightcurve observations supply independent and robust binary statistics regarding the near-Earth asteroid (NEA) population binary fraction. Using radar observations, Margot et al. (2002) reported that about 16% of radar observed binary systems larger than 200 m are binary systems. Updated statistics from radar observations agree well with the better determined value of about 17%: 31 binary systems out of 180 asteroid systems with absolute magnitudes $H < 21$ approximate diameters $D \gtrsim 250$ m for an $p = 0.18$ albedo asteroid (Taylor et al., 2012). Photometric lightcurve analyses report a binary detection rate of $15 \pm 4\%$ for NEAs with diameters $D \gtrsim 300$ m and inferred mass ratios $q > 0.006$ (Pravec et al., 2006). This agrees with an initial assessment by (Pravec et al., 1999) that 17% of near-Earth asteroid systems are binary. For small diameter MBA systems $D \lesssim 10$ km, Pravec and Harris (2006) determine that there is a similar

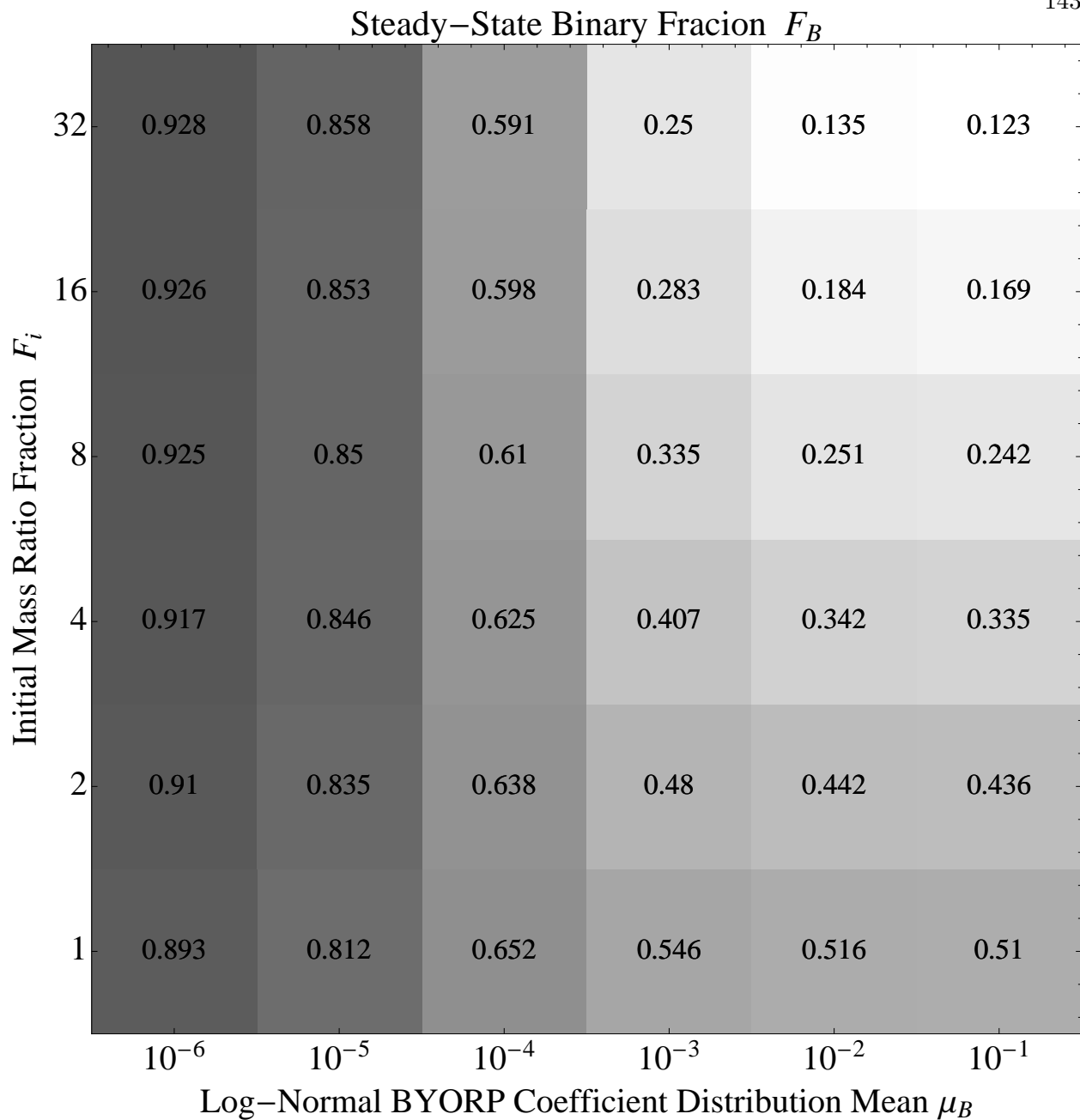


Figure 3.10: The binary fraction F_B of the model population is shown as a function of the two free parameters: the mean of the BYORP coefficient logarithmic normal distribution μ_B along the x-axis and the initial mass fraction F_i along the y-axis. Each grid point is determined from an independent run of the asteroid population evolution model with those values for the free parameters (otherwise the runs are identical).

binary fraction in the inner Main Belt and this is supported by the results of the Binary Asteroid

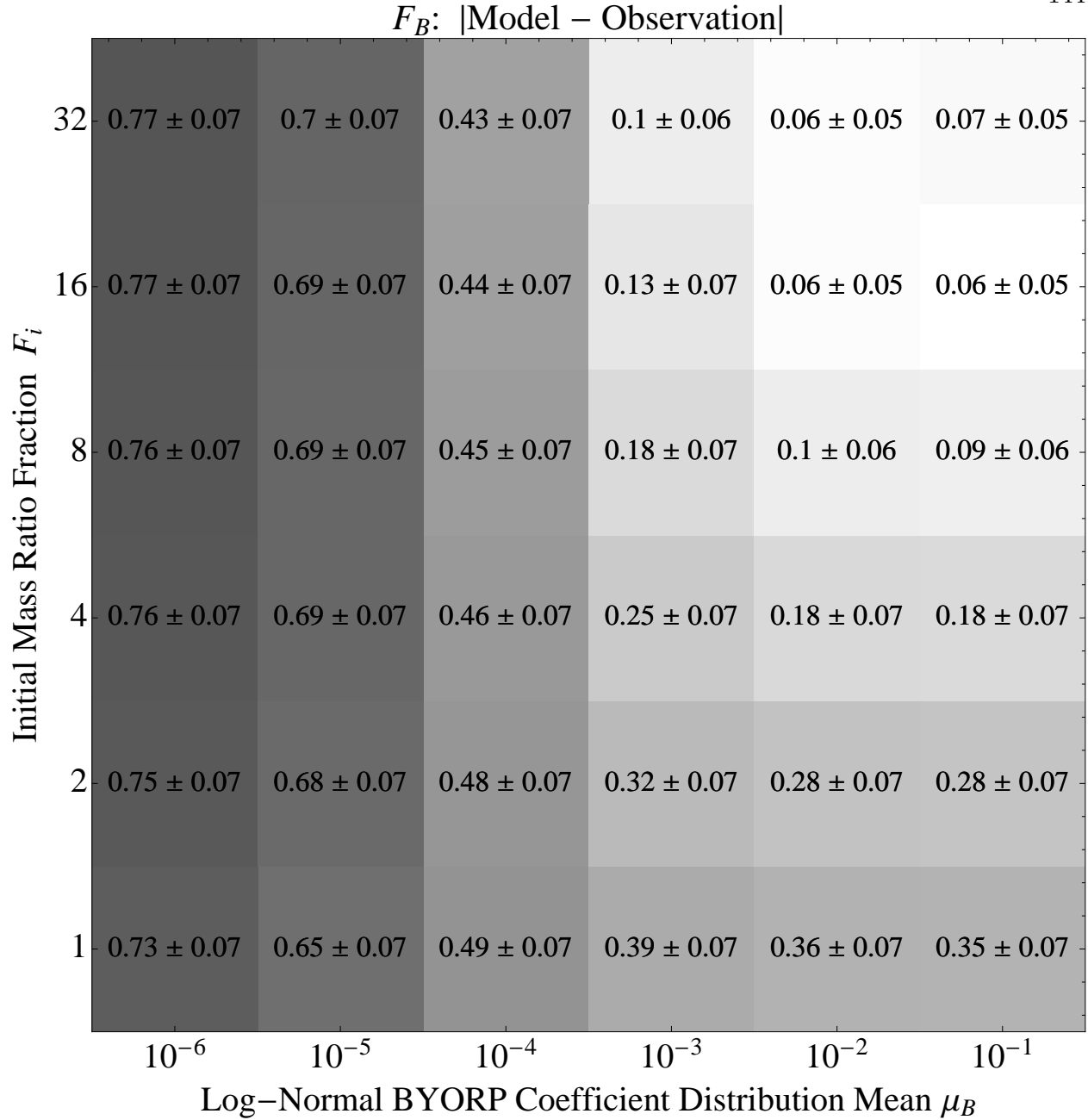


Figure 3.11: Each grid point shows the absolute difference between the model population and observation of the binary fraction F_b (i.e. a heat map identifying those free parameters that produce a model population closest to the observed population).

Photometric survey (Pravec et al., 2006, 2012). The near-Earth asteroid population is significantly easier to observe than similar sized Main Belt asteroids, but for the sizes observed $D \lesssim 10$ km,

rotational fission is expected to be the dominant formation mechanism. Tidal disruption of binary asteroids in the near-Earth asteroid population may slightly lower the binary fraction in that population relative to the Main Belt.

In Figure 3.11, the difference between the asteroid population evolution model and the observations are shown with uncertainties calculated from the observation. For this metric, we use the $16 \pm 7\%$ radar survey results from Taylor et al. (2012) assuming Poisson statistics for calculating the uncertainty. The best parameter fits occur when the log-normal BYORP coefficient distribution mean is low, either 10^{-1} or 10^{-2} and the initial mass ratio fraction is high.

Pravec et al. (2006) made a specific subpopulation observation that amongst fast-rotating binaries (spin periods between 2.2 and 2.8 hours) with diameters larger than 0.3 km the binary fraction becomes $66 \pm 12\%$. The asteroid population evolution model tracks the spin rate of single asteroids but since it does not evolve the system parameters of binaries, we rely on the binary evolution model to assume that all low mass ratio and no high mass ratio binaries will have rapidly rotating primaries. The fast rotating binary fraction as a function of the free parameters is shown in Figure 3.12. Similar to the overall binary fraction, a large initial mass ratio fraction produces a small fast rotating binary fraction. Unlike the overall binary fraction, the fast rotating binary fraction is not dependent on binary lifetimes since only low mass ratio systems have rapidly rotating primaries.

The difference between the model and the observational constraint is shown in Figure 3.13. There is a band around a initial mass fraction of 8 that produces the smallest difference between the model and observation, however this constraint is softer than the overall binary fraction since the nearby bins have similar values.

3.4.2 Steady-State Mass Ratio Fraction

The steady-state mass ratio fraction is the evolved initial mass ratio fraction, which as a reminder is the number of high mass ratio binaries divided by the number of low mass ratio binaries. It is shown as a function of the free parameters in Figure 3.14. Increasing the initial mass

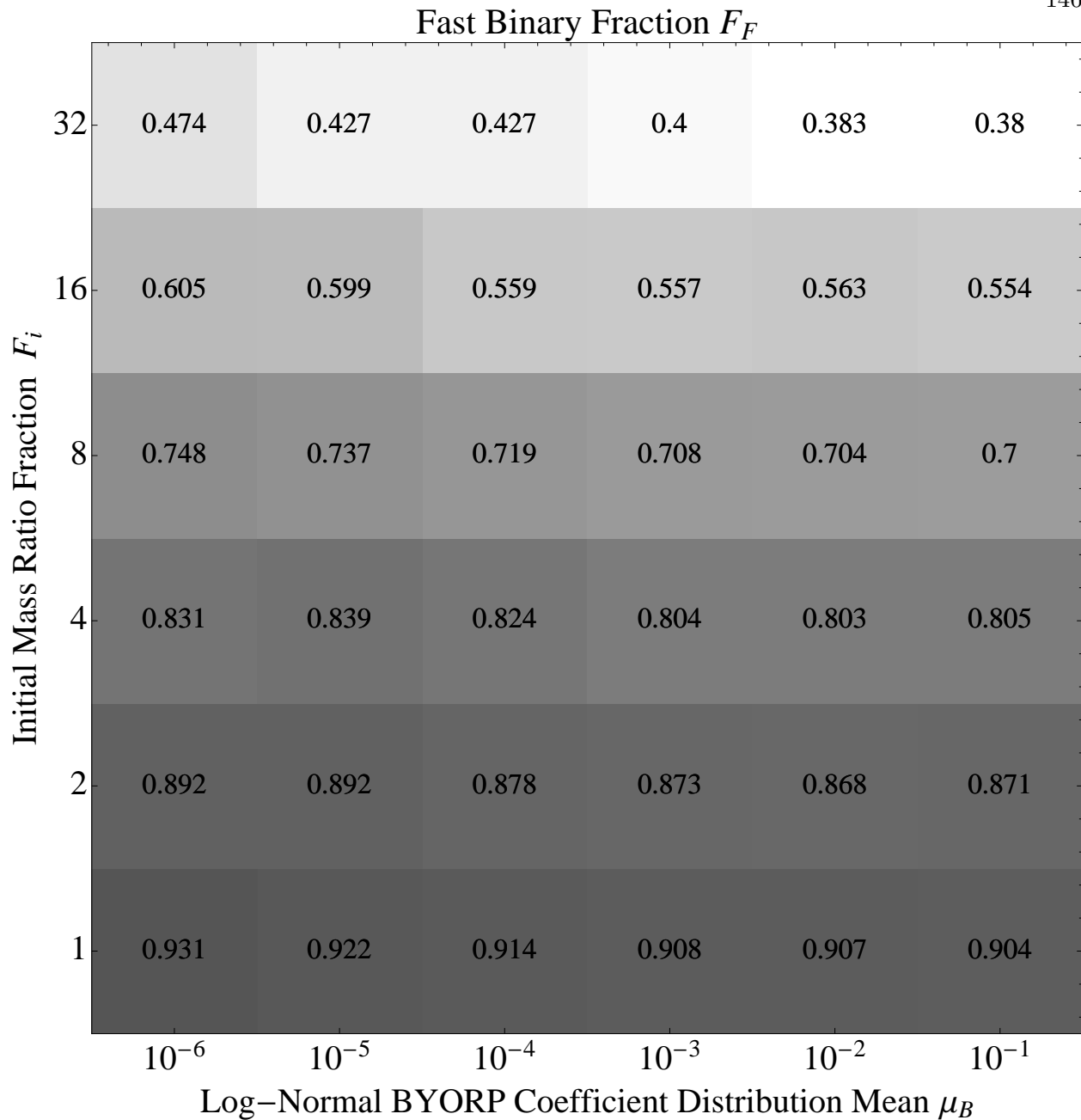


Figure 3.12: The fast rotating fraction F_F of the model population is shown as a function of the two free parameters: the mean of the BYORP coefficient logarithmic normal distribution μ_B along the x-axis and the initial mass fraction F_i along the y-axis. Each grid point is determined from an independent run of the asteroid population evolution model with those values for the free parameters (otherwise the runs are identical).

ratio fraction does increase the steady-state mass fraction, however that increase is mitigated when

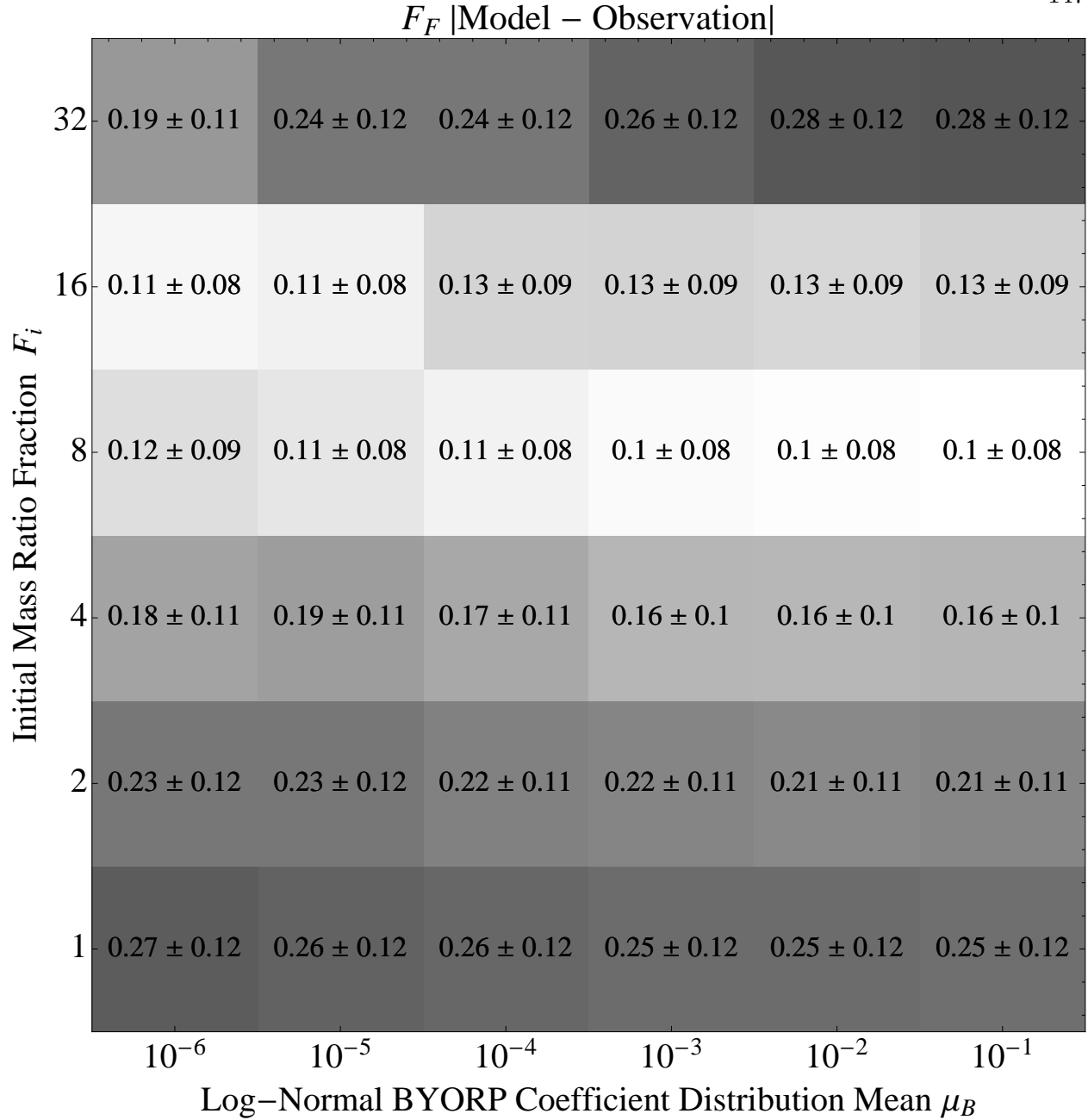


Figure 3.13: Each grid point shows the absolute difference between the model population and observation of the fast rotating binary fraction F_b (i.e. a heat map identifying those free parameters that produce a model population closest to the observed population).

high mass ratio systems do not survive for as long as low mass ratio systems. Also as the log-normal BYORP coefficient distribution mean decreases and binary lifetimes increase, the steady-state mass

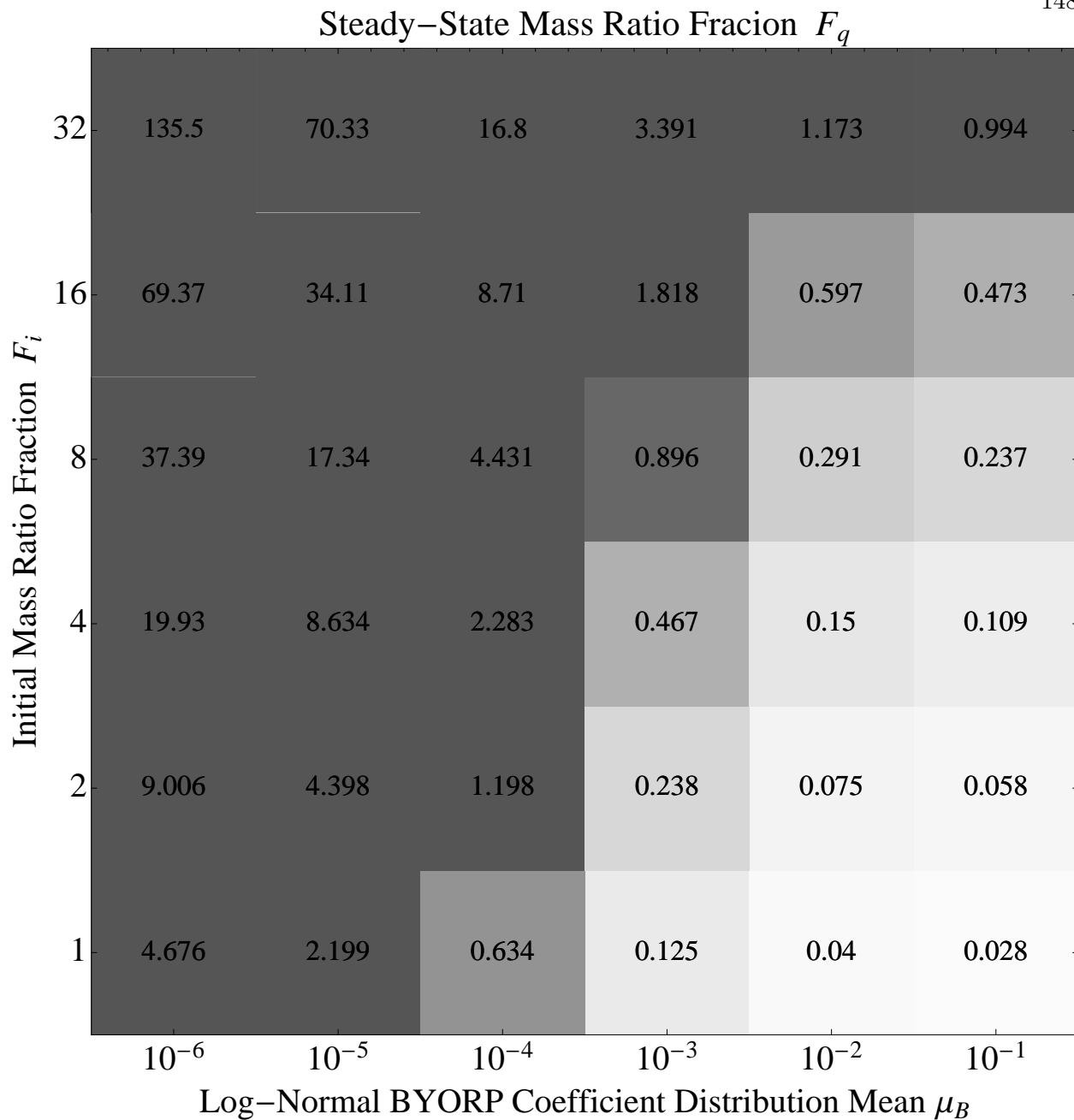


Figure 3.14: The mass ratio fraction F_q of the model population is shown as a function of the two free parameters: the mean of the BYORP coefficient logarithmic normal distribution μ_B along the x-axis and the initial mass fraction F_i along the y-axis. Each grid point is determined from an independent run of the asteroid population evolution model with those values for the free parameters (otherwise the runs are identical).

ratio fraction increases since the high mass ratio binaries are living longer relative to the low mass

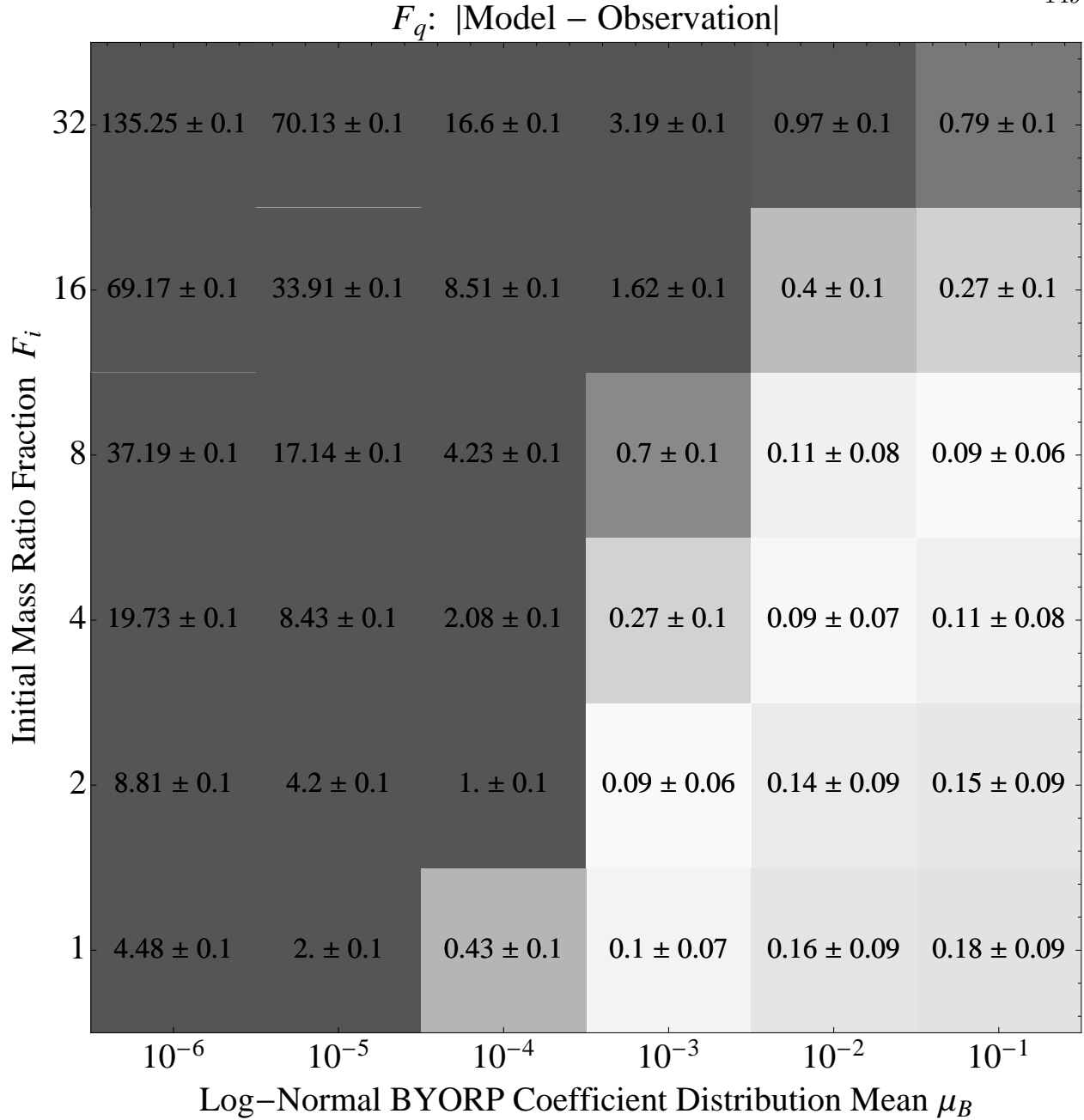


Figure 3.15: These plots are similar to Figure 3.3 but now show the steady-state mass ratio fraction F_q . The best fit parameters for this constraint is a diagonal line across the center of the plot.

ratio synchronous systems, which are in a long-term equilibrium.

The binary asteroid catalogue provided by Pravec et al. provides the best statistics regarding the steady-state mass ratio fraction. This ratio is shown in Figure 3.3 and is 0.2 ± 0.1 using Poisson

statistics. In Figure 3.15, the absolute difference between the model and the observation is shown. The best fits are a diagonal band from long binary lifetime and small initial mass ratio fractions to short binary lifetimes and high initial mass ratio fractions. This is sensible trade-off in parameters to arrive at similar values for the steady-state mass ratio fraction.

3.4.3 Contact Binary Fraction

In Figure 3.17, we show the model contact binary fraction as a function of the free parameters. Contact binaries are formed from the destruction of inward evolving high mass ratio binaries, so when high mass ratio binaries are created often (large initial mass ratio fraction) and when they are destroyed frequently (large log-normal BYORP coefficient distribution mean), the contact binary fraction is high.

Only radar imaging can conclusively determine whether a system is a contact binary, but even then it is often a subjective result. Taylor et al. (2012) provides the most recent estimate of $15 \pm 7\%$ using Poisson statistics. This number is perhaps more likely to be an underestimate relative to the asteroid population evolution model definition of a contact binary because contact binary formation involves the low velocity collision of two asteroids and collision geometry and internal structure may dictate whether a collapsing high mass ratio system is observable as a contact binary. In Figure 3.17, the absolute difference between the model and observations are shown. If the model is over-counting contact binaries because the model always creates them at the end of the collapsing high mass ratio track evolution track, then the band of best fits would contract some about the upper right-hand corner and come more into agreement with the initial mass ratio fractions that the other observable constraints impose.

3.4.4 Best Fit Parameters

We can combine each of these observables into a single log-likelihood estimator for determining the best fit for the free parameters. The log-likelihood metric we will use is a summation of the difference between the model output fraction F_j for each observable j and an observable

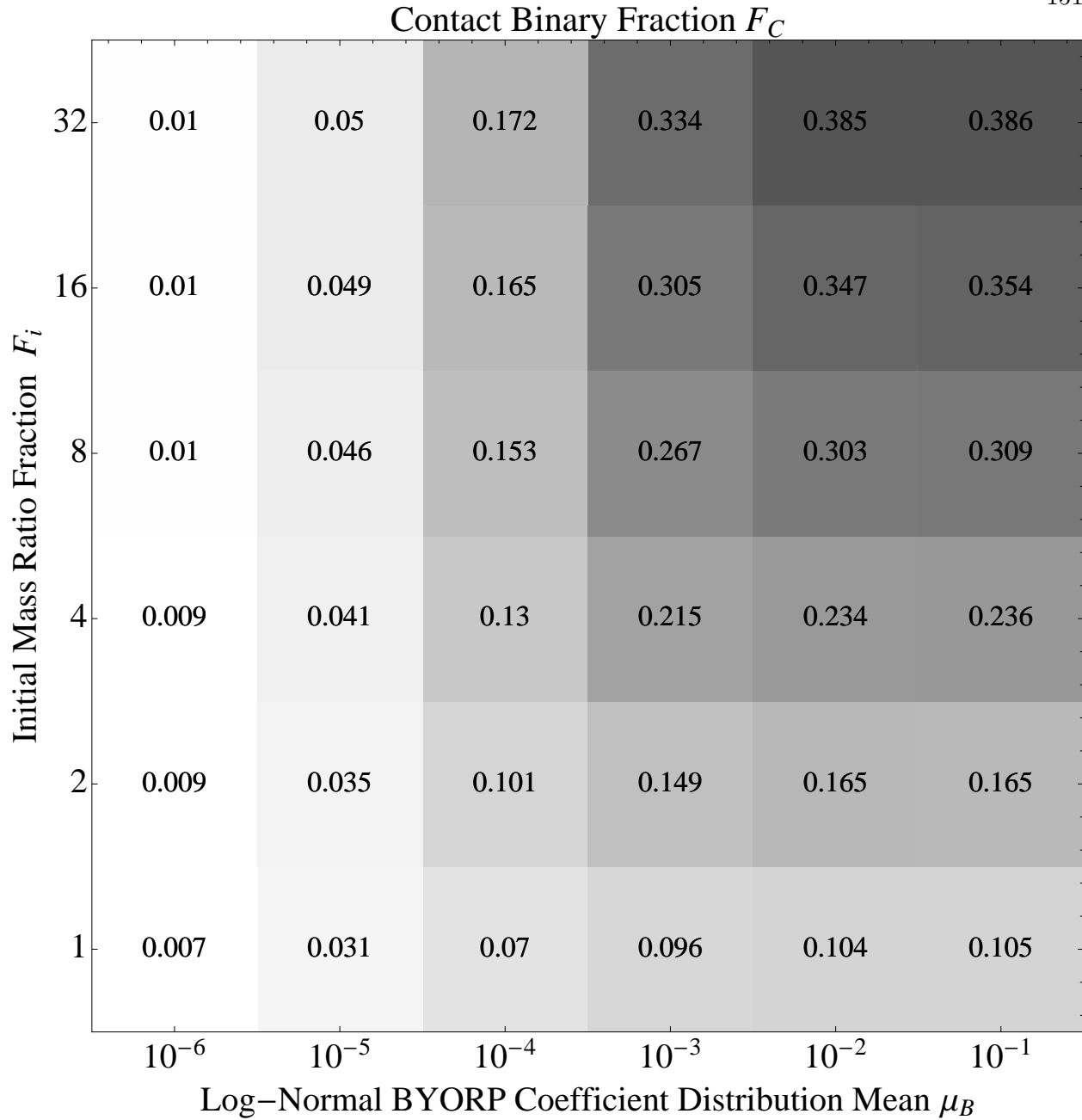


Figure 3.16: The contact binary fraction F_C of the model population is shown as a function of the two free parameters: the mean of the BYORP coefficient logarithmic normal distribution μ_B along the x-axis and the initial mass fraction F_i along the y-axis. Each grid point is determined from an independent run of the asteroid population evolution model with those values for the free parameters (otherwise the runs are identical).

fraction F_{obs} , which is drawn from a normal distribution with mean μ_j and standard deviation σ_j

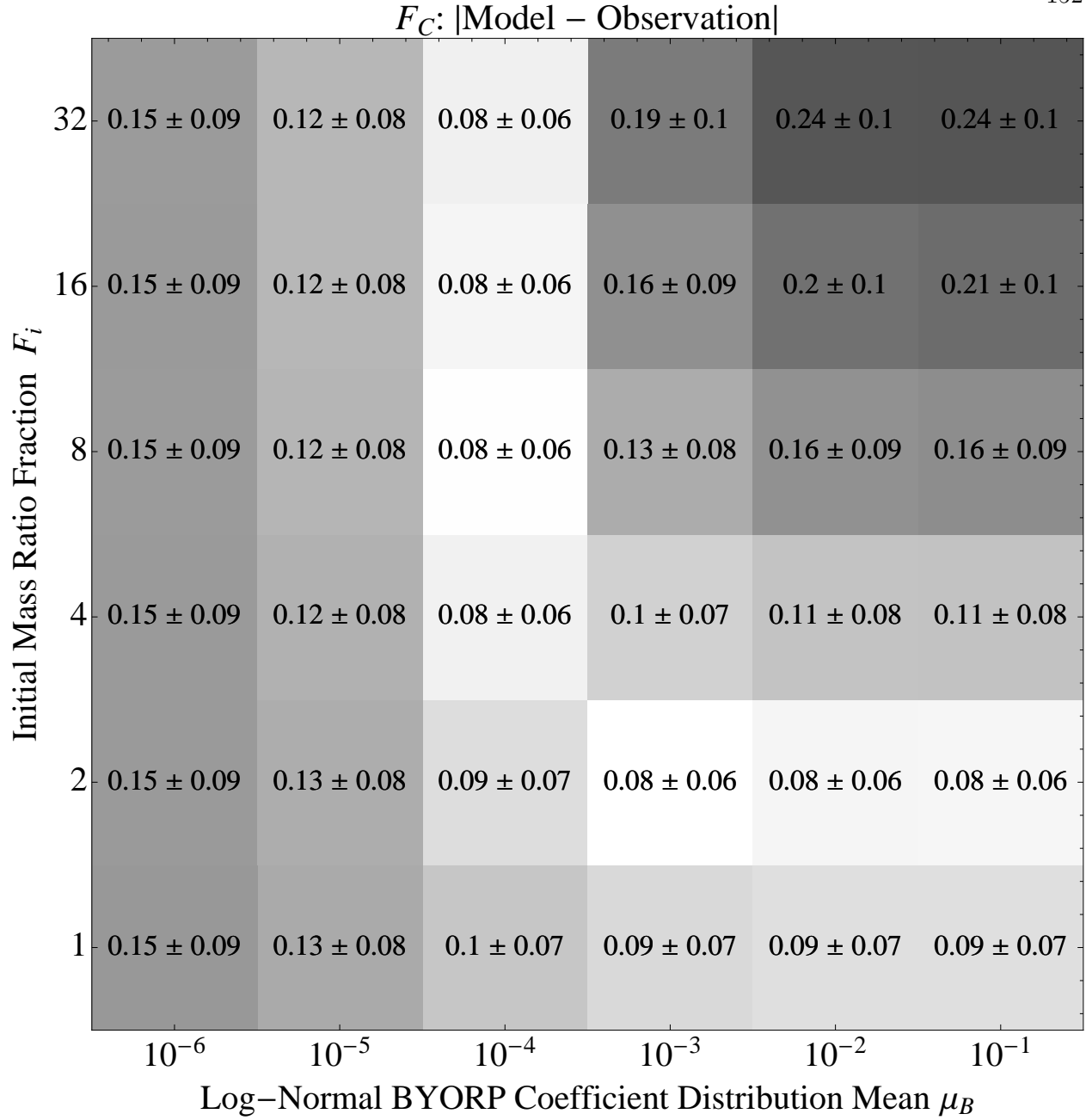


Figure 3.17: These plots are similar to Figure 3.3 but now show the contact binary fraction F_C . The best fit parameters for this constraint are in an L in the upper-left hand corner of the plot.

in accordance with the values in the previous sections.

$$\mathcal{L} = A \sum_j \frac{1}{2\sigma_j^2} (F_j - F_{obs}) \quad (3.17)$$

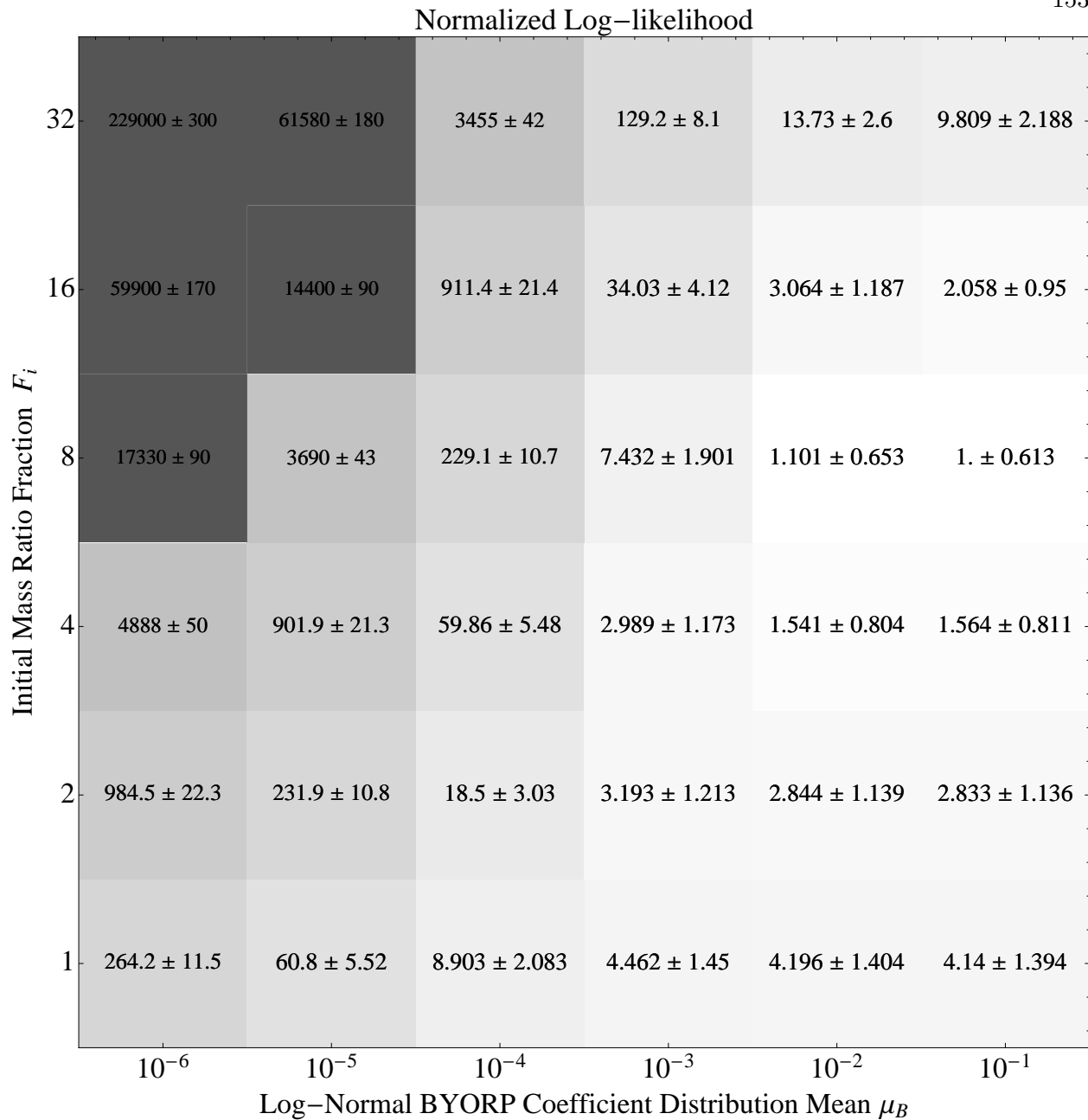


Figure 3.18: The normalized log-likelihood is shown as a function of the free parameters of the asteroid population evolution model. A low number means a higher probability.

A normalization is applied to make the best fit model have a value of 1. The larger the normalized log-likelihood the less likely those set of parameters are. Using Monte Carlo techniques, the uncertainty of the log-likelihood estimator can be determined. It is important to note that due to

computational constraints, the simulations are single runs and there is unaccounted for uncertainty. Although, a few cases were run more than once and they were consistent with small changes to the reported values. The log-likelihood metric is shown in Figure 3.18.

3.5 Discussion

The asteroid population evolution model identified a region in the phase space of the two free parameters in which the correct values are most likely to lie. The log-normal BYORP coefficient distribution mean is likely to be greater than -3 , which implies binary lifetimes less than 10^6 years for systems that do not end up in the tidal-BYORP equilibrium. These short binary lifetimes are consistent with the understanding that the tight asynchronous population (e.g. 2004 *DC*) are newly formed binary systems that have yet to tidally relax. The best fit initial mass ratio fraction of 8 is larger than a flat distribution of 4, and so weighted towards production of high mass ratio systems. The high mortality rate of low mass ratio systems in the “instantaneous” phase of binary formation is corrected by the synchronous low mass ratio binary population. This is consistent with the hypothesis that asteroids are more likely to rotationally fission along interior planes and “necks” than from small events at the surface that accumulate in orbit into a larger satellite (Sánchez and Scheeres, 2012; Holsapple, 2009; Walsh et al., 2008).

For these best fit parameters, the asteroid population evolution model provides some predictions regarding the Main Belt asteroid population. The asteroid pair population is predicted to be about 2% of the total population. That is within the last 2 Myrs, 2% of the population was a member of a binary pair that disrupted. These are mostly small asteroids, and it goes to less than 1% for asteroids larger than a kilometer in diameter.

Bibliography

- Agresti, A., Coull, B., 1998. Approximate is better than "exact" for interval estimation of binomial proportions. *American Statistician* , 119–126.
- Asphaug, E., Ryan, E.V., Zuber, M.T., 2002. Asteroid Interiors. *Asteroids III* , 463–484.
- Behrend, R., Bernasconi, L., Roy, R., Klotz, A., Colas, F., Antonini, P., Aoun, R., Augustesen, K., Barbotin, E., Berger, N., Berrouachdi, H., Brochard, E., Cazenave, A., Cavadore, C., Coloma, J., Cotrez, V., Deconihout, S., Demeautis, C., Dorseuil, J., Dubos, G., Durkee, R., Frappa, E., Hormuth, F., Itkonen, T., Jacques, C., Kurtze, L., Laffont, A., Lavayssière, M., Lecacheux, J., Leroy, A., Manzini, F., Masi, G., Matter, D., Michelsen, R., Nomen, J., Oksanen, A., Pääkkönen, P., Peyrot, A., Pimentel, E., Pray, D., Rinner, C., Sanchez, S., Sonnenberg, K., Sposetti, S., Starkey, D., Stoss, R., Teng, J.P., Vignand, M., Waelchli, N., 2006. Four new binary minor planets: (854) Frostia, (1089) Tama, (1313) Berna, (4492) Debussy. *ICARUS* 446, 1177–1184.
- Benner, L.A.M., Hudson, R.S., Ostro, S.J., Rosema, K.D., Giorgini, J.D., Yeomans, D.K., Jurgens, R.F., Mitchell, D.L., Winkler, R., Rose, R., Slade, M.A., Thomas, M.L., Pravec, P., 1999. Radar Observations of Asteroid 2063 Bacchus. *ICARUS* 139, 309–327.
- Benner, L.A.M., Nolan, M.C., Margot, J.L., Ostro, S.J., Giorgini, J.D., 2003. Radar Imaging of Binary Near-Earth Asteroid 1998 ST27. *ICARUS* 35, 959.
- Benner, L.A.M., Nolan, M.C., Ostro, S.J., Giorgini, J.D., Pray, D.P., Harris, A.W., Magri, C., Margot, J.L., 2006. Near-Earth Asteroid 2005 CR37: Radar images and photometry of a candidate contact binary. *ICARUS* 182, 474–481.
- Benz, W., Asphaug, E., 1999. Catastrophic Disruptions Revisited. *ICARUS* 142, 5–20.
- Bottke Jr, W.F., Durda, D.D., Nesvorný, D., Jedicke, R., Morbidelli, A., Vokrouhlický, D., Levison, H.F., 2005a. Linking the collisional history of the main asteroid belt to its dynamical excitation and depletion. *ICARUS* 179, 63–94.
- Bottke Jr, W.F., Durda, D.D., Nesvorný, D., Jedicke, R., Morbidelli, A., Vokrouhlický, D., Levison, H.F., 2005b. The fossilized size distribution of the main asteroid belt. *ICARUS* 175, 111–140.
- Bottke Jr, W.F., Nolan, M.C., Greenberg, R., Kolvoord, R.A., 1994. Velocity distributions among colliding asteroids. *ICARUS* 107, 255–268.

- Brozović, M., Benner, L.A.M., Taylor, P.A., Nolan, M.C., Howell, E.S., Magri, C., Scheeres, D.J., Giorgini, J.D., Pollock, J., Pravec, P., Galád, A., Fang, J., Margot, J.L., Busch, M.W., Shepard, M.K., Reichart, D.E., Ivarsen, K.M., Haislip, J.B., Lacluyze, A., Jao, J.S., Slade, M.A., Lawrence, K.J., Hicks, M.D., 2011. Radar and optical observations and physical modeling of triple near-Earth Asteroid (136617) 1994 CC. *ICARUS* 216, 241–256.
- Busch, M.W., Kulkarni, S.R., Brisken, W., Ostro, S.J., Benner, L.A.M., Giorgini, J.D., Nolan, M.C., 2010. Determining asteroid spin states using radar speckles. *ICARUS* 209, 535–541.
- Čapek, D., Vokrouhlický, D., 2004. The YORP effect with finite thermal conductivity. *ICARUS* 172, 526–536.
- Chesley, S.R., Ostro, S.J., Vokrouhlický, D., Čapek, D., Giorgini, J.D., Nolan, M.C., Margot, J.L., Hine, A.A., Benner, L.A.M., Chamberlin, A.B., 2003. Direct Detection of the Yarkovsky Effect by Radar Ranging to Asteroid 6489 Golevka. *Science* 302, 1739–1742.
- Ćuk, M., 2007. Formation and Destruction of Small Binary Asteroids. *The Astrophysical Journal* 659, L57–L60.
- Ćuk, M., Burns, J.A., 2005. Effects of thermal radiation on the dynamics of binary NEAs. *ICARUS* 176, 418–431.
- Davis, D.R., Chapman, C.R., Greenberg, R., Weidenschilling, S.J., Harris, A.W., 1979. Collisional evolution of asteroids - Populations, rotations, and velocities. *ICARUS* -1, 528–557.
- Davis, D.R., Ryan, E.V., Farinella, P., 1995. On How to Scale Disruptive Collisions. *ICARUS* 26, 319.
- Demura, H., Kobayashi, S., Nemoto, E., Matsumoto, N., Furuya, M., Yukishita, A., Muranaka, N., Morita, H., Shirakawa, K., Maruya, M., Ohyama, H., Uo, M., Kubota, T., Hashimoto, T., Kawaguchi, J., Fujiwara, A., Saito, J., Sasaki, S., Miyamoto, H., Hirata, N., 2006. Pole and Global Shape of 25143 Itokawa. *Science* 312, 1347–1349.
- Donnison, J.R., Wiper, M.P., 1999. Bayesian statistical analysis of asteroid rotation rates. *Monthly Notices of the Royal Astronomical Society* 302, 75–80.
- Durda, D.D., Greenberg, R., Jedicke, R., 1998. Collisional Models and Scaling Laws: A New Interpretation of the Shape of the Main-Belt Asteroid Size Distribution. *ICARUS* 135, 431–440.
- Fang, J., Margot, J.L., 2012. Binary Asteroid Encounters with Terrestrial Planets: Timescales and Effects. *The Astronomical Journal* 143, 25.
- Farinella, P., Davis, D.R., 1992. Collision rates and impact velocities in the Main Asteroid Belt. *Icarus* (ISSN 0019-1035) 97, 111–123.
- Farinella, P., Davis, D.R., Paolicchi, P., Cellino, A., Zappalà, V., 1992. Asteroid collisional evolution - an integrated model for the evolution of asteroid rotation rates. *Astronomy and Astrophysics* (ISSN 0004-6361) 253, 604–614.
- Fujiwara, A., Kawaguchi, J., Yeomans, D.K., Abe, M., Mukai, T., Okada, T., Saito, J., Yano, H., Yoshikawa, M., Scheeres, D.J., Barnouin-Jha, O., Cheng, A., Demura, H., Gaskell, R.W., Hirata, N., Ikeda, H., Kominato, T., Miyamoto, H., Nakamura, A.M., Nakamura, R., Sasaki, S., Uesugi, K., 2006. The Rubble-Pile Asteroid Itokawa as Observed by Hayabusa. *Science* 312, 1330–1334.

- Fulchignoni, M., Barucci, M.A., Di Martino, M., Dotto, E., 1995. On the evolution of the asteroid spin. *Astronomy and Astrophysics* 299, 929.
- Giblin, I., Martelli, G., Farinella, P., Paolicchi, P., Di Martino, M., Smith, P.N., 1998. The Properties of Fragments from Catastrophic Disruption Events. *ICARUS* 134, 77–112.
- Goldreich, P., 1963. On the eccentricity of satellite orbits in the solar system. *Monthly Notices of the Royal Astronomical Society* 126, 257.
- Goldreich, P., Peale, S.J., 1966. Spin-orbit coupling in the solar system. *Astronomical Journal* 71, 425.
- Goldreich, P., Sari, R., 2009. Tidal Evolution of Rubble Piles. *The Astrophysical Journal* 691, 54–60.
- Golubov, O., Krugly, Y.N., 2012. Tangential Component of the YORP Effect. *The Astrophysical Journal Letters* 752, L11.
- Higgins, D., Pravec, P., Kušnirák, P., Hornoch, K., Pray, D.P., Vilagi, J., Kornos, L., Gajdos, S., Husarik, M., Pikler, M., Cervak, G., 2008. Asteroid Lightcurve Analysis of Suspected Binary Asteroids. *Minor Planet Bulletin* 35, 173–175.
- Holsapple, K.A., 2007. Spin limits of Solar System bodies: From the small fast-rotators to 2003 EL61. *ICARUS* 187, 500–509.
- Holsapple, K.A., 2009. The Deformation of Asteroids from YORP Spin-Up. *Lunar and Planetary Institute Science Conference Abstracts* 40, 2053.
- Holsapple, K.A., 2010. On YORP-induced spin deformations of asteroids. *ICARUS* 205, 430–442.
- Hudson, R.S., Ostro, S.J., 1994. Shape of Asteroid 4769 Castalia (1989 PB) from Inversion of Radar Images. *Science* 263, 940–943.
- Ivezić, Ž., Tabachnik, S., Rafikov, R., Lupton, R.H., Quinn, T., Hammegren, M., Eyer, L., Chu, J., Armstrong, J.C., Fan, X., Finlator, K., Geballe, T.R., Gunn, J.E., Hennessy, G.S., Knapp, G.R., Leggett, S.K., Munn, J.A., Pier, J.R., Rockosi, C.M., Schneider, D.P., Strauss, M.A., Yanny, B., Brinkmann, J., Csabai, I., Hindsley, R.B., Kent, S., Lamb, D.Q., Margon, B., McKay, T.A., Smith, J.A., Waddell, P., York, D.G., 2001. Solar System Objects Observed in the Sloan Digital Sky Survey Commissioning Data. *ICARUS* 122, 2749–2784.
- Jacobson, S.A., Scheeres, D.J., 2011a. Dynamics of rotationally fissioned asteroids: Source of observed small asteroid systems. *ICARUS* 214, 161–178.
- Jacobson, S.A., Scheeres, D.J., 2011b. Long-term Stable Equilibria for Synchronous Binary Asteroids. *The Astrophysical Journal Letters* 736, L19.
- Jacobson, S.A., Scheeres, D.J., 2012. Forming the Observed Binary Asteroid Population. *LPI Contributions* 1667, 6092.
- Kaasalainen, M., Āurech, J., Warner, B.D., Krugly, Y.N., Gaftonyuk, N.M., 2007. Acceleration of the rotation of asteroid 1862 Apollo by radiation torques. *Nature* 446, 420–422.

- Love, S.G., Ahrens, T.J., 1996. Catastrophic Impacts on Gravity Dominated Asteroids. *ICARUS* 124, 141–155.
- Lowry, S.C., Fitzsimmons, A., Pravec, P., Vokrouhlický, D., Boehnhardt, H., Taylor, P.A., Margot, J.L., Galád, A., Irwin, M., Irwin, J., Kušnirák, P., 2007. Direct Detection of the Asteroidal YORP Effect. *Science* 316, 272–.
- MacDonald, G.J.F., 1964. Tidal friction. *Reviews of Geophysics* 2, 467–541.
- Margot, J.L., 2003. A Low-Density M-type Asteroid in the Main Belt. *Science* 300, 1939–1942.
- Margot, J.L., Nolan, M.C., Benner, L.A.M., Ostro, S.J., Jurgens, R.F., Giorgini, J.D., Slade, M.A., Campbell, D.B., 2002. Binary Asteroids in the Near-Earth Object Population. *Science* 296, 1445–1448.
- Marzari, F., Rossi, A., Scheeres, D.J., 2011. Combined effect of YORP and collisions on the rotation rate of small Main Belt asteroids. *ICARUS* 214, 622–631.
- McMahon, J.W., Scheeres, D.J., 2010a. Detailed prediction for the BYORP effect on binary near-Earth Asteroid (66391) 1999 KW4 and implications for the binary population. *ICARUS* 209, 494–509.
- McMahon, J.W., Scheeres, D.J., 2010b. Secular orbit variation due to solar radiation effects: a detailed model for BYORP. *Celestial Mechanics and Dynamical Astronomy* 106, 261–300.
- McMahon, J.W., Scheeres, D.J., 2012. Effect of Small Scale Surface Topology on Near-Earth Asteroid YORP and bYORP Coefficients. *AAS/Division of Dynamical Astronomy Meeting* 43.
- Michel, P., Benz, W., Tanga, P., Richardson, D.C., 2001. Collisions and Gravitational Reaccumulation: Forming Asteroid Families and Satellites. *Science* 294, 1696–1700.
- Mignard, F., 1979. The evolution of the lunar orbit revisited. I. *Moon and the Planets* 20, 301–315.
- Mignard, F., 1980. The evolution of the lunar orbit revisited. II. *Moon and the Planets* 23, 185–201.
- Murray, C.D., Dermott, S.F., 2000. *Solar System Dynamics*. Cambridge University Press.
- Nesvorný, D., Vokrouhlický, D., 2008. Analytic Theory for the Yarkovsky-O’Keefe-Radzievski-Paddack Effect on Obliquity. *The Astronomical Journal* 136, 291–299.
- Nolan, M.C., Howell, E.S., Becker, T.M., Magri, C., Giorgini, J.D., Margot, J.L., 2008. Arecibo Radar Observations of 2001 SN263: A Near-Earth Triple Asteroid System. *ICARUS* 40, 432.
- Nolan, M.C., Howell, E.S., Miranda, G., 2004. Radar Images of Binary Asteroid 2003 YT1. *ICARUS* 36, 1132.
- Nolan, M.C., Magri, C., Ostro, S.J., Benner, L.A., Giorgini, J.D., Howell, E.S., Hudson, R.S., 2007. The Shape and Spin of 101955 (1999 RQ36) from Arecibo and Goldstone Radar Imaging. *Bulletin of the American Astronomical Society* 39, 433.
- Ostro, S.J., Margot, J.L., Benner, L.A.M., Giorgini, J.D., Scheeres, D.J., Fahnestock, E.G., Broschart, S.B., Bellerose, J., Nolan, M.C., Magri, C., Pravec, P., Scheirich, P., Rose, R., Jurgens, R.F., De Jong, E.M., Suzuki, S., 2006. Radar Imaging of Binary Near-Earth Asteroid (66391) 1999 KW4. *Science* 314, 1276–1280.

- Pravec, P., Harris, A.W., 2006. Binaries among NEAs and Small Main Belt Asteroids: Angular Momentum and Other Properties. *American Astronomical Society* 38, 614.
- Pravec, P., Harris, A.W., 2007. Binary asteroid population. 1. Angular momentum content. *ICARUS* 190, 250–259.
- Pravec, P., Harris, A.W., Warner, B.D., 2007. NEA rotations and binaries. *Near Earth Objects* 236, 167–176.
- Pravec, P., Scheirich, P., 2010. Binary System Candidates for Detection of BYORP. *Bulletin of the American Astronomical Society* 42, 1055.
- Pravec, P., Scheirich, P., Kušnirák, P., Šarounová, L., Mottola, S., Hahn, G., Brown, P., Esquerdo, G., Kaiser, N., Krzeminski, Z., Pray, D.P., Warner, B.D., Harris, A.W., Nolan, M.C., Howell, E.S., Benner, L.A.M., Margot, J.L., Galád, A., Holliday, W., Hicks, M.D., Krugly, Y.N., Tholen, D.J., Whiteley, R.J., Marchis, F., Degraff, D.R., Grauer, A., Larson, S., Velichko, F.P., Cooney, W.R., Stephens, R.D., Zhu, J., Kirsch, K., Dyvig, R., Snyder, L., Reddy, V., Moore, S., Gajdoš, Š., Világi, J., Masi, G., Higgins, D., Funkhouser, G., Knight, B., Slivan, S.M., Behrend, R., Grenon, M., Burki, G., Roy, R., Demeautis, C., Matter, D., Waelchli, N., Revaz, Y., Klotz, A., Rieugné, M., Thierry, P., Cotrez, V., Brunetto, L., Kober, G., 2006. Photometric survey of binary near-Earth asteroids. *ICARUS* 181, 63–93.
- Pravec, P., Scheirich, P., Vokrouhlický, D., Harris, A.W., Kušnirák, P., Hornoch, K., Pray, D.P., Higgins, D., Galád, A., Világi, J., Gajdoš, Š., Kornoš, L., Oey, J., Husárik, M., Cooney, W.R., Gross, J., Terrell, D., Durkee, R., Pollock, J., Reichart, D.E., Ivarsen, K.M., Haislip, J.B., Lacluyze, A., Krugly, Y.N., Gaftonyuk, N.M., Stephens, R.D., Dyvig, R., Reddy, V., Chiorny, V., Vaduvescu, O., Longa-Peña, P., Tudorica, A., Warner, B.D., Masi, G., Brinsfield, J., Goncalves, R., Brown, P., Krzeminski, Z., Gerashchenko, O., Shevchenko, V.S., Molotov, I., Marchis, F., 2012. Binary asteroid population. 2. Anisotropic distribution of orbit poles of small, inner main-belt binaries. *ICARUS* 218, 125–143.
- Pravec, P., Vokrouhlický, D., 2009. Significance analysis of asteroid pairs. *ICARUS* 204, 580–588.
- Pravec, P., Vokrouhlický, D., Polishook, D., Scheeres, D.J., Harris, A.W., Galád, A., Vaduvescu, O., Pozo, F., Barr, A., Longa, P., Vachier, F., Colas, F., Pray, D.P., Pollock, J., Reichart, D.E., Ivarsen, K.M., Haislip, J.B., Lacluyze, A., Kušnirák, P., Henych, T., Marchis, F., Macomber, B., Jacobson, S.A., Krugly, Y.N., Sergeev, A.V., Leroy, A., 2010. Formation of asteroid pairs by rotational fission. *Nature* 466, 1085–1088.
- Pravec, P., Wolf, M., Šarounová, L., 1999. How many binaries are there among the near-Earth asteroids?, in: *Evolution and source regions of asteroids and comets : proceedings of the 173rd colloquium of the International Astronomical Union*, p. 159.
- Richardson, D.C., Elankumaran, P., Sanderson, R.E., 2005. Numerical experiments with rubble piles: equilibrium shapes and spins. *ICARUS* 173, 349–361.
- Rossi, A., Marzari, F., Scheeres, D.J., 2009. Computing the effects of YORP on the spin rate distribution of the NEO population. *ICARUS* 202, 95–103.
- Rozitis, B., Green, S.F., 2012. The influence of rough surface thermal-infrared beaming on the Yarkovsky and YORP effects. *Monthly Notices of the Royal Astronomical Society* 423, 367–388.

- Rubincam, D.P., 2000. Radiative Spin-up and Spin-down of Small Asteroids. *ICARUS* 148, 2–11.
- Sánchez, D.P., Scheeres, D.J., 2011. Simulating Asteroid Rubble Piles with A Self-gravitating Soft-sphere Distinct Element Method Model. *The Astrophysical Journal* 727, 120.
- Sánchez, D.P., Scheeres, D.J., 2012. DEM simulation of rotation-induced reshaping and disruption of rubble-pile asteroids. *ICARUS* 218, 876–894.
- Scheeres, D.J., 2007a. Rotational fission of contact binary asteroids. *ICARUS* 189, 370.
- Scheeres, D.J., 2007b. The dynamical evolution of uniformly rotating asteroids subject to YORP. *ICARUS* 188, 430.
- Scheeres, D.J., 2009a. Minimum energy asteroid reconfigurations and catastrophic disruptions. *Planetary and Space Science* 57, 154–164.
- Scheeres, D.J., 2009b. Stability of the planar full 2-body problem. *Celestial Mechanics and Dynamical Astronomy* 104, 103–128.
- Scheeres, D.J., 2012. Asteroid Shapes and Spins: How the Internal informs the External. *LPI Contributions* 1667, 6189.
- Scheeres, D.J., Hartzell, C.M., Sánchez, D.P., Swift, M., 2010. Scaling forces to asteroid surfaces: The role of cohesion. *ICARUS* 210, 968–984.
- Scheeres, D.J., Marzari, F., Rossi, A., 2004. Evolution of NEO rotation rates due to close encounters with Earth and Venus. *ICARUS* 170, 312–323.
- Scheirich, P., Pravec, P., Mottola, S., Mommert, M., Hornoch, K., Kušnirák, P., Pittichová, J., Jacobson, S.A., Pray, D., Polishook, D., Krugly, Y.N., Slyusarev, I., Pollock, J., Jehin, E., Manfroid, J., Gillon, M., Galád, A., Licandro, J., Alí-Lagoa, V., Brinsfield, J., Inasaridze, R.Y., Molotov, I.E., 2012. Zero Drift in Mean Anomaly of the Satellite of 1996 FG3 and its Implication for the BYORP Theory. *LPI Contributions* 1667, 6123.
- Shepard, M.K., Margot, J.L., Magri, C., Nolan, M.C., Schlieder, J., Estes, B., Bus, S.J., Volquardsen, E.L., Rivkin, A.S., Benner, L.A.M., Giorgini, J.D., Ostro, S.J., Busch, M.W., 2006. Radar and infrared observations of binary near-Earth Asteroid 2002 CE26. *ICARUS* 184, 198–210.
- Statler, T.S., 2009. Extreme sensitivity of the YORP effect to small-scale topography. *ICARUS* 202, 502–513.
- Stewart, S.T., Leinhardt, Z.M., 2009. Velocity-Dependent Catastrophic Disruption Criteria for Planetesimals. *The Astrophysical Journal Letters* 691, L133–L137.
- Tanga, P., Comito, C., Paolicchi, P., Hestroffer, D., Cellino, A., dell’Oro, A., Richardson, D.C., Walsh, K.J., Delbo, M., 2009. Rubble-Pile Reshaping Reproduces Overall Asteroid Shapes. *The Astrophysical Journal Letters* 706, L197–L202.
- Taylor, P.A., Howell, E.S., Nolan, M.C., Thane, A.A., 2012. The Shape and Spin Distributions of Near-Earth Asteroids Observed with the Arecibo Radar System, in: DPS, Reno, NV.
- Taylor, P.A., Margot, J.L., 2011. Binary asteroid systems: Tidal end states and estimates of material properties. *ICARUS* 212, 661–676.

- Taylor, P.A., Margot, J.L., Nolan, M.C., Benner, L.A.M., Ostro, S.J., Giorgini, J.D., Magri, C., 2008. The Shape, Mutual Orbit, and Tidal Evolution of Binary Near-Earth Asteroid 2004 DC. LPI Contributions 1405, 8322.
- Taylor, P.A., Margot, J.L., Vokrouhlický, D., Scheeres, D.J., Pravec, P., Lowry, S.C., Fitzsimmons, A., Nolan, M.C., Ostro, S.J., Benner, L.A.M., Giorgini, J.D., Magri, C., 2007. Spin Rate of Asteroid (54509) 2000 PH5 Increasing Due to the YORP Effect. *Science* 316, 274–.
- Vedder, J.D., 1996. Asteroid Collisions: Estimating Their Probabilities and Velocity Distributions. *ICARUS* 123, 436–449.
- Vedder, J.D., 1998. Main Belt Asteroid Collision Probabilities and Impact Velocities. *ICARUS* 131, 283–290.
- Vokrouhlický, D., Čapek, D., 2002. YORP-Induced Long-Term Evolution of the Spin State of Small Asteroids and Meteoroids: Rubincam's Approximation. *ICARUS* 159, 449–467.
- Vokrouhlický, D., Nesvorný, D., 2008. Pairs of Asteroids Probably of a Common Origin. *The Astronomical Journal* 136, 280–290.
- Walsh, K.J., Richardson, D.C., 2008. A steady-state model of NEA binaries formed by tidal disruption of gravitational aggregates. *ICARUS* 193, 553.
- Walsh, K.J., Richardson, D.C., Michel, P., 2008. Rotational breakup as the origin of small binary asteroids. *Nature* 454, 188–191.
- Walsh, K.J., Richardson, D.C., Michel, P., 2012. Spin-up of rubble-pile asteroids: Disruption, satellite formation, and equilibrium shapes. *ICARUS* 220, 514–529.
- Warner, B.D., Harris, A.W., Pravec, P., 2009. The asteroid lightcurve database. *ICARUS* 202, 134–146.
- Wisdom, J., 2004. Spin-Orbit Secondary Resonance Dynamics of Enceladus. *The Astronomical Journal* 128, 484–491.
- Wisdom, J., 2008. Tidal dissipation at arbitrary eccentricity and obliquity. *ICARUS* 193, 637.
- Yeomans, D.K., Barriot, J., Dunham, D.W., Farquhar, R.W., Giorgini, J.D., Helfrich, C.E., Konopliv, A.S., McAdams, J.V., Miller, J.K., Owen, W.M.J., Scheeres, D.J., Synnott, S.P., Williams, B.G., 1997. Estimating the Mass of Asteroid 253 Mathilde from Tracking Data During the NEAR Flyby. *Science* 278, 2106.